Pontifícia Universidade Católica
do Rio de Janeiro

Gustavo Schinazi

Bio-Based Flame Retardation of Acrylonitrile-Butadiene-Styrene

Tese de Doutorado

Thesis presented to the Programa de Pós-graduação em Engenharia Mecânica of PUC-Rio in partial fulfillment of the requirements for the degree of Doutor em Engenharia Mecânica.

Advisor: Prof. José Roberto Moraes d'Almeida
Co-Advisor: Prof. David A. Schiraldi
Co-Advisor: Prof. Jonathan K. Pokorski

Rio de Janeiro
October 2020

PONTIFÍCIA UNIVERSIDADE CATÓLICA
DO RIO DE JANEIRO

Gustavo Schinazi

Bio-Based Flame Retardation of Acrylonitrile-Butadiene-Styrene

Thesis presented to the Programa de Pós-graduação em Engenharia Mecânica of PUC-Rio in partial fulfillment of the requirements for the degree of Doutor em Engenharia Mecânica. Approved by the Examination Committee:

Prof. José Roberto Moraes d'Almeida
Advisor
Departamento de Engenharia Química e de Materiais – PUC-Rio

Prof. David A. Schiraldi
Co-Advisor
CWRU

Prof. Jonathan K. Pokorski
Co-Advisor
UCSD

Prof. Mônica Feijó Naccache
Departamento de Engenharia Mecânica – PUC-Rio

Prof. Amanda Lemette Teixeira Brandão
Departamento de Engenharia Química e de Materiais – PUC-Rio

Prof. Gary E. Wnek
CWRU

Prof. Hatsuo Ishida
CWRU

Prof. Ya-Ting T. Liao
CWRU

Rio de Janeiro, October 21st, 2020

Gustavo Schinazi

Graduated with a Bachelor's Degree in Industrial Engineering from PUC-Rio (Pontifícia Universidade Católica do Rio de Janeiro), with a minor in Mathematics, in 2009. Obtained a Master's Degree in Materials Science and Engineering from PUC-Rio in 2014. Earned PhD Degrees in Macromolecular Science and Engineering from CWRU (Case Western Reserve University) and in Mechanical Engineering from PUC-Rio in 2020. Performs research in the field of materials science and engineering with a focus on polymers and polymer composites, currently specializing in flame retardation of polymers. Scientific interests include material structure-property relationships, phase transformations, polymer processing, and flame retardation.

Bibliographic data

Schinazi, Gustavo

Bio-based flame retardation of acrylonitrile-butadiene-styrene / Gustavo Schinazi ; advisor: José Roberto Moraes d'Almeida ; co-advisors: David A. Schiraldi, Jonathan K. Pokorski. – 2020.
285 f. : il. color. ; 30 cm

Tese (doutorado) – Pontifícia Universidade Católica do Rio de Janeiro, Departamento de Engenharia Mecânica, 2020.
Inclui bibliografia.

1. Engenharia Mecânica – Teses. 2. Acrilonitrila-butadieno-estireno (ABS). 3. Retardamento de chama. 4. Retardantes de chama não-halogenados. 5. Materiais naturais. 6. Calorimetria por combustão. I. Almeida, José Roberto Moraes d'. II. Schiraldi, David A. III. Pokorski, Jonathan K. IV. Pontifícia Universidade Católica do Rio de Janeiro. Departamento de Engenharia Mecânica. V. Título.

CDD: 621

Dedicado à Vovó Geny
pelo seu amor incondicional e infinito.
Meu amor por você é maior do que o mundo inteiro.

Dedicated to my Grandma, Vovó Geny,
for your unconditional and infinite love.
My love for you is bigger than the entire world.

Acknowledgements

To my Advisor, Prof. David Schiraldi, for your support and guidance throughout my PhD. Thank you for your teachings, your positive and optimistic advising style, your patience during our long conversations, and your valuable advice related to my PhD, to my career, and to life in general.

To my Advisor, Prof. Jon Pokorski, for your support and advice throughout my research. Thank you for your guidance, your friendliness, your patience, your well measured nudges, your positive and constructive feedback, for making me feel supported even across a long physical distance, and for your valuable advice, which extended well beyond my PhD project.

To my Advisor, Prof. José Roberto d'Almeida, for your help and support during my PhD. Thank you for sharing your advice and feedback during different phases of my project, for the valuable discussions, for your patience during our long conversations, and for helping me overcome my difficulties.

To Prof. Hatsuo Ishida, for introducing me to the field of Fire Science through the excellently designed and taught course *Chemistry of Fire Safe Polymers and Composites* and for your valuable feedback as a Committee Member of my Research Qualifying Examination and of my PhD Dissertation Defense.

To the Committee Members of my PhD Dissertation Defense, Prof. Gary Wnek, Prof. Hatsuo Ishida, Prof. Ya-Ting Liao, Prof. Mônica Naccache, and Prof. Amanda Brandão, for your valuable insights, suggestions, and constructive feedback related to my PhD Dissertation.

To Prof. João Maia's Research Group for allowing me to use its melt-processing equipment and facilities – especially to Dr. Vivek Pandey for the training in batch mixing and compression molding techniques, Dr. Molin Guo for helping me during extrusion, and Dr. Tyler Schneider for discussions related to injection molding.

To Prof. Fumiaki Takahashi's Research Group, for allowing me to use their fire laboratory, especially the microscale combustion calorimeter.

To Lihan Rong, for performing the pyrolysis-gas chromatography-mass spectrometry analyses and training me in utilizing the related software and libraries.

To Prof. Miguel Sánchez-Soto and his research group, for performing the cone calorimetry experiments.

To Luiz Fernando Vieira, for introducing me to Design of Experiments and giving me the basis that I needed to begin to learn and use its techniques.

To Erik Price, for the valuable discussions and collaborations and for performing some of the microscale combustion calorimetry experiments.

To the Schiraldi Research Group members, Dr. Kim DeGracia, Hans Cheng, and Dr. Hua Sun, for your friendship, your support, the research-related brainstorming discussions, the life-related conversations, and for helping make the daily life in the office and in the lab more enjoyable.

To my Brazilian friends at Case Western Reserve University, especially Luiz Fernando, Lucivan, Erika, and Irlaine, for your friendship and your support, both related to my PhD research and related to life in general. Your support was very important to me, and you helped make the daily life in the department much more enjoyable.

To the entire Macromolecular Science and Engineering Department at CWRU, for creating such an amazing and collaborative work and social environment that was a joy to be a part of.

To Mitchell Balk, for all of your support, friendship, and generosity during my time living in Cleveland. You helped me feel at home through your support and kindness!

To Rabbi Mendy and Sara Alevsky, for helping me to feel at home in Cleveland, and to all of my other friends at Case Western Reserve University and in Cleveland.

To my Friends throughout the world – you know who you are – who always support me throughout my life. Thank you for always being there for me, helping me get through the difficult times, celebrating with me the victories, and enjoying life together!

To my Family, for always being here for me and supporting me. To my Mom, Sônia, for your unconditional support, guidance, and love throughout my life and throughout my PhD. Thank you for everything you have always given me and done for me and everything you continue to do for me. Thank you for always supporting and believing in me! To my brother, Daniel, for your support and friendship during my PhD and throughout my life. Thank you for the conversations, the many light, funny, and enjoyable moments, and for always being here with me! To my brother, Ale, for always supporting and rooting for me. Even though we are physically far, we are always together, and I can feel your support and how much you want me to be happy and succeed!

To my girlfriend, Gaby, for your support, caring, understanding, and for being here with me throughout all of the moments. Thank you for being who you are, and for allowing me to be genuinely myself when I am with you. Thank you for being with me in the good and in the hard moments, for your company, for all of the laughter, for cheering for me, for supporting me, and for believing in me!

To my Grandma, Vovó Geny, for everything! I love you more than anything in this world! You have always loved me, supported me, rooted and cheered for me, vibrated with all of my victories, comforted me, given me advice, and made me feel loved and at home. Your hugs were always the safest and warmest place to be in the world. Thank you for your teachings, your stories, your wisdom, and your love! Your memory will always make me smile and will always be a blessing!

To my Grandpa, Vovô Zaide, for your unconditional love, your teachings, your wisdom, your support, and your guidance throughout my life while you were here

with us. You always believed in my education and strived to give me the best education I could possibly get. I know you are smiling and very proud with this achievement! You planted beautiful seeds in this world! You have always been an example and a role model to me. Thank you for everything! Your memory will always be a blessing!

To Case Western Reserve University, Pontifícia Universidade Católica do Rio de Janeiro, and Capes, for having built this Dual-Degree Program and enabled me to have this wonderful and amazing experience that was so important in my life and that made me grow personally, academically, and professionally.

To CWRU, for the infrastructure, facilities, campus, events, and providing me a wonderful place to be and work in.

To Capes, for the financial support during my PhD (this study was financed in part by the Coordenação de Aperfeiçoamento de Pessoal de Nível Superior - Brasil (CAPES) - Finance Code 001).

To G-d, for giving me everything I have, for supporting me throughout my entire life, for giving me the gifts that He gives me, for giving me my spirituality and my connection to my religion, for giving me the strength, wisdom, knowledge, intellect, and determination to successfully complete my PhD, and for always being here with me and my family. Thank you G-d!

Abstract

Schinazi, Gustavo; d'Almeida, José Roberto Moraes (Advisor); Schiraldi, David A. (Co-Advisor); Pokorski, Jonathan K. (Co-Advisor). **Bio-Based Flame Retardation of Acrylonitrile-Butadiene-Styrene**. Rio de Janeiro, 2020. 285p. Tese de Doutorado – Departamento de Engenharia Mecânica, Pontifícia Universidade Católica do Rio de Janeiro.

Polymers are used in a wide variety of applications and are present in all aspects of people's daily lives; however, they are generally very flammable. Major advances have been made in developing flame retardants (FRs) to be used in polymers, but most commercial FR additives used today, mainly halogenated substances, are toxic to humans and the environment and are being increasingly banned throughout the world. Acrylonitrile-butadiene-styrene (ABS) is one of the most widely used polymers in the world but also one of the most flammable and most challenging to flame retard, and ABS is used commercially with toxic halogenated FRs. Research into the use of renewable products as FRs for polymers has grown exponentially, but very little work has been performed on reducing ABS's flammability using nature-derived or low-toxicity FRs. There is therefore an urgent need for the development of low-toxicity, bio-based FR systems to substitute halogenated FRs for commercial use in ABS.

The present work aims to contribute to the development of a bio-based flame-retardant solution for ABS, by (1) developing a flame-retardant grade of ABS using mainly nature-derived additives while maintaining acceptable mechanical properties and (2) comprehending the flame-retardation mechanisms of the bio-based FRs. The project consists of two phases: (1) a Screening Phase, during which the effects of 8 different FRs and combinations thereof on ABS's flammability are evaluated, using Design of Experiments techniques, through microscale combustion calorimetry; and (2) a Detailed Analysis and Mechanistic Study Phase, in which the most promising candidates from Phase 1 are further analyzed through a variety of techniques with the objectives of better understanding their flammability and mechanical performances and comprehending their flame-retardation mechanisms. Chapter 1 presents a brief introduction and a literature review. Chapter 2 contains the experimental methodology. Chapter 3 discusses the Screening Phase, providing details about experimental planning and presenting

screening results; the most promising samples and scientifically motivating synergies are identified. Chapter 4 contains Phase 2 results, presenting in-depth discussions and hypotheses to explain the flame-retardation mechanisms of the bio-based FRs in ABS. Chapter 5 provides the main conclusions of the research and recommendations for future work.

Keywords

Acrylonitrile-butadiene-styrene (ABS); flame retardation; non-halogenated flame retardants; bio-based materials; combustion calorimetry.

Resumo

Schinazi, Gustavo; d'Almeida, José Roberto Moraes (Orientador); Schiraldi, David A. (Co-Orientador); Pokorski, Jonathan K. (Co-Orientador). **Retardamento de Chama em Acrilonitrila-Butadieno-Estireno Utilizando Aditivos Naturais**. Rio de Janeiro, 2020. 285p. Tese de Doutorado – Departamento de Engenharia Mecânica, Pontifícia Universidade Católica do Rio de Janeiro.

Polímeros estão entre os materiais mais utilizados no mundo, sendo empregados em inúmeras aplicações e estando amplamente presentes na vida cotidiana das pessoas; no entanto, são, em geral, altamente inflamáveis. Muitos retardantes de chama (*flame retardants*, FR) foram desenvolvidos para reduzir a flamabilidade de polímeros; porém, a maioria dos aditivos FR usados comercialmente, principalmente os halogenados, são tóxicos para o meio-ambiente e para a humanidade e estão sendo cada vez mais banidos ao redor do mundo. Acrilonitrila-butadieno-estireno (ABS) é um dos polímeros mais utilizados no mundo mas também um dos mais inflamáveis e mais difíceis de solucionar, e ABS é usado comercialmente com retardantes de chama halogenados, que são tóxicos. A pesquisa sobre a utilização de materiais renováveis como retardantes de chama para polímeros vem crescendo exponencialmente, mas poucos trabalhos foram realizadas no âmbito de reduzir a flamabilidade de ABS utilizando FRs renováveis ou de baixa toxicidade. Há, portanto, uma necessidade urgente de se desenvolver sistemas FR de baixa toxicidade e baseados em materiais naturais para substituir os aditivos halogenados para uso comercial em ABS.

O presente trabalho pretende contribuir para o desenvolvimento de uma solução FR baseada em materiais naturais para uso em ABS. O primeiro objetivo é uma meta prática: desenvolver ABS de baixa flamabilidade utilizando principalmente aditivos naturais, mantendo propriedades mecânicas aceitáveis. O segundo objetivo é científico: compreender os mecânismos de retardamento de chama dos FRs naturais. O projeto é desenvolvido em duas etapas: (1) a Fase de Triagem, na qual os efeitos de 8 retardantes de chama e de suas combinações na flamabilidade de ABS são availados, utilizando-se técnicas de Planejamento de Experimentos, através de microcalorimetria por combustão (MCC); e (2) a Fase de Análise Detalhada e Estudo de Mecanismos, na qual os candidatos mais

promissores da primeira fase são analisados mais detalhadamente para se compreender melhor suas propriedades de flamabilidade e mecânicas e para se entender seus mecanismos de retardamento de chama. O Capítulo 1 contém uma breve introdução seguida de uma revisão bibliográfica. O Capítulo 2 apresenta a metodologia experimental utilizada durante a pesquisa. O Capítulo 3 discute a Fase de Triagem, detalhando o planejamento experimental, apresentando os resultados dos experimentos de triagem e identificando as amostras mais promissoras e as sinergias mais cientificamente motivadoras. O Capítulo 4 apresenta os resultados da segunda fase, com discussões aprofundadas e hipóteses acerca dos mecanismos de retardamento de chama dos FRs naturais em ABS. O Capítulo 5 contém as principais conclusões da pesquisa e recomendações para trabalhos futuros.

Palavras-chave

Acrilonitrila-butadieno-estireno (ABS); retardamento de chama; retardantes de chama não-halogenados; materiais naturais; calorimetria por combustão.

Table of Contents

List of Figures

List of Tables

List of Abbreviations

4VCH	4-Vinylcyclohexene
A	Acrylonitrile monomer
AA	Acrylonitrile dimer
ABS	Acrylonitrile-butadiene-styrene
a.c.	Area counts
Addit. Hypoth.	Additive hypothesis
APP	Ammonium polyphosphate
ATH	Alumina trihydrate
B	Butadiene monomer
BB	Butadiene dimer
BBB	Butadiene trimer
BEST-FR	Bio-sourced, environmentally safe, thermo-oxidative, and flame-retardant
BFR	Brominated flame retardant
Br-ABS	Brominated ABS
BS	1,4-Butane sultone
btc	Burned to clamp
CFR	Chlorinated flame retardant
CN-Np-PPN	[1-(4-Cyano-1,2,3,4-tetrahydronaphthyl)]propanenitrile
D	DNA
DBDPO	Decabromodiphenyl oxide
DNA	Deoxyribonucleic acid
DoE	Design of Experiments
DSC	Differential scanning calorimetry
dTG	Differential thermogravimetry
E_a	Activation energy
EDX	Energy-dispersive x-ray spectroscopy
EG	Expandable graphite
EGA	Evolved gas analysis
EHC	Effective heat of combustion
ESI	Electrospray ionization

EVA	Ethylene-vinyl acetate
F-lignin	Functionalized lignin
FG	Fish gelatin
FR	Flame retardant
frc	Flame reached clamp
FTIR	Fourier-transform infrared spectroscopy
GC	Gas chromatography
GC/MS	Gas chromatograph/mass spectrometer
HBCDD	Hexabromocyclododecane
HCA	Heart Cut Analysis
HCC	Heat of complete combustion
HDA	1,6-Hexanediamine
HDI	2-Heptadecylimidazole
HDPE	High-density polyethylene
HEP	Hydroxyethylpalmitamide
HIPS	High-impact polystyrene
HRR	Heat release rate
Irg	Irganox® 1010
L/D	Length-to-diameter
LbL	Layer-by-layer
LDH	Layered double hydroxide
LDPE	Low-density polyethylene
LOI	Limiting oxygen index
m-LDH	Modified layered double hydroxide
MA	Maleic anhydride
MCC	Microscale combustion calorimetry
ME	Melamine
MH	Magnesium hydroxide
MLR	Mass loss rate
MMT	Montmorillonite
MPP	Melamine polyphosphate
MS	Mass spectrometry
MSDS	Material safety datasheet

n/a	Not applicable
NBR	Nitrile-butadiene rubber
OBDPO	Octabromodiphenyl oxide
OC	Organic content
OSP	Oyster shell powder
PA	Phytic acid or Phytic acid salt or Phytic acid sodium salt
PA6	Nylon-6
PAN	Polyacrylonitrile
PB	Polybutadiene
PBB	Polybrominated biphenyl
PBDD	Polybrominated dibenzodioxin
PBDE	Polybrominated diphenyl ether
PBDF	Polybrominated dibenzofuran
PBT	Poly(butylene terephthalate)
PC	Polycarbonate
PCDD	Polychlorinated dibenzodioxin
PCDF	Polychlorinated dibenzofuran
PDSPB	Poly(4,4-diaminodiphenyl methane spirocyclic pentaerythritol bisphosphonate)
PE	Polyethylene
PEG	Poly(ethylene glycol)
PEI	Polyethyleneimine
PET	Poly(ethylene terephthalate)
PHRR	Peak heat release rate
Phyt	Phytic acid
PLA	Poly(lactic acid)
PMLR	Peak mass loss rate
PP	Polypropylene
PS	Polystyrene
PTFE	Polytetrafluoroethylene
PVA	Poly(vinyl alcohol)
PVC	Poly(vinyl chloride)
Py-GC-MS	Pyrolysis-gas chromatography-mass spectrometry

S	Styrene monomer
S6	Safire™ 600
SAN	Styrene-acrylonitrile copolymer
SbO	Sb_2O_3
SBR	Styrene-butadiene rubber
SEBS-g-MA	Polystyrene-*block*-poly(ethylene-*ran*-butylene)-*block*-polystyrene-*graft*-maleic anhydride
SEM	Scanning electron microscopy
SMA	Styrene-maleic anhydride random copolymer
SS	Styrene dimer
SSS	Styrene trimer
TA	Tannic acid
TAT	Tannic acid terephthalate
TBBPA	Tetrabromobisphenol-A
TBPE	Tribromophenoxy ethane
TGA	Thermogravimetric analysis
THR	Total heat release
THR_{eff}	Effective total heat release
TIC	Total ion chromatogram
TOCP	Tri-ortho-cresyl phosphate
TTI	Time to ignition
UL	Underwriters Laboratories
U.S.	United States
VC	Volatile content
WPC	Wood-plastic composite
XPS	X-ray photoelectron spectroscopy
μ	Char yield
χ	Combustion efficiency

1
Introduction and Literature Review

1.1.
Introduction, Objectives, and Methodology

Polymers are well known for their low densities, good processability, and versatility, enabling them to be used in a wide range of applications and to be present in all aspects of people's daily lives. One of the main drawbacks related to their use, however, is their flammability. The use of flame retardants (FRs) to suppress, reduce, and/or delay the combustion of polymers has long been explored, and major advances have been made in developing FR additives to be used commercially.

One of the largest and most effective classes of commercial flame-retardant additives is that of halogenated flame retardants [1,2]. Despite their efficacy, great environmental concerns have been raised surrounding their use: it has been shown that these FRs can leach out of everyday products during their lifetime, contaminating humans, animals, and the environment with toxic compounds; when exposed to fire, halogenated FRs release toxic and environmentally persistent byproducts; and the incineration or disposal of polymers into landfills at the end of their lifetime causes further contamination of the environment and of living organisms [1]. Many studies have detected the presence of these compounds in humans, animals, sediments, water, and air in various locations [3–12]. Halogenated FRs are being increasingly regulated or banned throughout the world as a result [10,13]. The toxicological concerns and ensuing restrictions related to halogenated flame retardants have created a need for environmentally friendly, low-toxicity flame retardants that can be used efficiently and safely in polymeric materials.

Driven by this societal need and by the increasing sustainability-focused global environmental awareness, research into the use of renewable products as FRs for polymers has grown exponentially in the past two decades. Many different nature-derived materials have since been used as FRs in various plastics. Costes et al. [14], Sonnier et al. [15], Hobbs [16], and Watson and Schiraldi [17] have

recently published comprehensive reviews describing the use of bio-based FRs in polymeric systems. Some examples of bio-based materials that have been explored as FRs in the past two decades, which are described in their reviews, are tannic acid (TA), phytic acid (PA), deoxyribonucleic acid (DNA), and fish gelatin (FG).

It is often desirable to combine nature-derived FRs with low-toxicity, commercially available FRs to explore more options for synergy, creating bio-based, environmentally friendly FR systems that improve flammability characteristics without reducing mechanical properties. Mineral hydroxides are good candidates for this purpose, being amongst the most widely used of all FRs but often needed in concentrations greater than 50 wt% when used independently [2]. Examples of this family are alumina trihydrate (ATH) and magnesium hydroxide (MH), the latter of which has been used synergistically with TA to flame retard different polymers [18,19]. Melamine (ME), which has been used synergistically with TA and FG in polyolefins [18]; melamine poly(magnesium phosphate) (Safire™ 600, S6), a commercial FR and smoke suppressant recently used in polystyrene (PS) [18]; and ammonium polyphosphate (APP), a usual element of intumescent systems [20–23], are also good candidates to be used in combination with bio-based FRs.

Bio-based FR systems have had a remarkable impact on the flammability of many polymers, but very little work has been carried out exploring the bio-based flame retardation of acrylonitrile-butadiene-styrene (ABS). ABS is one of the most widely used polymers in the world, finding applications in the electronics, consumer goods, and automobile industries (e.g. casings for electronic equipment, computer keycaps, home appliances and tools, car dashboards and light fixtures, wheel covers) [24–27]. These applications require the use of low-flammability components, since they deal with high electrical currents and temperatures and are found in everyday objects. ABS is, however, one of the most flammable polymers and one of the most challenging to flame retard due to its complex terpolymer structure. To reduce its flammability, ABS is currently used commercially with halogenated FRs, such as tetrabromobisphenol-A (TBBPA), which are extremely toxic and face global restrictions and bans [24,25,28]. There is therefore an urgent need for the development of low-toxicity, bio-based FR systems to substitute the halogenated FRs for commercial use in ABS.

Some work has been done in the past two decades using synthetic intumescent systems and/or nanofillers in ABS [20,29,30], but they have shown limited improvements and do not have the same environmental advantages as nature-derived FRs. A bio-based coating has been used on ABS [31], but coatings generally suffer from durability and washability issues. Very few reports of bio-based bulk FR additives in ABS have been published to date. Tributsch & Fiechter [32] blended tannins and tannin-containing tree barks with ABS, increasing the char yield and limiting oxygen index (LOI) and reducing polymer dripping during UL 94 tests; pristine and phosphorylated lignin were used by Song et al. [26,33] and Prieur et al. [27], respectively, to reduce the flammability of ABS, showing that lignin (and potentially other char formers) is a promising candidate for flame retarding ABS; and Moustafa et al. [34] used ground seashell waste to enhance the thermal and flammability properties of ABS. All of these studies, however, obtained restricted improvements in ABS's flammability and presented drawbacks. Overall, limited progress has been made in flame retarding ABS using nature-derived additives, creating a strong need for the development of bio-based FR systems for use in ABS.

The present work proposes to advance the field of bio-based flame retardation of polymers by seeking to find a flame-retardant solution for ABS using mainly nature-derived additives. The first objective of the study, a practical goal, was to develop a flame-retardant grade of ABS using bio-based and low-toxicity FRs with acceptable mechanical properties. The second objective, concerning a more scientific viewpoint, was to comprehend the mechanisms of flame retardation of bio-based FRs in ABS.

The methodology consisted of a two-phase approach, including a screening phase and a detailed analysis phase. In Phase 1, the Screening Phase, a systematic study was conducted, with the aid of Design of Experiments (DoE) techniques, to evaluate the flammability performances of 4 nature-derived FRs and 4 low-toxicity commercial FRs in ABS. Over 30 samples were produced, using the additives in combinations of up to 4 at a time, and tested through microscale combustion calorimetry (MCC); the most promising FRs and FR combinations were identified and scientifically motivating synergies among the components were detected. Phase 2, the Detailed Analysis and Mechanistic Study Phase, consisted of further analyzing the most promising samples from Phase 1, using techniques such as cone

calorimetry, thermogravimetric analysis (TGA), pyrolysis-gas chromatography-mass-spectrometry (Py-GC-MS), tensile testing, and impact testing; the objectives of this phase were to better understand the flammability and mechanical properties of these samples and to comprehend some of the additives' flame-retardation mechanisms.

1.2. Literature Review

1.2.1. The Combustion Cycle and Ways to Suppress It

In order to study ways to effectively prevent or retard the propagation of a fire or flame, it is important to understand the basic concepts of a fire. Two ways of describing these principles are by using what is known as the "Fire Triangle", or "Fire Tetrahedron", and by explaining the combustion cycle.

The "Fire Triangle", depicted in Figure 1.1, is a simple model that is widely used to represent the elements that must be present in order for a fire to occur [18,35,36]. These elements are: Ignition temperature, frequently represented as Heat; Oxygen, or an oxidizing agent; and Fuel. For a fire to be ignited and sustained, all three components must be present; in other words, extinguishing the fire can be achieved by removing any one of these elements. For example, cold water can be used to reduce the heat, a blanket can be utilized to prevent the oxygen from reaching the fuel, or the fuel itself (the burning material) can be physically relocated away from the sources of heat and oxygen. The role of each of the three components in a fire is explained below through the combustion cycle.

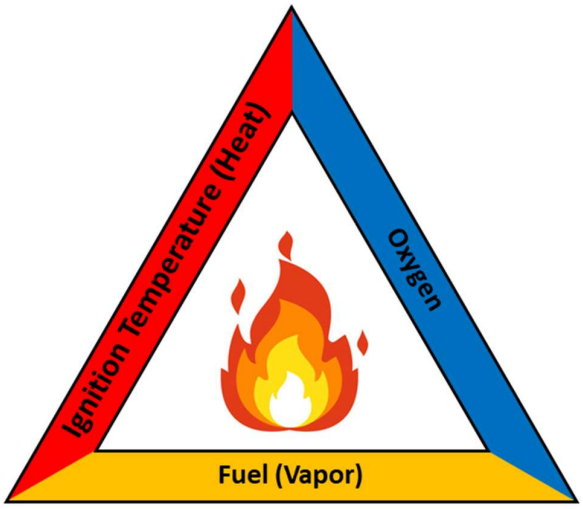

Figure 1.1. The "Fire Triangle" (adapted from [35]).

In 1962, Haessler suggested the use of a tetrahedron instead of a triangle [35–37]. The fourth element that he proposed is an Uninhibited Chemical Chain Reaction, without which a fire cannot occur. Figure 1.2 is one way to represent the tetrahedron, in which each side of the shape, representing one of the elements, is in contact with the other three. Haessler proposed that, even if the original three components are present, flaming combustion will only occur if the chemical processes of fuel degradation into radicals and radical-oxygen combination occur in a self-sustained manner; in other words, the radical-oxygen reactions, which are exothermic, must provide enough heat in order to sustain the degradation process, leading to a continuous cycle. The discovery of the tetrahedron is important, as it provides new ways of extinguishing fires [36]: instead of eliminating the heat, oxygen, or fuel, one can suppress the flames by inhibiting the self-sustained chain reaction, thus preventing the oxygen and the fuel from exothermically reacting, and effectively breaking the combustion cycle.

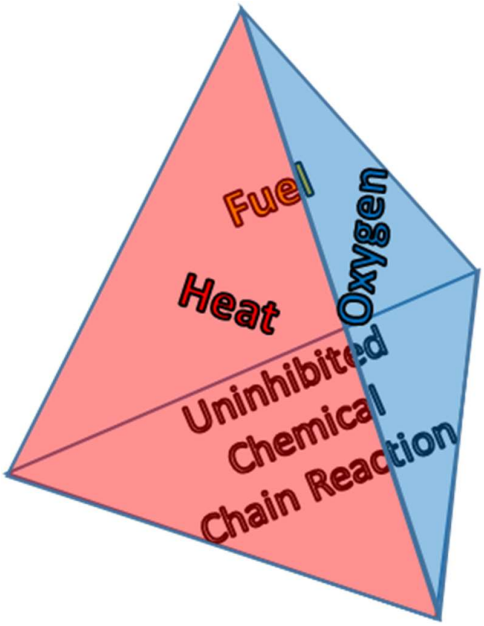

Figure 1.2. The "Fire Tetrahedron".

One example of how the cycle can be interrupted in such a way is through the use of halogenated flame retardants. When the material's temperature begins to rise, the halogen atoms are released before the polymer fragments. When the volatile polymer radicals are released, the halogens act as "radical scavengers", coupling with the fuel fragments and preventing them from exothermically combining with the oxygen. In this way, the oxygen, fuel, and heat are still present, but the chemical chain reaction is not allowed to occur. In other words, the removal of the fourth element can be enough to extinguish the fire.

The basic principles of fire, or flaming combustion, in a polymeric material can also be explained through the combustion cycle. According to Troitzsch [38], the four steps of the cycle are Preheating, Volatilization/Decomposition, Combustion, and Propagation. It can be described in the following manner:

(a) **Preheating:** The material is exposed to a source of thermal energy;

(b) **Volatilization/Decomposition:** An increase in the material's temperature causes bonds to be broken and radicals to be generated;

(c) **Combustion:** The radicals combine with oxygen atoms in the air. This bonding reaction is exothermic, releasing energy. If the temperature is high enough, this energy will be released in the form of visible and non-visible light (hence the flames and heat, respectively), and part of the heat will raise the temperature of the nearby polymer;

(d) **Propagation:** This increase in temperature will cause the material to continue to degrade, breaking more bonds, which will combine with more oxygen atoms, etc. As long as there is material to be burned, oxygen in contact with the system, and enough heat, the chemical reactions and, therefore, the burning will continue in a self-sustained manner.

The fire can be extinguished by interrupting the combustion cycle in any of its steps. The above description makes it easy to see how each of the elements of the "Fire Tetrahedron" is important. Heat is required to initiate (and sustain) degradation of the material by breaking chemical bonds, thus generating volatile radical fragments. Oxygen (or an alternative oxidizing agent) is necessary because it reacts with the fragments through an exothermic reaction, liberating more heat. Fuel (the material being burnt) is obviously necessary, because its fragments must combine with oxygen in order for the exothermic reaction to occur. Finally, an uninhibited chemical interaction between the fuel fragments and the oxygen is required in order to keep providing heat for the cycle to continue. Removing any one of these four elements would effectively interrupt the combustion cycle and extinguish the fire.

1.2.2.
Flame Retardants – Definition, Modes of Action, and Classification

A flame retardant (FR) can be defined as "a substance added or a treatment applied to a material in order to suppress, significantly reduce or delay the combustion of the material" [2]. In essence, the role of a flame retardant is to act in such a way that it interrupts the combustion cycle, preventing its host material from (or, at least, slowing down the process of) burning or propagating a flame. An FR additive can act in a number of different ways, since it can tackle *any* of the steps

of the combustion cycle by removing *any* of the elements of the "fire tetrahedron". The modes of action of FRs can be organized according to at least two different classifications. The first refers to the mode of action itself, which can be *physical* or *chemical*. The second relates to the location of the action, which can be the *condensed phase* or the *gas phase*.

1.2.2.1.
Physical Modes of Action

The main physical mechanisms through which an FR agent can act are through (1) cooling (i.e. acting as a heat sink), (2) dilution of the fuel and/or oxygen content, and (3) formation of a protective layer [2]. The mechanisms are described below:

(1) **Cooling/Heat Sink:** Some additives decompose endothermically, lowering the temperature of the reaction medium to below the combustion temperature. Examples are alumina trihydrate and magnesium hydroxide, which endothermically liberate water at about 200–300 °C.

(2) **Dilution/Inert Gases:** Some FRs liberate inert gases upon decomposition, such as H_2O, CO_2, and/or NH_3. These gases dilute the fuel and/or the oxygen supply, decreasing its concentration sufficiently to prevent ignition or sustained combustion.

(3) **Protective Layer:** Some FRs promote the formation of a solid or gaseous protective layer that covers the material's surface. A solid layer can be formed as a consequence of charring (formation of fused aromatic carbonaceous rings as a result of cross-linking, cyclization, and carbonization), and can be enhanced by the presence of elements such as silicon. A gaseous layer can be composed of inert gases evolved during the decomposition process. The solid or gaseous protective layer acts as a gas and thermal barrier: it prevents (or slows down) the volatile fragments from escaping the material and the oxygen atoms from diffusing into it, thus inhibiting the exothermic coupling reactions, and it

reduces the rate of heat transfer into the material, slowing down the pyrolysis of the polymer.

1.2.2.2. Chemical Modes of Action

FRs can also act through chemical mechanisms, such as radical scavenging (i.e. flame inhibition), promotion of accelerated crosslinking and charring, and promotion of accelerated decomposition [2]:

(1) **Radical Scavenging/Flame Inhibition:** This mechanism is initiated by the release of specific radicals, such as Br• or Cl•, which occurs through decomposition of the FR that contains these elements. When the polymer decomposes into volatile radical fragments, the Br• and Cl• radicals "scavenge" and capture these fuel fragments before they react with the oxygen atoms. Therefore, the exothermic processes are stopped or reduced, limiting the amount of heat generated by the combustion and interrupting the cycle. It is important to note that for an FR compound to be effective in this manner, its decomposition must occur before (i.e. at a lower temperature) than that of the polymer itself, so that the scavenger radicals are "ready" to capture the fuel fragments once these are released. The most favorable situation is when the FR compound decomposes at around 50 °C below the polymer [39].

(2) **Accelerated Crosslinking and Charring:** Some FRs, such as phosphorus-containing compounds, can accelerate the charring reaction, leading to a quicker formation of the protective layer described above. The enhanced crosslinking reactions also serve to limit the release of volatile fragments, since the atoms become bound to the polymer by a larger number of bonds, thus requiring more energy in order to be released.

(3) **Accelerated Decomposition:** Through this mechanism, which is somewhat counter-intuitive, the FR catalyzes the decomposition of the polymer. This leads to a rapid reduction in the polymer melt's viscosity, making it drip away from

the location of the flame. The fuel is thus removed from the source of heat, leading to eventual extinguishment of the flame due to the lack of fuel.

1.2.2.3.
Condensed Phase vs. Gas Phase

The above mechanisms can also be classified according to the location in which they act. Examples of actions occurring in the condensed phase are cooling through endothermic reactions (heat sink), formation of a solid protective layer, accelerated crosslinking/charring, and accelerated polymer decomposition. Mechanisms that can occur in the gas phase include dilution of the fuel or oxygen content, formation of a gaseous protective layer, and radical scavenging. Flame-retardant compounds can work in either or both of the phases, and in one or a combination of the mechanisms, in their quest to reduce the spreading of or to extinguish the fire.

1.2.3.
Commercial Flame Retardants

The idea of flame retardation and the use of flame-retardant compounds as a way to prevent or delay fire propagation dates back to ancient times. In around 450 BC, the Egyptians began to use alum to reduce the flammability of wood. About 250 years later, the Romans added vinegar to that mixture in their treatment of wood [40]. Table 1.1 lists some of the early developments in flame retardation.

Table 1.1

Early historical flame-retardant developments (adapted from [2]).

Development	Date
Alum used to reduce the flammability of wood by the Egyptians	~450 BC
Mixture of alum and vinegar used on wood by the Romans	~200 BC
Mixture of clay and gypsum used to reduce flammability of theater curtains	1638
Mixture of alum, ferrous sulfate, and borax used on wood and textiles by Wyld in Britain	1735
Alum used to reduce the flammability of balloons	1783
Gay-Lussac reported a mixture of $(NH_4)_3PO_4$, NH_4Cl, and borax to be effective on linen and hemp	1821
Perkin described a flame-retardant treatment for cotton using a mixture of sodium stannate and ammonium sulfate	1912

With the arrival of synthetic polymers in the 20th century and the increasing use of polymeric materials in a very large range of applications, flame retardants began to be more broadly researched and utilized since the latter half of that century. An example of the growth of FR usage in the past decades is the over-100% increase in the global market demand for brominated flame retardants between 1990 and 2000 [10]. In 2003, there were more than 175 chemicals classified as flame retardants [10].

The main commercial FRs utilized today can be grouped into four main categories: halogenated organic, organophosphorus, inorganic, and nitrogen-based [2]. The current section will describe the characteristics of and the issues posed by each of those classes.

1.2.3.1.
Halogenated Flame Retardants

1.2.3.1.1.
General Information

Halogenated flame retardants account for about 25% by volume of the worldwide FR production [2]. Their mode of action is by functioning as radical scavengers in the gas phase (i.e. flame inhibition), capturing fuel free-radicals before they have a chance to bond with oxygen atoms. Halogenated compounds are perhaps the most effective types of flame retardants.

In general, only bromine and chlorine are used in commercial halogenated FRs [2,10]. As mentioned previously, radical scavengers must be released from the material slightly before the polymer decomposes so that they can efficiently capture the volatile fragments. However, fluorinated compounds are generally very stable (because of the strength of the C–F bond), decomposing at higher temperatures than most polymers, so their halogens are released too late. On the other extremity, iodinated compounds are not stable enough and decompose at too low temperatures, besides being expensive. Therefore, in most cases, fluorine and iodine cannot be used as FRs [10,39]. Between bromine and chlorine, the larger bromine atom is more efficient in fire performance, since the radical-capturing efficiency of a halogen increases with its size. As a result, most commercial halogenated FR compounds are based on bromine, and they are often abbreviated as BFRs (brominated flame retardants) [10].

There is a large amount of different BFRs available in the market. Since, from a flammability point of view, the functional part of these compounds is the actual bromine atoms, there is no real restriction on the rest of the molecule. Therefore, these are chosen to make them compatible with the polymer to which they will be applied, thermally stable at the required processing temperature (although thermal stabilizers are often added), and stable during the product's lifetime [2,10].

The various BFRs can be generally classified as reactive or additive. Reactive BFRs are chemically bonded to the polymer, usually by either grafting or adding bromine atoms to the backbone. In the latter case, the resulting product often contains brominated and non-brominated monomers in the backbone. Additive

BFRs are physically mixed with the plastic [2]. Some of the main types of BFRs that have been used are polybrominated biphenyls (PBB), tetrabromobisphenol-A (TBBPA), polybrominated diphenyl ethers (PBDE), and hexabromocyclododecane (HBCDD). Brominated monomers such as brominated styrene or butadiene have also been used.

The following are some typical uses of BFRs. TBBPA is most often used in epoxy resins for printed circuit boards, in ABS, and in high-impact PS (HIPS). Decabromodiphenyl ether, a type of PBDE, can be used in virtually any type of polymer, including ABS, polyolefins, poly(vinyl chloride) PVC, and elastomers. It is widely utilized in HIPS for television and computer monitor cabinets. HBCDD is mainly applied in PS foam for building construction, and it is also used in the textile industry [2,10].

1.2.3.1.2.
Main Issues

Despite their high efficiency as flame retardants, halogenated compounds pose serious threats to the environment and to human health. Toxic halogenated byproducts can be released from their host materials during the lifetime, combustion, and/or disposal of everyday products, as will be described below. One of the greatest concerns is the emission of polybrominated dibenzofurans (PBDF) and polybrominated dibenzodioxins (PBDD) during heating or combustion. Some isomers of their chlorinated counterparts, polychlorinated dibenzofurans (PCDF) and polychlorinated dibenzodioxins (PCDD), are also toxic. Another potential issue is the formation of hydrogen bromide (HBr), a corrosive and powerful sensory irritant gas [2].

The release of the above-mentioned and other toxic compounds can occur during the lifetime and usage of products containing halogenated flame retardants. Some of the FR molecules or their derivatives can leach out of the products during their lifetime; this is more likely to occur with additive FRs, since they are only physically, as opposed to chemically, mixed with the polymer [10]. Humans are therefore exposed to these chemicals through simple skin contact with consumer products, such as televisions and textiles. BFRs and CFRs (chlorinated FRs), as well as their byproducts, can also leach into the environment.

PBDF and PBDD are also released when BFR-containing products are burned. These flame retardants can effectively delay the spread of fire, but the smoke released during the combustion is very toxic, as it contains, besides the "usual" toxic gases (such as CO), toxic PBDF and PBDD. In the case of a fire, not only is this a hazard to those directly involved (as they would be exposed to these toxic products), but PBDF and PBDD are released into the environment, contaminating the air, water, soil, and living creatures.

The disposal of polymeric products after they become waste is normally done via incineration or landfill. Many flame-retarded materials that had never been involved in a fire are purposely burned at the end of their lifetime. This leads to the release of large amounts of PBDF and PBDD into the environment. As for landfills, BFRs and their derivatives can leach out of the products over time, contaminating the environment.

It is important to note than these chemicals can spread via water, wind, and bioaccumulation once they are released into the environment. Areas that are not directly in the vicinity of fires, landfills, and consumer products can therefore become contaminated. Bioaccumulation can also lead to a hazard to humans through the food chain.

There are many examples of contamination of the environment by BFRs throughout the world. In 1973, PBBs were accidentally mixed into cattle feed in Michigan, contaminating many farm products [10]. TBBPA has been detected in sewage sludge from sewage treatment plants in Sweden [3] and Canada [8]. PBDEs have been encountered in human blood serum in Sweden and the U.S. [4,6], in peregrine falcon eggs in Sweden [5] and Norway [7], in sediments and sewage sludge from various locations, and in biota and breast milk in North America [10]. HBCDD has been found in various environmental compartments such as artic air and biota [9].

Because of the evidence that halogenated FRs are contaminating the environment and posing health hazards to humans, its usage has been reduced or banned in many countries, especially in Japan and the European Union. For example, hexabromobiphenyl (a type of PBB) FRs were banned in the U.S. in 1974 [13]. Other PBBs stopped being produced in the U.S., Germany, and France in 1979, 1985, and 2000, respectively [10]. The main types of PBDEs have been banned and withdrawn from the market in the European Union and in Japan since

the early years of the current century [10]. The use of BFRs has not yet been banned in the U.S., but it is possible that this will occur once alternative FR solutions that are as effective as BFRs (in terms of both flammability and cost) are discovered and become commercially available. As a conclusion, it is essential to develop effective non-toxic FRs to substitute the halogenated ones, in order to replace them in the already regulated markets and to provide alternatives that could lead to their ban where they are still in use.

1.2.3.2. Organophosphorus Flame Retardants

1.2.3.2.1. General Information

Phosphorus-containing compounds are another widely used group of FRs. This is the most important class of FR compounds used on cellulose in the textile industry [2]. The main types of organic phosphorus-based FRs are phosphate esters, phosphinates, and phosphonates [41]. Inorganic P-based FRs, such as red phosphorus and ammonium polyphosphate (APP), are also used. Phosphorus-nitrogen and phosphorus-halogen combinations are also commonly utilized as FRs. In the case of organophosphorus compounds, the P groups provide the flame retardance while the organic portion provides compatibility with the polymer.

Phosphorus-based FRs can act both in the condensed and in the gas phases to inhibit combustion. In the condensed phase, they catalyze crosslinking of the polymer, reducing the amount of volatile-fragment generation and leading to cyclization and enhanced char formation. As explained before, char protects the material from burning by reducing the diffusion of oxygen into and of fuel fragments out from the polymer and by decreasing the rate of heat transfer into the decomposing substance. In the gas phase, P also works as a radical scavenger, inhibiting the exothermic oxidative reactions. Because of its action in both phases, these FRs are often very effective.

1.2.3.2.2.
Main Issues

Although phosphorus-based FRs are less environmentally toxic than halogenated compounds, they are also potentially toxic. For example, studies have shown that delayed neurotoxicity due to tri-ortho-cresyl phosphate (TOCP) has been observed in humans [42]. Exposure of sediment-dwelling organisms near production plants to triphenyl phosphate may have been high enough to exert toxic effects [43]. Halogenated organophosphorus FRs such as bis and tris(2,3-dibromopropyl) phosphate were banned for use in children's clothing in 1977 in the U.S. and other countries because of concerns that the chemical might be a human carcinogen and because of the possibility of significant human exposure through contact with treated fabrics [44]. Besides this, PO_x and phosphoric acid, which are toxic, can be produced during pyrolysis of these FRs [2]. In Europe, other organophosphorus FRs, such as tris(1-aziridinyl)phosphine oxide, have also been banned [2].

1.2.3.3.
Inorganic Flame Retardants

1.2.3.3.1.
General Information

There are many different types of inorganic FRs in use. The most widely commercially used class is that of metal hydroxides. Other inorganic FRs are based on antimony, boron, phosphorus, and, to a lesser extent, molybdenum, titanium, zirconium, and zinc. The mechanism of action of these compounds is different depending on the elements used [2].

The main metal hydroxides in use are aluminum trihydrate (ATH; $Al_2O_3 \cdot 3H_2O$) and magnesium hydroxide (MH; $Mg(OH_2)$). ATH is one of the most widely used, by volume, of all FRs. These compounds impart flame retardance by endothermically decomposing, releasing water molecules. This action disrupts the combustion cycle in two ways: the endothermic reaction absorbs heat, cooling down the polymer and the flame (heat sink), while the released water vapor dilutes

the flammable gas mixture. The disadvantage of this group of FRs is that a very high concentration (typically 50–80 wt%) has to be used in order to be effective, which is often detrimental to the material's properties [2].

The most widely used antimony compound is antimony trioxide (Sb_2O_3), although other antimony oxides and antimonates are also used. These compounds are used as synergists with halogenated FRs, enhancing their efficiency and, sometimes, reducing the required amount of the latter [2]. For example, decabromodiphenyl ether combined with antimony oxide is used in processes that require high-temperature processing, such as HIPS used in television and computer-monitor cabinets [10]. In general, halogen acids released at high temperatures react with the antimony-containing substances, forming antimony-halogen compounds. These act in many different ways, both in the condensed and in the gas phases, to retard flame propagation. Typical concentrations of antimony compounds are 2–10 wt% [2].

As for boron compounds, the most widely used materials are boric acid (H_3BO_3), sodium borate (borax; $Na_2B_4O_7 \cdot 10H_2O$), and zinc borate. Boric acid and borax are mainly used in cellulosic materials, such as cotton and paper. Zinc borate is used in many plastic and rubber products, either substituting or acting in synergy with antimony trioxide. It acts mainly in the condensed phase, acting as a flame retardant and smoke suppressant [2].

Some of the main types of inorganic phosphorus-based FRs are red phosphorus and APP, as mentioned previously. These materials most likely act due to the oxidation of elemental phosphorus into phosphoric acid or phosphorus pentoxide during thermo-oxidative degradation, which then plays a role in both the condensed and the gas phases, as explained in Section 1.2.3.2. It is used mainly in polyamides and phenolic applications.

Molybdenum-containing FRs work mostly as smoke suppressants [38], appearing to act in the condensed phase. Some titanium and zirconium compounds are used in wool. Zinc stannate and the previously mentioned zinc borate are used as replacements for or synergists with antimony trioxide. Other compounds, such as ammonium sulfamate and ammonium bromide, are used in cellulose-based products and in forest fires [2].

1.2.3.3.2.
Main Issues

The main drawback of the largest class of inorganic FRs, that of metal hydroxides, is the very large amount of additives that must be used in order for the system to be effective, which can lead to deterioration of the product's properties (especially mechanical properties) [2]. This issue is also true of some other inorganic FRs, often limiting their use.

Other metallic compounds containing heavy metals, such as antimony-based FRs, can be detrimental to human health if they leach out of commercial products. Red phosphorus is a toxic substance that poses health risks to those involved in the production process, and, as mentioned previously, phosphorus-containing products have a potential toxic effect on humans and the environment.

Therefore, although inorganic FRs are, in general, much less hazardous than halogenated FRs, most of them are either somewhat toxic or, in most cases, have to be used in very large quantities. These drawbacks lead to potential commercial uses for non-toxic flame retardants that can be used in lower concentrations and/or that can be used synergistically with inorganic FRs, reducing the required amount of the latter. As will be discussed in Section 1.2.4, bio-based flame retardants are excellent candidates for such non-toxic FRs.

1.2.3.4.
Nitrogen-Based Flame Retardants

1.2.3.4.1.
General Information

Nitrogen-based flame retardants can be very attractive due to their low toxicity, low smoke production during combustion, and suitability for recycling [41]. However, they are not effective in a very wide range of polymers. They are mostly used in nitrogen-containing polymers, such as polyurethanes and polyamides, but can also be utilized in some polyolefins, PVC, PET, and PBT, for example [2]. There is a significant synergistic effect between nitrogen and

phosphorus, leading to the use of many FRs based upon a combination of N and P [41].

FRs in this class can act in both the condensed and the gas phases. In the condensed phase, they can catalyze char formation. In the gas phase, nitrogen-containing gases, such as N_2 and NH_3, are released from the compounds, diluting the oxygen and volatile-fuel concentrations and forming an inert gas barrier, which protects the combustible fuel from the oxygen [41]. They are also often used in intumescent systems [2], since compounds such as melamine or urea can act as bubbling agents due to the release of N-containing gases.

Some common examples of nitrogen-based FRs are melamine, melamine cyanurate, melamine polyphosphate, melamine ammonium polyphosphate, melamine poly(zinc/magnesium phosphate), ammonium polyphosphate, urea, and guanidine [2,18,41]. The usage of N and P in combination with each other becomes evident by these examples, many of which include both elements in a single compound.

1.2.3.4.2.
Main Issues

Perhaps the main issue of nitrogen-based flame retardants is that they are not so efficient when used alone. They can be very effective when used in combination with other elements, such as phosphorus, due to synergistic effects [41]. Another drawback is that they are only suitable as FRs for a limited number of polymers [2]. These issues are reflected in the fact that nitrogen-based flame retardants comprise only approximately 5% of the worldwide flame retardant production [10].

1.2.4.
Bio-Sourced Flame Retardants

The previous section has shown that, although many different classes of flame-retardant compounds exist and are commercially in use, most of them have adverse effects, mainly related to toxicity. Therefore, the search for flame-retardant solutions that are safe for the environment and for humans, in combination with the increasing overall global environmental awareness, has led to the search for flame

retardants that are environmentally friendly and non-toxic in a general sense. The past decade has shown increasingly growing research in flame-retardant materials that are non-toxic, biodegradable, and based on renewable resources. This section will briefly describe some of the work that has been published on nature-derived flame retardants since they began being consistently studied in the beginning of the current century. In each of the examples described below, the bio-sourced compound(s) is emphasized in bold.

To the best of our knowledge, the first document reporting the use of renewable compounds to improve the fire retardance of a polymer is a patent filed by Susumu Nikkeshi (inventor) in 2003 [45]. Nikkeshi utilized tannin compounds to increase the thermal stability and the fire resistance of thermoplastic polyester resins. More specifically, **tannic acid** copolymerized with poly(vinyl alcohol) (PVA) and poly(ethylene glycol) (PEG) was mixed with poly(ethylene terephthalate) (PET), poly(butylene terephthalate) (PBT), polycarbonate (PC), ABS, and/or blends thereof, in concentrations of 2 to 20,000 ppm. The invention describes an increase in the thermal stability of the thermoplastic polymer and a reduction or suppression of its combustion.

The discovery and use of other natural resources as potential flame retardants continued in the following years. In 2007, Gani & Naruse [46] published a study on the effect of cellulose and lignin content on the pyrolysis and combustion of many types of plants and vegetation. They demonstrated that increasing lignin content decreases the rate of pyrolysis, while increasing cellulose content increases it. This result suggests that **lignin** plays an important role in delaying the combustion of plants and fibers, making it a potential FR compound to be used in polymers.

In 2008, Tributsch & Fiechter [32], by investigating ecosystems that are naturally exposed to fires, learned that tannin, present in tree barks, is one of the key components that protects the trees from fires. Exploring the performances of different tree barks and of tannin extracted from some of the barks, they found that they display a large amount of char after being heated to 600 °C in argon atmosphere. They blended the barks and tannins with ABS and found that the polymer's char yield was greatly increased. Furthermore, the addition of tannin increased the LOI index and helped to achieve non-dripping behavior in the UL 94 tests. In summary, the authors discovered and demonstrated the important role of

tannin in imparting fire resistance to tree barks and successfully presented the application of tannin as a char-forming agent and potential flame retardant in ABS.

In 2008 and 2009, Tondi and coworkers [47,48] developed **tannin-based rigid foams** (prepared from 95% natural material) and compared them to synthetic, commercial, phenolic foams (which are known to have outstanding fire characteristics) in terms of fire resistance, mechanical resistance, and other important properties. They concluded that the novel renewable tannin-based foams could compete with synthetic phenolic foams and replace them in various applications, besides being "cheap, fast and easy to prepare". Moreover, the addition of boric and/or phosphoric acid can further improve their self-extinguishing and fire resistant characteristics.

In 2011, Ravichandran et al. [49] reported the synthesis and characterization of polycardanol, a new polyphenolic FR material based on cardanol. Cardanol is a renewable and biodegradable component derived from cashew nut shell liquid, a waste product of the cashew nut industry. Based on TGA, heat release rate and heat release capacity results, the authors classified the material as moderately fire resistant (according to classification parameters suggested in [50]). This finding suggests the potential use of **cardanol** and/or polycardanol as an effective FR additive for polymers.

In the same year, Zhang et al. [51] published a study on the thermal degradation and pyrolysis of calcium alginate fiber. Alginate is a polysaccharide abundantly found in seaweed, making it an easily accessible bio-sourced component. The authors demonstrated that alginate is an inherently flame-retardant material, displaying a limiting oxygen index (LOI) value of 48.0 and a peak heat release rate of less than 5 kW/m^2. Their results suggest the potential use of **alginate** as a flame-retardant additive.

Still in 2011, Song et al. [33] investigated the use of **lignin** to improve the thermal and flame-retardance properties of ABS. They found that lignin could slow down the polymer's degradation process and increase the char yield. Furthermore, lignin reduced the polymer's heat release rate and slowed down its combustion process. By analyzing the char residue, they concluded that the formation of a protective char layer of lignin was primarily responsible for the enhanced flame retardance.

In 2012, publications were issued by Laufer et al. [52,53] and by Carosio and coworkers [54,55] on innovations involving the application of **chitosan** and **phytic acid** as FR additives or coatings. Chitosan can be obtained from crustaceans and arthropods, and aspects of its thermal stability and of its pyrolysis characteristics had been investigated by Pawlak & Mucha in 2003 [56] and by Zeng et al. in 2011 [57], respectively. Phytic acid can be obtained from cereal grains, beans, and oil seeds. Laufer's group reported the preparation, via layer-by-layer (LbL) assembly, of chitosan-montmorillonite flame retardant nanocoatings applied to polyurethane foams and poly(lactic acid) films [52] and of chitosan-phytic acid intumescent and flame-retardant nanocoatings deposited onto cotton fiber [53]. According to the group, the latter application resulted in "the first completely renewable intumescent LbL assembly".

In the same year, Carosio's group also utilized the LbL assembly technique, depositing nanocoatings comprised of ammonium polyphosphate (APP) in combination with **chitosan** and/or silica nanoparticles onto polyester-cotton blends [54,55]. The partly renewable APP-chitosan coating indeed provided intumescence, coherent charring, and overall enhancement of the system's fire retardant properties.

Still in 2012, Tondi et al [58] reported the use of tannin-based solutions as preservatives impregnated into wood specimens. The **tannins** significantly improved the wood's fire resistance in terms of ignition time, self-extinguishing time, and weight loss during combustion. It was also demonstrated that the properties (especially afterglow time) could be further improved by adding boric or phosphoric acid.

In 2013, Alongi et al. [59] treated cotton fabrics with **DNA** in order to improve their flammability properties. Using 10 wt% and 19 wt% of DNA, they were able to achieve self-extinguishing behavior upon application of a methane flame and under cone-calorimetry tests, respectively. They observed that the additive produced char and released inert gases, acting like an intumescent system.

In the same year, Alongi and coworkers [60] also used the LbL technique to assemble layers of **DNA** and **chitosan** onto cotton. The FR coating successfully self-extinguished the cotton during horizontal flammability tests, increased its LOI, and reduced its heat release rate by 40%.

In 2014, Carosio, Alongi, and coworkers [61] published a review on their recent results utilizing biomacromolecules, such as **proteins** and **DNA**, as low-environmental-impact FRs for selected fabrics, such as cotton, polyester, and their blends. They also mentioned that biomacromolecules have been recently investigated as FR additives for ethylene vinyl-acetate copolymers and foamed polyurethane substrates.

In the same year, Lang [62] successfully produced aerogels based on sodium montmorillonite clay and epoxy with the addition of **tannic acid** as an FR. The flammability properties of the aerogels were improved by the addition of tannic acid.

Still in 2014, Wang et al. [63] synthesized poly(lactic acid) (PLA) foams with a phosphorus-containing FR and starch as a natural charring agent. The P-containing FR improved the polymer's flammability characteristics, but the addition of **starch** further improved its properties.

In 2015, Prieur et al. [27] were the second group to use **lignin** as an FR in ABS, successfully enhancing its flame retardance. They went on to produce phosphorylated lignin by grafting phosphorus onto the lignin, further improving the FR effect of the additive. They found that the phosphorylated lignin protects the polymer by reacting with ABS during thermal decomposition and catalyzing the formation of a cohesive char layer.

In the same year, Howell and Daniel [64] utilized the renewable compounds **isosorbide** (obtained from starch) and **10-undecenoic acid** (derived from castor oil) to prepare phosphorus esters. They showed that, upon thermal degradation (around 250–350 °C), the esters generate much char and liberate phosphorous acids, which are known to be good crosslinking agents and catalytic FRs. The authors then conclude that these mostly renewable phosphate esters have the potential to serve as effective solid-phase FRs for polymers, liberating phosphorous acid and producing char if the material is exposed to a large amount of heat.

Still in 2015, Costes et al. [65] investigated the use of **metallic phytates** as bio-sourced P-containing FR additives for PLA. Starting from nature-derived sodium phytate, they produced aluminum, iron, and lanthanum phytates. They then applied the metallic phytates independently and in combination with native sodium phytate to PLA. The best results were achieved by utilizing aluminum phytate together with sodium phytate; the former was responsible for the significant FR

effect, and the latter was required to maintain thermal stability during processing. With this formulation, peak heat release rate was significantly decreased, and a V-2 UL 94 rating was achieved.

In the same year, Wang et al. [66] used **cardanol** as a flame retardant to improve the thermal properties of epoxy resins. Firstly, cardanol was combined with 1,4-butane sultone (BS) to produce cardanol-BS. Secondly, cardanol-BS was used to prepare a modified layered double hydroxide (m-LDH). Finally, the m-LDH was incorporated into an epoxy resin. Compared to the epoxy resins prepared with pristine (unmodified) layered double hydroxide (LDH), the epoxy resins prepared with the cardanol-BS-modified LDH presented greatly enhanced fire resistance, with significant improvements in LOI, UL 94, and combustion properties. This comparison clearly demonstrated the important role of cardanol in imparting flame retardance to the system being studied.

In 2016, Schiraldi and coworkers reported the use of **alginate** both as an intrinsically flame-retardant aerogel [67] and in a flame-retardant coating to polyurethane foam [68]. In the former, alginate aerogels were prepared with and without the addition of inorganic nanofillers, and with and without the application of a post-cross-linking step with Ca^{2+}. The neat alginate aerogels presented excellent flame-retardant characteristics, with an LOI of 47.7 and a V-0 UL 94 rating. The addition of nanofillers and/or the crosslinking step further improved the aerogels' flame-retardant properties, achieving an LOI > 60, completely preventing flame during combustion tests, and promoting the formation of a large quantity of residual char. Once again, the potential use of alginate as an FR compound for polymers was suggested. The group demonstrated this in the latter paper, in which alginate/clay aerogels were used as coatings on polyurethane foams. The flame retardance of the synthetic foams was greatly improved by the application of the partly renewable coating.

In the same year, Pokorski and coworkers [69] utilized **DNA** as an FR additive for low-density polyethylene (LDPE). They compared the performance of DNA to that of melamine polyphosphate (MPP), a standard intumescent FR additive for plastics. They found that the biomacromolecule has a much higher compatibility with the LDPE matrix and performs better than MPP in horizontal burn tests, greatly reducing the burn distances. The authors state that this result

potentially expands the use of DNA as an FR for commodity plastics, as it had previously been used only in textiles and specialty polymers.

Still in 2016, Liu et al. [70] used functionalized **lignin** (F-lignin) as an FR agent in wood-plastic composites (WPC). The F-lignin was produced by grafting phosphorus, nitrogen, and copper elements onto lignin. This bio-based FR additive greatly enhanced the flame retardance of WPCs, even more so than the unmodified lignin. The presence of P, N, and Cu^{2+} catalyzed char formation, continuously producing a compact char that was the main responsible for the improved flame retardance properties.

In the same year, Kiratitanavit et al. [71] utilized **tannic acid** as an intumescent, char-forming additive for nylon-6 by melt blending the two components. The nylon's heat release capacity and total heat release were significantly reduced.

In 2017, Deans [18] successfully flame retarded different polyolefins (namely LDPE, high-density polyethylene (HDPE), PP, and PS) using mainly nature-derived additives. Interestingly, different FR systems were required for each polymer. For LDPE, a V-0 UL 94 rating was achieved when **tannic acid** (as a charring agent) was used in combination with **fish gelatin** (as a crosslinking enhancer, blowing agent, and anti-drip agent), magnesium hydroxide, or melamine cyanurate. The latter two are not bio-based but are also not toxic. It is important to note that other secondary additives, such as an antioxidant (to protect tannic acid during processing), a compatibilizer, and an anti-foaming agent were also required. For HDPE, a V-0 rating was achieved by using fish gelatin (as a char former and blowing agent) in combination with melamine (as a blowing agent), along with a nucleating aid (a sorbitol derivative). PP was successfully flame retarded by using fish gelatin in combination with the nucleating aid dibenzylidene sorbitol. The flammability properties of PS were improved by using either fish gelatin with melamine or tannic acid with magnesium hydroxide or melamine. PS was able to be further flame retarded in order to withstand larger fires through the incorporation of tannic acid in combination with Safire™ 400 (melamine poly(zinc phosphate)) or Safire™ 600 (melamine poly(magnesium phosphate)). **Lecithin** was also shown to have a potential as an FR additive for polyolefins. In summary, different polyolefins were effectively flame retarded by using a combination of nature-derived char-forming FRs (tannic acid, fish gelatin, or potentially lecithin) in

combination with non- or low-toxicity commercial FRs (such as magnesium hydroxide, melamine, melamine cyanurate, or a melamine poly(metallic phosphate)), especially those containing nitrogen or nitrogen and phosphorus.

In the same year, Costes et al. [14] published a comprehensive review on the potential use of many bio-based compounds (biomass) as flame retardants. The compounds described by the authors include: saccharide-based products, such as **cellulose**, **hemicellulose**, **starch**, **cyclodextrin**, **isosorbide**, **chitosan**, **tea saponin**, and **tartaric acid**; bio-based aromatic products, such as **lignin**, **phloroglucinol**, **levulinic acid**, and **cardanol**; **DNA**; proteins, such as **casein**, **hydrophobins**, and **whey protein**; **phytic acid**; and vegetable oils, such as **soybean oil** and **castor oil**. The principle mechanism by which these compounds can improve the flame retardance of polymers is inducing char formation, since they have an outstanding char-forming ability under certain circumstances. Some can also be used as a part of intumescent systems, normally as the carbonizing agent. It is important to note, however, that these compounds often have to be combined with other FR agents (such as N- and/or P-containing FRs) and/or chemically modified (e.g. phosphorylated) in order to be truly effective as flame retardants.

Still in 2017, Shah et al. [41] published a review on the fire retardance of natural fiber and bio-based composites. Among the possible flame-retardant additives that can be used on polymers and polymer-matrix composites, the author described a number of natural FR additives in use, such as: **chitosan**, **oyster shell powder (OSP)**, **egg shells**, **lignin**, **biochar** (defined as “any charcoal that is composed from biomass”), **human hair**, and **DNA**. Although publications on the use of OSP, egg shells, biochar, and human hair are very limited, they are worth being mentioned as possible bio-sourced FRs.

Also in 2017 [72], Costes et al. used **phytic acid** in combination with **lignin** to improve the thermal and flammability properties of PLA. The pair worked synergistically, with phytic acid improving lignin’s dispersion in the matrix and lignin reducing the composite’s hygroscopy. Peak heat release rates (PHRR) in cone calorimetry were reduced by up to 44%, V-2 classifications were obtained in UL 94 tests, and ductility was even improved for one formulation.

In the same year, Schiraldi and co-workers [73] incorporated bio-based gelatins (**fish gelatin** and **porcine gelatin**) into poly(vinyl alcohol) (PVA)/montmorillonite clay (MMT) aerogels to improve their flame retardance,

thermal stability, and strength. The aerogels' self-extinguishing times were cut in half in combustion tests, LOI values increased, and PHRR from cone-calorimetry tests decreased with the addition of the gelatins. The compressive moduli of the aerogels also increased greatly, reaching improvements of almost 200%.

Moustafa et al. [34] used ground **seashell** waste to enhance the thermal, flammability, and mechanical properties of ABS in 2017. Low amounts of the filler were able to increase the polymer's storage modulus, glass transition temperature, and tensile strength. Enhanced thermal stability was observed, and HRRs were decreased during combustion.

In 2018, Xia et al. [74] chemically modified **tannic acid** to produce tannic acid terephthalate (TAT), which is a crosslinked network of tannic acid molecules. TAT was used as a coating on nylon-66 fabric, resulting in quick self-extinguishing behavior and reduced burn lengths in vertical burn tests. Enhanced char formation was responsible for the improved flame retardance.

In the same year, Wang and co-workers [75] synthesized a bio-based nitrogen- and phosphorus-containing FR from **phytic acid** and 1,6-hexanediamine (HDA, which can be obtained from bio-based **5-hydroxymethylfurfural**, despite being conventionally produced from petroleum). The synthesized FR (PA-HDA) was used in a toughened PLA composite, achieving a UL 94 V-0 rating and increasing its LOI value with only a 5-wt% loading. The composite's crystallinity was increases and its mechanical performance was not compromised with the employment of the FR agent.

Still in 2018, Sonnier et al. [15] published a comprehensive review on bio-based flame retardant polymers, in which they discussed both the use of conventional FRs in bio-based polymers and the use of bio-based FRs in polymers. They presented detailed discussions of bio-based FRs, or raw materials used in the production of FRs, by grouping them into different categories: carbohydrates (**cellulose**, **starch**, **cyclodextrin**, **isosorbide**, **itaconic acid**, **tartaric acid**, **phytic acid**, **chitosan**, and **alginates**); proteins (**DNA**); lipids (**undecylenic acid** and **cardanol**); and phenolic compounds (**lignin** and **tannins**).

In the same year, Laoutid et al. [76] synthesized a novel bio-based flame retardant composed of **phytic acid** and **tannic acid** grafted with polyethyleneimine (Phyt/PEI-TA) and used it to improve the thermal and flammability properties of PLA. The use of 20 wt% of the additive increased the polymer's char yield and

decreased the PHRR by 36% in cone calorimetry. The main mode-of-action of the FR was identified as a condensed phase action, promoting the formation of char.

Cheng, DeGracia, and Schiraldi [77,78] used PVA, **tannic acid**, and sodium hydroxide to prepare low-flammability, mechanically strong, environmentally friendly aerogels in the same year. PHRR and total heat release (THR), as measured by cone calorimetry, were reduced by 69% and 54%, respectively, compared to PVA aerogels. The aerogel's compressive modulus was increased by almost 20 times, which the authors attributed to a strong interaction between tannic acid and PVA through hydrogen bonding.

In 2019, Yang et al. [79] synthesized a novel flame retardant composed of **phytic acid** and tromethamol and employed it in PLA at a 3-wt% loading level. LOI values were increased, V-0 ratings were achieved in UL 94 tests, and mechanical properties were not compromised.

Cayla et al. [80], in the same year, used **lignin** alone and in combination with APP as a flame retardant in polyamide 11. The use of lignin delayed the polymer's thermal degradation and decreased the PHRR by 66% through a charring effect. When lignin and APP were used together, the fire reaction was further improved (although the two components did not present synergy), and intumescence was obtained for specific lignin/APP ratios.

DeGracia [81] reported the use of **porcine gelatin** in combination with melamine poly(magnesium phosphate) and polytetrafluoroethylene (PTFE) to flame retard PBT in 2019. The author also proposed a mechanism of flame retardation of porcine gelatin in the polymer.

In the same year, Gao et al. synthesized a new bio-based flame retardant based on **phytic acid** and piperazine and employed it in PP [82]. The polymer's LOI value increased by 39%, UL 94 V-0 ratings were obtained, and PHRR, THR, and smoke release were reduced in cone calorimetry tests. The authors claimed that the flame-retarding efficiency of the bio-based additive was superior to that of traditional intumescent FR systems that contain APP or pentaerythritol.

Hobbs [16] published a comprehensive review, still in 2019, on recent advances in the use of bio-based FR additives in synthetic polymers. The author described the main characteristics and recent uses of bio-derived FRs such as **tannic acid** and related materials, **phytic acid** and its salts, **isosorbide**, **diphenolic acid**, **DNA**, **lignin**, and **β-cyclodextrin**.

In 2020, Song and co-workers [83] published a review on the use of lignin-derived compounds as bio-based FRs for polymeric materials. They focused on the flame retardance effects of pristine **lignin** and lignin chemically modified with nitrogen and/or phosphorus, as well as on the synergistic interactions between lignin-based FRs and other existing FR additives. The uses of lignin-derived FRs in a variety of polymeric matrices were discussed, and future perspectives and opportunities were presented.

Also in 2020, Watson and Schiraldi [17] published a complete review on the use of biomolecules as FR additives for polymers. The authors summarized the known bio-sourced, environmentally safe, thermo-oxidative, and flame-retardant (BEST-FR) additives and reviewed their effects on the flame retardance and, when available, mechanical properties of polymers. The FR additives discussed were grouped into four categories: proteins (**wool**, **feathers**, **eggshell**, **whey**, **casein** and **hydrophobins**, **gelatin**, **zein**, and **gluten**); amino acids and oils (**phenylalanine**, **DNA**, and **vegetable oil derivatives**); carbohydrates (**cellulosic fibers**, **lignin**, **alginate**, **starches**, and **cyclodextrin**); and polyphenols/polyhydroxyphenols (antioxidants), including **tannins and extracts** and **polydopamine**.

From the examples cited in this section, one can perceive that there are numerous possibilities when it comes to using bio-sourced compounds as FR additives for polymers, either by themselves or in combination with non-toxic commercial FRs. These nature-derived compounds come from sources that can be abundantly found in nature, and they are renewable, often cost-effective, non-toxic, safe, and environmentally friendly. Through scientific research, the right combination of these compounds has been and can potentially be found to flame retard many different polymers, potentially leading to their commercial use as flame retardants for polymers in the near future.

1.2.5. Acrylonitrile-Butadiene-Styrene (ABS)

Acrylonitrile-butadiene-styrene (ABS) is a widely used thermoplastic copolymer. Because of its good mechanical properties, chemical resistance, ease of processing, and recyclability, it is used in a variety of applications, especially in the electronics and automotive industries [24–27]. It is one of the principal materials

used in housings and cabinets for electrical and electronic equipment and in a variety of home appliances and tools [24]. All of these applications require components that do not easily catch on fire, since they deal with high electrical currents and/or high temperatures and are all around people in their daily lives.

Despite its advantages, ABS is a very flammable polymer. For this reason, many commercial flame retardants are utilized in this plastic in order to reduce its combustibility and increase its applicability and safety. The FR compounds do reduce ABS's flammability quite effectively; the problem is that the vast majority of FRs used in this material are halogen-based (especially brominated) systems [28]. The main brominated FRs used in ABS are octabromodiphenyl oxide (OBDPO), decabromodiphenyl oxide (DBDPO) (both in the class of PBDEs), tribromophenoxy ethane (TBPE), and tetrabromobisphenol-A (TBBPA) [24]. The toxicity and environmental issues involved with these compounds are many, as has been described above.

These environmental issues have led to the necessity of developing alternative, non-toxic flame retardants for ABS. In the past two decades, there has been some work in the development of non-halogenated FRs, mainly phosphorus-based FRs, for use in ABS. Some research has also been performed utilizing nanofillers and/or intumescent systems. In 2007, Ma et al. [29] synthesized a new phosphorus–nitrogen intumescent FR, poly(4,4-diaminodiphenyl methane spirocyclic pentaerythritol bisphosphonate) (PDSPB), which reduced ABS's flammability and increased its thermal stability mainly due to the formation of a cohesive, intumescent char. In the following year, the same researchers grafted PDSPB onto carbon nanotubes to create an even more effective FR [30]. In 2012, Ge et al. [20] applied expandable graphite (EG) in combination with APP, leading to a new intumescent system. The synergy between EG and APP improved ABS's flammability performance, achieving a UL 94 V-0 rating. Once again, the main responsible mechanism for the improved flame retardance was the formation of a compact, intumescent char layer.

Nevertheless, even with these developments, there is still a limited number of non-halogenated FR systems that have shown success in ABS, and almost none are available commercially. The compounds listed above are also not nature-derived; there is a great benefit in using nature-derived products: they are naturally abundant, often easily accessible, renewable, often low-cost, non-toxic, and environmentally

friendly. Furthermore, many bio-based compounds are readily available, often in excess, as by-products of industry processes (e.g. lignin from the papermaking industry [26] and cardanol from the cashew nut industry [49]), so it is important to find new applications for them in order to prevent them from being wasted or incinerated. As a result, there is a large need for the development of bio-based, environmentally friendly FRs for use in ABS.

There have been very few reports on the successful usage of bio-based FRs in ABS to date. Tributsch & Fiechter [32] blended tannins and tannin-containing tree barks with ABS in 2008. They were able to increase the polymer's char yield and the LOI index, demonstrating the potential use of tannin as an FR. They did not, however, perform a comprehensive study on the composites' flammability and other properties. Lignin was utilized to flame retard ABS by Song et al. (2011) [33] and by Prieur et al. (2015) [27]. The former added 20 wt% of lignin together with a compatibilizing agent, achieving a 32% reduction in PHRR from cone calorimetry experiments; the latter incorporated 30 wt% of a phosphorylated lignin, obtaining a 58% reduction in PHRR. Both systems relied on char formation to enhance the flame retardance. These studies show that lignin (and potentially other char formers) is a promising candidate for flame retarding ABS. When investigating the composites' mechanical properties, however, Song et al. found that a 5-wt% lignin content marginally increased the tensile strength and Young's modulus, but this is far lower than the concentration required to achieve improved flammability results. The required concentration (20 wt%) causes large reductions in tensile strength, ductility, and impact strength (33%, 50%, and 87%, respectively). The use of a compatibilizer can somewhat lessen the tensile-strength and ductility reductions, but it is detrimental to the Young's modulus and flexural strength. In other words, the required loading of lignin to achieve significant improvements in ABS's flammability properties is detrimental to the material's mechanical properties, limiting its benefits. Another drawback of the systems investigated by the authors is that the time to ignition was reduced by the addition of lignin. Furthermore, the phosphorylation of lignin, proposed by Prieur's group (who did not report effects on the mechanical properties), although an interesting approach, is less commercially interesting than the use of a nature-derived product as-is, since it would add an additional step (thus, additional cost) to the manufacturing process. Moustafa et al. [34] used ground seashell waste to enhance the thermal and

flammability properties of ABS in 2017; the ductility of the polymer, however, was compromised.

In conclusion, there is a high need for the development of bio-based FR systems for ABS that are fire-resistant, cost-effective, commercially viable, and non-detrimental to the material's other properties. The strong importance and presence of halogenated flame retardant ABS products currently in the market (especially in the electronics industry), allied to the increasing global environmental awareness, creates a commercial and environmental demand for these systems, giving reason to believe that a successful, environmentally friendly, commercially viable, flame-retardant ABS product based on nature-derived additives and having good mechanical properties is very much needed and has a high potential of being absorbed into the market. Advancing the current scientific knowledge on the flame-retardation mechanisms and effects of bio-based FR systems in ABS is fundamental in order to progress towards effective, commercially viable, environmentally friendly, and low-flammability ABS products that can substitute halogenated-based ABS systems in the near future.

2
Experimental

2.1.
Materials

Acrylonitrile-butadiene-styrene (ABS; Terluran® GP-35, Ineos Styrolution), with a density of 1.040 g/cm^3 and a melt flow index of 3.1 g/10 min (200 °C, 5.0 kg), was used as received. Polystyrene-*block*-poly(ethylene-*ran*-butylene)-*block*-polystyrene-*graft*-maleic anhydride (SEBS-g-MA; Sigma-Aldrich), with a maleic anhydride content of approximately 2 wt%, a density of 0.91 g/cm^3, and a melt flow index of 21 g/10 min (230 °C, 5.0 kg), and a styrene-maleic anhydride random copolymer (SMA; XIRAN® SZ08250, Polyscope Polymers), with a maleic anhydride content of 8 wt% and a density of 1.080 g/cm^3, were used as received as compatibilizers. A commercial brominated flame-retardant grade of ABS (Br-ABS; LG Chemical AF312A, Polymer Technology & Services) containing tetrabromobisphenol-A and antimony(III) oxide, with a density of 1.19 g/cm^3 and a melt flow index of 55 g/10 min (220 °C, 10.0 kg), was used as received as a positive control. Powdered flame-retardant additives were used as received: tannic acid (TA; molecular weight 1701.23 g/mol, Acros Organics), gelatin from cold water fish skin (FG; Sigma-Aldrich), phytic acid sodium salt hydrate from rice (PA; Na content ≥ 5 mol/mol, Sigma-Aldrich), DNA from herring sperm (D; Sigma-Aldrich), magnesium hydroxide (MH; Vertex® 100 SF, J.M. Huber Corporation), alumina trihydrate (ATH; Micral® 632, J.M. Huber Corporation), melamine poly(magnesium phosphate) (S6; Safire™ 600, J.M. Huber Corporation), melamine (ME; Sigma-Aldrich), and ammonium polyphosphate (APP; Exolit® AP 422, crystal phase II, Clariant). Pentaerythritol tetrakis(3-(3,5-di-tert-butyl-4-hydroxyphenyl)propionate) (Irg; Irganox® 1010, Ciba Geigy) was used as received as an antioxidant. Table 2.1 lists all of the materials used and their respective functions.

Table 2.1

List of materials used in the present study, as well as their functions

	Category	Materials	
Matrix	Polymer	**Acrylonitrile-butadiene-styrene** (ABS) *Commercial injection-molding grade*	
Matrix	Compatibilizer	**SEBS-g-MA** Polystyrene-*block*-poly(ethylene-*ran*-butylene)-*block*-polystyrene-*graft*-maleic anhydride **OR** **SMA** Styrene-maleic anhydride random copolymer	
Additives	Flame Retardants	Nature-derived FRs	**Tannic Acid** (TA) *tree bark, grape skin*
			Fish Gelatin (FG) *fish skin*
			Phytic Acid Sodium Salt (PA) *grains*
			DNA (D) *fish*
		Commercial low-toxicity FRs	**Magnesium Hydroxide** (MH)
			Alumina Trihydrate (ATH)
			Safire™ 600 (S6) Melamine Poly(magnesium phosphate)
			Melamine (ME)
			Ammonium Polyphosphate (APP)
Additives	Antioxidant	**Irganox® 1010** (Irg) – *Only when TA is used* Pentaerythritol tetrakis(3-(3,5-di-tert-butyl-4-hydroxyphenyl)propionate)	
	Positive Control	**Brominated ABS** (Br-ABS) *Commercial halogenated flame-retardant ABS, containing TBBPA + Sb_2O_3*	

2.2. Methodology and Terminology

Figure 2.1 portrays the experimental methodology used in the present research, which was organized into two phases. Phase 1, the "Screening Phase", had the objective of evaluating the effects of 8 different bio-based or low-toxicity FRs and their combinations on the flammability of ABS. Design of Experiments techniques were employed in order to plan the screening experiment, which included the production of a large number of filled ABS samples through batch mixing followed by compression molding and their analysis through vertical burn testing and microscale combustion calorimetry (MCC).

The most promising samples from the Screening Phase were taken to Phase 2, the "Detailed Analysis and Mechanistic Study Phase". The objectives of Phase 2 were to better understand the flammability and mechanical behaviors of the most promising compositions and to elucidate the flame-retardation mechanisms of some of the FR agents. Scaled-up samples were produced through extrusion followed by either compression molding or injection molding and analyzed through cone calorimetry, thermogravimetric analysis (TGA), pyrolysis-gas chromatography-mass spectrometry (Py-GC-MS), tensile testing, and Izod impact testing.

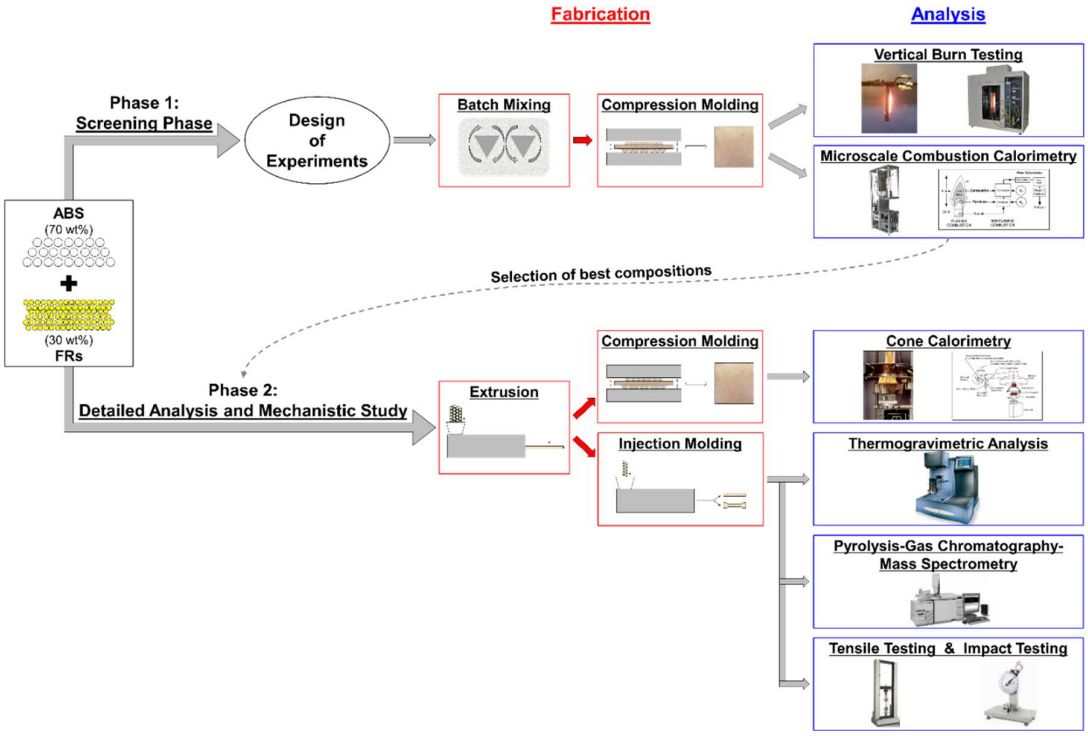

Figure 2.1. Overview of the experimental methodology used in the present study.

It can be discussed whether the most appropriate term to be used for the flame-retarded ABS samples fabricated in the present study is *composites*, *blends*, *filled polymers*, or another expression. A *composite* can be defined as a "multicomponent material comprising multiple different (nongaseous) phase domains in which at least one type of phase domain is a continuous phase" [84], which is an appropriate description of the FR ABS samples. The notion that the resulting material has new, desirable properties, combining the best characteristics of each of the starting materials, is often included in the description of a *composite*

material; this concept also mostly applies to the melt-processed samples fabricated in this project, which aim to combine the polymer's light weight, ease of processability, specific strength, and toughness with the additives' improved flammability properties. A *blend* can be defined as a "macroscopically homogeneous mixture of two or more different species of polymer" [84]; most of the additives used herein cannot be considered polymers nor macromolecules (with the possible exceptions of melamine poly(magnesium phosphate), ammonium polyphosphate, DNA, and fish gelatin), so *blend* does not seem to be an appropriate term to describe all of the FR ABS samples. The term *filled polymer* often applies to a polymer filled with particulate additives that have the objective of improving properties other than mechanical ones; this phrase, which has a similar meaning as the expression *particle-filled polymeric composite*, seems to be appropriate in most cases in this study. For simplicity, the term *composite* was chosen and will be used throughout this study to refer to the ABS samples containing flame-retarded additives.

2.3. Sample Preparation

2.3.1. Drying of Starting Materials

Materials were dried prior to being melt processed. TA, PA, MH, ATH, and ME were dried at 110 °C under vacuum for approximately 24 h. FG, S6, Irg, SEBS-g-MA, and SMA were dried at 60 °C under vacuum for approximately 24 h. ABS and Br-ABS were dried at 80 °C in air for 2 to 4 h. D and APP were not dried. Dried materials were stored in a desiccator until being melt processed.

2.3.2. Melt Processing for Phase 1 (Screening Phase)

During the Screening Phase, composite samples for vertical burn testing and MCC were prepared by batch mixing followed by compression molding. Control samples were also submitted to the same processing method for consistency. For

each processing step (i.e. batch mixing and compression molding), samples were generally produced in a random order.

2.3.2.1. Batch Mixing

Dried raw materials were weighed in the appropriate proportions for each sample (according to Table 3.3 and Table 3.4 in Chapter 3) in batches of 60 g. For each sample, the FR powders were manually mixed amongst themselves, the pellets (ABS and SEBS-g-MA or SMA compatibilizer) were manually mixed amongst themselves, and then pellets and powders were manually mixed together. Manual mixing was performed by stirring, kneading, and shaking the components within a plastic bag. The solid mixture was then processed in a Haake Polylab OS Rheodrive 7 batch mixer (Thermo Fisher Scientific, Hillsboro OR, USA) equipped with roller rotors at 160 °C. The motor speed was set at 20 rpm during feeding (which typically took 30–60 s) and for 1 additional minute, then at 60 rpm for 4 minutes, generating a total residence time of 5.5 to 6 minutes. The material was immediately cut into small pieces after being removed from the equipment, while it was still soft.

2.3.2.2. Phase 1 Compression Molding

Batch-mixed materials were then compression molded into thin plates (127 mm x 127 mm x 1.6 mm) using a Carver Model C hydraulic press (Carver Inc., Wabash IN, USA). Samples were placed between two sheets of Teflon™-coated fiberglass fabric, which were placed between two metallic plates. This assembly was inserted into the equipment and pressed at 160 °C for 5 minutes under the following pressure program: 2.5 minutes under a residual amount of pressure (to allow the material to soften), and 2.5 minutes under a cyclic loading pattern (to avoid formation of air bubbles), by which the load was set to 8 metric tons, allowed to decrease naturally to ~6 metric tons, released, immediately reapplied at 8 metric tons, allowed to decrease to ~6.5 metric tons, released, immediately reapplied at 8 metric tons, allowed to decrease for the remainder of the time period, and released. The assembly was then cooled for about 2.5 to 4 minutes between two metallic

plates kept cold by running water flowing through an internal hose system. The samples were then removed from the mold.

2.3.2.3.
Sample Cutting for Vertical Burn Testing

For vertical burn testing, rectangular bars (127 mm x 12.7 mm x 1.6 mm) were cut out from the Phase 1 compression-molded plates using a box-cutter. To perform the cuts, a metallic ruler was initially used to guide the box-cutter lightly along the surface of the sample in a straight line, creating a light groove. After a few iterations, when the groove was deep enough to guide the blade on its own, the ruler was removed and the box-cutter was passed repeatedly along the line with gradually increasing pressure. When the groove was deep enough, the sample was gently bent back and forth using both hands until it broke along the grooved line, yielding a rectangular bar. The procedure was repeated up to 9 times per compression-molded plate, yielding up to 10 rectangular-bar specimens for each composition.

2.3.3.
Melt Processing for Phase 2 (Detailed Analysis and Mechanistic Study Phase)

During Phase 2, composite samples were prepared by extrusion followed by either compression molding (for cone calorimetry) or injection molding (for TGA, Py-GC-MS, and mechanical testing). Control samples were also submitted to the same processing method for consistency.

2.3.3.1.
Extrusion

Dried raw materials were weighed in the appropriate proportions for each sample (according to Table 3.3 and Table 3.4 in Chapter 3) in batches of 2 kg. For each sample, the powders were manually mixed amongst themselves in a plastic bag, and then the pellets (ABS and SEBS-g-MA compatibilizer) were added to the

bag and manually mixed with the powders. Manual mixing was performed by stirring, kneading, and shaking the components within the bag. The solid mixture was then fed into a Prism Eurolab 16 co-rotating twin screw extruder (Thermo Fisher Scientific, Hillsboro OR, USA) with 16-mm-diameter screws and a length-to-diameter (L/D) ratio of 40 through a feeder at a feeding rate of about 30–40 g/min. Screw speed was 200 rpm, and the temperature profile was set at 170-180-190-210-220-220-220-220-220-220 °C (equally spaced heating zones from feeder to die). The extrudate was immediately cooled in a water bath at room temperature and cut into pellets in a Thermo Scientific pelletizer (Thermo Fisher Scientific, Hillsboro OR, USA). The pellets were then dried at 80 °C under vacuum for approximately 24 h.

2.3.3.2.
Phase 2 Compression Molding

Dried extruded materials were compression molded using a Carver Model C hydraulic press into square plates (100 mm x 100 mm) with an average thickness of 3.3 mm. Samples were placed between two sheets of Teflon™-coated fiberglass fabric, which were placed between two metallic plates. This assembly was inserted into the equipment and pressed at 200 °C. For the first 2.5 minutes, the samples were under a residual amount of pressure to allow the material to soften. Next, a cyclic loading pattern was used to avoid formation of air bubbles, by which the following pattern was performed a total of 3 times: the load was set to 8 metric tons, allowed to decrease naturally to 6 metric tons, slowly released, and left at 0 metric tons for 30 s. After the third load release (without waiting 30 s at 0 metric tons), the assembly was removed from the press and cooled for approximately 5 minutes between two metallic plates kept cold by running water flowing through an internal hose system. The samples were then removed from the mold.

2.3.3.3.
Injection Molding

Dried extruded materials were injection molded in a BOY 22-S injection-molding machine (BOY Machines, Exton PA, USA) equipped with a two-cavity

family mold that included an ASTM Type IV tensile dog bone and an ASTM flexural bar. Screw speed was 150 rpm; barrel/nozzle temperatures were set at 220/220 °C for pure ABS, 185/182 °C for Br-ABS and TA, TA-FG, and PA composites, and 175/175 °C for PA-TA composites; mold temperature was set at 25 °C (60 °C for pure ABS); injection, holding, and back pressures were respectively 140, 50, and 15 bar; mold clamping pressure was approximately 210 bar; pressure holding time was 10 s; and cooling time within the mold was an additional 10 s (20 s for pure ABS).

2.4. Characterization

2.4.1. Vertical Burn Testing

UL 94-inspired vertical burn tests were performed on rectangular bars (127 mm x 12.7 mm x 1.6 mm) cut out from the Phase 1 compression-molded plates during the Screening Phase. Tests were performed in a fume hood with the sash closed, in a fume hood with the sash open, and in an SL-S29 UL 94 Horizontal-Vertical Flame Chamber (Skyline Instruments, Guangdong, China). In all three configurations, the specimen was clamped in vertical position using a metal clamp, and a blue flame with a height of 20 mm was applied to the lower extremity of the sample for 10 s. The base of the flame was positioned 10 mm below the sample, in such a way that there was a 10-mm overlap between the flame and the sample. After the 10-s application period, the flame was removed. If the specimen self-extinguished, the flame was reapplied for an additional 10 s. Up to 3 specimens were tested for each composition in each testing configuration, and the experiments were performed in a random order for each configuration. Each sample's UL 94 classification was recorded; the existing classifications are listed in Table 2.2.

Table 2.2
UL 94 classifications

Classification	Description
Not rated	Sample burns to the clamp or self-extinguishes in more than 30 s for at least one of the flame applications
V-2	Burning stops within 30 s for both flame applications; drips of flaming particles are allowed
V-1	Burning stops within 30 s for both flame applications; drips of particles are allowed, as long as they are not inflamed
V-0	Burning stops within 10 s for both flame applications; drips of particles are allowed, as long as they are not inflamed

2.4.2. Microscale Combustion Calorimetry

Microscale combustion calorimetry (MCC) was performed on a Fire Testing Technology FAA Micro Calorimeter (Fire Testing Technology, East Grinstead, UK) during the Screening Phase. Specimens weighing 5–10 mg were cut out from the Phase 1 compression-molded plates and placed in a ceramic cup. Samples were heated in the pyrolyzer from 150 to 700 °C at 1 °C/s under nitrogen, and volatiles were swept into the combustor, which was kept at 900 °C with a N_2 flow rate of 80 cm^3/min and an O_2 flow rate of 20 cm^3/min. Heat release rate (HRR) per unit mass was measured as a function of temperature based on the oxygen consumption, and peak heat release rate (PHRR; highest point on the HRR curve) and total heat release (THR; time-integral of the HRR curve) were determined from the curves. Char yield was determined by weighing the samples before and after the experiment, and heat of complete combustion of the volatiles (HCC) was calculated by dividing the THR by one minus the char yield. Each composition was tested at least 3 times, and the experiments were performed in a random order. Melt-processed pure ABS (sample 1.1) was tested approximately 30 times (at least once on almost every test day) to ensure repeatability of results and to detect possible drifts. As an additional control, ABS/MA (sample 1.2) was tested at least 8 times.

The FR agents were tested individually as powders after being dried according to subsection *Drying*. The masses of the powdered samples varied

between 5 and 20 mg, depending on each compound's expected oxygen consumption. At least 2 repetitions of each FR were performed.

2.4.3.
Cone Calorimetry

Cone calorimetry was performed on a BECC cone calorimeter (INELTEC, Barcelona, Spain) during the Detailed Analysis and Mechanistic Study Phase; ISO 5660 standard procedure was followed, with the exception that each composition was tested twice. The Phase 2 compression-molded specimens (100 mm x 100 mm, average thickness of 3.3 mm) were irradiated with a constant heat flux of 50 kW/m2, using a constant distance of 25 mm between the electrical resistance and the specimens. There was no grid on top of the specimens. Heat release rate (HRR) per unit surface area and sample mass were measured as a function of time, and parameters such as time to ignition (TTI; time at which the HRR curve departs from 0), peak heat release rate (PHRR; highest point on the HRR curve), total heat release (THR; time-integral of the HRR curve), and char yield (final-mass to initial-mass ratio) were determined from the curves. Effective heat of combustion of the volatiles (EHC) was calculated by dividing the THR by one minus the char yield, and combustion efficiency was calculated by dividing the EHC by the MCC-obtained HCC. Each composition was tested twice.

2.4.4.
Thermogravimetric Analysis

Thermogravimetric analysis (TGA) of ABS and its composites was performed on a TGA Q50 thermogravimetric analyzer (TA Instruments, New Castle DE, USA). Specimens weighing 15–20 mg were cut out from the Phase 2 injection-molded flexural bars and placed in a platinum pan, which was inserted into the furnace. Samples were heated from 50 to 600 °C at 10 °C/min under nitrogen. The N2 flow rate was 60 mL/min for the sample purge and 40 mL/min for the balance purge. Sample mass and mass-loss rate were measured as a function of temperature, yielding TGA and differential-thermogravimetry (dTG) curves, respectively. Each composition was tested once.

The FR agents (tannic acid, phytic acid sodium salt, fish gelatin, and ammonium polyphosphate) were tested individually as powders on a TGA Q500 thermogravimetric analyzer (TA Instruments, New Castle DE, USA) under the same conditions as ABS and its composites. The temperature range was extended to 700 °C for TA, PA, and FG and to 800 °C for APP. Sample masses of 7–10 mg were used; each compound was tested once.

The initial water content of each sample was estimated by reading the mass loss (vertical-axis value on the TGA curves) corresponding to the inflection point after the first mass-loss event (i.e. corresponding to the local minimum after the first peak in the dTG curves); the temperature corresponding to this point was recorded as the end-of-water-loss temperature. "Water-corrected" TGA and dTG curves were calculated by dividing the raw values by one minus the water content. The temperature at which 10% of the mass was lost (T_{d10}), the temperature at the onset of decomposition (T_{onset}; calculated as the temperature value of the intersection between a line tangent to the TGA curve at the point of maximum mass-loss rate and a line tangent to the TGA curve at the inflection point immediately preceding the main mass-loss event), the temperature at which the mass-loss rate was the highest (T_{dmax}), the peak mass-loss rate (PMLR), and the char yield (mass % reading at the end of the test) were determined from the water-corrected curves.

2.4.5. Pyrolysis-Gas Chromatography-Mass Spectrometry

Pyrolysis-gas chromatography-mass spectrometry (Py-GC-MS) was conducted on an Agilent 5973 inert Gas Chromatograph/Mass Spectrometer (GC/MS; Quantum Analytics, Foster City CA, USA) equipped with an EGA/PY-3030D Multi-Shot Pyrolyzer (Frontier Laboratories Ltd., Koriyama, Japan). Evolved Gas Analysis (EGA) and Heart Cut Analysis (HCA) experiments were performed. A short Ultra ALLOY® UA-DTM deactivated metal capillary column (2.5 m length, 0.15 mm inner diameter, 0.47 mm outer diameter; Frontier Laboratories Ltd., Koriyama, Japan) with a dimethylpolysiloxane stationary phase was used for the EGA measurements, while a long Ultra ALLOY® UA+-5 metal capillary column (30 m length, 0.25 mm inner diameter, 0.47 mm outer diameter, 0.25 μm film thickness; Frontier Laboratories Ltd., Koriyama, Japan) with a 5%

diphenyl-dimethylpolysiloxane stationary phase was used for the HCA measurements.

For the EGA experiments, specimens weighing ~0.2 mg were cut out from the Phase 2 injection-molded flexural bars using a blade and placed in a sample cup. The sample cup was placed into the pyrolyzer, which was preheated at 100 °C. The samples were then heated in the pyrolyzer from 100 to 800 °C at 20 °C/min, and the evolved gas was injected directly into the short capillary column during heating. The interface between the pyrolyzer and the capillary column was maintained at 200 °C, and the column temperature was maintained at 300 °C.

For the HCA experiments, specimens weighing ~0.4 mg were cut out from the Phase 2 injection-molded flexural bars using a blade and placed in a sample cup. The sample cup was placed into the pyrolyzer, which was preheated at 100 °C. Four temperature zones were defined based on the EGA results and were used for all samples: 100 to 220 °C (Zone A), 220 to 370 °C (Zone B), 370 to 400 °C (Zone C), and 400 to 500 °C (Zone D). These temperature ranges correspond to the following time ranges in the EGA curves: 0 to 6 min, 6 to 13.5 min, 13.5 to 15 min, and 15 to 20 min, respectively. The heating process was as follows: (1) the sample was heated from 100 to 220 °C at 40 °C/min (Zone A); (2) the sample was quickly cooled down to 100 °C and maintained at this temperature for 26 min while the gases evolved from Zone A were being processed by the GC/MS; (3) the sample was quickly heated until 220 °C (initial Zone B temperature) and maintained at this temperature for ~2 min; (4) the sample was then heated from 220 to 370 °C at 40 °C/min (Zone B); (5) the sample was quickly cooled down to 100 °C and maintained for 26 min during Zone B gas processing; (6) quickly heated until 370 °C (initial Zone C temperature) and maintained for ~2 min; (7) heated from 370 to 400 °C at 40 °C/min (Zone C); (8) quickly cooled to 220 °C and maintained for 26 min during Zone C gas processing; (9) quickly heated to 400 °C (initial Zone D temperature) and maintained for ~2 min; (10) heated from 400 to 500 °C at 40 °C/min (Zone D). The gases evolved from the sample during each thermal zone (steps 1, 4, 7, and 10) were trapped using an MJT-1035E MicroJet Cryo-Trap (Frontier Laboratories Ltd., Koriyama, Japan); when the final temperature of the zone was reached, the trap was heated and the compounds were immediately released and injected into the long capillary column using an SS-1010E Selective Sampler (Frontier Laboratories Ltd., Koriyama, Japan). Once the gases were released into the column, the column was

kept at 40 °C for 2 min, heated from 40 to 320 °C at 20 °C/min, and kept at 320 °C for 10 min. The gases evolved from the sample during the cooling, 26-min waiting, heating, and ~2-min waiting periods between zones (steps 2, 3, 5, 6, 8, and 9) were disposed. The interface between the pyrolyzer and the capillary column was maintained at 300 °C.

The compounds exiting the columns were detected using an Agilent Technologies 5973 Mass Selective Detector (Quantum Analytics, Foster City CA, USA) using an electrospray ionization (ESI) source. Identification of the evolved compounds was performed based on mass spectrometry spectra using F-Search libraries and search software (version 3.5.2; Frontier Laboratories Ltd., Koriyama, Japan) and NIST Mass Spectral Program for the NIST/EPA/NIH Mass Spectral Library (version 2.2; National Institute of Standards and Technology, Gaithersburg MD, USA). Semi-automatic gas-chromatography-peak area measurements were performed using an automatic integrator included in the MSD Chemstation software (Agilent Technologies, Inc., Santa Clara CA, USA) followed by manual adjustments.

2.4.6. Tensile Testing

Uniaxial tensile testing was performed on an MTS Insight 5 twin-column tabletop universal tester (MTS Systems Corporation, Eden Prairie MN, USA) equipped with a 5-kN load cell according to ASTM D638. Testing was performed on the injection-molded Type IV dog bone specimens. Nominal testing speed was 5 mm/min; this rate was chosen to ensure that the ABS specimens would rupture in 0.5 to 5 minutes, as recommended by the ASTM standard. The distance between grips was 65 mm, and the gauge length (L_o, length of the thin part of the specimen) was 33 mm. The applied load was measured as a function of specimen elongation, and the load and elongation values were converted into stress (dividing by the specimen's original cross-sectional area) and strain (dividing by the gauge length, 33 mm), respectively. Elastic modulus, tensile strength (highest stress on the curve), strain at break, and toughness (area under the curve) were determined from the stress-strain curves. For samples that reached a yield point (first local maximum stress on the curve), the tensile strength was denominated "yield strength"; for

samples that ruptured before reaching a yield point, the tensile strength was called "tensile strength at break". 5 specimens were tested for each composition. The orientation of the samples relative to the direction of the melt flow during injection molding was varied: for each composition, 3 of the specimens were placed with the flow direction pointing downwards and 2 were placed with the flow direction pointing upwards. The experiments were carried out in a random order.

2.4.7. Impact Testing

Notched Izod impact testing was performed on a QPI-IC-12J Analog Universal Impact Tester (Qualitest International Inc., Ft. Lauderdale FL, USA), equipped with a pendulum with a maximum capacity of 12 J, in Izod configuration according to ASTM D256. Specimens for impact testing were obtained by cutting the injection-molded flexural bars in half. The specimens were notched using a Model 899 Automatic Specimen Notcher for Plastics (Tinius Olsen Testing Machine Co., Horsham PA, USA) at a specimen feed speed of approximately 90 mm/min and a cutter speed of approximately 150 m/min, to produce a notch with the dimensions given by the ASTM standard. Groups of 10 or 20 specimens were placed in the notching sample holder at a time, with the addition of 2 "dummy bars" at the end of each group to ensure that the last specimen would be notched correctly, as recommended by ASTM.

For Izod impact testing of the specimens, a procedure similar to Test Method C of ASTM D256 was used since many of the specimens had a notched Izod impact resistance less than 27 J/m. The testing procedure consisted of clamping the specimen in place, releasing the pendulum from its original height, and recording the Izod impact energy indicated by the analog pointer. For all specimens that presented a complete break, an additional procedure was performed in order to estimate the energy required to toss the broken piece: the tossed section was replaced on top of the clamped part, and the pendulum was again released from its original height. The energy recorded after the second pendulum release was the "estimated toss energy", which was then subtracted from the original Izod impact energy to obtain the net Izod impact energy. The original and net Izod impact energies were divided by the specimen width (3.19 mm) to obtain the original and

net Izod impact resistances, respectively, of the specimens. The system was regularly “calibrated” during testing by adjusting the pointer knob so that a free swing of the pendulum would take the pointer to the 0 J mark. 10 specimens of each composition (i.e. the top and bottom halves of 5 injection-molded flexural bars) were tested. Specimens were tested in a random order.

3

Bio-Based Flame Retardation of ABS Evaluated by Microscale Combustion Calorimetry

3.1. Introduction

Polymers are well known for their low densities, good processability, and versatility, enabling them to be used in a wide range of applications and to be present in all aspects of people's daily lives. One of the main drawbacks related to their use, however, is their flammability. The use of flame retardants (FRs) to suppress, reduce, and/or delay the combustion of polymers has long been explored, and major advances have been made in developing FR additives to be used commercially.

One of the largest and most effective classes of commercial flame-retardant additives is that of halogenated flame retardants [1,2]. Despite their efficacy, great environmental concerns have been raised surrounding the use of halogenated additives: it has been shown that these FRs can leach out of everyday products during their lifetime, contaminating humans, animals, and the environment with toxic compounds; when exposed to fire, halogenated FRs release toxic and environmentally persistent byproducts; and the incineration or disposal of polymers into landfills at the end of their lifetime causes further contamination of the environment and of living organisms [1]. Many studies have detected the presence of these compounds in humans, animals, sediments, water, and air in various locations [3–12]; halogenated FRs are being increasingly regulated or banned throughout the world as a result [10,13]. The toxicological concerns and ensuing restrictions related to halogenated flame retardants have created a need for environmentally friendly, low-toxicity flame retardants that can be used efficiently and safely in polymeric materials.

Driven by this societal need and by the increasing sustainability-focused global environmental awareness, research into the use of renewable products as FRs for polymers has grown exponentially in the past two decades. Many different nature-derived materials have since been used as FRs in various plastics. Costes et

al. [14], Sonnier et al. [15], Hobbs [16], and Watson and Schiraldi [17] have recently published comprehensive reviews describing the use of bio-based FRs in polymeric systems. Some examples of bio-based materials that have been explored as FRs in the past two decades, which are described in their reviews, are tannic acid, phytic acid, deoxyribonucleic acid (DNA), and fish gelatin. Tannic acid (TA), a naturally occurring polyphenolic compound found abundantly throughout the plant kingdom [74], is one of the key elements protecting trees from fires [32]. It is a good char former, a strong antioxidant, and an inherently intumescent compound. Researchers have used TA to reduce the flammability of aerogels [62,77,78,85], poly(lactic acid) (PLA) [76], nylon-6 (PA6) [19,86], polyesters and polyester/ABS blends [45], and polyolefins such as low-density polyethylene (LDPE) and polystyrene (PS) [18]. Phytic acid (PA) is the main storage form of phosphorus in plant seeds; its high P content (28 wt% and P/C atomic ratio of 1), readily carbonizable glucose ring, and natural intumescence make it attractive as an FR agent [17,72]. PA or its salts have been used in FR coatings for cotton [53,87], PLA [88], and wood [81] and as bulk FR additives in PLA [65,72,75,76] and polypropylene (PP) [82]. TA and PA have recently been used synergistically in PLA [76]. DNA (D) is an inherently intumescent compound that combines P and N atoms, which are known to act synergistically, in a single molecule. It has been used in coatings for cotton fabrics [59,60,89], ethylene-vinyl acetate (EVA) [90], poly(ethylene terephthalate) (PET) foams [91], and other polymers (PP, ABS, PA6, and bulk PET) [31] and as a bulk additive in EVA [92] and LDPE [69]. Fish gelatin (FG) has been used to reduce the flammability and improve the mechanical properties of PLA aerogels [73] and polyolefins (polyethylene (PE), PP, and PS) [18], showing synergy with TA when used in the polyolefins. It is hypothesized to work as an FR through crosslinking and the release of non-flammable gases [17,18,81].

It is often desirable to combine nature-derived FRs with low-toxicity, commercially available FRs to explore more options for synergy, creating bio-based, environmentally friendly FR systems that improve flammability characteristics without reducing mechanical properties. Mineral hydroxides are good candidates for this purpose, being amongst the most widely used of all FRs but often needed in concentrations greater than 50 wt% when used independently [2]. Examples of this family are alumina trihydrate (ATH) and magnesium

hydroxide (MH), the latter of which has been used synergistically with TA to flame retard LDPE, PS, and PA6 [18,19]. Melamine (ME), a strong blowing agent, can potentially be used with natural char formers and phosphate-rich compounds (such as TA, PA, and/or DNA) to produce intumescence and/or combine P and N atoms; ME has been used synergistically with TA and FG in polyolefins [18]. Melamine poly(magnesium phosphate) (Safire™ 600, S6), a P- and N-containing commercial FR and smoke suppressant, can potentially be used synergistically with natural char formers and other FRs for an optimized performance; it has recently been used in PS films and foams [18].

Bio-based FR systems have had a remarkable impact on the flammability of many polymers, but very little work has been carried out exploring the bio-based flame retardation of acrylonitrile-butadiene-styrene (ABS). ABS is one of the most widely used polymers in the world, finding applications in the electronics, consumer goods, and automobile industries (e.g. casings for electronic equipment, computer keycaps, home appliances and tools, car dashboards and light fixtures, wheel covers) [24–27]. These applications require the use of low-flammability components, since they deal with high electrical currents and temperatures and are found in everyday objects. ABS is, however, one of the most flammable polymers and one of the most challenging to flame retard due to its complex terpolymer structure. To reduce its flammability, ABS is currently used commercially with halogenated FRs, such as tetrabromobisphenol-A (TBBPA), which are extremely toxic and face global restrictions and bans [24,25,28]. There is therefore an urgent need for the development of low-toxicity, bio-based FR systems to substitute the halogenated FRs for commercial use in ABS.

Some work has been done in the past two decades using synthetic intumescent systems and/or nanofillers in ABS [20,29,30], but they have shown limited improvements and do not have the same environmental advantages as nature-derived FRs. A bio-based coating has been used on ABS [31], but coatings generally suffer from durability and washability issues. Very few reports of bio-based bulk FR additives in ABS have been published to date. Tributsch & Fiechter [32] blended tannins and tannin-containing tree barks with ABS, increasing the char yield and limiting oxygen index (LOI) and reducing polymer dripping during UL 94 tests; a comprehensive study on the flammability and mechanical properties of the blends was not reported, however. Pristine and phosphorylated lignin were used

by Song et al. [26,33] and Prieur et al. [27], respectively, to reduce the flammability of ABS, showing that lignin (and potentially other char formers) is a promising candidate for flame retarding ABS; the drawbacks related to their studies are that the amount of lignin required for effective flame retardation worsened the polymer's mechanical properties, phosphorylation of lignin adds an additional step to the manufacturing process, and lignin has a large structural diversity and compositional variability, so its performance depends strongly on its origin and the extraction process used [93,94]. Moustafa et al. [34] used ground seashell waste to enhance the thermal and flammability properties of ABS, but the ductility of the polymer was compromised. Overall, limited progress has been made in flame retarding ABS using nature-derived additives, creating a strong need for the development of bio-based FR systems for use in ABS.

In the present work, a systematic, two-phase approach was used to investigate the flammability performances of different bio-based and low-toxicity FR additives in ABS. Phase 1, the Screening Phase, consisted of a screening experiment, planned using Design of Experiments (DoE) techniques, in which 30 ABS composites were produced through melt processing and analyzed through vertical burn testing and microscale combustion calorimetry (MCC); the objective of this phase was to identify the most promising FRs and FR combinations and detect synergies among the components in a relatively fast and systematic way. The second phase consisted of analyzing the most promising Phase 1 samples in more detail using other analytical methods, with the objectives of better understanding their flammability and mechanical properties and comprehending their flame-retardation mechanisms.

The present chapter focuses on Phase 1, the Screening Phase, the overview of which is portrayed in Figure 3.1. The Design of Experiments and experimental-planning procedure are described first, including a description of the material-selection process, the justification for the fabrication and analysis techniques chosen, results from preliminary experiments, and an explanation of the DoE techniques used to define the compositions to be produced and tested. Analysis results, including outcomes from vertical burn testing and MCC, are then presented and discussed. Finally, identification and selection of the most promising compositions is described; further analysis of these compositions, which occurred in Phase 2, are discussed in the next chapter.

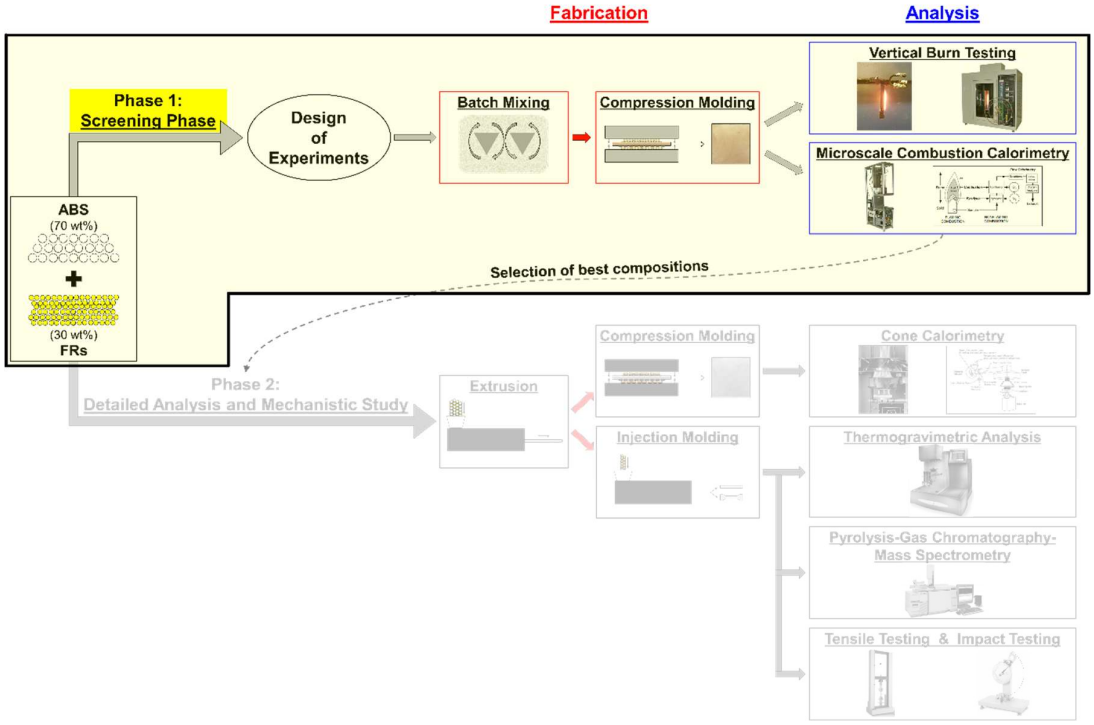

Figure 3.1. Overview of the Screening Phase (Phase 1), which is discussed in the present chapter, in the context of the complete experimental methodology of the current project.

3.2.
Experimental Planning and Design of Experiments

3.2.1.
Material Selection

The selection of flame-retardant additives to be used in ABS throughout this study was based on a number of factors. The goal was to select nature-derived or low-toxicity materials that: have been used successfully as FRs in other polymeric systems; are diverse amongst each other in terms of their flame-retardation mechanisms and compositions; have presented synergistic effects when used with each other in other polymers; and/or have the potential to interact synergistically with each other based on their compositions. Based on these factors, tannic acid (TA), DNA (D), fish gelatin (FG), phytic acid sodium salt hydrate (PA), melamine poly(magnesium phosphate) (Safire™ 600; S6), magnesium hydroxide (MH), alumina trihydrate (ATH), and melamine (ME) were selected to be used as flame retardants in this study; typical chemical structures for these compounds are shown

in Figure 3.2. Due to the hydrophilic nature of the selected flame retardants, a compatibilizing agent was used in order to improve the compatibility between the ABS matrix and the FR additives; polystyrene-*block*-poly(ethylene-*ran*-butylene)-*block*-polystyrene-*graft*-maleic anhydride (SEBS-g-MA) and a styrene-maleic anhydride random copolymer (SMA) were selected as candidates for this function. An antioxidant was also used in order to protect tannic acid from undergoing thermo-oxidative degradation during melt processing; Pentaerythritol tetrakis(3-(3,5-di-tert-butyl-4-hydroxyphenyl)propionate) (Irganox® 1010; Irg) was selected for this role.

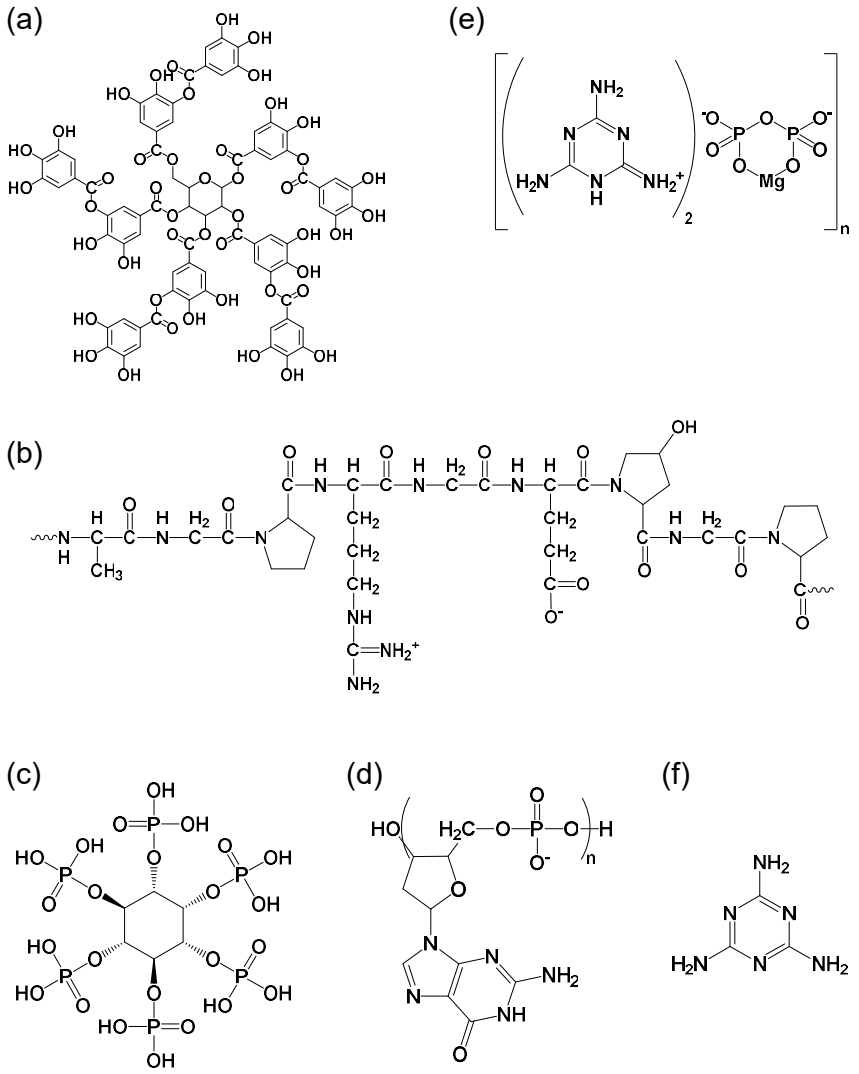

Figure 3.2. Typical chemical structures of FR additives: (a) tannic acid, (b) gelatin, (c) phytic acid, (d) DNA, (e) Safire™ 600 (melamine poly(magnesium phosphate)), and (f) melamine.

Tannic acid (TA) acts mainly in the solid phase as a char former due to its polyphenolic structure, shown in Figure 3.2a. It is an inherently intumescent compound, possessing the three characteristics required for that function: it is an acid source (containing many ester groups), a good carbon source and char former (composed mainly of benzene rings), and a blowing agent (releasing CO_2 during decomposition) [71,86]. Researchers have used tannic acid, either alone or in combination with other additives, to reduce the flammability of epoxy aerogels [62,85], PLA aerogels [77,78], PLA resin [76], PA6 [19,86], polyesters and polyester/ABS blends [45], and polyolefins such as LDPE and PS [18]. Another naturally occurring polyphenolic compound, lignin, has been used in ABS to reduce its flammability [26,27,33]; tannic acid has a similar structure and char-forming capacity as lignin, with the advantage of having a greater structural and compositional regularity, making it a promising candidate for use in ABS. Since TA functions mainly as a char former, it can be used synergistically with FRs that catalyze char formation, such as phytic acid or other compounds that contain phosphate groups.

Fish gelatin (FG) has been used as a flame retardant by Schiraldi and co-workers [73] in PVA aerogels and by Deans [18] in polyolefins (PE, PP, and PS), successfully reducing the flammability and improving the mechanical properties of the materials. The addition of fish gelatin into LDPE greatly reduced polymer dripping during combustion and increased the tensile elastic modulus by over 200%; FG-induced crosslinking was suspected to be responsible for the improvements. Gelatins have also been hypothesized to act in the gas phase, diluting the concentration of flammable gases by releasing CO_2 and NH_3 during decomposition [81,95,96]. FG also presents the potential to work synergistically with other bio-based or low-toxicity FRs: Deans found that using FG in conjunction with TA or ME further reduces the flammability of the polyolefins [18], and the typical N-containing structure of gelatins (Figure 3.2b) suggests that FG can also be used synergistically with P-containing compounds, since the two elements are known to enhance each other's FR effects.

Phytic acid and its salts (generically abbreviated herein as PA) have been used, either independently or combined with other compounds, as FR additives in PLA [65,72,75,76] and PP [82] and in FR coatings for cotton [53,87], PLA fabric [88], and wood [81]. PA's most common commercial form is phytic acid sodium

salt, or sodium phytate [15]. With a high P content (Figure 3.2c), PA can potentially work in both the solid phase (as a catalyst for char formation) and the gas phase (as a radical scavenger) [27,72]. As a catalyst for char formation, PA can be used synergistically with TA, a natural char former, to enhance and accelerate the latter's char-forming capability; Laoutid and coworkers recently used PA and TA synergistically to synthesize a new FR additive for PLA [76], and PA has been used in synergy with another polyphenolic char former (lignin) [72]. PA is also inherently intumescent, having phosphoric acid groups (acid source), containing 6-membered C rings (carbon source), and releasing H_2O during decomposition (blowing agent). Exploring its particular strength as an acid source, it can potentially be combined with TA (strong char former) and melamine (strong blowing agent) to provide a more pronounced intumescent effect than when PA or TA is used alone. PA can also be used synergistically with nitrogen-containing compounds, exploring the P-N synergy for flame retardation.

DNA (D) is a naturally intumescent compound [60,97] due to the presence of phosphate groups (acid source), N atoms (blowing agent), and cyclic groups (carbon source) in its structure (Figure 3.2d). It also makes use of the P-N synergy for flame retardation. Its intumescence has allowed it to be used as an FR coating for cotton [59,60,89], EVA [90], PET foams [91], and other polymers (PP, ABS, PA6, and bulk PET) [31]. It has found limited use so far as a bulk FR additive, having been applied in EVA [92] and LDPE [69]. In the latter system, investigated by Pokorski and coworkers [69], results comparable to melamine polyphosphate (MPP), one of the industry-standard FRs for plastics, were achieved.

Melamine poly(magnesium phosphate) (Safire™ 600, S6) is a flame retardant and smoke suppressant developed for use mainly in polybutylene terephthalate (PBT) and polyamides. However, Deans [18] recently used Safire™ 600 to reduce the flammability of PS films and foams, making it an interesting candidate for use in styrenic polymers, such as ABS. Rich in phosphorus and nitrogen (Figure 3.2e), S6 makes use of the P-N synergy for flame retardation. As an acid source (phosphate groups) and blowing agent (N atoms), it can potentially be combined with a natural char former, such as TA, to catalyze char formation and possibly provide intumescence.

Magnesium hydroxide (MH) and alumina trihydrate (ATH) act mainly in the solid phase as "heat sinks", lowering the burning material's temperature as they

endothermically decompose into magnesium oxide and aluminum oxide, respectively, and release water. One drawback related to their use is that these additives are normally needed in large quantities in order to be effective, which often diminishes the polymer's mechanical properties [19]; this can potentially be mitigated by using them in lower quantities in combination with other FR additives that work through different mechanisms and are not as harmful to the mechanical properties. Wang et al. [19] used MH together with TA-iron complexes in PA6, improving both the flame resistance and the mechanical properties of the polymer. MH has also been used synergistically with TA to flame retard LDPE and PS [18].

Melamine (ME), rich in nitrogen (Figure 3.2f), acts mainly in the gas phase, diluting the fuel concentration by evaporating and releasing ammonia [98,99]. Due its high gas release, it is also often used as a blowing agent in intumescent systems [23,100], so the use of ME in combination with TA (carbon source) and PA (acid source) can potentially form an effective intumescent FR system while also taking advantage of the P-N synergy. Deans [18] recently used ME-TA and ME-FG combinations to flame retard polyolefins.

Polystyrene-*block*-poly(ethylene-*ran*-butylene)-*block*-polystyrene-*graft*-maleic anhydride (SEBS-g-MA) and a styrene-maleic anhydride random copolymer (SMA) were chosen to be used as reactive compatibilizers in order to improve the interfacial adhesion between the ABS matrix and the FR additives, the latter of which contain mostly hydrophilic end groups. Maleated polymers are often used to improve the compatibilization in particle-filled polymeric systems, building bridges between the components as the compatibilizer's polymeric backbone blends with the matrix and the maleic anhydride (MA) groups bond with the hydrophilic additives. Copolymers based on MA and styrene can be especially effective in styrenic polymers, such as ABS [28]. SEBS-g-MA has been used in styrenic polymers (PS and HIPS) to improve their compatibility with nature-derived additives, including TA, FG and ME [18,101]; other styrene- and MA-based copolymers have been used as compatibilizers in ABS composites, including those filled with a bio-based FR agent, lignin [26,33,102].

Irganox® 1010 (Irg), a sterically hindered antioxidant designed to protect organic substrates from thermo-oxidative degradation, has been shown to be important in protecting tannic acid from thermo-oxidative degradation during

processing in polyolefins [18]. Irg was therefore selected to be used in every TA-containing sample in this study.

3.2.2.
Selection of Fabrication and Analysis Techniques

The fabrication and analysis methodologies of the Screening Phase were selected so as to enable a large number of samples to be produced and tested using a relatively small amount of raw material and in a short amount of time. The fabrication technique selected was batch mixing followed by compression molding, which allows for a quick production of samples using as little as 60 g of raw material each. Two analysis techniques were chosen: UL 94-inspired vertical burn testing and MCC. Vertical burn testing was selected because it can be performed extremely quickly and is a flaming test, showing the materials' actual behaviors in the presence of a flame. Drawbacks related to this testing method are: (1) the samples are only tested in the presence of a small flame, which often does not represent large-fire scenarios; (2) results are strongly dependent on testing conditions, such as sample thickness; and (3) the test basically has a pass-no pass criteria, making it difficult to compare a large number of samples if the majority of them either pass or don't pass the test. In other words, the test can be useful as a screening tool if only a small group of samples achieve V-0 classification, as the successful samples would be selected for Phase 2; however, if many samples achieve a V-0 or V-1 rating or if none of the samples obtain such a classification, the selection of the "most promising samples" would become subjective, reducing the validity and the scientific content of the screening experiment. It was decided to utilize vertical burn testing despite these drawbacks, since it is clearly the fastest flammability-testing technique and because it could still be useful as a screening tool if only some of the samples achieved a UL 94 classification. The other analysis method chosen, MCC, provides a number of benefits: it allows for a relatively quick analysis, requires only a small amount of sample, has been indicated as a rapid screening tool to estimate the fire performances of flame-retarded materials [103–105], has been shown to correlate to flaming combustion tests (especially when polymers that contain non-halogenated flame retardants are analyzed) [103–107], is based on intrinsic thermodynamic properties rather than being dependent on test-specific conditions,

and can be directly related, through the peak heat release rate (PHRR) parameter, to one of the best single indicators of the fire hazard of a material, the heat release capacity [108]. The main disadvantages of this method are the absence of an actual flame (raising questions about its representability of real fire scenarios) and the fact that barrier effects and flame inhibition are not captured by it [103,104,108]; despite its shortcomings, this technique can be considered an adequate flammability screening tool.

3.2.3. Preliminary Experiments

3.2.3.1. Determination of Melt-Processing Parameters

Batch-mixing and compression-molding parameters for compounding ABS and its composites were determined based on a combination of: documented information (ABS's technical datasheet and reports in the literature), differential scanning calorimetry (DSC) results, and empirical compounding experiments. Ineos Styrolution's technical datasheet for Terluran® GP-35 ABS recommends that the product be injection molded with a melt temperature of 220–260 °C; no recommendations are given for other processing techniques. Previous authors [109,110] have reported utilizing twin-screw-extruder die temperatures of 220 to 230 °C and injection-molding barrel temperatures of 210 to 230 °C to produce ABS/short glass fiber composites. Another group [111] used a single-screw extruder with a die temperature of 240 °C followed by compression molding at 260 °C for the production of ABS/ZnO composites. Batch mixing typically has a much higher residence time than extrusion and injection molding, so it was expected that the optimal temperature for batch mixing ABS would be below the extrusion and injection-molding temperatures listed above (i.e. below the 210–260 °C temperature range obtained from the combined data) to avoid polymer degradation. Batch mixing followed by compression molding was used by Prieur et al. [27] to fabricate ABS/lignin composites and by Shofner et al. [112] to produce ABS/single wall carbon nanotubes composites; the former performed batch mixing at 200 °C for 10 min (50-rpm motor speed, 200-g batches) and compression molding at 200

°C, while the latter batch mixed the material at 140 °C for 10 min (60-rpm motor speed, 30-g batches) and compression molded the samples at 150 °C. It was therefore expected that the optimal temperature for batch mixing and compression molding ABS would be within (or close to) the range of 140–200 °C.

Differential scanning calorimetry (DSC) was performed on a pristine, as-received ABS pellet; the specimen was heated, cooled, and re-heated within the range of 30 to 300 °C at 10 °C/min. The resulting curve shows that all thermal events (glass transitions corresponding to styrene and acrylonitrile) occur below 150 °C, suggesting that a processing temperature close to 160 °C might be appropriate to ensure that all of the material is sufficiently melted.

Batch-mixing experiments were then performed on ABS in order to empirically confirm the optimal temperature for melt processing. 60-g batches of ABS were batch mixed at 140, 160, 180, 200, and 220 °C. The target residence time was 4 to 5 min, but adjustments had to be made at the lowest temperature to ensure that the material completely melted; motor speed was kept at 20 rpm until the torque stabilized, and then raised to 60 rpm for the remainder of the time period. At 140 °C, it was clear, based on the torque behavior and on the presence of "scrubbing" sounds as still-solid pellets were being mixed, that the material took too long to melt (the residence time was increased to 8 min to ensure complete melting), indicating that this temperature was too low. At 200 and at 220 °C, on the other hand, the presence of a considerable amount of smoke and a strong odor during processing suggested that significant degradation was occurring, indicating that these temperatures were too high; it was considered that these qualitative experimental observations were sufficient, so it was decided not to perform detailed analysis of the extent of degradation using techniques such as Fourier-transform infrared spectroscopy (FTIR). At 180 °C, no smoke could be seen, but there was still a strong odor after 5 min of residence time, suggesting that some degradation was taking place; this temperature could potentially be used, but with a residence time of less than 5 min. At 160 °C, the material seemed to melt adequately and no vapors nor odors were present after the 5-min procedure, suggesting that this was an appropriate temperature. Batches of Br-ABS were also produced successfully at 150 and 170 °C. It was therefore determined that batch mixing of ABS and its composites would be performed at 160 °C for a residence time of approximately 5 min, as described (in more detail) in Section 2.3.2.1. Compression molding was

tested for ABS, Br-ABS, and a number of preliminary compositions (composed mainly of ABS and tannic acid) at 160 °C, achieving successful products; it was therefore determined that the same temperature would be used for compression molding. Further details of the compression-molding procedure can be found in Section 2.3.2.2.

3.2.3.2. Evaluation of Processing Effect on Material Properties

Once the parameters and procedures for batch mixing and compression molding were defined, it was important to determine whether the melt-processing steps would alter the materials' properties in such a way that would have an effect on their flammability behaviors. Microscale combustion calorimetry (MCC) was used to perform the comparison between unprocessed and processed material; vertical burn tests were not performed, since it is not possible to test unprocessed material using this method (some kind of processing would be necessary in order to transform the raw materials, available in pellet or powder form, into bar-shaped specimens).

As-received pellets of neat ABS and of a commercial brominated grade of ABS (Br-ABS) were cut with a blade into 5–8-mg specimens and tested by MCC in two repetitions each. Melt-processed ABS and Br-ABS specimens were cut out from square plates fabricated through batch mixing followed by compression molding (details in Section 2.3.2) and tested as well; throughout the present project, 27 melt-processed ABS specimens and 3 melt-processed Br-ABS specimens were analyzed using MCC. Figure 3.3 shows representative heat release (HRR) curves for the 4 samples, and Figure 3.4 presents average MCC results for all as-received and melt-processed ABS and Br-ABS specimens.

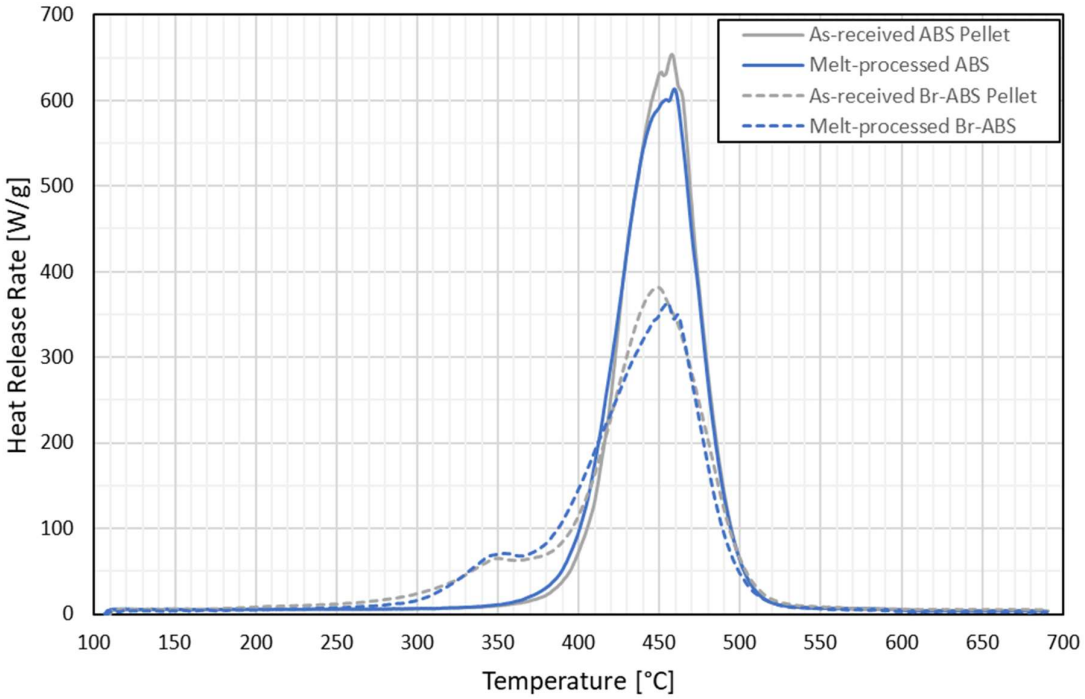

Figure 3.3. Representative heat release rate (HRR) curves, obtained by MCC, for as-received and melt-processed ABS and Br-ABS.

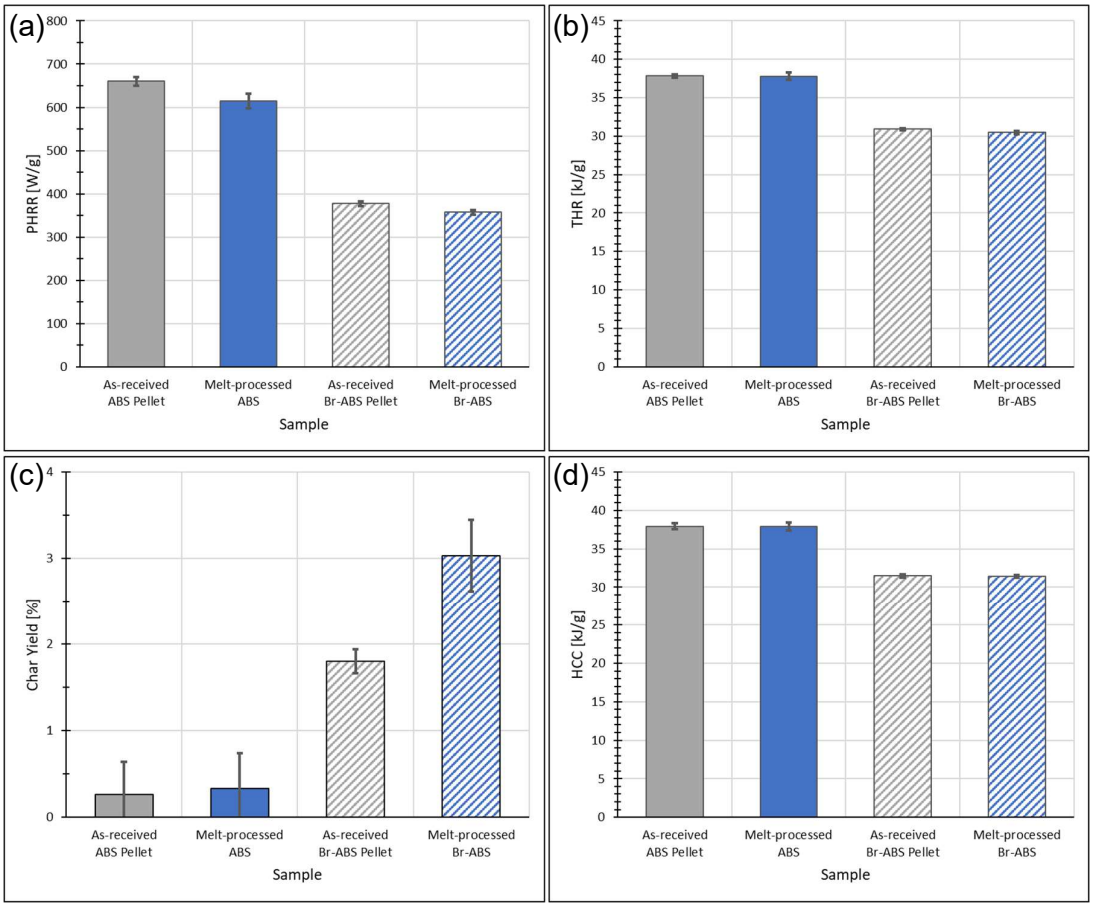

Figure 3.4. (a) Peak heat release rate, (b) total heat release, (c) char yield, and (d) heat of complete combustion of as-received and melt-processed ABS and Br-ABS, obtained by MCC. Error bars indicate standard deviations.

The results indicate that melt processing did not have a significant impact on the samples. The total heat release (THR) and heat of complete combustion (HCC) showed no change for both ABS and Br-ABS, indicating that the total amount and the nature of the gases evolved from the samples remained the same. There was a slight decrease in peak heat release rate (PHRR) for both ABS and Br-ABS; knowing that the THR (area under the curve) does not change from the as-received to the melt-processed samples, the decreases in PHRR can be explained by the fact that the main peak of the melt-processed sample (blue) begins to rise earlier than that of the as-received pellet (gray) for both ABS and Br-ABS (Figure 3.3), widening and, consequently, "flattening" the curves. The earlier rising of the melt-processed samples' peaks suggests that ABS volatiles are beginning to be released earlier than in the as-received samples; partial degradation during processing can

possibly be responsible for this behavior. An increase in char yield (from 2 to 3%, which has almost no practical significance) can be seen for Br-ABS, while no change occurs in ABS's char yield. Overall, the results and the appearances of the curves are very similar between the as-received and the melt-processed samples, indicating that the compounding step did not have a significant nor a practical impact on the samples.

3.2.3.3.
Selection of Type and Amount of Compatibilizer

Bio-based compounds tend to contain hydrophilic end groups, and the same is true for many commercial low-toxicity flame retardants. It was determined, therefore, that a compatibilizing agent would be used in the present study in order to improve the compatibility between ABS and the FR additives, providing better interfacial adhesion between the components and better dispersion of the fillers. Maleated coupling agents are often chosen for this function, as the hydrophobic portion of the compound can blend well with the polymeric matrix while the maleic anhydride (MA) groups can react with the fillers' hydrophilic end groups. Styrenic compounds grafted or copolymerized with MA are good candidates to be used in ABS due to the presence of styrene in the terpolymer; styrene- and MA-based compatibilizers have been used frequently in ABS composites [18,26,33,101,102].

Two different compounds were selected as candidates to be used as the compatibilizer throughout this research: polystyrene-*block*-poly(ethylene-*ran*-butylene)-*block*-polystyrene-*graft*-maleic anhydride (SEBS-g-MA) and a styrene-maleic anhydride random copolymer (SMA). Magnesium hydroxide (MH) and a combination of Safire™ 600 (S6) with fish gelatin (FG) were chosen as the additives to test and compare the performances of the compatibilizers, since these FR systems showed a positive performance in preliminary vertical burning tests. ABS/MH composites were produced with SEBS-g-MA and SMA in two different loading levels each (MH/5 SEBS, MH/15 SEBS, MH/5 SMA, and MH/15 SMA), and ABS/S6-FG composites were fabricated with SEBS-g-MA in two different loading levels (S6-FG/5 SEBS and S6-FG/15 SEBS). In all samples, the total flame-retardant content was 30 wt%. The two loading levels for the compatibilizers were defined as 5 and 15 wt% of the matrix, corresponding to 3.5 and 10.5 wt% of the

sample, respectively. The six formulations are described in Table 3.1. The samples were produced through batch mixing followed by compression molding, using the previously defined processing parameters, according to the drying and melt-processing procedures described in Sections 2.3.1 and 2.3.2. Analyses were performed using vertical burn testing and MCC.

Table 3.1

Compositions of ABS composites used to compare different types and amounts of compatibilizer

Sample Name	ABS	SEBS-g-MA[a]	SMA[a]	MH[a]	S6[a]	FG[a]
MH/5 SEBS	66.5	3.5	-	30	-	-
MH/15 SEBS	59.5	10.5	-	30	-	-
MH/5 SMA	66.5	-	3.5	30	-	-
MH/15 SMA	59.5	-	10.5	30	-	-
S6-FG/5 SEBS	66.5	3.5	-	-	15	15
S6-FG/15 SEBS	59.5	10.5	-	-	15	15

[a] SEBS-g-MA = polystyrene-*b*-poly(ethylene-*r*-butylene)-*b*-polystyrene-*g*-maleic anhydride, SMA = styrene-maleic anhydride random copolymer, S6 = Safire™ 600, FG = fish gelatin, MH = magnesium hydroxide.

3.2.3.3.1. Vertical Burn Testing for Compatibilizer Evaluation

Vertical burn tests, following a procedure similar to the UL 94 protocol, were performed on rectangular bars (127 mm x 12.7 mm x 1.6 mm), cut out from the compression-molded plates, in a fume hood. All samples were tested both with the sash closed and with the sash open, since the two configurations provide very distinct testing conditions and results. When the sash is closed, an upward air stream is formed due to the ventilation system, making the test more difficult to be passed as the flame is swept upward along the bars. When the sash is open, however, there is an air flow moving from the front to the back of the hood, making the test easier to be passed because the flame is moved mostly to the backside of the sample and volatiles can be swept away from the specimen. Two to three specimens were tested in each configuration for MH/5 SEBS and S6-FG/5 SEBS, and one specimen was tested in each configuration for all other samples.

When the tests were performed with the sash closed, all of the specimens burned completely. With the sash open, however, all specimens but one were able

to self-extinguish following the first or both 10-s flame applications, as shown in Table 3.2. When comparing the two types of compatibilizers (SEBS-g-MA and SMA), no difference was seen: the MH formulations with a low compatibilizer loading level (MH/5 SEBS.1, MH/5 SEBS.3, and MH/5 SMA) were able to extinguish the 1st flame in under 10 s and the 2nd flame in over 30 s, and the MH formulations with a high loading level (MH/15 SEBS and MH/15 SMA) were able to extinguish the 1st flame immediately but were unable to extinguish the 2nd flame, independent of the type of compatibilizer used. When evaluating the amount of compatibilizer in the MH compositions, it appears that a lower content is slightly preferable, since only the specimens with lower amounts of compatibilizer were able to extinguish the 1st and the 2nd flames, while the samples with higher loading levels were only able to extinguish the 1st flame. The advantage of the lower amount is not clear though, since the second low-compatibilizer-loading specimen was not able to extinguish even the first flame (MH/5 SEBS.2). For the S6-FG samples, it is unclear whether the higher or lower amount of SEBS-g-MA performed better: the higher amount extinguished the 1st flame immediately but was unable to extinguish the 2nd flame, while the lower amount took over a minute to extinguish the 1st flame but was able to extinguish the 2nd flame in 11 s for one of the specimens. In conclusion, both compatibilizers had equivalent performances, and it is unclear whether a loading level of 5 or of 15 wt% of the matrix is advantageous. There may be a small preference for the lower loading level, since only low-content specimens were able to extinguish both flames.

Table 3.2

Self-extinguishing times from vertical burn tests for ABS composites with different types and amounts of compatibilizer[a]

Sample	Time to Self-Extinguish[b] [s]		Fraction of Specimen Covered by Flame[c] [%]
	1st Flame	2nd Flame	
MH/5 SEBS.1	0	77	60%
MH/5 SEBS.2	frc	-	-
MH/5 SEBS.3	10	74	33%
MH/15 SEBS	0	frc	-
MH/5 SMA	5	47	25%
MH/15 SMA	0	frc	-
S6-FG/5 SEBS.1	80	11	65%
S6-FG/5 SEBS.2	64	frc	-
S6-FG/15 SEBS	0	frc	-

[a] Tests were performed in a fume hood with the sash open.

[b] frc = flame reached clamp.

[c] Fraction of the rectangular bar that was covered by the 2nd flame before it was extinguished; only applies to samples that self-extinguished following both flame applications, since the remaining samples were 100% covered by the flame.

3.2.3.3.2. Microscale Combustion Calorimetry for Compatibilizer Evaluation

MCC tests were also performed in order to compare the two different types and amounts of compatibilizer. Analyses were performed on 5–10-mg specimens cut out from the compression-molded plates for the 6 samples described in Table 3.1. Each composition was tested 3 times. Figure 3.5 presents average PHRR, THR, and char yield results; data from pristine ABS are also included as a reference.

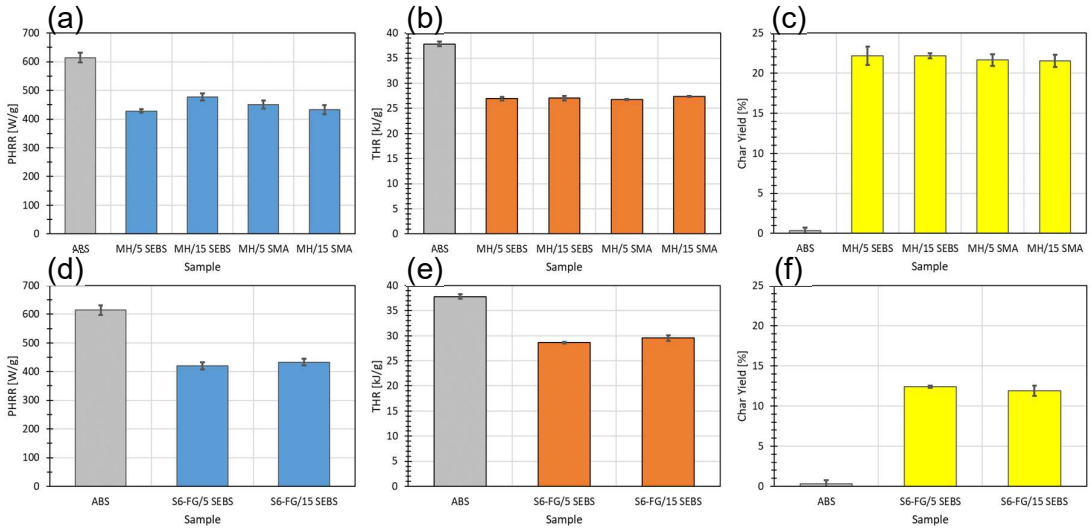

Figure 3.5. (a, d) Peak heat release rate, (b, e) total heat release, and (c, f) char yield results, obtained by MCC, for ABS/MH (top) and ABS/S6-FG (bottom) composites with different types and amounts of compatibilizer.

For the S6-FG samples (bottom row), very little difference was seen when the level of SEBS-g-MA was varied; PHRR and char yield results were statistically unchanged, while a small increase was seen in THR when the level of SEBS-g-MA was increased. When MH was used (top row), the 4 samples had statistically identical char yields and almost equivalent THR results; the only statistically significant differences in THR are slightly better performances by MH/5 SEBS and MH/5 SMA in relation to MH/15 SMA, again pointing to a small advantage of using a lower amount of compatibilizer. The PHRR results for the MH samples also suggest that less compatibilizer might be slightly better, showing a clear increase when the SEBS-g-MA content was increased and no change when the SMA level was increased. The results are inconclusive as to the best type of compatibilizer: in terms of PHRR, SEBS-g-MA performed better than SMA for the lower loading level while SMA performed better for the higher level; in terms of THR and char yield, the 2 compatibilizers had identical performances.

Two general conclusions can be made from the vertical burn tests and the MCC analyses. The first is that SEBS-g-MA and SMA had equivalent performances, with no clear advantage of one over the other. The second conclusion is that there is very little difference between using the compatibilizer at 5 or at 15 wt% of the matrix, with a slightly better performance at the lower loading level. A

possible explanation for the slightly worsened results when the loading level was increased is that the compatibilizers themselves are more flammable than ABS, having PHRRs close to 900 W/g (compared to 600 W/g for ABS), as can be seen in Table 3.8; it is likely, therefore, that no improvement was achieved in dispersion and interfacial adhesion in a way that would enhance the FR effects of the additives, while the increased amount of compatibilizer simply increased the flammable content of the samples. Based on the above results, SEBS-g-MA was selected as the compatibilizer to be used further throughout the research because it was available in higher amounts in our laboratory, and the lower loading level of 5 wt% of the matrix was chosen for the continuation of the study.

3.2.4.
Design of Experiments for Determination of Sample Compositions

Design of Experiments was employed in order to determine the compositions of the samples to be produced and tested during the Screening Phase. Two sets of samples were defined, fabricated and analyzed sequentially; the analysis results from the first set were used to define the samples of the second set. A Mixture Design was used to define the compositions. It was not possible to largely reduce the number of samples to be tested using, for example, fractional factorial designs, because these kinds of designs don't provide information on the interactions between the components, making the assumption that they are not significant; on the contrary, interactions are frequently very significant in flammability performance and were important to be studied, since different FRs interact with the matrix in different ways and FRs can interact with each other to produce synergistic effects such as char-formation catalysis or intumescence. The rest of this section describes the process for determining the compositions for the Screening Phase.

3.2.4.1.
First Set of Samples

The FRs analyzed in the first set of samples were tannic acid, Safire™ 600, DNA, fish gelatin, and magnesium hydroxide. The compositions of the first set of samples, shown in Table 3.3, were selected based on Design of Experiments using

a Mixture Design. Two definitions were made prior to applying the mixture design: (1) all of the composite samples would contain the compatibilizing agent, SEBS-g-MA, as part of the matrix at a fixed ABS:SEBS-g-MA ratio of 95:5 (w/w) in order to improve the compatibility between the matrix and the additives; and (2) all of the tannic acid-containing samples would contain the antioxidant, Irganox® 1010 (Irg), at a fixed tannic acid:Irg ratio of 29:1 (w/w) in order to protect tannic acid during processing. The six components of the mixture design were then defined as: Matrix (ABS and SEBS-g-MA compatibilizer at a fixed ratio of 95:5 (w/w)), TA (tannic acid and Irganox® 1010 at a fixed ratio of 29:1 (w/w)), S6 (Safire™ 600), D (DNA), FG (fish gelatin), and MH (magnesium hydroxide).

Table 3.3

Compositions of the 1st set of samples of the Screening Phase (wt%)[a]

Sample #	Sample Name	ABS	SEBS-g-MA[b]	TA[b]	D[b]	S6[b]	FG[b]	MH[b]	Irg[b]	TBBPA[b,c]	SbO[b,c]	Others[c]
1.1	ABS	100	-	-	-	-	-	-	-	-	-	-
1.2	ABS/MA	95	5	-	-	-	-	-	-	-	-	-
1.3	TA	66.5	3.5	29	-	-	-	-	1	-	-	-
1.4	D	66.5	3.5	-	30	-	-	-	-	-	-	-
1.5	S6	66.5	3.5	-	-	30	-	-	-	-	-	-
1.6	FG	66.5	3.5	-	-	-	30	-	-	-	-	-
1.7	MH	66.5	3.5	-	-	-	-	30	-	-	-	-
1.8	TA-D	66.5	3.5	14.5	15	-	-	-	0.5	-	-	-
1.9	TA-S6	66.5	3.5	14.5	-	15	-	-	0.5	-	-	-
1.10	TA-FG	66.5	3.5	14.5	-	-	15	-	0.5	-	-	-
1.11	TA-MH	66.5	3.5	14.5	-	-	-	15	0.5	-	-	-
1.12	D-S6	66.5	3.5	-	15	15	-	-	-	-	-	-
1.13	D-FG	66.5	3.5	-	15	-	15	-	-	-	-	-
1.14	D-MH	66.5	3.5	-	15	-	-	15	-	-	-	-
1.15	S6-FG	66.5	3.5	-	-	15	15	-	-	-	-	-
1.16	S6-MH	66.5	3.5	-	-	15	-	15	-	-	-	-
1.17	FG-MH	66.5	3.5	-	-	-	15	15	-	-	-	-
1.18	TA-D-S6	66.5	3.5	9.7	10	10	-	-	0.3	-	-	-
1.19	TA-D-FG	66.5	3.5	9.7	10	-	10	-	0.3	-	-	-
1.20	TA-D-MH	66.5	3.5	9.7	10	-	-	10	0.3	-	-	-
1.21	TA-S6-FG	66.5	3.5	9.7	-	10	10	-	0.3	-	-	-
1.22	TA-S6-MH	66.5	3.5	9.7	-	10	-	10	0.3	-	-	-
1.23	TA-FG-MH	66.5	3.5	9.7	-	-	10	10	0.3	-	-	-
1.24	S6-FG-MH	66.5	3.5	-	-	10	10	10	-	-	-	-
1.25	Br-ABS[c]	70 - 90	-	-	-	-	-	-	-	5 - 20	2 - 6	0 - 9

[a] Gray = control samples, Green = ABS composites containing 1, 2, or 3 different FRs (in progressively darker shades).

[b] SEBS-g-MA = polystyrene-*b*-poly(ethylene-*r*-butylene)-*b*-polystyrene-*g*-maleic anhydride, TA = tannic acid, D = DNA, S6 = Safire™ 600, FG = fish gelatin, MH = magnesium hydroxide, Irg = Irganox® 1010, TBBPA = tetrabromobisphenol-A, SbO = antimony(III) oxide.

[c] Br-ABS (brominated ABS) is a commercial product. The approximate composition given here was taken from its material safety datasheet (MSDS). "Others" refers to an impact modifier, stabilizers, and lubricants.

Figure 3.6 illustrates the five-dimensional design space of the experiment. The FR content of the samples (excluding the controls) was fixed at 30 wt%. Fixing the matrix at a constant value (70 wt%) allowed for the development of a simpler

design, with only 5 pseudocomponents (TA, S6, D, FG, and MH), each having minimum and maximum values of 0 and 30 wt%, respectively, with a total sum of 30 wt%. A 2nd degree simplex centroid design was used, with the addition of 7 out of the 10 3rd degree compositions (this four-dimensional 5-pseudocomponent design subspace is represented by the 10 smaller triangles within the tetrahedra in Figure 3.6). In other words, 22 ABS composite samples were produced and tested, including: each FR individually at a 30 wt% content (samples 1.3–1.7 in Table 3.3 (light green); vertices of smaller triangles in Figure 3.6); combinations of 2 FRs at 15 wt% each (1.8–1.17 in Table 3.3 (medium green); edges of triangles in Figure 3.6); and combinations of 3 FRs at 10 wt% each (1.18–1.24 in Table 3.3 (darker green); centers of triangles in Figure 3.6). In addition, 3 control samples were included (gray lines in Table 3.3): pure ABS (1.1 in Table 3.3; not represented in Figure 3.6); ABS with SEBS-g-MA at a 95:5 (w/w) ratio (pure "Matrix", or ABS/MA; 1.2 in Table 3.3; top vertex of tetrahedra in Figure 3.6); and a commercial brominated FR grade of ABS (Br-ABS; 1.25 in Table 3.3; not represented in Figure 3.6).

The 25 samples, including the controls, were subjected to the same melt-processing steps and conditions in order to eliminate the effects of processing when comparing results. All samples were tested by MCC under the same conditions in at least 3 repetitions. Sample production and testing occurred in random orders.

MCC was also run on each individual FR (TA and Irg, D, S6, FG, and MH) in order to enhance the 6-component Mixture Design and enable analysis of the interactions between each FR and the matrix. Since it is not possible to melt process the FRs independently (i.e. without the presence of the matrix), the MCC runs were performed directly on the powders (bottom vertices of tetrahedra in Figure 3.6). Together with sample 1.2 (ABS/MA, top vertex of tetrahedra), these samples represent the vertices of the 5-dimensional design space, which are the compositions that contain 100% of each component (i.e. the pure components of the mixture design).

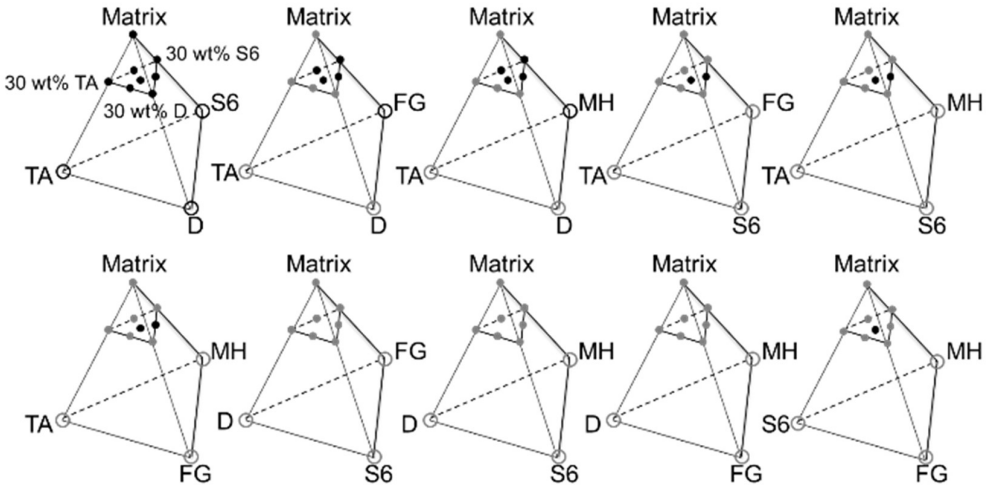

Figure 3.6. Representation of the design space for the 1st set of samples. The 23 black filled circles represent the melt-processed composites and ABS/MA (samples 1.2–1.24); the 5 black empty circles represent the samples that were tested as powders (individual FRs); and the gray circles refer to samples that were already accounted for in the previous tetrahedra. Vertices of tetrahedra represent the pure components of the mixture design. The subspace defined by the smaller triangles (5-pseudocomponent 2nd degree simplex centroid design with the addition of 7 3rd degree compositions) represents the 1-, 2-, and 3-additive composites (triangle vertices, edges, and centers, respectively), which contain 70 wt% matrix and 30 wt% FRs. Samples 1.1 (pure ABS) and 1.25 (Br-ABS) are not shown.

3.2.4.2. Second Set of Samples

A second set of samples, with the inclusion of 3 new FR agents, was defined and tested, as shown in Table 3.4. Phytic acid sodium salt (PA) and melamine (ME) were chosen to be tested along with TA and FG, because (1) TA and TA-FG had the best performance from the first set, as can be seen later in this chapter; (2) phytic acid has been shown to present synergy with tannic acid [76] and with lignin (which has a similar structure as tannic acid) [72]; (3) a PA-TA-ME system has the potential to present intumescence because it contains an acid source, a carbon source, and a blowing agent, respectively; and (4) FG has been demonstrated to work in synergy with TA and with ME [18]. Therefore, ABS composite samples containing PA, TA, FG, and ME in combinations of 1, 2, 3, and 4 FRs at a time (samples 2.1–2.7) were produced and tested. An additional sample, containing only alumina trihydrate as an FR (ATH, sample 2.8), was included in the second set in

order to be compared with the MH sample, since the two mineral fillers act through the same flame-retardation mechanism. The 8 samples of Set 2 were produced and tested in random orders under the same conditions as the 25 samples of Set 1. MCC was also run on PA, ME, and ATH individual powders in order to enable analysis of the interactions between each FR and the matrix.

Table 3.4

Compositions of the 2nd set of samples of the Screening Phase (in wt%)[a]

Sample #	Sample Name	ABS	SEBS-g-MA[b]	PA[b]	TA[b]	ME[b]	FG[b]	ATH[b]	Irg[b]
2.1	PA	66.5	3.5	30	-	-	-	-	-
2.2	PA-TA	66.5	3.5	15	14.5	-	-	-	0.5
2.3	PA-TA-ME	66.5	3.5	10	9.7	10	-	-	0.3
2.4	PA-TA-ME-FG	66.5	3.5	7.5	7.25	7.5	7.5	-	0.25
2.5	ME	66.5	3.5	-	-	30	-	-	-
2.6	PA-ME	66.5	3.5	15	-	15	-	-	-
2.7	PA-ME-FG	66.5	3.5	10	-	10	10	-	-
2.8	ATH	66.5	3.5	-	-	-	-	30	-

[a] Light Green = samples of the PA/TA/ME/FG group, Darker Green = mineral-filler-containing sample.

[b] SEBS-g-MA = polystyrene-*b*-poly(ethylene-*r*-butylene)-*b*-polystyrene-*g*-maleic anhydride, PA = phytic acid sodium salt hydrate, TA = tannic acid, ME = melamine, FG = fish gelatin, ATH = alumina trihydrate, Irg = Irganox® 1010.

Figure 3.7 illustrates the four-dimensional design space for the PA-TA-ME-FG group (the blue color represents the 4th dimension), with Matrix (ABS + SEBS-g-MA), PA (phytic acid sodium salt), TA (tannic acid + Irg), FG (fish gelatin), and ME (melamine) as the components (vertices of the hypertetrahedron). The enlarged tetrahedron (inset) symbolizes the three-dimensional 4-pseudocomponent subspace obtained by fixing the matrix at a constant value (70 wt%), and it represents the 10 compositions from the PA-TA-ME-FG group (out of 15 possible permutations) that were tested during the Screening Phase: 3 of them had already been tested in the first set of samples (TA, FG, and TA-FG (Table 3.3); gray filled circles in the enlarged tetrahedron in Figure 3.7), and the other 7 were tested in the second set (samples 2.1–2.7 in Table 3.4; black filled circles in Figure 3.7). The MCC runs on the individual PA and ME powders are represented by the 2 black empty circles at the vertices of the hypertetrahedron in Figure 3.7. The ATH composite sample (2.8) and the ATH individual powder are not shown in the figure.

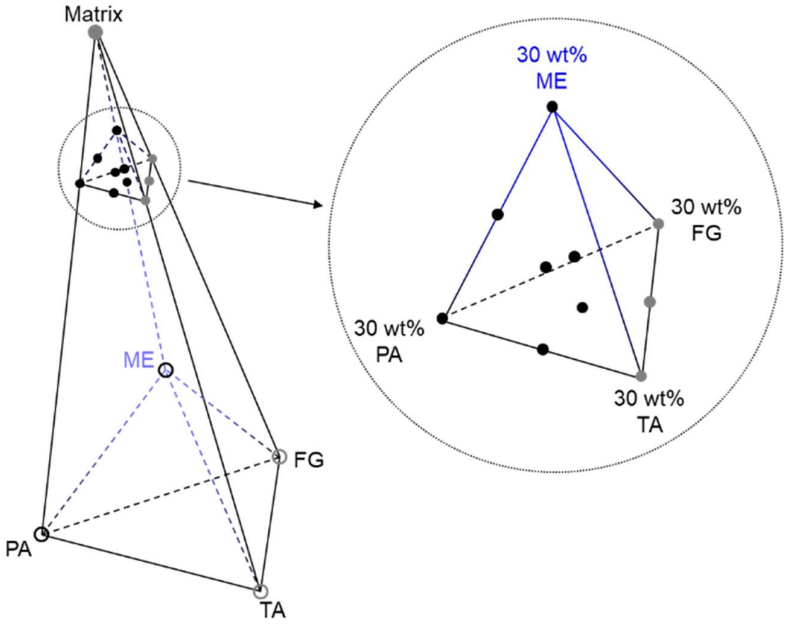

Figure 3.7. Representation of the 4-dimensional design space for the PA-TA-ME-FG group (the 4th dimension is symbolized by the tone of blue). Gray circles represent samples from the 1st set, and black circles represent samples from the 2nd set. Filled circles represent the melt-processed samples, and empty circles represent the samples that were tested as powders (individual FRs). The 5 vertices of the hypertetrahedron represent the pure components of the mixture design for the PA-TA-ME-FG group. The design subspace defined by the enlargement on the right represents the 1-, 2-, 3-, and 4-additive composites containing 70 wt% matrix and 30 wt% FRs. Sample 2.8 (ATH) and the ATH individual powder are not shown.

3.3.
Flammability Results and Discussion

3.3.1.
Vertical Burn Testing

Vertical burn testing was performed on the ABS controls and composites, following a procedure similar to the UL 94 protocol, as a preliminary flammability screening tool. Specimens were cut out from the Phase 1 compression-molded plates in the shape of rectangular bars (127 mm x 12.7 mm x 1.6 mm). The first round of tests was performed in a fume hood with the sash closed. Almost all compositions were tested in repetitions of 1, 2, or 3. Detailed notes were taken on aspects of the samples' burning behaviors, such as:

- Time to self-extinguish the 1st flame;
- Time to self-extinguish the 2nd flame (if applicable);
- Afterglow/ember time after self-extinguishing (if applicable);
- Length of bar covered by flame before self-extinguishing (if applicable);
- Amount and color of smoke (subjective, based on visual observation);
- Amount and description of bubbling (subjective, based on visual observation);
- Whether or not the specimen elongated/stretched before breaking (if applicable);
- Whether the specimen dripped or broke into pieces;
- Number of pieces that broke off from the specimen;
- Time until initial specimen breakage and until break-off of each subsequent piece;
- Time until flame reached the clamp and extinguished;
- Time until the broken pieces extinguished;
- Description of the char;
- General description of the burning process.

Table 3.5 presents some of the parameters that were observed in the closed-sash fume-hood tests: time until 1st and 2nd flame extinguishments, average time until initial specimen breakage, average smoke amount (subjective score from 0 (no smoke) to 1 (much smoke)), and average amount of bubbling (subjective score from 0 (no bubbling) to 1 (much bubbling)). Some samples were not tested in this configuration but are included in the table for the sake of completion; these samples' results are marked as "-". All of the samples, except for the commercial brominated grade of ABS (Br-ABS), burned until the flame reached the clamp ("burned to clamp", btc); Br-ABS, as expected, extinguished the 1st and 2nd flames immediately. Almost none of the samples, including ABS, dripped considerably; instead, they began to elongate after a certain amount of time and, eventually, pieces began breaking off of the specimens. Since all non-commercial samples burned completely, other parameters, such as flame-spread rate and time until sample breakage, were taken into account in order to qualitatively compare their performances. MH and FG-MH (darker golden shade in Table 3.5) were the

samples that took the longest time to break and for which the flame seemed to spread the slowest. The next longest-to-break samples were S6-FG-MH, D-FG, FG, and ATH (lighter golden shade). It is not surprising that MH- and ATH-containing samples remained intact for a relatively long time, since the mineral hydroxides produce a large amount of char as they convert into magnesium oxide and aluminum oxide, respectively; it is worth noting, however, that the "intact" portion of the specimen was only char (as opposed to intact ABS covered in char), which crumbled into ashes when touched. The other FR agent that had a positive effect on the time until breakage was fish gelatin, which was present in most of the samples listed above. The FG-containing samples seemed to contain "fibers" that held the specimen together when it began to elongate, and the after-test residue seemed relatively tough. These observations are in accordance with Deans's hypothesis that fish gelatin might induce cross-linking within thermoplastic samples during melt processing and/or burning [18]. A general observation made during the tests with the sash closed was that there was a significant upward air flux due to the hood's exhaust system, which helped the flame to spread upward along the samples; consequently, these tests imposed more difficult conditions, making it harder for samples to be successful.

Table 3.5

Results from vertical burn testing performed in the fume hood with the sash closed[a]

Vertical Burn Tests in the Hood with the Sash Closed							
Sample #	Sample Name	Specimen	Time to Self-Extinguish[b] [s]		Time until Sample Breakage [s]	Bubbling Amount[c]	Smoke Amount[c]
			1st Flame	2nd Flame			
1.1	ABS	1	btc	n/a	30 ± 5	1.0	1.0
		2	btc	n/a			
1.2	ABS/MA	1	btc	n/a	33 ± 4	0.8	1.0
		2	btc	n/a			
1.3	TA	1	btc	n/a	30 ± 4	0.9	0.8
		2	btc	n/a			
1.4	D	1	btc	n/a	38 ± 18	0.5	0.8
		2	btc	n/a			
1.5	S6	1	btc	n/a	35 ± 7	0.3	0.8
		2	btc	n/a			
1.6	FG	1	btc	n/a	61 ± 37	0.5	0.3
		2	btc	n/a			
1.7	MH	1	btc	n/a	105 ± 7	0.3	0.5
		2	btc	n/a			
1.8	TA-D	1	btc	n/a	38 ± 11	0.3	0.8
		2	btc	n/a			
1.9	TA-S6	1	btc	n/a	33 ± 11	0.4	1.0
		2	btc	n/a			
1.10	TA-FG	-	-	-	-	-	-
1.11	TA-MH	1	btc	n/a	54 ± 1	0.9	0.6
		2	btc	n/a			
1.12	D-S6	1	btc	n/a	39 ± 16	0.3	0.5
		2	btc	n/a			
1.13	D-FG	1	btc	n/a	69 ± 54	1.0	0.8
		2	btc	n/a			
1.14	D-MH	-	-	-	-	-	-
1.15	S6-FG	1	btc	n/a	40 ± 0	0.4	0.7
		2	btc	n/a			
1.16	S6-MH	-	-	-	-	-	-
1.17	FG-MH	1	btc	n/a	138 ± 32	0.5	0.9
		2	btc	n/a			

(continued on next page)

[a] Yellow = samples that self-extinguished at least once, Darker Gold = samples that took the longest to break or did not break, Lighter Gold = samples that took the next-longest before breaking.

[b] btc = burned to clamp.

[c] Bubbling Amount and Smoke Amount are in scales of 0 to 1 based on subjective visual observations (0 = no bubbling/smoke, 1 = much bubbling/smoke).

[d] Results marked as "-" refer to samples that were not tested in this configuration.

[e] Question marks ("?") refer to data that was not clearly observed or recorded.

Table 3.5 (cont.)

Results from vertical burn testing performed in the fume hood with the sash closed[a]

Vertical Burn Tests in the Hood with the Sash Closed (cont.)							
Sample #	Sample Name	Specimen	Time to Self-Extinguish[b] [s]		Time until Sample Breakage [s]	Bubbling Amount[c]	Smoke Amount[c]
			1st Flame	2nd Flame			
1.18	TA-D-S6	1 2	btc btc	n/a n/a	43 ± 11	0.6	1.0
1.19	TA-D-FG	1 2 3	btc btc btc	n/a n/a n/a	42 ± 17	0.5	0.8
1.20	TA-D-MH	1 2	btc btc	n/a n/a	37 ± 5	0.4	0.6
1.21	TA-S6-FG	1 2	btc btc	n/a n/a	22 ± 2	0.7	0.9
1.22	TA-S6-MH	1 2	btc btc	n/a n/a	40 ± 0	0.2	0.5
1.23	TA-FG-MH	1 2	btc btc	n/a n/a	55 ± 7	0.3	0.8
1.24	S6-FG-MH	1 2 3	btc btc btc	n/a n/a n/a	82 ± 10	0.1	0.4
1.25	Br-ABS	1 2	0 0	0 0	did not break	n/a	n/a
2.1	PA	-	-	-	-	-	-
2.2	PA-TA	-	-	-	-	-	-
2.3	PA-TA-ME	-	-	-	-	-	-
2.4	PA-TA-ME-FG	-	-	-	-	-	-
2.5	ME	-	-	-	-	-	-
2.6	PA-ME	1	btc	n/a	?	?	?
2.7	PA-ME-FG	1	btc	n/a	45	?	?
2.8	ATH	1	btc	n/a	60	?	?

[a] Yellow = samples that self-extinguished at least once, Darker Gold = samples that took the longest to break or did not break, Lighter Gold = samples that took the next-longest before breaking.

[b] btc = burned to clamp.

[c] Bubbling Amount and Smoke Amount are in scales of 0 to 1 based on subjective visual observations (0 = no bubbling/smoke, 1 = much bubbling/smoke).

[d] Results marked as "-" refer to samples that were not tested in this configuration.

[e] Question marks ("?") refer to data that was not clearly observed or recorded.

A second round of tests was performed in the fume hood, this time with the sash open. Since none of the samples were able to self-extinguish in the first round of tests and because of the particularly difficult conditions imposed by the closed-sash configuration, it was decided to ease the testing conditions by opening the sash, with the expectation that, by "lowering the bar", it would be easier to distinguish between more and less successful samples as some would potentially be able to self-extinguish in the new configuration. Testing conditions changed considerably when the sash was open; instead of having a strong upward air stream, there was a significant air flux flowing from the front to the back of the hood, causing the flame to be blown to the backsides of the samples. The specimens, therefore, initially caught fire only on their backsides, while the front remained intact; for some specimens, the flame continued climbing only along the back of the sample, while for others, the flame wrapped around the sample and began to spread along its entirety. It is likely that the inward air flow also swept away some of the combustible volatiles from the area of the flame. The open-sash configuration thus had the opposite effect than the closed-sash one, making it easier for samples to be successful. Almost all samples were tested in the open-sash configuration, in 1, 2, or 3 repetitions. Detailed notes were taken regarding the same aspects as for the closed-sash tests.

Table 3.6 presents some of the parameters that were observed in the open-sash fume-hood tests: time until 1st and 2nd flame extinguishments, average time until initial specimen breakage, average smoke amount (subjective score from 0 to 1), and average amount of bubbling (subjective score from 0 to 1). Some samples were not tested in this configuration but are included in the table for the sake of completion; these samples' results are marked as "-". Once again, pristine ABS burned completely while gradually elongating and breaking into a number of pieces, while Br-ABS self-extinguished immediately following both flame applications. This time, however, a number of ABS composites were able to self-extinguish as well (highlighted in yellow in Table 3.6). Five compositions were able to extinguish both the 1st and the 2nd flames: PA-ME, PA-ME-FG, MH, ATH, and S6-FG. The phytic acid- and melamine-containing samples (PA-ME and PA-ME-FG) were the most successful, extinguishing the 1st flame immediately and the 2nd flame in 48 or 65 s, after it had covered approximately 25 and 50% of the sample, respectively. PA-ME came close to achieving what would be equivalent to a UL 94

V-1 classification (which requires the 1st and 2nd flames both to be extinguished in less than 30 s without dripping flaming particles), although it must be taken into account that the open sash provides an easier testing condition than that present in the UL 94 chamber. Unfortunately, the other PA- and/or ME-containing compositions (samples 2.1 to 2.5) were not tested or did not have their results recorded; it is likely that their performances would have been noteworthy as well. The next-best samples were the ones containing mineral hydroxides: 2 out of the 3 MH specimens and the ATH specimen self-extinguished in under 10 s for the 1st flame and in approximately 75 s for the 2nd flame, having 60, 33, and 50% of their lengths, respectively, covered before self-extinguishing for the 2nd time. The third MH specimen burned completely. S6-FG had a peculiar performance: both specimens were able to self-extinguish following the 1st flame application, but only after the flame had traveled up the backside of the bar for over 1 minute, covering approximately 65% of its length. One specimen quickly extinguished the 2nd flame as well due to the char that had accumulated near the bottom of the sample, while the other specimen burned completely as the 2nd flame covered both the front and the back of the bar. Three other samples were able to extinguish the 1st but not the 2nd flame: one S6 specimen extinguished the 1st flame immediately, but the 2nd flame reached the clamp; one FG specimen extinguished the 1st flame immediately, while the 2nd flame reached the clamp; and one TA-D-FG specimen extinguished the 1st flame in 27 s but burned completely after the 2nd flame application. The second specimen of each of these compositions were unable to self-extinguish. In summary, the flame retardants that performed the best when the tests were held in the open-sash configuration were PA and/or ME, followed closely by the mineral hydroxides (MH and ATH), followed by Safire™ 600 and fish gelatin. In terms of time until sample breakage, which only applies to the specimens that did not extinguish both flames, MH and FG once again took the longest time to break (light golden shaded in Table 3.6).

Table 3.6

Results from vertical burn testing performed in the fume hood with the sash open[a]

Vertical Burn Tests in the Hood with the Sash Open							
Sample #	Sample Name	Specimen	Time to Self-Extinguish[b] [s]		Time until Sample Breakage [s]	Bubbling Amount[c]	Smoke Amount[c]
			1st Flame	2nd Flame			
1.1	ABS	1	btc	n/a	68 ± 11	1.0	1.0
		2	btc	n/a			
1.2	ABS/MA	1	btc	n/a	66	1.0	1.0
1.3	TA	1	btc	n/a	100	0.7	0.6
1.4	D	1	btc	n/a	138	0.0	0.4
1.5	S6	1	0	frc	103 ± 18	0.6	0.6
		2	frc	n/a			
1.6	FG	1	0	frc	193 ± 39	0.0	0.2
		2	frc	n/a			
1.7	MH	1	0	77	did not break	0.0	0.2
		2	btc	n/a	230		
		3	10	74	did not break		
1.8	TA-D	1	btc	n/a	130	0.2	0.8
1.9	TA-S6	1	btc	n/a	120	0.0	1.0
1.10	TA-FG	-	-	-	-	-	-
1.11	TA-MH	1	btc	n/a	97	0.8	1.0
1.12	D-S6	1	btc	n/a	100	0.4	0.3
1.13	D-FG	1	btc	n/a	64 ± 51	1.0	0.8
		2	btc	n/a			
1.14	D-MH	-	-	-	-	-	-
1.15	S6-FG	1	80	11	did not break	0.5	0.5
		2	64	btc	91		
1.16	S6-MH	-	-	-	-	-	-
1.17	FG-MH	1	btc	n/a	125	1.0	1.0
1.18	TA-D-S6	1	btc	n/a	100	0.6	1.0
1.19	TA-D-FG	1	27	btc	151 ± 30	0.2	0.6
		2	btc	n/a			
1.20	TA-D-MH	1	btc	n/a	70	1.0	0.4
1.21	TA-S6-FG	1	btc	n/a	70	0.8	0.7
1.22	TA-S6-MH	1	btc	n/a	130	0.0	0.5
		2	btc	n/a			
1.23	TA-FG-MH	1	btc	n/a	105	0.0	0.8
1.24	S6-FG-MH	1	frc	n/a	125 ± 35	0.3	0.4
		2	frc	n/a			
1.25	Br-ABS	1	0	0	did not break	n/a	n/a
2.1	PA	-	-	-	-	-	-
2.2	PA-TA	-	-	-	-	-	-
2.3	PA-TA-ME	-	-	-	-	-	-
2.4	PA-TA-ME-FG	-	-	-	-	-	-
2.5	ME	-	-	-	-	-	-
2.6	PA-ME	1	0	48	did not break	0.0	0.2
2.7	PA-ME-FG	1	0	65	did not break	0.0	?
2.8	ATH	1	5	78	did not break	0.0	?

[a] Yellow = samples that self-extinguished at least once, Light Gold = samples that took the longest to break or did not break.

[b] btc = burned to clamp, frc = flame reached clamp.

[c] Bubbling Amount and Smoke Amount are in scales of 0 to 1 based on subjective visual observations (0 = no bubbling/smoke, 1 = much bubbling/smoke).

[d] Results marked as "-" refer to samples that were not tested in this configuration.

[e] Question marks ("?") refer to data that was not clearly observed or recorded.

Almost all compositions from the 1st set of samples were also tested in a UL 94 Horizontal-Vertical Flame Chamber, again in the vertical configuration. Testing conditions in the chamber are very similar to those in the fume hood when the sash is closed, only having an apparently weaker upward air flux. The results, shown in Table 3.7, are qualitatively identical to the closed-sash fume-hood configuration: all samples except for Br-ABS burned completely, while the samples that remained intact for the longest amount of time were FG-MH (did not break) and MH. Samples not tested in this configuration have results marked as "-". Samples not tested in this configuration have results marked as "-".

Table 3.7

Results from vertical burn testing performed in the UL 94 Flame Chamber[a]

Vertical Burn Tests in the UL 94 Chamber						
Sample #	Sample Name	Specimen	Time to Self-Extinguish[b] [s]		Time until Sample Breakage [s]	Smoke Amount[c]
			1st Flame	2nd Flame		
1.1	ABS	1	btc	n/a	48	1.0
1.2	ABS/MA	1	btc	n/a	35	1.0
1.3	TA	1	btc	n/a	41	1.0
		2	btc	n/a		
1.4	D	1	btc	n/a	45	0.7
1.5	S6	1	btc	frc	45	1.0
1.6	FG	1	btc	frc	60	?
1.7	MH	1	btc	77	116	0.5
1.8	TA-D	1	btc	n/a	60	1.0
1.9	TA-S6	1	btc	n/a	45	0.5
1.10	TA-FG	-	-	-	-	-
1.11	TA-MH	1	btc	n/a	65	0.5
1.12	D-S6	1	btc	n/a	54	0.7
		2	btc	n/a		
1.13	D-FG	1	btc	n/a	60	1.0
1.14	D-MH	-	-	-	-	-
1.15	S6-FG	1	btc	11	50	1.0
1.16	S6-MH	-	-	-	-	-
1.17	FG-MH	1	btc	n/a	did not break	0.5
		2	btc	n/a		
1.18	TA-D-S6	1	btc	n/a	69	0.8
		2	btc	n/a		
1.19	TA-D-FG	1	btc	btc	70	1.0
1.20	TA-D-MH	1	btc	n/a	40	?
		2	btc	n/a		
1.21	TA-S6-FG	1	btc	n/a	39	1.0
1.22	TA-S6-MH	1	btc	n/a	53	0.7
1.23	TA-FG-MH	1	btc	n/a	63	?
1.24	S6-FG-MH	1	btc	n/a	70	1.0
1.25	Br-ABS	1	0	0	did not break	n/a

[a] Yellow = samples that self-extinguished at least once, Light Gold = samples that took the longest to break or did not break.

[b] btc = burned to clamp.

[c] Smoke Amount is in a scale of 0 to 1 based on subjective visual observations (0 = no smoke, 1 = much smoke).

[d] Results marked as "-" refer to samples that were not tested in this configuration.

[e] Question marks ("?") refer to data that was not clearly observed or recorded.

It is possible to conclude that the mineral hydroxides (MH and ATH) and PA and/or ME were the most successful FR agents in the vertical burn tests, as these were present in the only compositions that managed to quickly extinguish the 1st flame and eventually extinguish the 2nd flame in the open-sash tests; it cannot be concluded whether the success of the PA- and ME-containing samples should be credited to PA, ME, both, or a synergistic combination of the two. In terms of sample breakage, MH, ATH, and FG kept the sample intact for the longest amounts of time. Smoke release was generally worse in samples containing Safire™ 600, tannic acid, or DNA (although the latter had a better smoke-release performance for open-sash tests) and better in samples containing magnesium hydroxide or fish gelatin; this inference was reached by using a simple weighted-average calculation that considered that, for each FR, each sample had a weight of *1/n* (where *n* was the number of different FRs in that sample), thus dividing the "responsibility" of the smoke release evenly between the FRs of a given sample. These results, if looked at by themselves, would have led to the selection of samples containing MH, FG, PA, and ME to be further studied in Phase 2 (Detailed Analysis Phase); however, it is clear that the results from the vertical burn tests are very subjective, none of the samples had an exceptionally good performance, and the results were dependent upon testing conditions. It was therefore decided to base the selection of samples for Phase 2 on a more objective and quantitative screening experiment that was not based on a pass-no pass criteria but, instead, would provide unbiased numerical parameters for every sample. Microscale combustion calorimetry (MCC) was chosen as the analysis method to be used for the remainder of the Screening Phase.

3.3.2.
Microscale Combustion Calorimetry

3.3.2.1.
MCC Curves and Results

Microscale combustion calorimetry (MCC) was used to determine the flammability of the controls, composites, and individual components during the Screening Phase. This technique was chosen because it allows for a relatively fast analysis using small samples (when compared to cone calorimetry, for example),

making it possible to test a large quantity of materials in a short amount of time. Furthermore, previous authors have shown that there are correlations between MCC results and those from other combustion or flammability tests (e.g. cone calorimetry, limiting oxygen index (LOI), and UL 94 tests) when analyzing polymers that contain non-halogenated flame retardants [103,104,106,107], and MCC has been indicated as an appropriate tool to conduct rapid flammability screening of FR compounds [103–105]. A combustor temperature of 900 °C was used to ensure complete combustion of the samples.

Three parameters were extracted from the MCC experiments and analyzed: the peak heat release rate (PHRR), the total heat release (THR), and the amount of residue remaining at the end of the test (char yield). The PHRR is a very important parameter in flammability studies [88,108], because it measures how fast heat is being released from a burning material at the peak of combustion. In a real-world scenario, the amount of heat released per unit time from a burning object can make the difference of whether or not nearby objects reach their flash point and begin to burn as well. Therefore, flame spread is strongly influenced by the PHRR. The THR is also an important parameter, as it measures the total amount of thermal energy released by an object while it is burning, which can also influence the spread of a fire to nearby objects. Char yield plays an important role in a fire scenario, since a burning object's structural integrity can depend on how much of the material has burned and how much has remained intact.

Table 3.8 presents average MCC results for the individual components: melt-processed ABS, each FR (tested as a powder), the antioxidant (Irg), and the 2 compatibilizers originally considered for this study (SEBS-g-MA and SMA). All of the FR agents are much less flammable than ABS, as expected; Irg is also less flammable than the control. The two compatibilizers, on the other hand, have a significantly higher flammability. The FRs are listed in order of increasing flammable content, which correlates to the compounds' organic contents (OC): the mineral fillers (ATH and MH) are inorganic, having THR and PHRR values close to 0 and a high char yield; PA has a small OC, having only a slightly higher PHRR; S6 and D have some OC, but still contain inorganic elements (Mg and/or P), showing slightly higher PHRR and/or THR values and lower char yields; TA, ME, and FG are fully organic, having even higher PHRR and THR results and leaving less residue. The reason for the inclusion of the "HRR(454 °C)" column, which

refers to the compounds' HRR values at 454 °C (ABS's average PHRR temperature), will be explained in the next sub-section.

Table 3.8

MCC results of individual components (neat ABS, FR additives, antioxidant, and compatibilizers)[a]

Compound[b]	Physical Form	PHRR[f] [W/g]	HRR(454 °C)[d] [W/g]	THR[f] [kJ/g]	Char Yield [%]
ABS[c]	melt-processed	614 ± 17	599 ± 17	37.8 ± 0.5	0 ± 0
ATH[f]	powder	2 ± 0	1.5 ± 0.2	0.0 ± 0.0	69 ± 1
MH[f]	powder	6 ± 1	4.0 ± 1.2	0.3 ± 0.0	77 [e]
PA[f]	powder	19 ± 2	1.9 ± 0.3	0.5 ± 0.1	81 ± 0
S6[f]	powder	18 ± 1	13.2 ± 0.3	2.8 [e]	51 ± 2
D[f]	powder	41 [e]	8.9 [e]	4.9 [e]	44 [e]
TA[f]	powder	142 ± 30	5.7 ± 1.0	7.4 ± 0.1	23 ± 2
ME[f]	powder	161 ± 2	2.8 ± 0.1	11.5 ± 0.8	0 ± 0
FG[f]	powder	167 ± 9	16.7 ± 2.1	12.6 ± 0.5	22 ± 3
Irg[f]	powder	321 ± 29	299 ± 36	31.4 ± 1.0	4 ± 2
SMA[f]	pellet	869 [e]	210 [e]	38.5 [e]	0 [e]
SEBS-g-MA[f]	pellet	890 [e]	859 [e]	40.2 [e]	0 [e]

[a] Gray = control, Green = FR additives, Light Blue = antioxidant, Darker Blue = compatibilizers.

[b] All compounds listed, with the exception of ABS, are pure, as-received materials.

[c] Pure ABS melt processed through batch mixing followed by compression molding.

[d] HRR(454 °C) is the heat release rate at the temperature of 454 °C, which is the average PHRR temperature for neat ABS.

[e] Only one valid repetition was performed that allowed the determination of this result, so the standard deviation is not available.

[f] ATH = alumina trihydrate, MH = magnesium hydroxide, PA = phytic acid sodium salt hydrate, S6 = Safire™ 600, D = DNA, TA = tannic acid, ME = melamine, FG = fish gelatin, Irg = Irganox® 1010, SMA = styrene-maleic anhydride random copolymer, SEBS-g-MA = polystyrene-*b*-poly(ethylene-*r*-butylene)-*b*-polystyrene-*g*-maleic anhydride, PHRR = peak heat release rate, THR = total heat release.

Figure 3.8 exhibits representative heat release rate (HRR) curves for ABS, ABS/MA, Br-ABS, and the ABS composites containing 1 FR additive. It is evident that all of the flame retardants are successful in reducing ABS's PHRR and THR (area under the curve); the TA composite even achieves the PHRR level of Br-ABS, the commercial halogenated product. The small peaks or shoulders to the left of the main peaks (~300–380 °C) refer to the degradations of the additives themselves,

which always occur before the polymer's decomposition (main peaks, ~400–500 °C). It is interesting to note that most of the FRs cause a small anticipation in the main peak, which refers to ABS's decomposition. Figure 3.9 and Figure 3.10 show the composites' curves in more detail, presenting them in pairs and comparing them to ABS and Br-ABS, the two "extremities"; Figure 3.9 presents the samples that contain bio-based FRs, while Figure 3.10 portrays the compositions that contain low-toxicity commercial FRs. TA and PA composites (Figure 3.9a) reach the closest results to halogenated Br-ABS. It is relevant to briefly discuss the peaks or shoulders that refer to the degradation of the FR additives (~300–380 °C) in terms of their possible impacts on flame spread in real fire scenarios. These peaks occur at lower temperatures than the polymer's degradation peak; if they are excessively high, there is a potential risk that enough heat will be released per unit time to begin to spread the fire to nearby objects before the main PHRR is reached, essentially making the fire spread faster than in the case of the pure polymer, which is the opposite of the desired effect. This undesired situation would not be expected to occur, however, if the materials produced in this study were scaled up and exposed to large fires, as long as the FR loading level was maintained; it should be noted that the important parameter to determine whether a fire will spread to nearby objects (PHRR) is not the *total* amount of heat released per unit time at the peak of decomposition, but the amount of heat released *per unit area* of a burning surface per unit time, which translates into the increase in the energy *density* (i.e. per unit volume) in the environment surrounding the burning material. If the FR content is maintained at approximately 30 wt%, the size of the initial peak/shoulder, in terms of HRR *per unit mass* or *per unit surface area*, should not increase, regardless of how large the material is, because the concentration of the additives is not increased; therefore, the size of the initial peak/shoulder, which refers to the degradation of the FR additives, is not expected to be an issue even if the material is scaled up and exposed to a large fire scenario.

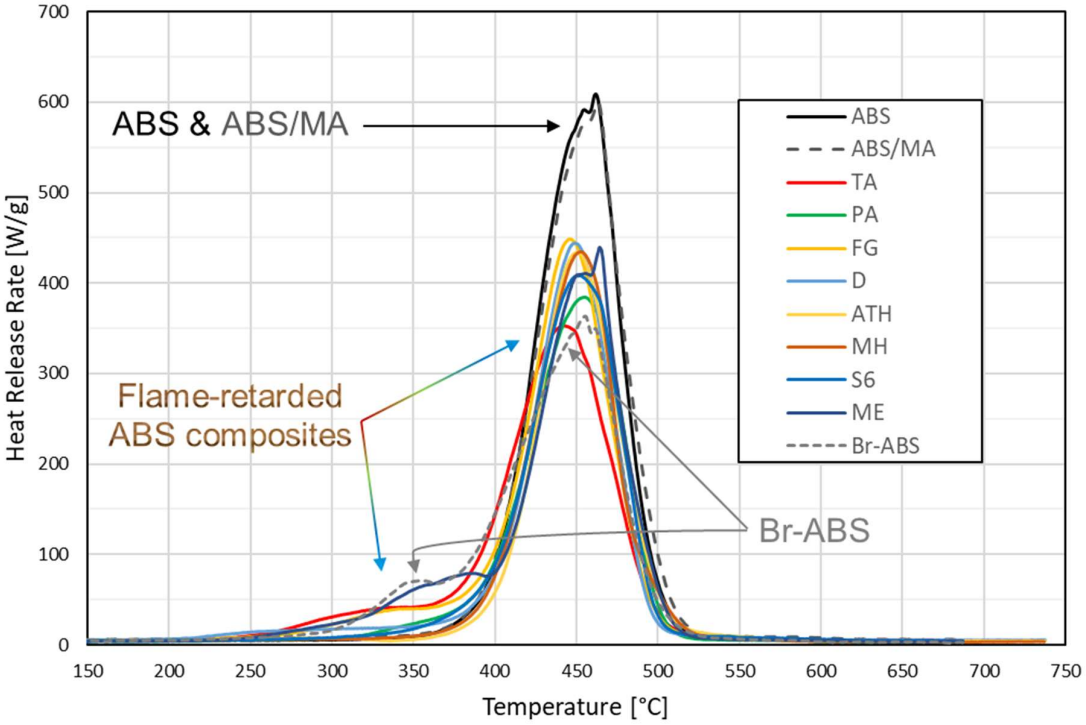

Figure 3.8. Representative HRR curves, obtained by MCC, for ABS, ABS/MA, Br-ABS, and the 8 ABS composites that contain 1 FR additive: tannic acid, phytic acid sodium salt, fish gelatin, DNA, alumina trihydrate, magnesium hydroxide, Safire™ 600, and melamine.

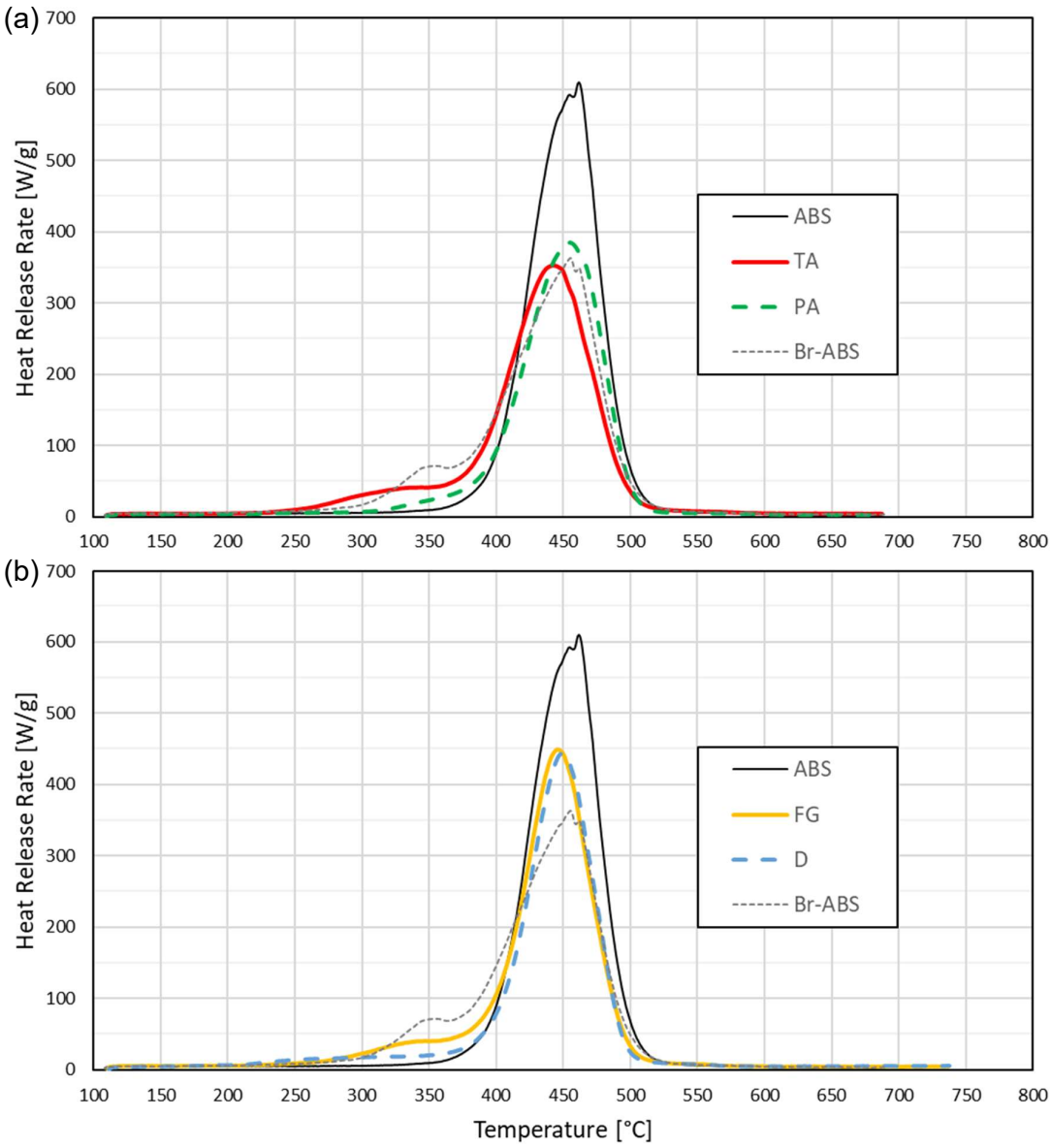

Figure 3.9. Representative HRR curves, obtained by MCC, for ABS composites containing 1 bio-based flame retardant: (a) tannic acid and phytic acid sodium salt and (b) fish gelatin and DNA. Controls ABS and Br-ABS are shown for comparison.

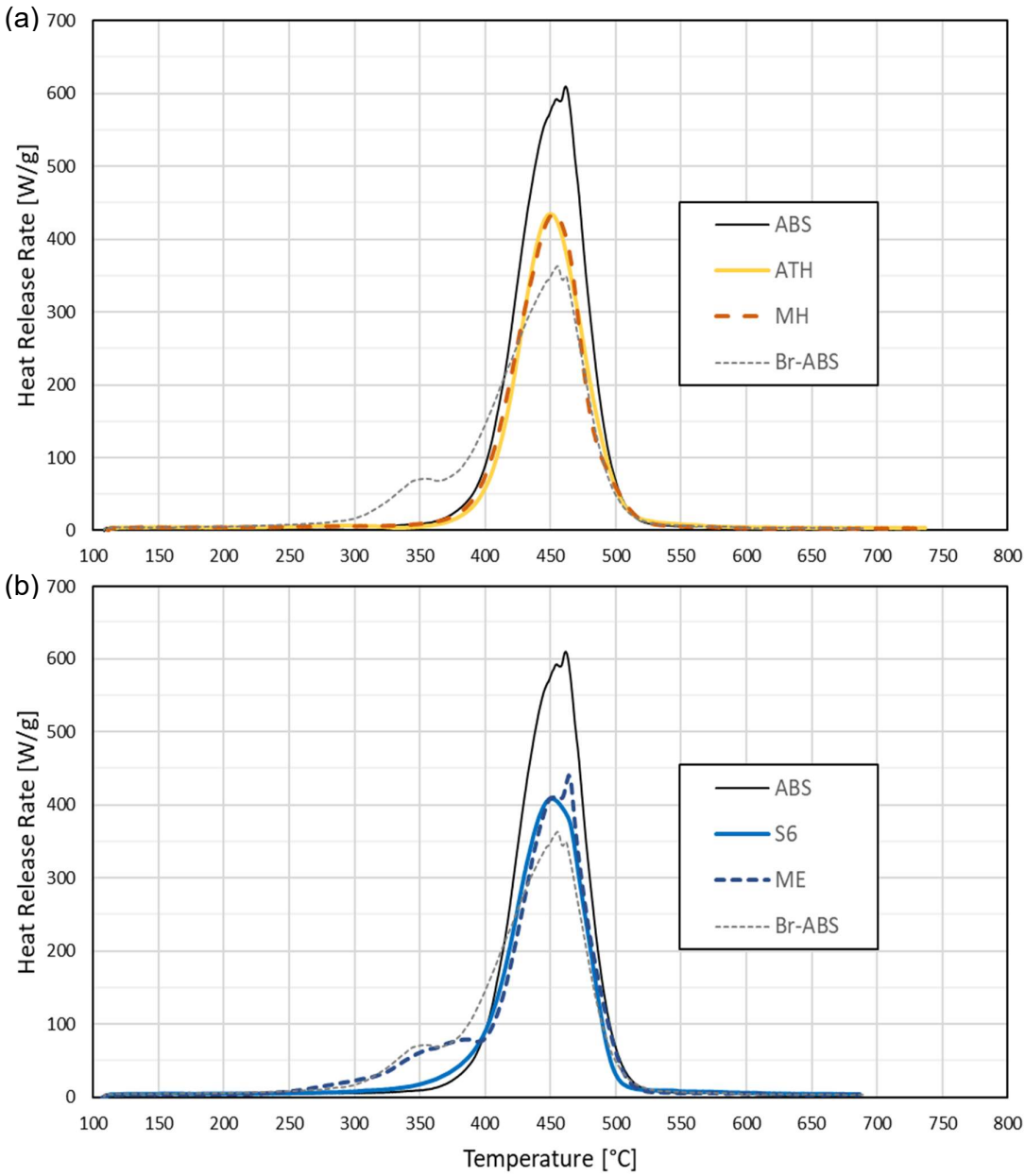

Figure 3.10. Representative HRR curves, obtained by MCC, for ABS composites containing 1 low-toxicity commercial flame retardant: (a) mineral fillers (alumina trihydrate and magnesium hydroxide) and (b) Safire™ 600 (melamine poly(magnesium phosphate)) and melamine. Controls ABS and Br-ABS are shown for comparison.

Average PHRR, THR, and char yield results for each of the control and composite samples are presented in Figure 3.11. A quick analysis of the data reveals that the FRs reduced the flammability of ABS, since all of the composites have lower PHRR (26–43% reduction), lower THR (16–29% reduction), and higher char yield than the neat polymer. The reduction of flammability was expected, because the addition of FR compounds into the polymer, at the very least, reduces the flammable content of the material. In other words, each of the FRs individually is much less flammable than ABS, so they dilute the fuel content. ABS and ABS/MA presented statistically equivalent results for all of the parameters, indicating that the compatibilizer did not affect the performance of the pure polymer.

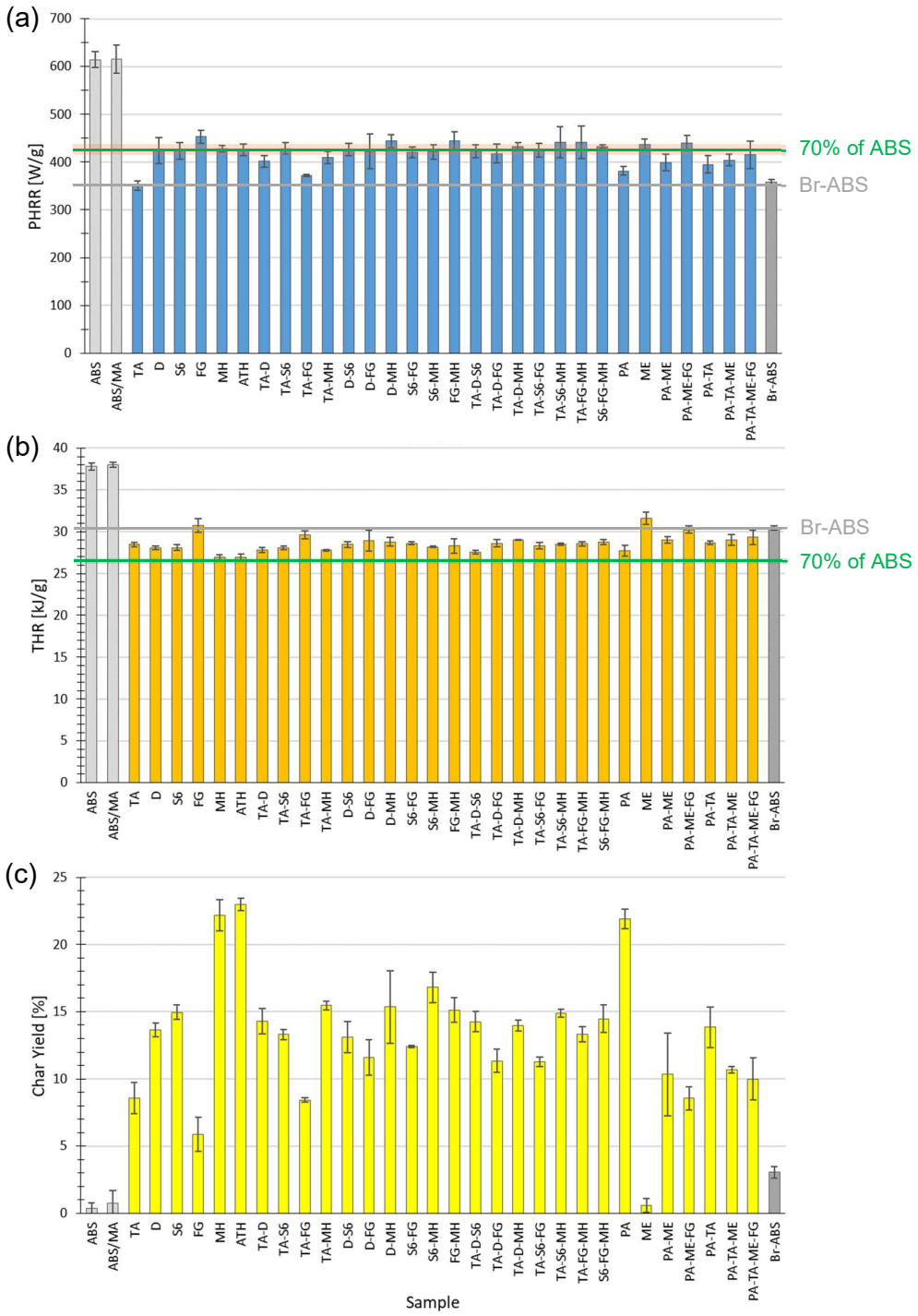

Figure 3.11. (a) Peak heat release rate, (b) total heat release, and (c) char yield results of unmodified ABS and flame-retarded ABS samples, obtained by MCC. Gray bars represent control samples, and colored bars represent FR ABS composites. Error bars indicate standard deviations. The 30% reduction lines (green horizontal lines) in (a) and (b) are accompanied by their standard deviations (light green shaded rectangles).

Figure 3.11a shows that all of the composites presented large reductions in PHRR (between 26 and 43%) compared to neat ABS. The fact that reductions above 30% were observed (bars below the horizontal green line) indicates that some of the FRs do more than just dilute the fuel content, since the FR content of the samples is only 30 wt%. Instead, these FRs (most notably tannic acid and phytic acid sodium salt) interact synergistically with the matrix and effectively slow down its rate of combustion, either by slowing down its decomposition into volatile radicals or by retarding the radicals' reactions with oxygen. Furthermore, some of the samples, especially TA, achieved results comparable to the commercial halogenated flame-retardant product, Br-ABS, which is a promising result. The composites with tannic acid (TA), tannic acid and fish gelatin (TA-FG), and phytic acid sodium salt (PA) presented the best performances, showing improvements of 43, 39, and 38%, respectively, relative to neat ABS.

THR reductions between 16 and 29% were observed in relation to neat ABS (Figure 3.11b). Many composites presented reductions smaller than 30% (bars above the horizontal green line) because most of the FRs used contain organic components; even though these organic components are responsible for slowing down the decomposition of ABS, effectively reducing the PHRR, they do eventually decompose exothermically, contributing to the total heat released by the sample. The relative performances between the composites were directly related to the organic contents (OC) of the FR additives that they contain (represented by the order in which they are listed in Table 3.8), as expected. The lowest THR values were obtained by the mineral fillers (MH and ATH), since these minerals have no OC and do not contribute to the THR (as can be seen in Table 3.8), releasing only water upon decomposition. PA, S6, and D, which have some OC, had intermediate results. The largest values were presented by samples containing fish gelatin (FG) and melamine (ME), which have the largest OC out of the FRs used in this study. The only exception to the trend is that TA, despite being an organic compound (large OC), actually performed as well as PA, S6, and D, all of which contain inorganic elements, further suggesting that tannic acid reduces the flammability of ABS by doing more than just diluting the fuel content. Almost all of the composites presented results better than those of the commercial halogenated product, Br-ABS.

The char yield results (Figure 3.11c) presented the same trend as the THR results, with a negative correlation; this was expected, since samples with a large

amount of residue naturally produce less fuel during the process, resulting, in general, in less total heat released. All of the composites, with the exception of ME, left a larger amount of residue at the end of the test than both neat ABS (~0%) and halogenated Br-ABS (3%). The highest char yields (22–23%) were produced by MH, ATH, and PA (little to no OC), since these FR additives retain most of their masses (~75, 70, and 80%, respectively) when tested individually. S6 and D (some OC) had intermediate results, outperforming TA and FG (high OC). ME (high OC) presented the lowest char yield (~0%), evaporating almost completely [98,99].

3.3.2.2. Additive Hypothesis and the Quantification of Synergy

Further analysis of the data was performed in order to "quantify the synergy" between the FRs and the ABS matrix in each sample – that is, to determine the extent to which the FRs interact synergistically (or antagonistically) with the ABS matrix, as opposed to being simply passive diluents – through a data analysis methodology proposed in the present study. The analysis is based on the assumption, herein called the "additive hypothesis", that if two or more components of a given sample do not interact, the heat release rate (HRR) of the sample will simply be a weighted average of the HRRs of the individual components at any given temperature, within error. Mathematically, this can be expressed as:

$$HRR_{pred,no\_int}(T) = w_A * HRR_A(T) + w_B * HRR_B(T) + \cdots \quad (1)$$

where *A*, *B*, etc. are the components of a given sample, $HRR_{pred,no\_int}(T)$ is the **pred**icted heat release rate of the sample as a function of temperature assuming that there are **no int**eractions between the components, $HRR_i(T)$ is the heat release rate of each individual component as a function of temperature, and w_i is the weight fraction of each component within the sample.

The validity of the additive hypothesis, represented by eq. (1), was supported by the realization of an additional MCC experiment, illustrated in Figure 3.12. A piece of the ABS/MA control sample and a small amount of tannic acid powder*

(weighed at a ratio of 70:30 (w/w)) were placed side-by-side in a single MCC sample holder, but kept separate from one another, forcing there to be no solid- or liquid-phase interactions between the components (dark gray sample in the figure). (*An appropriately small amount of Irg was mixed into the tannic acid powder, since all TA-containing composites contain the antioxidant at a 1:29 (w/w) ratio with TA.) If the hypothesis was correct, the resulting HRR curve would be very similar to the additive hypothesis-based no-interaction prediction because of the forced lack of interactions in the experiment. The resulting HRR curve ("ABS/MA + TA separate", solid dark gray) is indeed almost identical to the proposed no-interaction "Additive Hypothesis Prediction" curve (dotted light gray, obtained as a weighted average of the individual components' HRR curves (blue and dark green)), suggesting that the additive hypothesis is valid. The experiment was also performed with phytic sodium salt powder instead of tannic acid, in two repetitions; the resulting curves are also very similar to the predicted curve, further supporting the hypothesis.

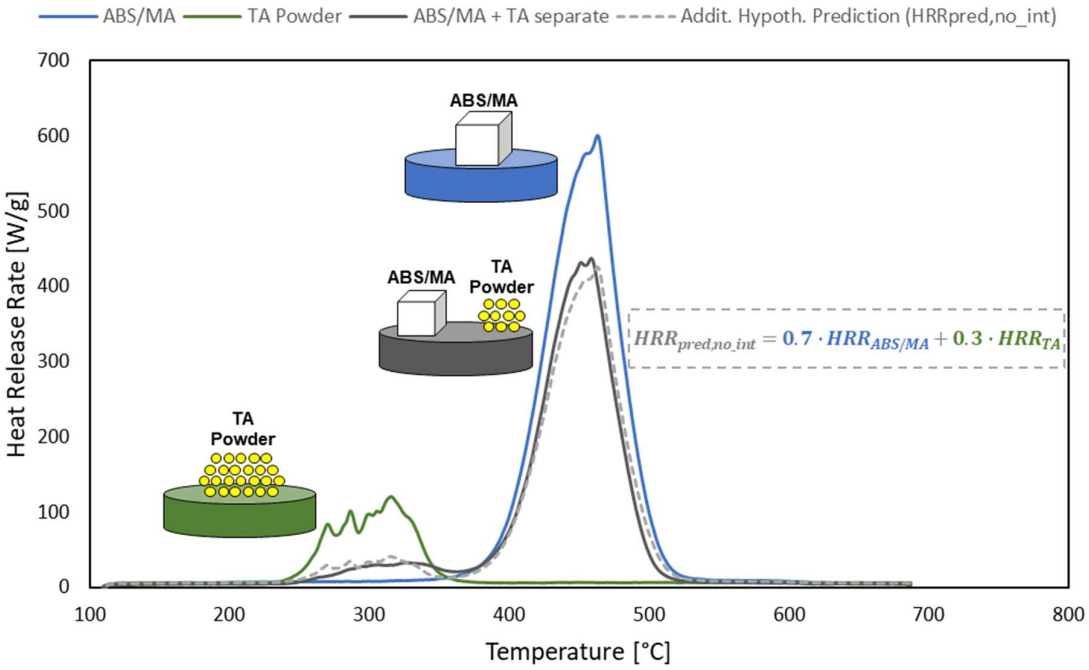

Figure 3.12. Validation of the additive hypothesis. Each of the solid curves represents the HRR, as a function of temperature, resulting from the color-matching MCC experiment to the left: ABS/MA (a blend of ABS and SEBS-g-MA at a 95:5 (w/w) ratio, sample 1.2), tannic acid powder, and ABS/MA and tannic acid powder placed in the same sample holder but kept separate. The dotted curve and equation represent the predicted HRR for a material composed of 70 wt% ABS/MA and 30 wt% tannic acid, *assuming that there are no interactions between the components*; it was calculated as a weighted average of the ABS/MA and TA Powder curves. The similarity between the "ABS/MA + TA separate" and "Addit. Hypoth. Prediction (HRR_{pred,no_int})" curves suggests that the additive hypothesis is valid.

Considering the samples used in this study, which contain a matrix (composed of ABS and SEBS-g-MA compatibilizer at a fixed ratio, thus named "ABS/MA") and at least one flame retardant, eq. (1) can be rewritten as:

$$HRR_{pred,no\_int}(T) = w_{ABS/MA} * HRR_{ABS/MA}(T) + \sum_i \left[w_{FR_i} * HRR_{FR_i}(T)\right]$$

$$= 0.70 * HRR_{ABS/MA}(T) + \sum_i \left[w_{FR_i} * HRR_{FR_i}(T)\right] \quad (2)$$

where *ABS/MA* represents the matrix (which is being considered here as a single "component" containing 95 wt% ABS and 5 wt% SEBS-g-MA) and FR_i represents each individual flame retardant contained in the sample. All of the terms on the right side of this equation are known: (1) $HRR_{ABS/MA}(T)$, which is the heat release rate curve of a "component" containing 95 wt% ABS and 5 wt% SEBS-g-MA, was experimentally determined by analyzing sample 1.2 (ABS/MA) through MCC; (2) $HRR_{FRi}(T)$, which is the heat release rate curve of each individual flame retardant, was also experimentally determined when each individual FR powder was tested by MCC; and (3) the weight fractions of all components in each sample are known (see Table 3.3 and Table 3.4). Therefore, HRR_{pred,no_int}, which is the predicted no-interaction heat release rate, can be calculated for any sample at any given temperature.

Since ABS/MA's HRR curve has a much higher peak than any of the FRs' HRR curve (seen in Figure 3.12 for tannic acid, for example, and listed for all FRs in Table 3.8) and ABS/MA has a higher weight fraction than any of the FRs, the $w_{ABS/MA} * HRR_{ABS/MA}(T)$ term in eq. (2) will always be dominant, so the peak of the sample's predicted HRR curve will occur at about the same temperature as the peak of ABS/MA's HRR curve (see Figure 3.12, for example), which was experimentally determined to be approximately 454 °C, on average. Therefore, by setting *T* in eq. (2) to 454 °C, one can calculate the predicted no-interaction PHRR of each sample:

$$HRR_{pred,\mathrm{no\_int}}(454\ ℃) = 0.70 * HRR_{ABS/MA}(454\ ℃) + \sum_i [w_{FR_i} * HRR_{FR_i}(454\ ℃)] \quad (3)$$

which can be rewritten as

$$PHRR_{pred,no\_int} = 0.70 * PHRR_{ABS/MA} + \sum_i \left[w_{FR_i} * HRR_{FR_i}(454\ ℃)\right] \quad (4)$$

Also, since the THR is the integral of the HRR curve, the THR of each sample, assuming that there are no interactions between the components, can be predicted by:

$$THR_{pred,no\_int} = 0.70 * THR_{ABS/MA} + \sum_i \left(w_{FR_i} * THR_{FR_i}\right) \quad (5)$$

Adopting the same hypothesis for the mass-loss-rate curve, the predicted no-interaction char yield can be calculated in the same fashion:

$$CharYield_{pred,no\_int} = 0.70 * CharYield_{ABS/MA} + \sum_i \left(w_{FR_i} * CharYield_{FR_i}\right) \quad (6)$$

All of the variables on the right sides of eqs. (4), (5), and (6) are known and can be found in Figure 3.11 ($PHRR_{ABS/MA}$, $THR_{ABS/MA}$, $CharYield_{ABS/MA}$), Table 3.8 ($HRR_{FRi(454\ °C)}$, THR_{FRi}, $CharYield_{FRi}$), and Table 3.3 and Table 3.4 (w_{FRi}), allowing the calculation of $PHRR_{pred,no\_int}$, THR_{pred,no_int}, and $CharYield_{pred,no\_int}$ to be performed for any sample in this study.

The next step is to compare the predicted no-interaction parameters with the actual experimental values, for which the "Δ parameters" are introduced:

$$\Delta PHRR = PHRR_{experimental} - PHRR_{pred,no\_int} \quad (7)$$

$$\Delta THR = THR_{experimental} - THR_{pred,no\_int} \quad (8)$$

$$\Delta CharYield = CharYield_{experimental} - CharYield_{pred,no\_int} \quad (9)$$

where $PHRR_{experimental}$, $THR_{experimental}$, and $CharYield_{experimental}$ are the experimental PHRR, THR, and char yield of each sample, respectively.

For ΔPHRR and ΔTHR, significantly large negative numbers indicate that there are synergistic interactions between the components, while large positive

numbers indicate antagonistic interactions. The opposite is true for ΔCharYield, since higher char yields are desirable. For all of the Δ parameters, small values indicate little or no interaction between the matrix and the FRs. Figure 3.13 graphically shows the calculation of ΔPHRR for the TA composite and visually depicts how the additive hypothesis can be used to distinguish between a simple diluent effect and actual synergistic effects. The illustrations in the figure represent 4 MCC experiments that were performed to analyze the interactions between the matrix (ABS/MA) and tannic acid in ABS-TA composites; the resulting HRR(T) curves are shown in matching color. The experiments analyzed ABS/MA individually, tannic acid individually, both materials side-by-side (but forced not to interact, validating the additive hypothesis), and mixed within the ABS-TA composite (sample 1.3). The dotted curve and equation indicate the composite's predicted HRR *assuming that the components do not interact*, representing the additive hypothesis. The difference between the blue and gray curves occurs simply because the fuel content is being decreased, representing a dilution effect; the further reduction from the gray to the dark yellow curves demonstrates the synergistic interaction occurring between tannic acid and the matrix, and graphically represents the ΔPHRR parameter.

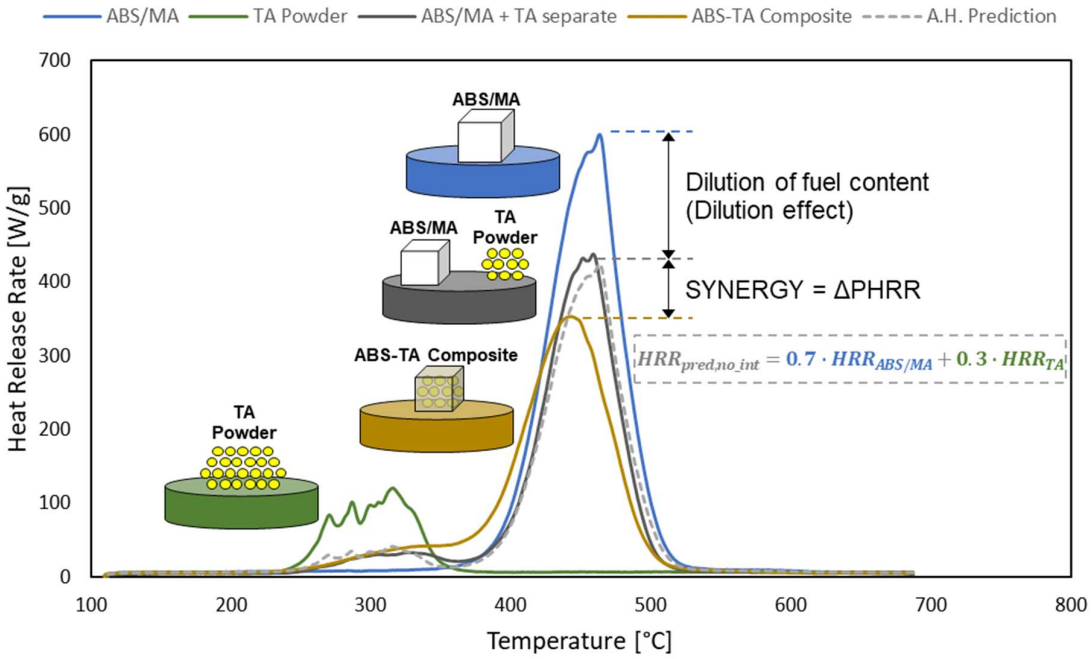

Figure 3.13. Graphical representation of the additive hypothesis – showing how it can be used to quantify the synergy between the FRs and the matrix by distinguishing between a simple dilution effect and actual synergistic effects – and of ΔPHRR.

Finally, standard deviations (σ) for the Δ parameters were calculated through propagation of error based on the standard deviations of the composites' and the pure components' experimental parameters. The uncertainties associated to the different samples' measurements were considered not to be correlated. Mathematically, the standard deviations were calculated as follows, with *Property* referring to PHRR, THR, or Char Yield:

$$\sigma_{Property_{pred,no\_int}} = \sqrt{\left(0.70 * \sigma_{Property_{ABS/MA}}\right)^2 + \sum_i \left[\left(w_{FR_i} * \sigma_{Property_{FR_i}}\right)^2\right]} \quad (10)$$

$$\sigma_{\Delta Property} = \sqrt{\left(\sigma_{Property_{experimental}}\right)^2 + \left(\sigma_{Property_{pred,no\_int}}\right)^2} \quad (11)$$

where $\sigma_{Property\_experimental}$ is the standard deviation related to the composite's PHRR, THR, or char yield and $\sigma_{Property\_ABS/MA}$ and $\sigma_{Property\_FRi}$ are the standard deviations

related to the PHRR, THR, or char yield of the pure components (ABS/MA and each flame retardant, respectively).

In conclusion, mathematical development of the additive hypothesis leads to the possibility of predicting the PHRR, THR, and char yield of any composite sample based on the individual components' results, assuming that the components of the sample do not interact. The difference between each sample's predicted no-interaction results and its actual experimental results indicates the amount of synergistic or antagonistic interaction between the ABS matrix and the FRs (and/or between the different FRs) contained in the sample, allowing one to distinguish between a simple dilution effect and actual synergistic effects by using eqs. (7), (8), and (9). This "quantification of synergy" is graphically depicted in Figure 3.13: when an additive does not interact with the matrix (dark gray), the HRR is reduced from the blue curve (neat ABS/MA) to the gray curves (non-interacting components) because the additive is simply diluting the fuel content; when the additive *does* interact synergistically with the matrix, the HRR is further reduced from the gray curves to the dark yellow curve (ABS-TA composite), representing a quantification of the synergy.

3.3.2.3.
Synergistic Analysis Based on MCC Results

Figure 3.14 presents the ΔPHRR, ΔTHR, and ΔCharYield results for all of the composite samples in this study. Values significantly different than 0 indicate that there is an interaction between the components of a sample (synergistic or antagonistic, as indicated to the right of each graph), and values close to 0 indicate that the components of a sample do not significantly interact in a way that affects its combustion properties. As mentioned earlier, there is no significant interaction between ABS and the compatibilizer SEBS-g-MA in terms of flammability properties, as shown by the gray bars on the left. Also, as expected, no interaction is seen between the components in the experiments that were performed to validate the additive hypothesis (green bars on the right), since the TA and PA powders were not mixed with ABS in those experiments, forcing there to be no interactions. All of the other bars represent the interactions between the components (i.e. the extent

to which the FRs interact with the ABS matrix and/or with each other) in each composite sample analyzed in this study.

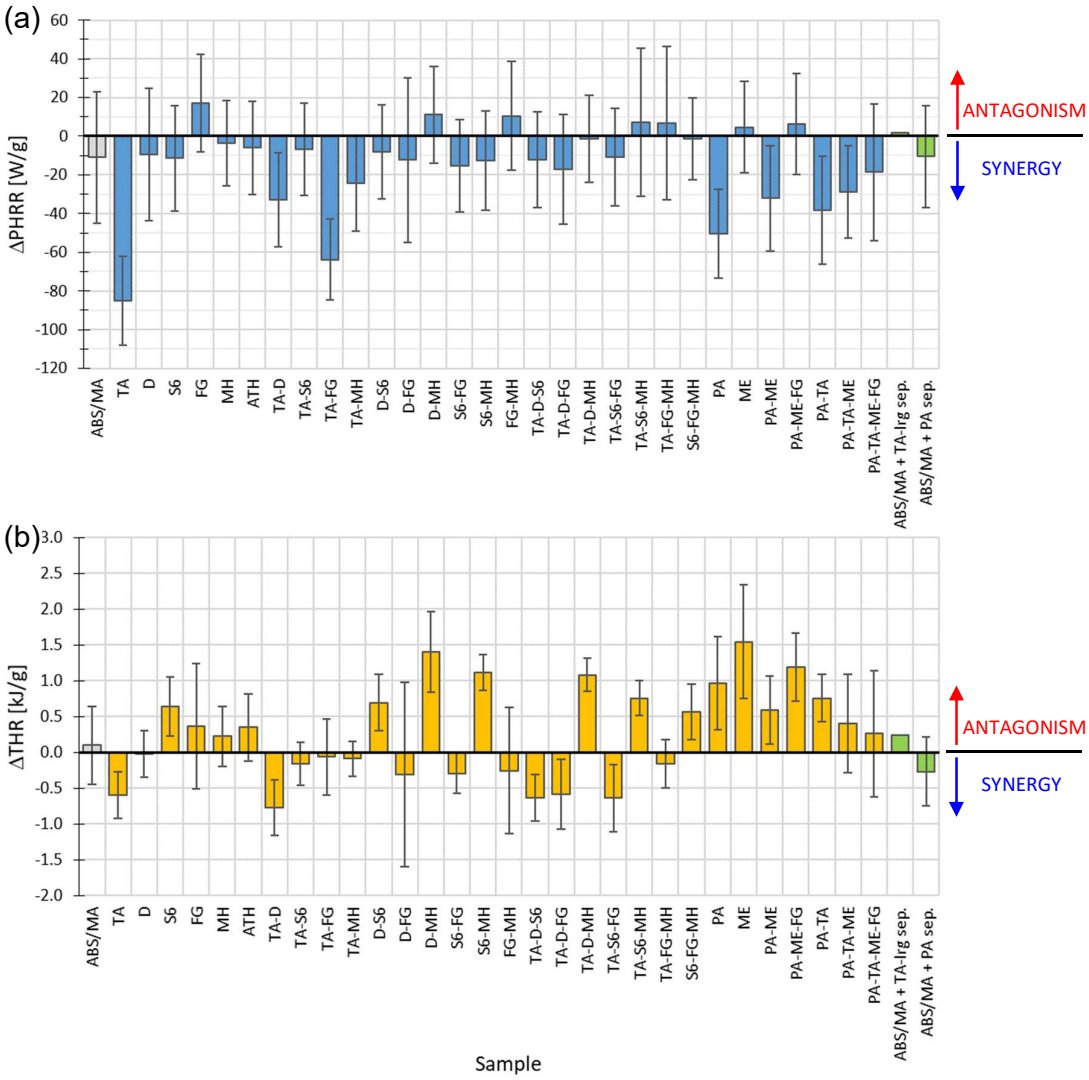

(continued on next page)

Figure 3.14. Quantification of synergy between components in ABS composites, calculated as the difference between each sample's experimental result and its predicted no-interaction result, represented as: (a) ΔPHRR, (b) ΔTHR, and (c) ΔCharYield. Blue, orange, and yellow bars represent interactions between ABS and the FR additives in each composite; gray bars represent interactions between ABS and SEBS-g-MA in the ABS/MA control sample; and green bars represent the experiments performed to validate the additive hypothesis, in which the FRs were forced not to interact with ABS (see Figure 3.12 (dark gray sample)).

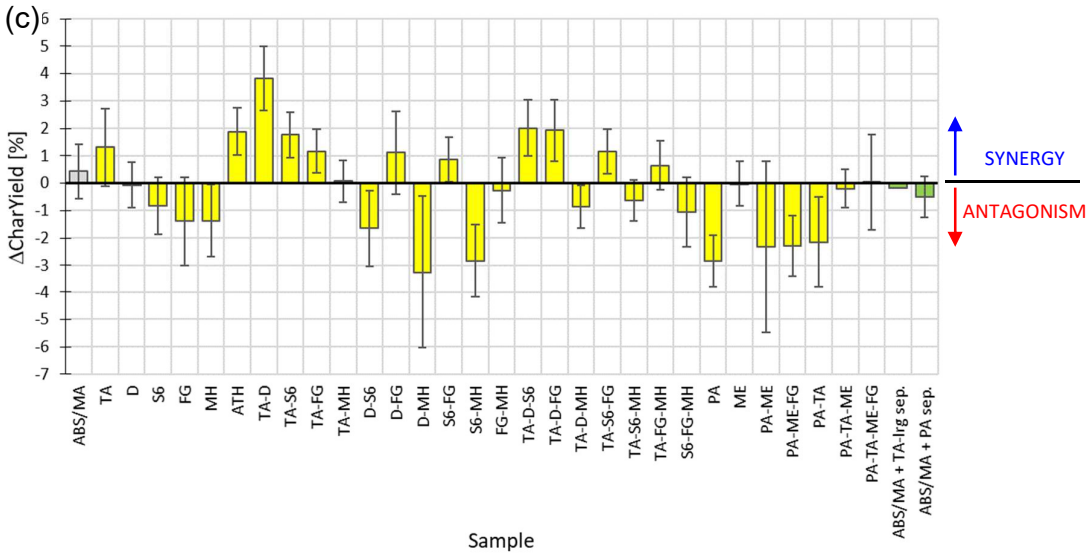

Figure 3.14. (cont.) Quantification of synergy between components in ABS composites, calculated as the difference between each sample's experimental result and its predicted no-interaction result, represented as: (a) ΔPHRR, (b) ΔTHR, and (c) ΔCharYield. Blue, orange, and yellow bars represent interactions between ABS and the FR additives in each composite; gray bars represent interactions between ABS and SEBS-g-MA in the ABS/MA control sample; and green bars represent the experiments performed to validate the additive hypothesis, in which the FRs were forced not to interact with ABS (see Figure 3.12 (dark gray sample)).

The most interesting results can be seen in Figure 3.14a. A number of samples have a very negative ΔPHRR – most notably TA, TA-FG, and PA (approx. -85, -65, and -50 W/g, respectively) –, indicating that the FRs in these samples are not simply acting as diluents, but are interacting synergistically with the matrix and/or with each other to reduce the PHRR beyond the predicted value. In other words, tannic acid, phytic acid sodium salt hydrate, and a tannic acid-fish gelatin mixture are each protecting ABS during combustion, effectively slowing down its decomposition and release of heat. In the case of TA-FG, the negative data point, when analyzed independently, shows there is synergy between any two of the components (tannic acid, fish gelatin, and ABS) and/or between all three of them. It is likely that the synergy between ABS and tannic acid seen in sample TA is maintained in the TA-FG sample, but the fact that the PHRR of TA-FG is much lower than the average of TA's and FG's PHRRs suggests that there is also synergy between tannic acid and fish gelatin, which is in accordance with Deans's findings when the two components were used together in LDPE [18]. Some synergy can also be seen in the ABS/PA-TA and ABS/TA-D systems. None of the composites

presented statistically significant antagonistic interactions. It is interesting to note that the fully nature-derived components and combinations (TA, PA, TA-FG, and to a lesser extent PA-TA and TA-D) led to better results and interact more synergistically with ABS than the synthetic FRs. Tannic acid's successful results, when used both individually and in combination with other FRs, is also noteworthy.

Figure 3.14b and c shows that there is little interaction between the FRs and the matrix in terms of altering the THR and the char yield, since all of the values are close to 0. In other words, even though some of the FRs successfully slow down the combustion of ABS (significantly reducing the PHRR beyond the predicted value), they do not protect the polymer throughout the entire duration of the test. This result was expected, because pyrolysis and combustion are forced to completion in MCC experiments due to the high pyrolysis temperature, small sample size, excess amount of oxygen, and high combustor temperature, causing virtually all of the organic material to decompose and the volatiles to undergo complete combustion by the end of the test [108,113]. It is noteworthy that only TA-containing composites presented some synergy in terms of THR or char yield (with the exception of ATH's char yield), although the amount of synergy is small. Some of the samples, on the other hand, presented slightly positive ΔTHR and/or negative ΔCharYield values, suggesting a small antagonistic effect between the components. In the case of PA, a possible explanation for this is that when phytic acid powder is tested alone, efficient crosslinking is suspected to take place (reducing the amount of volatiles) and significant intumescence occurs (protecting and trapping volatile fragments within the compact char formed on the surface); however, when phytic acid is dispersed in the matrix, it cannot crosslink as effectively nor form as cohesive a char layer, causing more phytic acid degradation products to be generated and to escape than when the compound is tested alone. The synergies and antagonisms seen, however, are small in the case of ΔTHR and ΔCharYield, having little practical value.

Finally, interactions between pairs of FRs were evaluated using a procedure similar to the one based on the additive hypothesis (described in the previous sub-section). The analysis begins by assuming that if 2 given FRs (FR_A and FR_B) do not interact with each other in the environment of an ABS matrix, nor do they interfere with the other one's interactions with the matrix itself, then the parameters of the FR_A-FR_B sample (composite containing both FRs) should be the average of the FR_A

sample's and the FR_B sample's parameters, because FR_A-FR_B contains equal amounts of each FR (15 wt%). Thus, the Δ_2 parameters are introduced:

$$\Delta_2 PHRR = PHRR_{FR_A-FR_B} - \frac{PHRR_{FR_A} + PHRR_{FR_B}}{2} \quad (12)$$

$$\Delta_2 THR = THR_{FR_A-FR_B} - \frac{THR_{FR_A} + THR_{FR_B}}{2} \quad (13)$$

$$\Delta_2 CharYield = CharYield_{FR_A-FR_B} - \frac{CharYield_{FR_A} + CharYield_{FR_B}}{2} \quad (14)$$

If the experimental FR_A-FR_B value is similar to the average of the FR_A and the FR_B values (i.e. Δ_2 is close to 0), then there is no significant interaction between the 2 concerned FRs. On the other hand, if Δ_2 is significantly different than 0 in the direction of synergy, then the 2 FRs interact synergistically with each other and/or improve each other's interaction with ABS. If Δ_2 is significantly different than 0 in the antagonistic direction, then the 2 FRs interact antagonistically with each other and/or worsen each other's interaction with ABS.

Figure 3.15 shows the Δ_2 parameters for each of the samples that contain 2 FRs, indicating if each pair interacts synergistically or antagonistically or if it doesn't interact. One of the most notable values is the synergistic interaction between tannic acid and fish gelatin (sample TA-FG) in reducing the PHRR, which was suggested during the discussion on Figure 3.14a and is in accordance with Deans's findings when the two components were used together in LDPE [18]. This means that when the two FRs are used together, TA and FG help each other to slow down the degradation of ABS. TA-S6, TA-MH, and PA-TA, on the other hand, present antagonistic interactions in terms of PHRR; it is possible that Safire™ 600, magnesium hydroxide, and phytic acid sodium salt interfere negatively with the strong ABS-TA synergy described earlier. Regarding THR and char yield, synergy is generally observed in samples S6-FG, TA-D, and possibly TA-S6, while antagonistic interactions can be seen in samples D-MH, S6-MH, and possibly PA-TA. It is difficult to draw general conclusions from these results, but one can say that fish gelatin tends to interact beneficially with the other flame retardants

(possibly by inducing crosslinking, which gives the other FRs more time to act by delaying the formation of volatiles), while magnesium hydroxide tends to interact prejudicially.

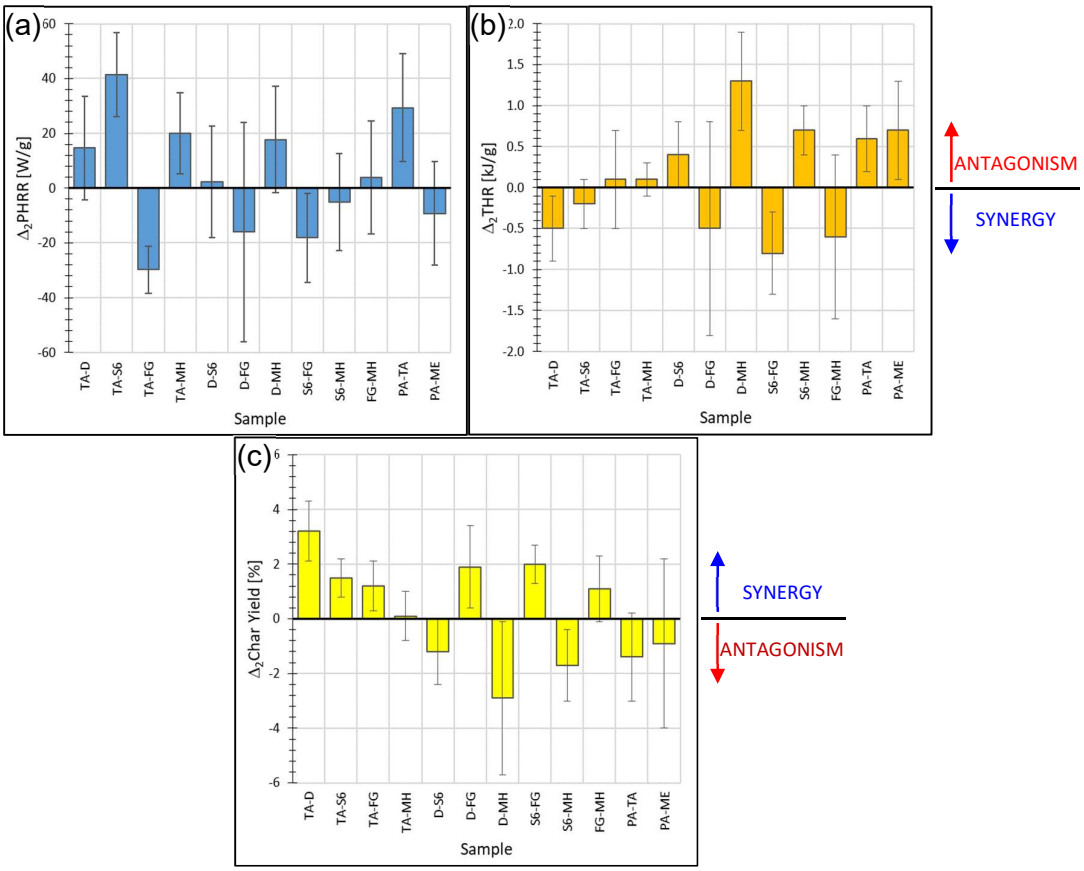

Figure 3.15. Interactions between pairs of FRs: (a) Δ_2PHRR, (b) Δ_2THR, and (c) Δ_2CharYield values, with standard deviations, for ABS composites that contain 2 different FRs. The Δ_2 parameter values represent the difference between the value for a given 2-FR composite and the average value of the composites containing each FR individually. Values significantly different than 0 indicate that there is a net interaction between the 2 FRs in the sample (synergistic or antagonistic, as indicated to the right of each graph); values close to 0 indicate no significant net interaction between the 2 FRs.

3.4. Conclusions

A screening experiment was successfully designed and executed. Materials, experimental techniques, and sample compositions, using Design of Experiments, were selected and planned, and samples were fabricated and tested in order to

evaluate the effects of 8 different bio-based or low-toxicity FR additives and their combinations on the flammability of ABS.

The first flammability analysis method utilized, UL 94-inspired vertical burn testing, did not yield useful results. The FRs that performed the best were, in general, magnesium hydroxide, alumina trihydrate, and phytic acid sodium salt and/or melamine. However, none of the samples were able to achieve a UL 94 rating, sample performances depended on testing conditions, and comparisons between samples were based on subjective observations. This analysis technique was, therefore, not used in the determination of samples to be furthered studied in Phase 2.

MCC was also used to screen the samples' flammability performances, and interesting results were obtained. TA presented the most promising results when tested by MCC, as it greatly reduced ABS's PHRR – achieving results equivalent to or better than a commercial brominated product (Br-ABS) – and was shown to interact synergistically with ABS, improving its PHRR and THR results beyond the predicted no-interaction values. The combination of tannic acid and fish gelatin (TA-FG) also significantly reduced ABS's PHRR beyond the expected amount, which was caused by synergies both between ABS and TA and between TA and FG. The third best composite was PA, which also reduced ABS's PHRR well beyond the expected value, suggesting that there is synergistic interaction between this FR and the matrix. It is quite interesting to note that the best performances were achieved by nature-derived FRs rather than by synthetic or inorganic ones.

The compositions that showed the most interesting results in the MCC tests were chosen, along with the controls, to be studied further. PHRR was selected as the defining parameter, since in a real-world scenario it can be the determinant of whether or not a fire will begin and spread to nearby objects. It is also the parameter in which the largest improvements and synergies were observed in these experiments. TA, TA-FG, and PA clearly showed the best results in terms of both PHRR (raw values) and ΔPHRR (synergy). PA-TA also presented very good results in terms of PHRR and ΔPHRR, and it was a good candidate to be studied further since TA and PA both presented great results when used individually. Therefore, the samples that were selected to be further analyzed in Phase 2 of this study, the Detailed Analysis and Mechanistic Study Phase, were TA, TA-FG, PA, PA-TA, and the controls ABS and Br-ABS.

4

Detailed Analysis and Mechanistic Study of Bio-Based Flame-Retardant ABS Composites

4.1.
Introduction

The previous chapter described a screening experiment, by which the effects of 8 different bio-based or low-toxicity flame retardants on ABS's flammability were evaluated through the fabrication and analysis of 30 FR ABS composites. The most promising samples from the Screening Phase, as evaluated through MCC, were ABS composites filled with tannic acid (TA), tannic acid and fish gelatin (TA-FG), phytic acid sodium salt (PA), and phytic acid sodium salt and tannic acid (PA-TA). These samples were selected, along with 2 controls – neat ABS and a commercial halogenated ABS product (Br-ABS) – to be scaled up and further analyzed in Phase 2 of the present study, the Detailed Analysis and Mechanistic Study Phase. The compositions of the selected samples were the same as previously used in Phase 1 (Table 3.3 and Table 3.4), and are re-presented in Table 4.1 for simplicity.

Table 4.1

Compositions of Phase 2 samples (wt%)[a]

Sample #[b]	Sample Name	ABS	SEBS-g-MA[c]	PA[c]	TA[c]	FG[c]	Irg[c]	TBBPA[c,d]	SbO[c,d]	Others[d]
E1	ABS	100	-	-	-	-	-	-	-	-
E2	Br-ABS[d]	70 - 90	-	-	-	-	-	5 - 20	2 - 6	0 - 9
E3	PA	66.5	3.5	30	-	-	-	-	-	-
E4	PA-TA	66.5	3.5	15	14.5	-	0.5	-	-	-
E5	TA	66.5	3.5	-	29	-	1	-	-	-
E6	TA-FG	66.5	3.5	-	14.5	15	0.5	-	-	-

[a] Gray = control samples, Green = bio-based FR composites.

[b] "E" refers to Extrusion, since all Phase 2 samples were produced through extrusion followed by injection or compression molding.

[c] SEBS-g-MA = polystyrene-*b*-poly(ethylene-*r*-butylene)-*b*-polystyrene-*g*-maleic anhydride, PA = phytic acid sodium salt hydrate, TA = tannic acid, FG = fish gelatin, Irg = Irganox® 1010, TBBPA = tetrabromobisphenol-A, SbO = antimony(III) oxide.

[d] Br-ABS (brominated ABS) is a commercial product. The approximate composition given here was taken from its MSDS. "Others" refers to an impact modifier, stabilizers, and lubricants.

The objectives of the Detailed Analysis and Mechanistic Study Phase were to better understand the flammability and mechanical behaviors of the most promising compositions and to try to comprehend the flame-retardation mechanisms of some of the FR agents. The general experimental methodology of this phase is portrayed in Figure 4.1. The main fabrication technique chosen was extrusion followed by injection molding, facilitating transferability of successful or promising products to industry since this process is widely used in industrial settings. Extrusion followed by compression molding was also used, in order to fabricate samples that would be tested by cone calorimetry, which requires plate-shaped specimens. Cone calorimetry and thermogravimetric analysis (TGA) were selected as analysis techniques; besides providing direct information about flammability behavior and thermal stability, they can potentially provide insights into flame-retardation mechanisms when their results are combined with MCC data [107]. Pyrolysis-gas chromatography-mass spectrometry (Py-GC-MS) was also used to analyze the materials; qualitative and semi-quantitative information about the gases released during pyrolysis can provide valuable mechanistic information as well. Finally, mechanical testing was performed in order to verify the impact of the addition of the FR compounds on the mechanical properties of the polymer: tensile testing was used because it is a standard mechanical-testing technique, and impact testing was selected because ABS is known for its high impact toughness.

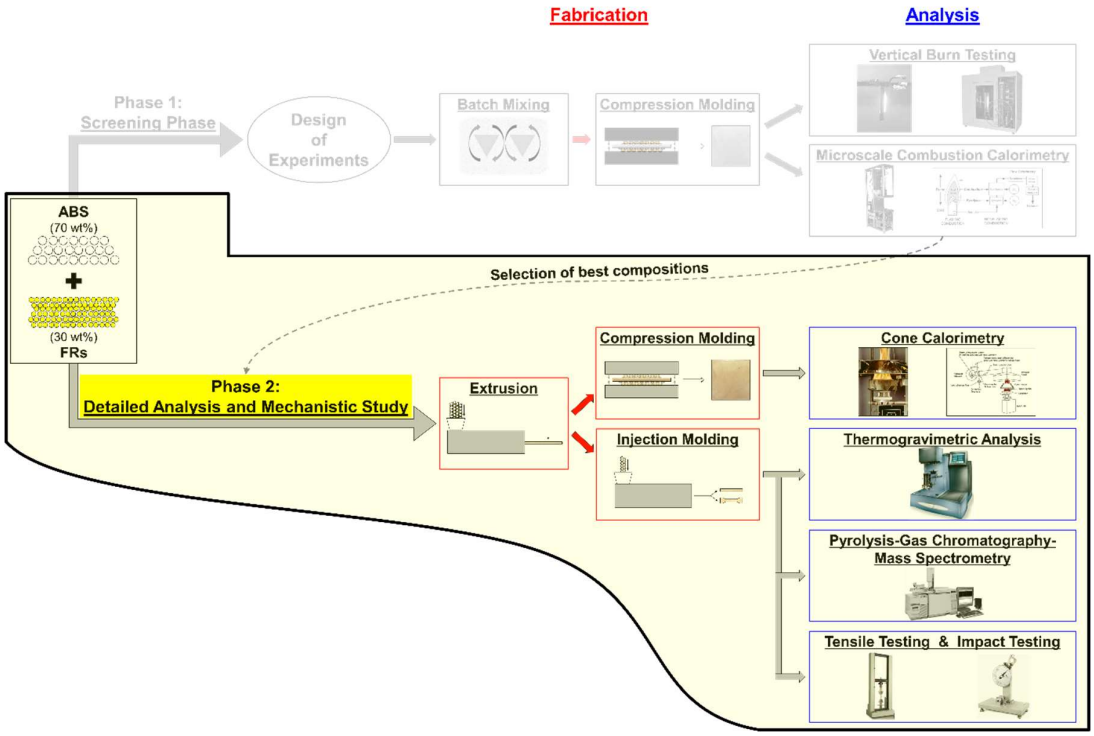

Figure 4.1. Overview of the Detailed Analysis and Mechanistic Study Phase (Phase 2), which is discussed in the present chapter, in the context of the complete experimental methodology of the current project.

4.2.
Cone Calorimetry

Cone calorimetry was used to evaluate the flammability of the six Phase 2 samples. One objective of using this technique was to verify if the FR composites would repeat their promising MCC results when subjected to a medium-scale flaming experiment, which comes closer to representing a real-world fire scenario. Another reason for using cone calorimetry was that it can provide information on flame-retardation mechanisms, especially when its results are compared to those from MCC [107]. Two specimens of each composition were prepared through extrusion followed by compression molding and subsequently tested.

Parameters that were chosen to be analyzed in this work include: time to ignition (TTI), peak heat release rate (PHRR), effective total heat release (THR_{eff}), char yield, and effective heat of combustion (EHC). Four parameters derived from comparisons between cone calorimetry and MCC were also studied: THR Ratio, combustion efficiency (χ), MCC PHRR Ratio (R1), and Cone Calorimetry PHRR

Ratio (R2). The TTI represents the time that it takes for a material to ignite and begin to burn in a fire scenario. The importance of PHRR, THR, and char yield were described in the discussion regarding MCC. The THR_{eff}, which is the THR divided by the mass, is discussed in this section rather than the THR itself; since the HRR in cone calorimetry is normalized by the sample's surface area rather than by its weight, heavier samples can display a higher THR than lighter samples simply because the total amount of material (i.e. fuel) is larger, so the THR_{eff} is a more neutral way to compare values between samples with different masses. The remaining parameters will be described in detail in Section 4.2.2 and are briefly summarized here: (1) the EHC, which is the THR_{eff} divided by (1 – char yield), indicates the amount of heat released per gram of volatiles; (2) dividing the EHC by the equivalent parameter from MCC (the heat of complete combustion, HCC) yields χ, which provides valuable information about the occurrence of gas-phase mechanisms; (3) the THR Ratio (THR_{eff} from cone calorimetry divided by THR from MCC) also gives information about gas-phase mechanisms; and (4) R1 and R2 are related to measures of PHRR in MCC and cone calorimetry and can provide information about condensed-phase mechanisms.

4.2.1. Direct Cone-Calorimetry Results

Figure 4.2 shows the heat release rate curves for the 6 compounds; both specimens are shown for each composition (specimen 1 in (a) and specimen 2 in (b)). It is clear that all of the FRs were able to significantly reduce the polymer's PHRR. All of the compounds showed similar HRR curves for both specimens. ABS presented a single combustion peak with a small shoulder on the left as the entire sample rapidly burned; this behavior is typical of a thermally thin (theoretically no shoulder) or intermediate-thickness (theoretically more noticeable shoulder), non-charring sample [114]. TA-FG did not significantly alter the shape of the curve, lowering the HRR but presenting a single peak with a small shoulder as well; this suggests that this sample was also mostly non-charring. TA, PA, and PA-TA, on the other hand, showed evidence of char formation. TA's HRR curves are typical of a charring sample with intermediate thermal thickness that goes through the steps of (1) initial burning (initial sharp increase in HRR); (2) formation of an efficient

protective char layer that acts as a thermal and gas barrier, protecting the sample underneath (1st peak and subsequent decrease in HRR); (3) cracking of the char layer, exposing the sample to heat and oxygen (2nd increase in HRR, leading up to the 2nd and final peak); and (4) consumption of the remaining fuel (2nd peak and final decrease in HRR) [114]. PA's curves present a sharp change in slope (but not an initial peak) at ~55 s, suggesting that the sample was attempting to form a char layer, which partially protected the specimen (significantly reducing the rate of HRR increase) but was not strong enough or did not form fast enough to actually form a peak and reduce the HRR; despite taking longer to form, the char in this sample appears to have formed just an effective a barrier as the one formed in TA, since the PHRR was kept lower for PA than for TA. PA-TA's HRR curves indicate that the sample was able to rapidly form a strong and cohesive char layer, presenting the best performance out of the bio-based composites: (1) although the initial burning rate (initial slope) was the same as for TA and TA-FG, the 1st peak occurred much quicker (and at a lower HRR value) than for TA, suggesting that char formation occurred very fast; (2) the subsequent reduction in HRR is more pronounced than for TA (especially for specimen 1), suggesting that the char formed was stronger, thicker, and more cohesive; (3) a 2nd intermediate peak was quickly reached (before the final peak) after the HRR began to rise again, showing that the sample was able to quickly re-form the protective char layer after it had begun to crack; and (4) only after the 2nd char forming-char cracking cycle did the curve reach its 3rd and final peak and decrease as the remaining fuel was consumed [114]. It is very interesting that PA-TA performed better than both PA and TA, suggesting that there is a strong flame-retardation synergy between the 2 FRs when used in ABS. The brominated compound, Br-ABS, significantly reduced ABS's HRR without much changing the curve's shape (except for a more pronounced shoulder to the left and an additional lower shoulder or peak to the right of the main peak (~150 s)), showing a close-to-typical behavior for a non-charring sample with intermediate thermal thickness [114]; the absence of char formation was expected, since it is known that halogenated FRs act in the gas phase as radical scavengers rather than in the solid phase as char formers.

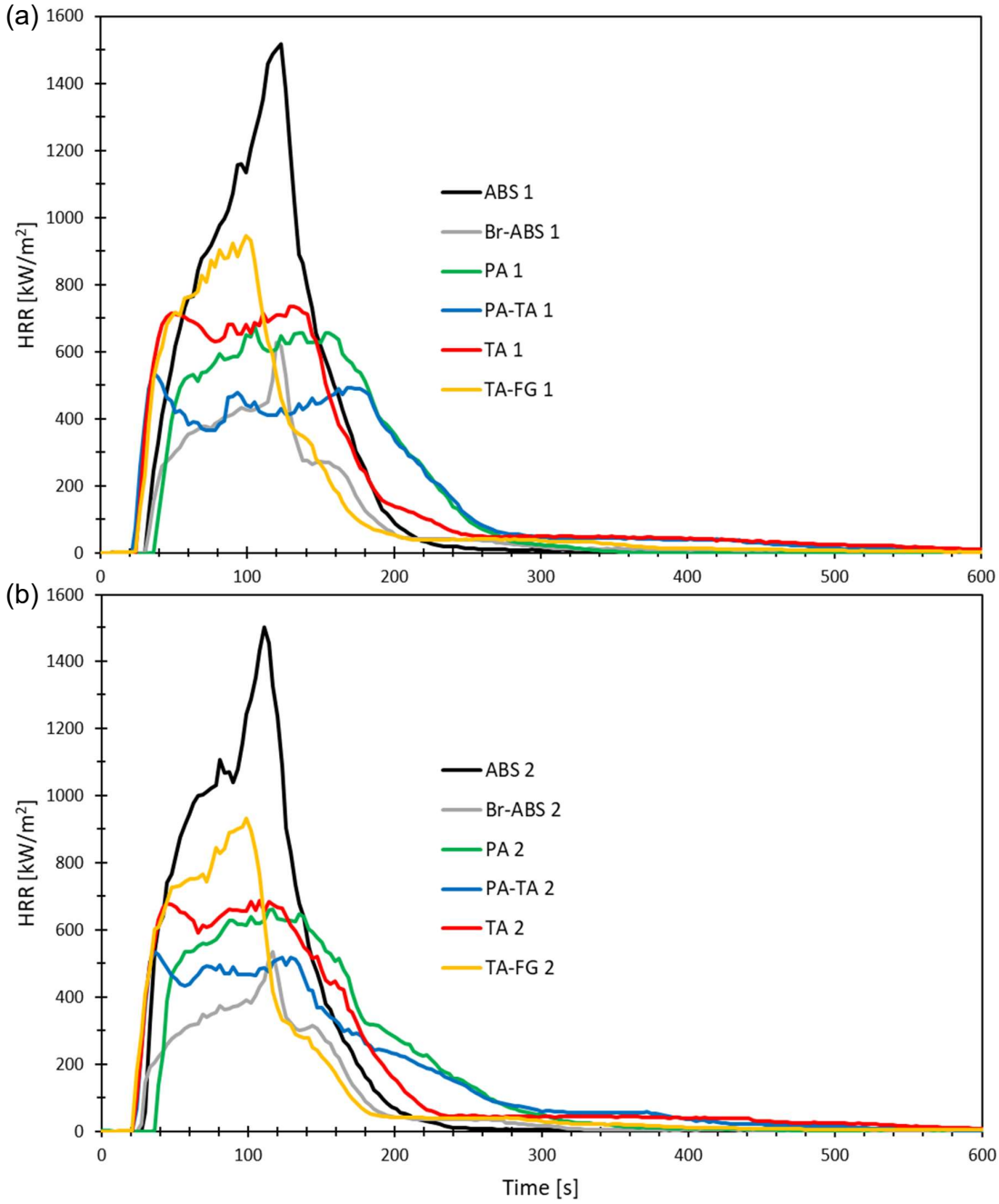

Figure 4.2. Heat release rate curves, obtained by cone calorimetry, for (a) specimen 1 and (b) specimen 2 of neat ABS, commercial halogenated Br-ABS, and bio-based FR ABS composites.

Table 4.2 presents the averages and standard deviations of each sample's flammability properties (TTI, PHRR, THR, THR_{eff}, and char yield). The TTI of ABS was reduced by the addition of tannic acid, as all of the samples containing this additive (PA-TA, TA, and TA-FG) had a smaller TTI than pristine ABS. The reduction can be explained by the fact that tannic acid is an organic molecule that

begins to degrade and release heat at a much lower temperature than the polymer, as can be seen in Figure 3.13. Phytic acid sodium salt (PA), on the other hand, delayed ABS's ignition when used as the only additive. No difference was observed between the commercial brominated ABS and the pristine polymer in terms of TTI.

Table 4.2

Cone calorimetry results of ABS, commercial brominated ABS, and bio-based FR ABS composites[a]

Sample Name	Weight [g]	TTI[b] [s]	PHRR[b] [kW/m^2]	% PHRR Reduction[c]	THR[b] [MJ/m^2]	THR_{eff}[b] [MJ/m^{2}g]	% THR_{eff} Reduction[c]	Char Yield [%]
ABS	33 ± 0	**32 ± 2**	1509 ± 13	---	127 ± 3	3.8 ± 0.0	---	**0 ± 0**
Br-ABS	35 ± 0	**30 ± 4**	580 ± 65	**62 ± 4**	55 ± 4	1.6 ± 0.1	**59 ± 3**	**0 ± 0**
PA	38 ± 1	**39 ± 0**	669 ± 12	**56 ± 1**	102 ± 1	2.7 ± 0.0	**30 ± 1**	**20 ± 11**
PA-TA	32 ± 1	**24 ± 0**	535 ± 3	**65 ± 0**	97 ± 3	3.0 ± 0.0	**22 ± 1**	**1 ± 0**
TA	33 ± 0	**26 ± 2**	711 ± 34	**53 ± 2**	111 ± 4	3.3 ± 0.1	**13 ± 3**	**0 ± 0**
TA-FG	26 ± 0	**26 ± 2**	939 ± 9	**38 ± 1**	92 ± 3	3.5 ± 0.1	**9 ± 3**	**0 ± 0**

[a] Gray = controls, Green = bio-based FR composites.

[b] TTI = time to ignition, PHRR = peak heat release rate, THR = total heat release, THR_{eff} = effective total heat release (THR divided by Weight).

[c] Reductions in relation to neat ABS.

All of the composites presented a significant reduction in PHRR (between 38 and 65% reduction) in relation to neat ABS. The fact that all of the reductions were greater than 30%, which is the weight fraction of the FRs in the composites, suggests that synergistic interactions occurred between the FRs and the matrix in terms of slowing down the release of heat. Surprisingly, PA-TA presented the lowest PHRR out of all of the materials tested (65 ± 0% reduction from ABS), being clearly better than both PA (56 ± 1% reduction) and TA (53 ± 2% reduction); taking into consideration that the total FR content is the same for all composite samples, this suggests that there is strong synergy between tannic acid and phytic acid sodium salt in slowing down the burning of ABS in the presence of a medium-sized flame. PA-TA also performed at least as well as the commercial brominated product (Br-ABS, 62 ± 4% reduction) in terms of PHRR, which is a promising result. When used individually in the present study, PA performed slightly better than TA, although the difference between them is at the limit of the experimental error. Adding fish gelatin was detrimental, as TA-FG presented the worst result, showing only a 38 ± 1% improvement in relation to ABS; it cannot be determined, however, whether or not the synergy seen between tannic acid and fish gelatin in MCC also

occurs in cone calorimetry, since FG was not tested by itself through the latter technique.

In terms of THR_{eff}, Br-ABS presented a significant superiority in the cone calorimetry experiments (59 ± 3% reduction in relation to neat ABS). This superiority was not seen in MCC, because brominated flame retardants act as radical scavengers in the gas phase, a mechanism which occurs significantly in cone calorimetry tests but not in MCC analyses because the latter test forces complete combustion of the volatiles [103,104,108]. The bio-based composites did not compete with Br-ABS in terms of THR_{eff}, but they all performed better than ABS. Among the composites, the order of performance followed the same order as the organic content (OC) of the FR additives (similarly to what was seen in MCC): PA (smaller OC) performed the best (30 ± 1% reduction from ABS); PA-TA displayed the next best results (22 ± 1% reduction); TA (higher OC) did not perform as well (13 ± 3% reduction); and TA-FG (fish gelatin also has a high OC) had a similar performance (9 ± 3% reduction). These results are consistent with the THR and char yield results of the individual FR powders when tested by MCC, shown in Table 3.8: phytic acid sodium salt released almost no heat (0.5 kJ/g) and yielded 81% of char, tannic acid had a higher THR (7.4 kJ/g) and a char yield of only 23%, and fish gelatin had an even higher THR (12.6 kJ/g) and a similar char yield (22%). It should be noted that the THR does not follow the same order as the THR_{eff} because of the weight differences between the samples. The fact that the THR_{eff} results of the composites followed the same trend as the flammable content of the FRs that they contain suggests that, although the FR additives reduced the fire spread rate towards the beginning of the test, they did not fully protect the polymer during the entire test.

ABS and Br-ABS did not produce any char, as shown in Table 4.2 and repeated in Table 4.3 alongside the MCC char yields; this was expected, since ABS is not a char-forming polymer and brominated FRs do not contribute to char formation, and is consistent with the shapes of the HRR curves shown in Figure 4.2 and with the low char yields seen for these compounds in MCC. Surprisingly, PA-TA, TA, and TA-FG also had very low char yields, despite yielding 14, 9, and 8%, respectively, in MCC experiments; TA and TA-FG had residual amounts, while PA-TA displayed a clearly visible amount but that equals only 1% of the sample's mass. Even if a protective char layer was formed towards the beginning of the tests

that effectively reduced the PHRR (which seems to be the case for PA-TA and TA, based on their HRR curve shapes (Figure 4.2)), the char burned completely by the end of the test, an event which did not occur in MCC. A possible explanation for the complete burning of the char is the occurrence of thermo-oxidative degradation at the later stages of the cone calorimetry tests, possibly after the flame had gone out [107]. Even though there is evidence that the degradation that occurs at a burning surface during flaming combustion is anaerobic because the flame consumes all of the available oxygen [115], oxygen can be present when a flame has decreased or after it has gone out, allowing thermo-oxidative degradation to take place while the temperature is still sufficiently high [107]. A close look at Figure 4.3 (which is a magnification of the final portions of the cone calorimetry curves shown in Figure 4.2) reveals that all of the samples that presented a lower char yield in cone calorimetry than in MCC (PA-TA, TA, TA-FG, and Br-ABS) exhibit a plateau towards the end of the test (with HRR values of ~40–60 kW/m^2), while ABS and PA's HRR curves don't exhibit the plateau, going directly to 0 kW/m^2; this observation supports the explanation that the residues of PA-TA, TA, TA-FG, and even Br-ABS suffered thermo-oxidative degradation towards the end of the tests. This phenomenon did not occur in MCC experiments because the entire degradation process takes place in an oxygen-free chamber. PA was the only compound that presented a significant char yield (20 ± 11%), similar to its MCC result (22 ± 1%), indicating that the char formed during the combustion of this sample had a higher thermal stability in the presence of oxygen than the residues formed from the other samples, staying intact until the end of the test. It is quite surprising that PA's HRR curve shape suggests a slower or initially weaker char formation for this sample than for TA and PA-TA (as described in the discussion on Figure 4.2), yet the char formed was the most thermally stable, being the only one to remain intact until the end of the test.

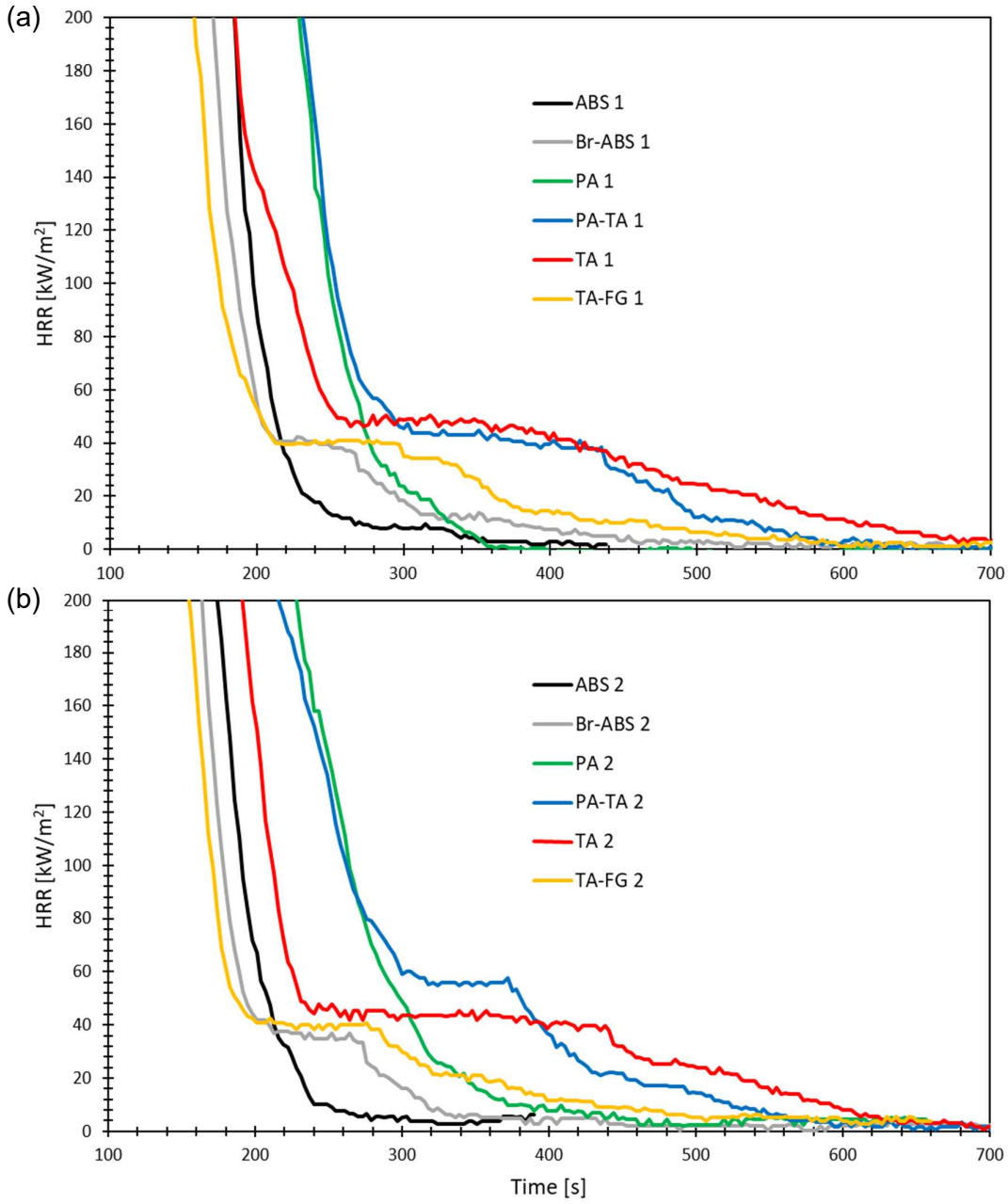

Figure 4.3. Magnification of the heat release rate curves shown in Figure 4.2, showing the final portion of the burning process: (a) specimen 1 and (b) specimen 2 of neat ABS, commercial halogenated Br-ABS, and bio-based FR ABS composites.

4.2.2.
Results and Mechanisms from MCC-Cone Calorimetry Comparisons

Table 4.3 presents a comparison between data from cone calorimetry and MCC, providing parameters that can shed a light on FR mechanisms. In order to

compare the THR values obtained by the two instruments, the units must be the same (kJ/g), so the THR_{eff} values from cone calorimetry were multiplied by the exposed area of the specimens (A) to yield the $THR_{eff}*A$ values shown in Table 4.3; the term "THR" will henceforth refer to this "corrected" value, in kJ/g. The ratio between the THR values obtained by cone calorimetry and by MCC is shown in Table 4.3 for each sample (THR Ratio). The effective heat of combustion (EHC) of a burning sample is the amount of heat released by its volatile gases per gram of volatile gas, and it is calculated as shown in eq. (15), where μ is the char yield:

$$EHC\ \left[\frac{kJ}{g-volatiles}\right] = \frac{THR\quad \left[\frac{kJ}{g-sample}\right]}{(1-\mu)\ \left[\frac{g-volatiles}{g-sample}\right]} \tag{15}$$

Combustion is forced to completion in MCC under normal testing conditions (i.e. excess oxygen and combustor temperature of 900 °C), so the effective heat of combustion measured from an MCC experiment is called the heat of complete combustion (HCC, often referred to as h_c^0) of the gases:

$$HCC = \frac{THR_{MCC}}{(1-\mu_{MCC})} \tag{16}$$

Combustion is normally incomplete in flaming tests and real fire scenarios due to low oxygen concentration, insufficient reaction time, low temperature in the combustion zone, poor ventilation, and/or the presence of combustion inhibitors [104,116], so the EHC from cone calorimetry is almost always lower than the HCC for a given sample. The flaming combustion efficiency, χ, is a measure of the "completeness" of combustion and is defined as the ratio between the EHC of the volatiles from a burning sample and the HCC of those gases; the combustion efficiency of samples in cone calorimetry experiments can therefore be calculated by using eq. (17) [104,115–117]:

$$\chi = \frac{EHC_{Cone}}{HCC_{MCC}} = \frac{\frac{THR_{Cone}}{(1-\mu_{Cone})}}{\frac{THR_{MCC}}{1-\mu_{MCC}}} \quad (17)$$

Table 4.3

Parameters derived from the comparison between cone calorimetry and MCC for ABS, commercial brominated ABS, and bio-based FR ABS composites[a]

	Char Yield (Cone vs MCC)		Total Heat Release (Cone vs MCC)			Effective Heat of Combustion (Cone vs MCC)		
Sample Name	Char Yield from Cone [%]	Char Yield from MCC [%]	THR_{eff}*A from Cone[b,c] [kJ/g]	THR[b] from MCC [kJ/g]	THR Ratio[d] [%]	EHC[b] from Cone [kJ/g]	HCC[b] from MCC [kJ/g]	χ [%][b]
ABS	0 ± 0	0 ± 0	34 ± 0	38 ± 0	89 ± 1	34 ± 0	38 ± 0	89 ± 1
Br-ABS	0 ± 0	3 ± 0	14 ± 1	30 ± 0	45 ± 3	14 ± 1	31 ± 0	44 ± 3
PA	20 ± 11	22 ± 1	24 ± 0	28 ± 1	86 ± 2	30 ± 4	36 ± 1	84 ± 12
PA-TA	1 ± 0	14 ± 2	26 ± 0	29 ± 0	92 ± 1	27 ± 0	33 ± 0	80 ± 1
TA	0 ± 0	9 ± 1	29 ± 1	28 ± 0	104 ± 4	29 ± 1	31 ± 0	95 ± 3
TA-FG	0 ± 0	8 ± 0	31 ± 1	30 ± 0	104 ± 4	31 ± 1	32 ± 0	95 ± 4

[a] Gray = controls, Green = bio-based FR composites.

[b] THR_{eff} = effective total heat release, A = exposed area of specimen, THR = total heat release, EHC = effective heat of combustion, HCC = heat of complete combustion, χ = flaming combustion efficiency.

[c] Total heat released per gram of sample, having the same units and physical significance as the THR in MCC.

[d] Ratio between the previous 2 columns $\left(\frac{\text{THR}_{\text{Cone}}\ [\text{kJ/g}]}{\text{THR}_{\text{MCC}}\ [\text{kJ/g}]}\right)$.

Neat ABS presented a combustion efficiency of 89 ± 1% in cone calorimetry, being less than 100% because of incomplete combustion of the volatiles; one of the causes of χ values less than 1 is the propensity of a compound to form smoke or soot, and ABS forms a large amount of soot due to the presence of aromatic groups (styrene), which are the "building blocks" for soot formation, in its structure [116]. This value is slightly higher than those reported in literature (78 ± 5% [115], 79% [116], and ~85% [107,118]). Br-ABS presented a very low χ (44 ± 3%), which was expected because halogenated FRs act in the gas phase through flame inhibition (radical scavenging), reducing the oxygen consumption in the flame zone and the efficiency of combustion; Lyon and Janssens [116] reported a similar value (38%) for "FR-ABS", an unspecified flame-retardant grade of ABS likely containing halogenated additives. Combustion efficiency can provide an indication of whether or not an FR acts in the gas phase (as opposed to the condensed phase); however, a threshold has not been defined to delimit the mechanisms. Lin et al. [103] found χ

values of 50–60% for halogenated FR compounds and 70–80% for non-halogenated ones; Lyon et al. [115] estimated 40–80% for halogenated and 80–100% for non-halogenated plastics; and Sonnier et al. [107,118] measured χ to be ~85% for neat ABS, ~40–80% for ABS containing halogenated FRs, and ~80–90% for ABS containing phosphorus-based FRs. Halogenated FRs always act in the gas phase, but P-based and other FRs can work in either or both phases; there is, therefore, a range (~70–90%) for which it cannot be directly determined whether an FR acts in the gas phase (through flame inhibition) or by other mechanisms. PA-TA and PA presented χ values within this intermediary range (80 ± 1% and 84 ± 12%, respectively). PA's value cannot be distinguished from ABS's χ value because of the former's large standard deviation; PA-TA's χ value, however, is lower than ABS's combustion efficiency, suggesting that either the FRs present some extent of gas-phase action or the degradation products from the additives undergo a more incomplete combustion than ABS's products. TA and TA-FG presented high χ values (95 ± 3% and 95 ± 4%, respectively), higher than ABS's, indicating that they do not act through gas phase mechanisms. The increase in χ from ABS to TA and TA-FG can possibly be explained by the thermo-oxidative degradation of the char described earlier: char has a high EHC because it is a carbon-rich product [107], so the degraded char increases the average EHC of these samples in cone calorimetry; this does not occur in MCC, because the char does not degrade. Therefore, while ABS's EHC in cone calorimetry decreases in relation to its HCC because of its incomplete combustion, TA and TA-FG's EHCs suffer a reduction because of ABS's incomplete combustion, but also experience an increase because of the high EHC contribution of the "new" degradation products (from the degraded char). The smaller reduction in EHC leads to a higher combustion efficiency.

The ratio between THR values from cone calorimetry and from MCC can be expressed, by rearranging eq. (17), as:

$$THR\ Ratio = \frac{THR_{Cone}}{THR_{MCC}} = \chi * \frac{1 - \mu_{Cone}}{1 - \mu_{MCC}} \tag{18}$$

ABS's THR Ratio was 89 ± 1% due the incomplete combustion of its volatiles. Br-ABS had a THR Ratio of 45 ± 3% because of the flame-inhibition action of the

halogenated additive. PA's THR Ratio (86 ± 2%) was statistically equivalent to ABS's, suggesting that no gas-phase mechanisms were present. All 3 samples had a THR Ratio similar to its respective χ value, since their char yields did not change from MCC to cone calorimetry (see eq. (18)). PA-TA, TA, and TA-FG all showed higher THR Ratios than ABS, likely due to the thermo-oxidative degradation of the char: additional material was volatilized and combusted in these samples, leading to a higher THR in cone calorimetry.

Table 4.4 proposes a breakdown of the THR Ratios into physio-chemical phenomena that can cause reductions or increases in the cone-calorimetry THR values; Table 4.5 shows the equivalent breakdown of χ, showing the changes in cone-calorimetry EHC values caused by the same phenomena. Columns 1 to 4 contain the contributions of each phenomenon to each sample; column 5 contains the total explained THR Ratio or χ, obtained by adding the sum of columns 1 to 4 to 100%; column 7 contains the actual THR Ratio or χ, which is the deviation between the experimental MCC values and the experimental cone-calorimetry values; and column 6 contains the THR Ratio or χ considering the actual cone-calorimetry values and the predicted no-interaction MCC values (i.e. $\frac{\mathrm{THR_{Cone}}}{\mathrm{THR_{MCC_{pred,no\_int}}}}$ or $\frac{\mathrm{EHC_{Cone}}}{\mathrm{HCC_{MCC_{pred,no\_int}}}}$), which ignores any synergies or antagonisms seen in MCC and focuses only on mechanisms seen in cone calorimetry. All samples suffered an 11% reduction in THR and in EHC from MCC to cone calorimetry because of incomplete combustion of the volatiles (column 1), leading to ABS's THR Ratio and χ of 89%. Gas-phase mechanisms (flame inhibition; column 4) led to the remaining 44–45% reduction for Br-ABS. Column 2 shows that PA-TA, TA, and TA-FG experienced an increase in $\mathrm{THR_{Cone}}$ and $\mathrm{EHC_{Cone}}$ (and therefore in THR Ratio an χ, respectively) because of the thermo-oxidation and combustion of the char originally formed from tannic acid and fish gelatin; the additional fuel increased the THR simply because more fuel was available to release heat, and it increased the average EHC because the EHC of carbon-rich char is likely higher than the average EHC of the rest of the sample. PA-TA experienced half of the increase of the other 2 samples because it contains only 15 wt% of TA or FG as opposed to 30 wt%. The column-2 values allocated to this phenomenon (+6 or +12% for THR Ratio, +2 or +5% for χ) consider that the volatilized char had an average EHC of ~50 kJ/g (which is a reasonable estimate given that the highest

HCC for over 100 polymers and small molecules was found to be ~52 kJ/g [119] and carbon-rich char is considered to have "a very high EHC" [107]), raising the total heat released and the average EHC (previously 27–30 kJ/g for the rest of the sample). These estimates can explain the total THR Ratio and χ for TA and TA-FG (column 5 ≈ column 6). The portion of PA-TA's char that was originally formed from phytic acid would have caused an additional increase of as large as 20% in THR Ratio and 7% in χ for this sample if the same EHC of 50 kJ/g was considered, because phytic acid's original char yield is much higher than tannic acid's and fish gelatin's (Table 3.8), thus adding more "new" fuel from the volatilized char; however, this residue contains Na, P, and O atoms, which cause a reduction in the char's average EHC. Making the considerations listed hereafter, an EHC of between 17 and 44 kJ/g was considered for the volatilized phytic acid-originated portion of the char: (1) phytic acid's chemical formula was considered to be $C_6H_{12}O_{24}P_6.6Na.7H_2O$ (taken from [120], who reportedly used the same product as in the present study); (2) all of the Na and P atoms remained in the original char; and (3) Na does not contribute to the THR (EHC = 0), P groups contribute with an EHC between 0 and 50 kJ/g, and O groups contribute with an EHC between 25 and 50 kJ/g. These approximations led to an increase in THR Ratio of ~7–18% and a change in χ of between -4% and +5%. The THR Ratio necessarily increases simply because "new" fuel is being considered, so the total amount of heat released is necessarily larger. χ, on the other hand, depends on the average EHCs of the components: since the char's EHC (being considered as ~17–44 kJ/g) could be either higher or lower than the rest of the sample's average EHC (~27–30 kJ/g), the change in χ can be either positive or negative. In order to reach the THR Ratio and χ described in column 6 (95 ± 1% and 81 ± 1%, respectively), a further reduction of ~6–19% in THR and ~5–16% in χ would have to be explained (column 4); this reduction can possibly be attributed to a gas-phase mechanism, which can be accredited either to radical scavenging performed by the phosphorus atoms of phytic acid or to dilution in oxygen concentration due to the release of CO_2 from tannic acid and/or H_2O from phytic acid (or to both). Since neither TA nor PA exhibited gas-phase mechanisms, meaning that the levels of CO_2 and H_2O released were not sufficient to significantly dilute the oxygen concentration and that phosphorus did not act as a radical scavenger (likely remaining in the residue, not being volatilized) in those samples, it is possible that the gas-phase mechanism seen

in PA-TA refers to radical scavenging performed by phosphorus atoms only during combustion of the char towards the end of the test. If this is the case, most of the burning process would exhibit only the phenomenon in column 1, and the combustion of the char towards the end of the test would experience an event described by columns 2–4 combined, which could be called "combustion of char from PA and from TA with simultaneous flame inhibition from phosphorus groups, reducing the EHC of the combusting char". This event would account for the remaining (i.e. after application of column 1) changes in THR Ratio (+5%) and χ (-8%) if an average EHC of ~12 kJ/g was considered for the char; the burning char would still add to the total heat released, but it would decrease the average EHC of the sample, decreasing χ. The extent of the possible gas-phase action, however, is small compared to that of Br-ABS. PA's reduction in THR Ratio and χ can be attributed solely to the incomplete combustion of the volatiles (column 1), indicating that there were likely no gas-phase mechanisms, since its char residue was the same between MCC and cone calorimetry (i.e. there were no "new" volatiles).

Table 4.4

Proposed phenomenological breakdown of THR Ratio values[a]

Sample	1 Incomplete combustion of volatiles	2 Combustion of char from TA and FG (organic)	3 Combustion of char from PA (partially inorganic)	4 Gas-phase mechanism	5 Total Explained THR Ratio[b]	6 THR Ratio considering predicted MCC THR values[c]	7 Actual THR Ratio[d]
ABS	- 11%	-	-	-	**89%**	**89 ± 1%**	89 ± 1%
Br-ABS	- 11%	-	-	- 44%	**45%**	**45 ± 3%**	45 ± 3%
PA	- 11%	-	-	-	**89%**	**89 ± 1%**	86 ± 2%
PA-TA	- 11%	+ 6%	+ 7–18%	- 6–19%	**94–96%**	**95 ± 1%**	92 ± 1%
TA	- 11%	+ 12%	-	-	**101%**	**103 ± 4%**	104 ± 4%
TA-FG	- 11%	+ 12%	-	-	**101%**	**105 ± 4%**	104 ± 4%

[a] Gray = controls, Green = bio-based FR composites.

[b] Column 5 = 100% + sum of columns 1 to 4.

[c] Column 6 = $\frac{\mathrm{THR_{Cone}}_{\mathrm{experimental}}\left[\frac{\mathrm{kJ}}{\mathrm{g}}\right]}{\mathrm{THR_{MCC}}_{\mathrm{pred,no\_int}}\left[\frac{\mathrm{kJ}}{\mathrm{g}}\right]}$.

[d] Column 7 = THR Ratio $= \frac{\mathrm{THR_{Cone}}_{\mathrm{experimental}}\left[\frac{\mathrm{kJ}}{\mathrm{g}}\right]}{\mathrm{THR_{MCC}}_{\mathrm{experimental}}\left[\frac{\mathrm{kJ}}{\mathrm{g}}\right]}$.

Table 4.5

Proposed phenomenological breakdown of combustion efficiency (χ) values[a]

Sample	1 Incomplete combustion of volatiles	2 Combustion of char from TA and FG (organic)	3 Combustion of char from PA (partially inorganic)	4 Gas-phase mechanism	5 Total Explained χ[b]	6 χ considering predicted MCC HCC values[c]	7 Actual χ[d]
ABS	- 11%	-	-	-	**89%**	**89 ± 1%**	89 ± 1%
Br-ABS	- 11%	-	-	- 45%	**44%**	**44 ± 3%**	44 ± 3%
PA	- 11%	-	-	-	**89%**	**85 ± 12%**	84 ± 12%
PA-TA	- 11%	+ 2%	- 4% – + 5%	- 5–16%	**80–82%**	**81 ± 1%**	80 ± 1%
TA	- 11%	+ 5%	-	-	**94%**	**95 ± 3%**	95 ± 3%
TA-FG	- 11%	+ 5%	-	-	**94%**	**97 ± 4%**	95 ± 4%

[a] Gray = controls, Green = bio-based FR composites.

[b] Column 5 = 100% + sum of columns 1 to 4.

[c] Column 6 = $\frac{\mathrm{EHC_{Cone_{experimental}}}\left[\frac{\mathrm{kJ}}{\mathrm{g}}\right]}{\mathrm{HCC_{MCC_{pred,no\_int}}}\left[\frac{\mathrm{kJ}}{\mathrm{g}}\right]}$.

[d] Column 7 = $\chi = \frac{\mathrm{EHC_{Cone_{experimental}}}\left[\frac{\mathrm{kJ}}{\mathrm{g}}\right]}{\mathrm{HCC_{MCC_{experimental}}}\left[\frac{\mathrm{kJ}}{\mathrm{g}}\right]}$.

The extent of each sample's condensed-phase action can be evaluated by the introduction of 2 new parameters, R1 and R2, which exploit the discrepancies between MCC and cone calorimetry results [121]:

$$R1 = \frac{PHRR_{flame-retarded\ polymer}}{PHRR_{pure\ polymer}}\ in\ MCC \tag{19}$$

$$R2 = \frac{PHRR_{flame-reta\quad polymer}}{PHRR_{pure\ polymer}}\ in\ cone\ calorimetry \tag{20}$$

R2 is almost always less than or equal to R1 [121], because cone calorimetry enables more FR mechanisms than MCC (e.g. flame inhibition and barrier effects), allowing FR additives to be more effective in cone calorimetry than in MCC. Other possible causes of discrepancy between MCC and cone calorimetry results are differences in thermal stability, thermal conductivity, reflectivity, and heat absorption between the materials, which can cause changes in cone-calorimetry HRR curves but have no effect in MCC tests [107]. Assuming that no major changes occurred in the latter properties between pure ABS and the FR ABS samples, differences between R1 and R2 can be attributed to condensed-phase (e.g.

thermal/gas barrier) and gas phase (e.g. flame inhibition) effects: for samples where R1 ≈ R2, these mechanisms are not present; for samples where R2 < R1, at least one of these mechanisms is likely present. The difference (or quotient) between R1 and R2, combined with gas-phase-mechanism information obtained from χ, can qualitatively indicate the extent of condensed-phase action in each sample.

Figure 4.4 presents a graph of R1 plotted against R2 for the 5 FR ABS samples (the 4 bio-based FR composites and Br-ABS). It is clear that PA-TA presents the largest deviation from the "R1 = R2" line, demonstrating that condensed- and/or gas-phase mechanisms are significantly present; since it was determined from the χ values that Br-ABS has a much stronger gas-phase action than PA-TA, yet PA-TA has a considerably larger R1/R2 ratio than Br-ABS, it can be concluded that PA-TA contains a significant condensed-phase flame-retardation mechanism. This result is consistent with the discussion regarding the cone-calorimetry HRR curves (Figure 4.2), where it was suggested that PA-TA quickly forms a cohesive char layer that is able to rapidly limit the HRR growth multiple times by forming a protective barrier. PA has the next most pronounced condensed-phase mechanism, equivalent to Br-ABS's flame-inhibition action in terms of reducing the flammability. TA has a lower R1/R2 ratio, indicating either that it has a smaller char-layer barrier effect in cone calorimetry than PA or that it has a similar barrier effect but the strong ABS-TA synergy seen in MCC (Figure 3.14a) is not present in cone calorimetry. TA-FG presents almost no barrier or flame-inhibition effects (R1 = R2), which is consistent with the fact that the shape of its HRR curve is very similar to that of ABS's curve (Figure 4.2), indicating little or no protective char formation.

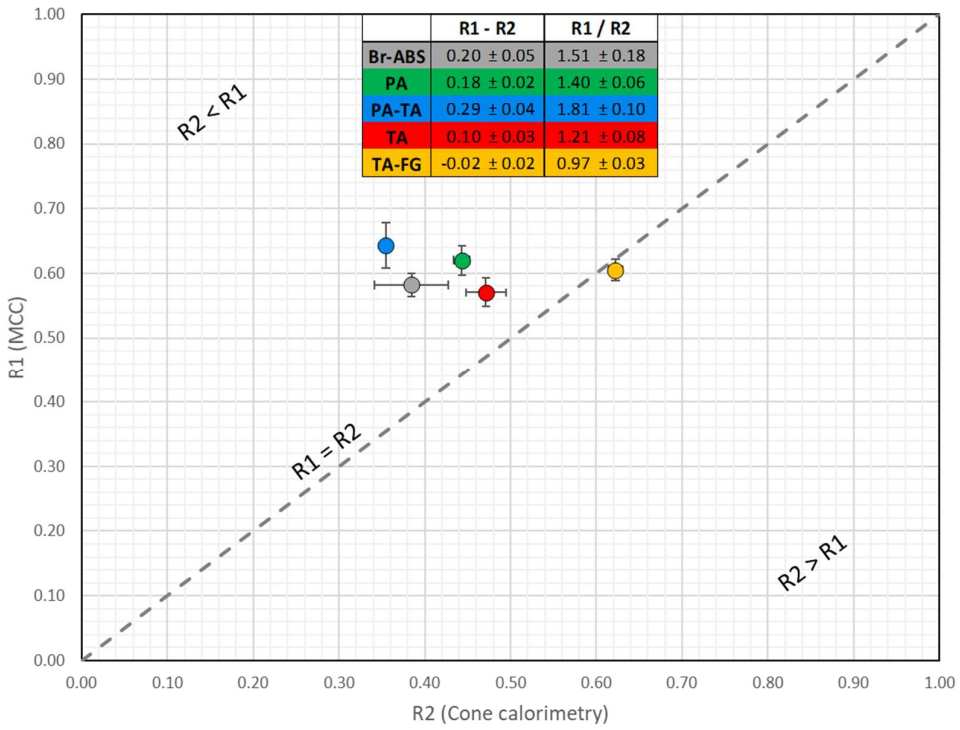

Figure 4.4. R1 vs. R2 for bio-based FR ABS composites and Br-ABS.

In terms of overall performance of the bio-based FR composites, the promising results seen in MCC were generally reproduced in cone calorimetry: ABS's PHRR was significantly reduced by the additives, achieving results comparable to a commercial brominated ABS product, and ABS's THR was reduced as well. The significant reduction in PHRR has important practical results, as this parameter can be determinant as to whether or not a fire will spread to nearby objects in a real-world scenario.

It can be concluded, from the detailed analysis of and comparison between data from cone calorimetry and MCC, that the FR additives in PA-TA, PA, and TA act mainly through condensed-phase mechanisms, likely forming protective char layers that serve as thermal and gas barriers, thus reducing the flammability of the samples. TA-FG, on the other hand, does not present efficient condensed-phase nor gas-phase FR mechanisms. An efficient char takes longer to form in PA than in TA and PA-TA, which might be caused by a delayed ignition in PA, making the temperature take longer to rise, thus delaying the decomposition and char-forming processes; despite having a slower formation, the char barrier formed in PA is at least as effective as the one formed in TA in terms of reducing the PHRR. PA's

char residue is also the most thermally stable, as PA is the only sample to present a considerable char yield at the end of the experiment; TA, PA-TA, and TA-FG's residues likely undergo thermo-oxidative degradation towards the end of the test, so these samples leave almost no char. PA-TA had the best performance out of the bio-based FR composites. The condensed-phase mechanism of PA-TA is more pronounced than those of PA and TA, indicating that there is strong synergy between tannic acid and phytic acid in ABS during flaming combustion. A faster, stronger, and more effective char barrier is suspected to have been formed than for any of the other samples, limiting the PHRR to a considerably lower value, equivalent to Br-ABS's PHRR. The synergy between PA and TA is hypothesized to be caused by phytic acid sodium salt releasing phosphate groups that catalyze tannic acid's char formation, forming a cohesive protective layer that acts as a thermal and gas barrier, shielding the sample from the flame. The hypothesis is based on the facts that phosphorus is known to act as a catalyst for char formation when it works in the solid phase; polyphenols are inherent char formers; and, in systems that contain an acid source and a carbon source (such as intumescent systems), it is known that the phosphate groups of the acid source (in this case, PA) can catalyze char formation of the carbon source (in this case, TA) [23,76]. PA-TA also appears to present some level of gas-phase flame-retardation action, although its extent is lower than that of PA-TA's condensed-phase mechanisms and that of Br-ABS's gas-phase flame-inhibition action. PA-TA's gas-phase mechanism can possibly be attributed to radical scavenging (flame inhibition) caused by phytic acid's high phosphorus content and/or to dilution of the oxygen concentration through the release of CO_2 by tannic acid and/or H_2O by phytic acid. It is interesting, however, that none of these gas-phase mechanisms seem to be present when tannic acid and phytic acid is used individually (in TA and PA, respectively). A possible explanation could be that radical scavenging by phosphorus groups is indeed responsible for PA-TA's gas-phase mechanism, but it only occurs during combustion of the remaining char during the final stages of the test; this is, in fact, supposedly the only instance, among all of the samples, that phosphorus is released into the gas phase (since PA retains its residue, which likely contains all of the sample's phosphorus, at the end of the test), being, consequently, the only instance in which phosphorus-based flame inhibition occurs.

4.3.
Microscale Combustion Calorimetry and Thermogravimetric Analysis

4.3.1.
Revisiting Microscale Combustion Calorimetry

Revisiting MCC data from Phase 1 can provide more information on the modes-of-action of the FRs. This subsection discusses results from the ABS, Br-ABS, PA, PA-TA, TA, and TA-FG samples that were produced and tested in Phase 1; the results were already presented in Chapter 3, but they are re-discussed here with a focus on these 6 samples and with an emphasis on aspects not examined previously.

Figure 4.5 exhibits MCC heat-release-rate curves for the pure components: pure ABS (melt processed through the Phase 1 procedure) and as-received phytic acid sodium salt, tannic acid, and fish gelatin powders. All of the FRs degrade before ABS, a desired condition for effective flame retardation. Tannic acid decomposes between ~250 and ~350 °C in multiple steps; fish gelatin degrades between ~280 and ~400 °C, with a long "tail" afterwards; and phytic acid decomposes between ~340 and ~400 °C, releasing very little heat. ABS's degradation occurs from ~390 to ~500 °C. Two peaks can be seen at very similar temperatures, with a possible additional shoulder occurring just before them; these possibly represent the 3 ABS monomers, which have been shown to decompose independently at very close temperatures [122]. Because of their proximity, it is possible to approximate ABS's degradation as occurring in a single step.

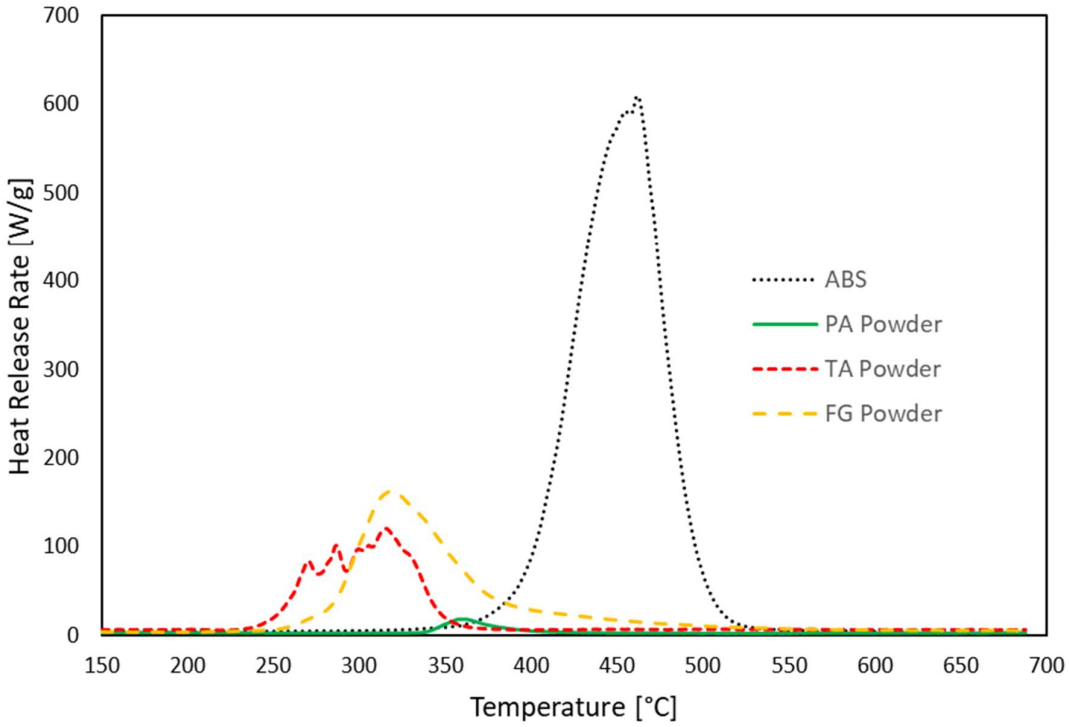

Figure 4.5. Representative HRR curves, obtained by MCC, for melt-processed pure ABS and for as-received phytic acid sodium salt, tannic acid, and fish gelatin powders.

HRR curves for the six Phase 2 samples (melt processed through the Phase 1 procedure) are shown in Figure 4.6. In the smaller images, each bio-based FR composite is shown separately and compared to the two controls, to facilitate visualization. The initial shoulders or peaks refer to the decompositions of the FR additives: tannic acid's earlier degradation (c, d, e); fish gelatin's decomposition, in a similar range, overlapping with TA's and the beginning of ABS's peaks (e), phytic acid's later and less noticeable (i.e. lower) peak, just before the polymer's degradation (b, c); and the degradation of TBBPA and Sb_2O_3 in Br-ABS's curve (b–e). It is noteworthy that TA anticipated ABS's decomposition, bringing the start and the peak of degradation to earlier temperatures, as can be seen in Figure 4.6d; the end of decomposition, however, was not changed. A similar anticipation can be seen for TA-FG, but it is much less pronounced. Such occurrence cannot be clearly observed for the phytic acid-containing samples. Br-ABS did not alter the peak's temperature, but seems to have anticipated the beginning of ABS's degradation; it is not clear, however, if the early rise is caused by a "tail" in the additives' degradation peak or by an anticipation of ABS's degradation.

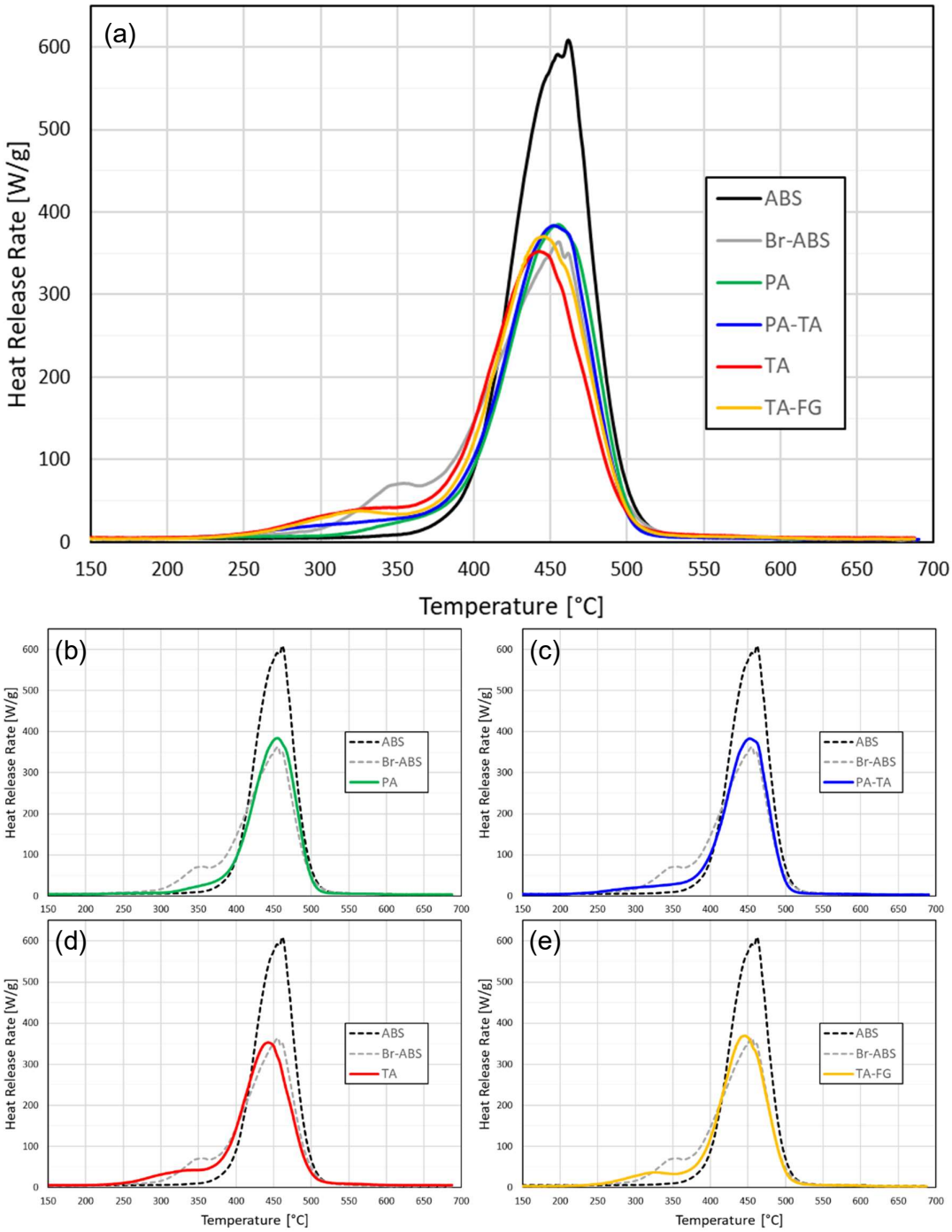

Figure 4.6. (a) Representative HRR curves, obtained by MCC, for ABS, commercial halogenated Br-ABS, and bio-based FR ABS composites. (b–e) Each bio-based FR composite's curve from (a) is shown individually and compared to ABS and Br-ABS's curves.

In order to analyze the effects of the FRs on ABS's degradation and heat release, it is useful to compare each sample's experimental HRR curve to its predicted, no-interaction curve (HRR_{pred,no_int}), obtained as a weighted average of representative HRR curves of the individual components (see eqs. (1) and (2) in Chapter 3). Figure 4.7 presents such a comparison for PA, TA, and PA-TA. It is clear that TA brought the onset and the peak of decomposition to lower temperatures than expected, as described earlier, and significantly reduced the PHRR beyond the predicted value; the end of decomposition, however, was barely anticipated in relation to the shifts in the onset and peak temperatures, leading to a wider curve than expected. PA did not significantly change the temperature of the peak, but the PHRR was reduced and the onset of degradation was slightly anticipated; the end of the peak was not changed, leading to a slightly wider curve as well. PA-TA is compared to two different predictions: "PA-TA predicted" was obtained as a weighted average of the individual components' (ABS, phytic acid powder, and tannic acid powder's) HRR curves, and "Average PA & TA" was calculated as the average between representative HRR curves of the PA and TA composites. The latter prediction results in a lower and earlier curve than the former because of the TA composite's performance, which was lower and more to the left than expected. PA-TA's performance was in between the two predictions, meaning that the additives still lowered the PHRR and the degradation temperature beyond the expected when used together, but phytic acid partially inhibited tannic acid's ability to anticipate the onset and the peak of degradation. The latter statement can be seen more clearly in (d), which shows that PA-TA's curve overlaps almost completely with PA's curve instead of occurring halfway between PA and TA.

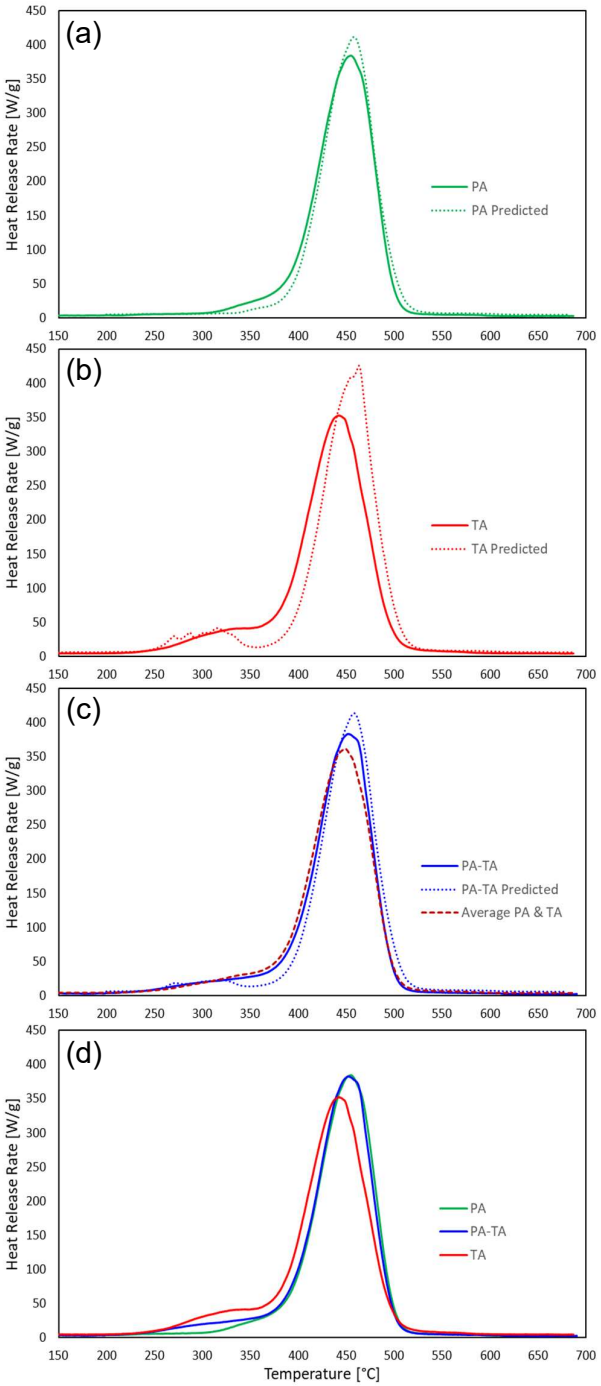

Figure 4.7. (a–c) Comparison between experimental and predicted MCC HRR curves for (a) PA, (b) TA, and (c) PA-TA. (d) Comparison between PA, TA, and PA-TA's experimental curves. Predicted (dotted) curves were calculated as weighted averages of the individual components' HRR curves. The dashed curve in (c) is the average of PA's and TA's experimental curves.

It is important to take into consideration that the 3 samples presented THR values close to the expected, as shown in Figure 3.14b; in other words, the areas under the solid and dotted curves are almost the same for each image in Figure 4.7. Given that the experimental peaks start earlier but end close to the predicted peaks, the PHRRs are significantly lower, and the total areas are the same, it can be postulated, based on geometry, that the experimental peaks are lower than expected simply because they are wider. The curves are widened and, consequently, "flattened". In other words, the synergy between these FR additives and the matrix in terms of PHRR reduction, which was observed and discussed in Chapter 3, can possibly be explained by a catalytic action of the FRs, anticipating the beginning of ABS's degradation. This is especially true for TA, which presented the largest anticipation of the beginning of the peak (thus the largest curve-widening) and the largest PHRR reduction out of all of the samples (see Figure 3.14a), suggesting that tannic acid catalyzes the beginning of ABS's decomposition. This action is not so clear for PA; the experimental curve is slightly higher than the predicted curve in the 320–400 °C temperature range, which could represent either ABS degradation products that began to be released sooner or a larger amount of phytic acid degradation products than expected. Phytic acid's heat of combustion is very low, so there is a fair possibility that the terpolymer is indeed degrading earlier; however, the action is much less pronounced than in the case of tannic acid. When the two additives are used together, it seems that phytic acid interferes with tannic acid's catalysis of ABS's degradation, greatly reducing this effect (Figure 4.7d).

4.3.2. Thermogravimetric Analysis

Thermogravimetric analysis (TGA) was performed on the Phase 2 samples; results are shown in Figure 4.8 for the pure components (melt-processed ABS and as-received phytic acid, tannic acid, and fish gelatin powders) and in Figure 4.9 for ABS, Br-ABS, and the bio-based FR composites; the main parameters are summarized in Table 4.6. In both figures, image (a) contains the raw TGA curves; image (b) portrays the TGA curves corrected to account for the approximate water contents of the samples ("water-corrected curves"), so that 100% mass corresponds to the approximate dried weight of each sample, after the initial water loss; and

image (c) presents the differential-thermogravimetry (dTG) curves, also known as the mass loss rate (MLR) curves, obtained by differentiating the water-corrected TGA curves. The data in Table 4.6 refer to the water-corrected curves. For each melt-processed sample, two specimens were tested, but one of them was interrupted just before the peak of decomposition; therefore, results in Table 4.6 are either averages of two specimens (numbers with standard deviations) or single-run values (numbers without standard deviations). Each FR powder was tested once.

Table 4.6

TGA results for ABS, commercial brominated ABS, bio-based FR ABS composites, and as-received FR powders[a]

Sample	Water Content [%]	End of Water Loss [°C]	T_{d10}[b,c] [°C]	T_{onset}[b,c] [°C]	T_{dmax}[b,c] [°C]	PMLR[b,c] [%/min]	Char Yield[c] [%]	Predicted Char Yield[d] [%]	Char Yield from MCC [%]
ABS	0 ± 0	-	400 ± 1	403	428	19.8	1.4	-	0.3 ± 0.4
Br-ABS	0 ± 0	-	318 ± 0	399	427	10.9	4.1	-	3.0 ± 0.4
PA	9 ± 1	174 ± 5	369 ± 2	403	428	12.5	24.4	25.4	21.9 ± 0.7
PA-TA	5 ± 0	172 ± 1	301 ± 11	398	425	12.1	16.4	17.0	13.9 ± 1.5
TA	3 ± 0	188 ± 1	293 ± 1	388	414	10.4	11.3	8.6	8.6 ± 1.2
TA-FG	3 ± 0	175 ± 2	290 ± 0	400	424	12.7	10.5	7.9	8.4 ± 0.2
PA Powder	7	172	323	186	330	1.4	81.2	-	80.8 ± 0.1
TA Powder	4	140	239	227	247	7.7	25.3	-	23.1 ± 1.7
FG Powder	11	201	292	281	335	6.7	20.8	-	22.5 ± 2.6

[a] Gray = controls, Green = bio-based FR composites, Light Blue = as-received FR powders.

[b] T_{d10} = temperature at 10% mass loss, T_{onset} = temperature at the onset of the main decomposition step, T_{dmax} = temperature at the point of maximum decomposition (i.e. mass-loss) rate, PMLR = peak mass loss rate.

[c] Calculated from the water-corrected TGA curves.

[d] Weighted average of the individual components' char yields (weighted by each component's original mass fraction in the sample).

In Figure 4.8, the initial mass loss for the FR additives (~40–180 °C) refers to water loss, since the compounds are hygroscopic and were not dried prior to being tested. Tannic acid degrades between ~200 and ~330 °C in two steps, fish gelatin decomposes from ~230 to ~500 °C (with the main part occurring before 400 °C), and phytic acid has a first degradation step from ~180 to ~360 °C (with a more pronounced peak from ~300 to ~360 °C) and a second short step from ~370 to ~400°C. All of the additives have most of their degradation occur before ABS's degradation (~350–480 °C), a desired condition for effective flame retardation. The char yields are identical to those observed in MCC: 81% in both TGA and MCC for phytic acid, 25% in TGA (compared to 23 ± 2% in MCC) for tannic acid, and

21% in TGA (compared to 22 ± 3% in MCC) for fish gelatin. ABS left almost no char (1.4% compared to 0.3 ± 0.4% in MCC).

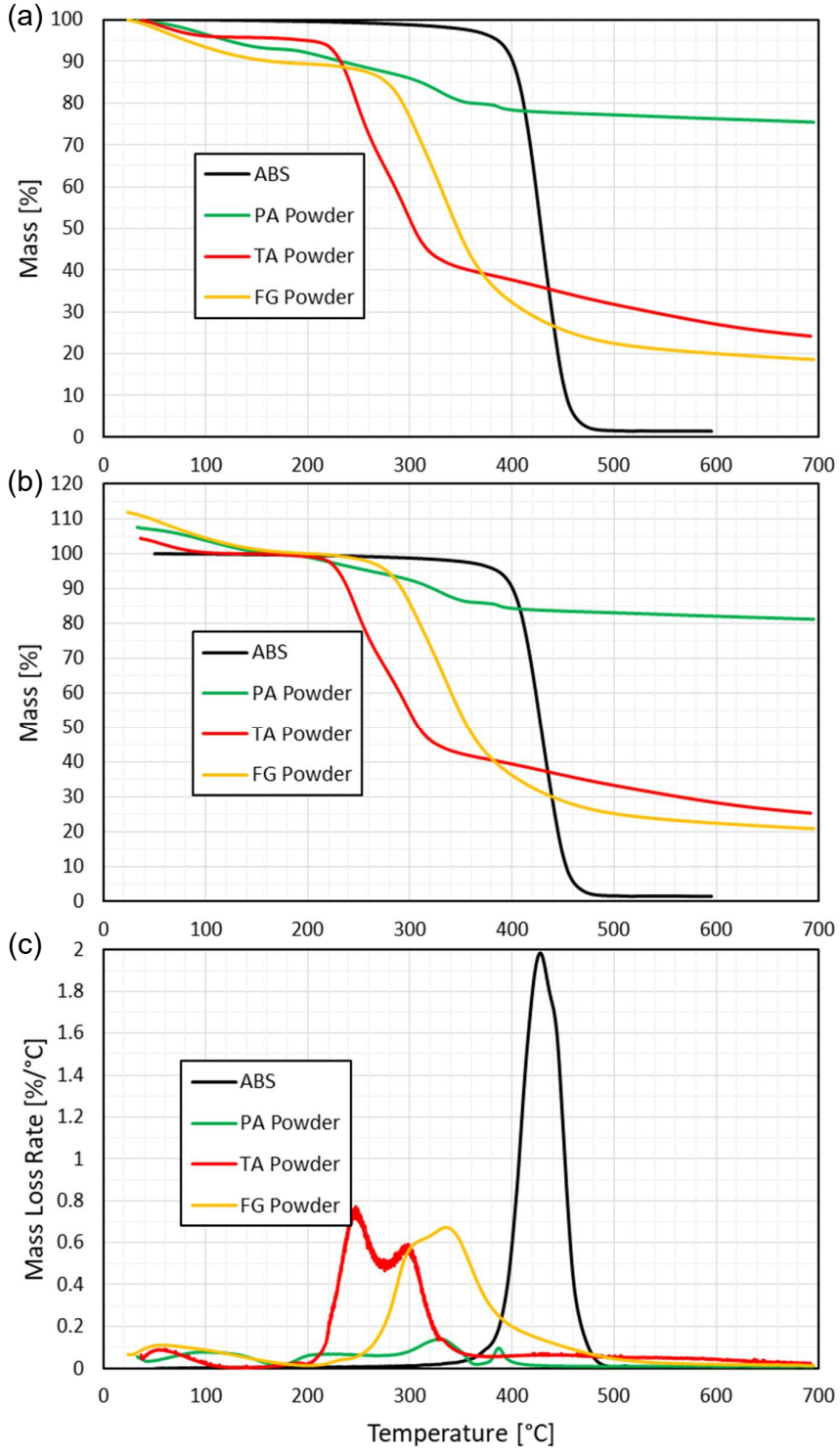

Figure 4.8. TGA results for melt-processed pure ABS and as-received phytic acid sodium salt, tannic acid, and fish gelatin powders: (a) original TGA curves, (b) water-corrected TGA curves, and (c) dTG curves.

Figure 4.9 presents the results for the six Phase 2 samples. The initial dTG peaks at around 120–160 °C for the 4 bio-based FR composites correspond to water loss; the FR additives are hygroscopic, leading to water accumulation by the samples (which were not dried prior to the tests) over time. ABS and Br-ABS did not contain water. The next mass-loss event (~210–370 °C) corresponds to the degradation of the additives (phytic acid, tannic acid, fish gelatin, and TBBPA with Sb_2O_3). The main and final event (~350–500 °C) corresponds to ABS's decomposition. The temperature at 10% mass loss (T_{d10}), shown in Table 4.6, is dominated by the FR additives' thermal stabilities, since the expected mass losses corresponding to the volatilization of the additives were ~6, 14, 22, and 23% for PA, PA-TA, TA, and TA-FG, respectively (calculated as $\sum w_i(1-\mu_i)$, where w_i is the original mass fraction of each FR in the sample and μ_i is the char yield of each FR when tested individually as a powder): TA and TA-FG had the lowest T_{d10}, followed by PA-TA, Br-ABS, PA, and ABS (in increasing order). It is clear from the table and from the figures that TA anticipated ABS's degradation, in terms of both the onset (T_{onset}; 388 °C compared to 403 °C for ABS) and the peak (T_{dmax}; 414 °C compared to 428 °C for ABS) of decomposition, just as seen in MCC. Br-ABS also exhibited an early start of the main mass-loss event (visually clear in Figure 4.9b and c, but not reflected in the T_{onset} probably because the additives' mass-loss peak overlaps significantly with ABS's), but did not anticipate the dTG peak, also in accordance with MCC results. PA-TA and TA-FG only slightly anticipated ABS's onset and peak of decomposition, while PA presented the same temperatures as ABS. TA and Br-ABS exhibited the lowest peak mass loss rates (PMLR; vertical-axis reading of the peak of the dTG curves), while PA, PA-TA, and TA-FG had slightly faster decomposition rates; all of the FR samples reduced ABS's PMLR by over 30%. Char yields were almost the same as those observed for MCC, but slightly higher: Br-ABS yielded 4% for TGA and 3 ± 0% for MCC, TA-FG presented 11% for TGA and 8 ± 0% for MCC, TA left 11% for TGA and 9 ± 1% for MCC, PA-TA presented 16% for TGA and 14 ± 2% for MCC, and PA left 24% (correcting for the initial water content) or 22% (considering the initial water) for TGA and 22 ± 1% for MCC. PA and PA-TA's char yields were close to the predicted no-interaction char yields (calculated as weighted averages of the individual components' char yields), while TA and TA-FG presented higher char yields than predicted.

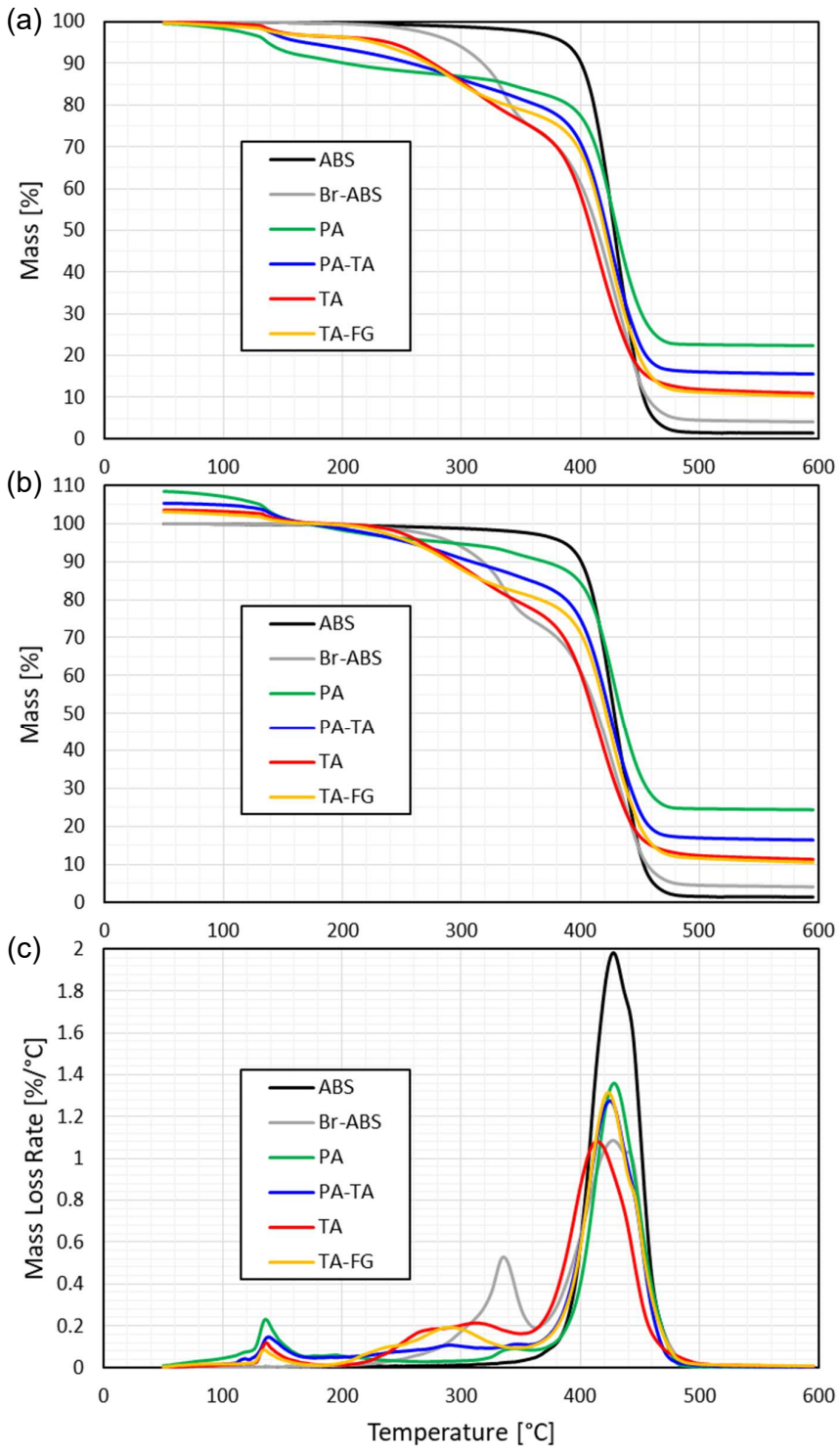

Figure 4.9. TGA results for ABS, commercial halogenated Br-ABS, and bio-based FR ABS composites: (a) original TGA curves, (b) water-corrected TGA curves, and (c) dTG curves.

Figure 4.10 presents the comparison between each bio-based FR composite's experimental curves and its predicted no-interaction curves (calculated as the average of the individual components' curves, weighted by their respective original mass fractions in the composite) for PA, TA, and PA-TA, as was done for MCC. PA did not change the matrix's degradation behavior, but it slightly increased the mass loss corresponding to phytic acid's degradation; the same behavior had been observed for MCC. TA clearly anticipated ABS's decomposition, since the main mass-loss event begins and peaks significantly earlier for TA than for ABS; the end of ABS's degradation was kept at the same temperature, however, leading to a widening of the curve. The same behavior was observed in the MCC results. It is also noteworthy that the decomposition of tannic acid itself seems to have been delayed. ABS stabilized tannic acid; tannic acid, in turn, catalyzed ABS's decomposition, which began earlier but occurred at a slower rate than expected. PA-TA is compared to the individual-component-based predicted no-interaction curves and to the PA composite-TA composite average curves. As for MCC, PA-TA's performance was in between the two predictions, meaning that the PMLR and the T_{dmax} were reduced slightly further than expected based on the individual components, but phytic acid interfered with tannic acid's catalysis of ABS's degradation and peak-widening, reducing these effects in PA-TA. Tannic acid's degradation also seems to have been delayed in this sample. All of the char yields were close to the predicted ones, but TA and TA-FG presented small increases (see Table 4.6).

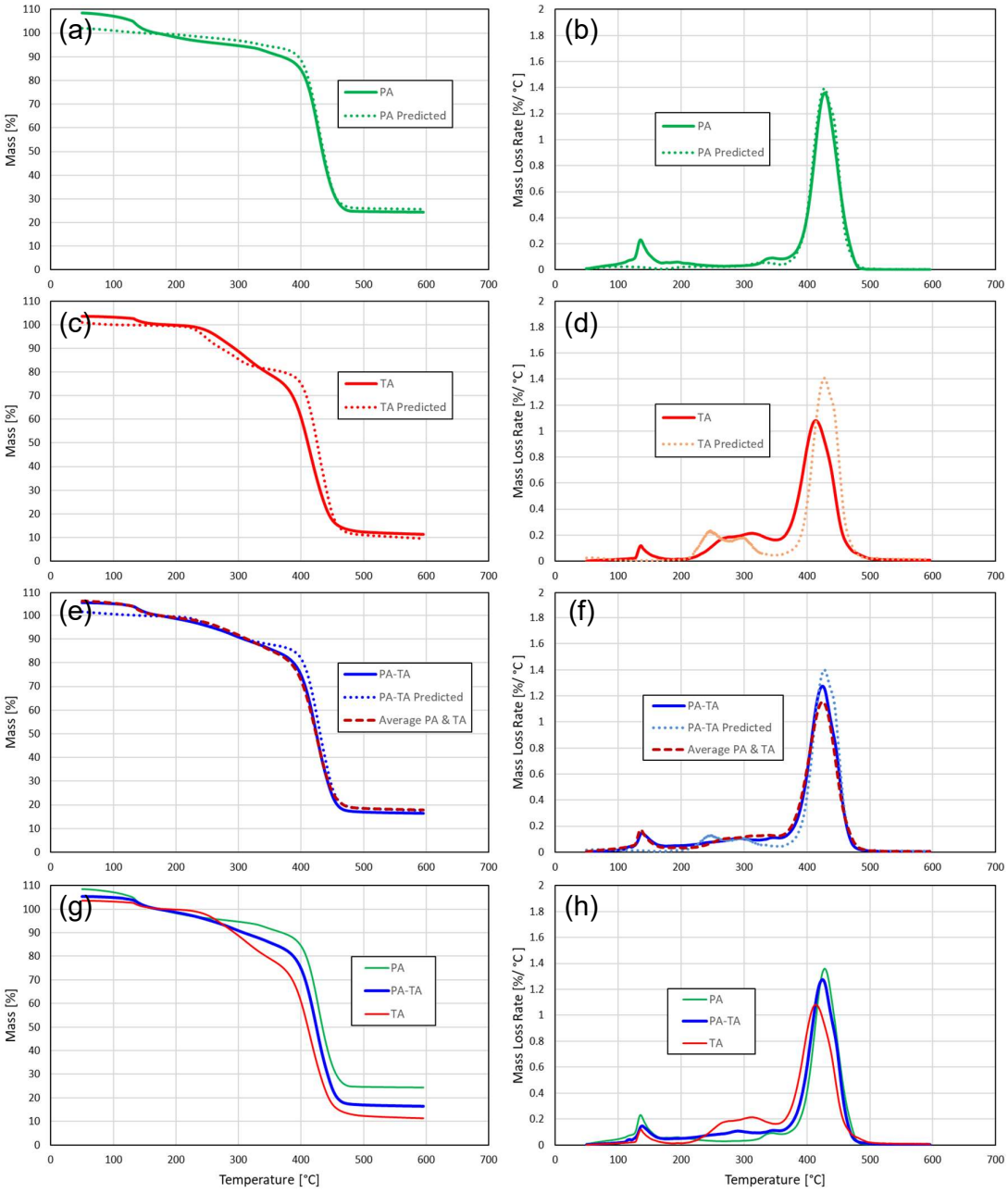

Figure 4.10. (a–f) Comparisons between experimental and predicted TGA (left) and dTG (right) curves for (a, b) PA, (c, d) TA, and (e, f) PA-TA. (g, h) Comparison between PA, TA, and PA-TA's experimental TGA (left) and dTG (right) curves. Predicted (dotted) curves were calculated as weighted averages of the individual components' curves. The dashed curves in (e) and (f) are the averages of PA's and TA's experimental curves.

4.3.3.
MCC-TGA Comparison and Activation Energy

TGA results corresponded very well with MCC results. Figure 4.11 presents a comparison between HRR curves from MCC and dTG curves from TGA. The proportion between the heat release rate scale in the HRR curves and the mass loss rate scale in the dTG curves is the same for all of the graphs. The results depict the close correspondence and agreement between the two tests. The comparisons do not provide much additional information that was not already known, but it is worthwhile to point out some interesting facts regarding the discrepancies in the curves: (1) almost all of the MCC peaks are shifted to the right in relation to the TGA peaks – this is caused by the faster heating rate in MCC (60 °C/min) than in TGA (10 °C/min) [104]; (2) the water-loss peaks seen at the beginning of the mass-loss-rate curves for the 4 bio-based FR composites (c–f), and also visible for PA Powder and FG Powder (g, i) are not seen at all in the MCC curves – this is because water does not react with oxygen and undergo combustion, so it does not release any heat after being volatilized; (3) in the FR composites' curves (b–f), the peaks corresponding to the additives' decompositions (~200–350 °C) are always lower in MCC than in TGA (while the peaks corresponding to ABS's degradation were normalized to be the same size) – this reflects the fact that the FR additives are less flammable than ABS, having a lower heat of combustion (EHC or HCC) and releasing less heat per gram of material; (4) the same effect is visible for the FR powders (g–i), which exhibit clearly lower MCC than TGA peaks for the same reason; (5) PA Powder (g) exhibits longer, more pronounced, and many more mass-loss events than heat-release events – this is because phytic acid's main degradation product is water, which is likely responsible for most of the mass loss but doesn't release any heat; (6) the relative sizes of the 2 main peaks in TA Powder's degradation (h) are inverted, with a larger 1st peak for TGA but a larger final peak for MCC – it is probable that the volatilization products from the 1st degradation step (which likely include non-combustible CO_2) have a lower average heat of combustion than the volatilization products from the final degradation step.

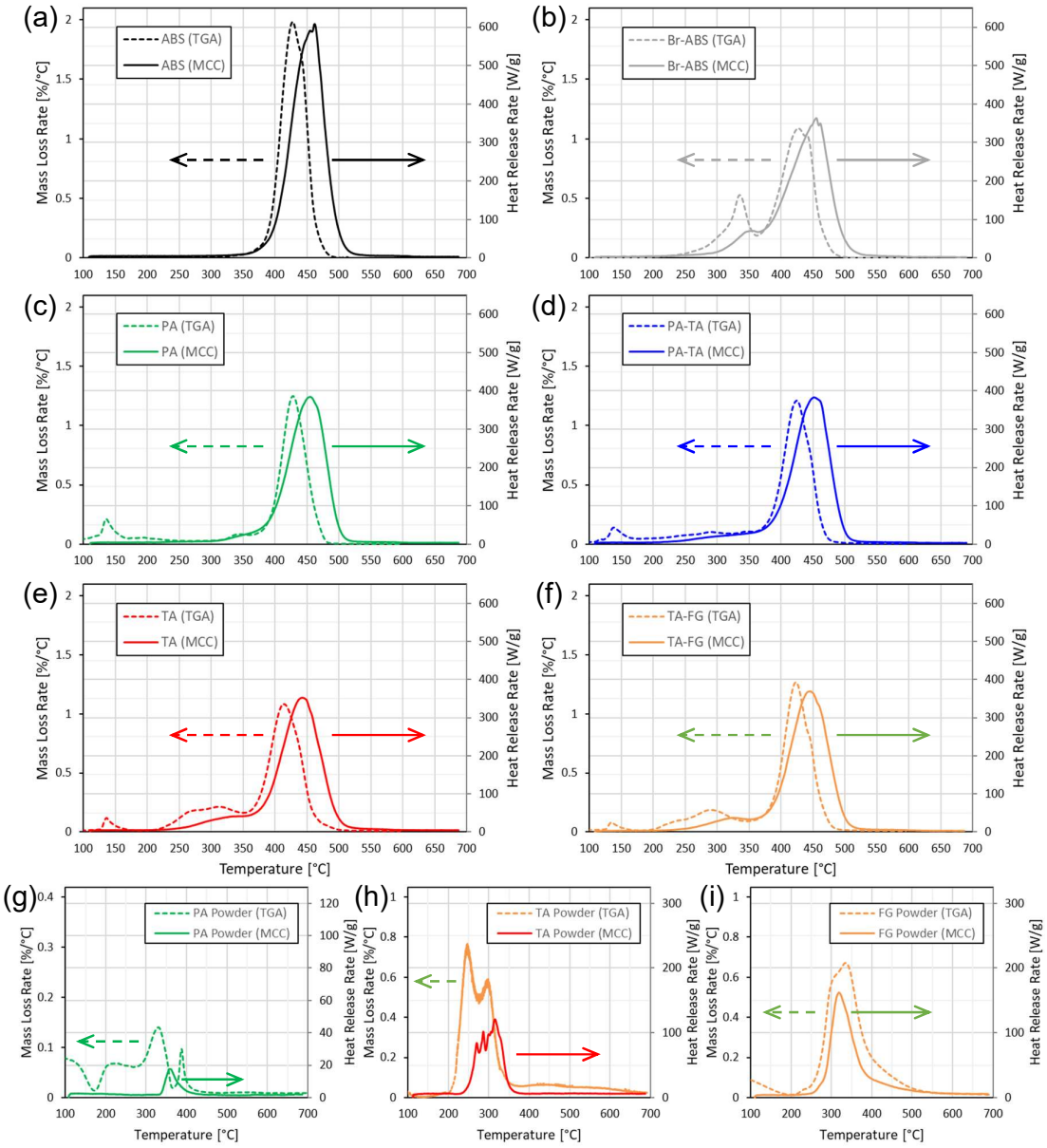

Figure 4.11. Comparisons between HRR curves from MCC and dTG curves from TGA for (a) ABS, (b) commercial halogenated Br-ABS, (c–f) bio-based FR ABS composites, and (g–i) individual FR powders.

The most interesting conclusions from the MCC and the TGA tests are the same: (1) TA significantly anticipates the beginning and the peak of ABS's degradation, but it does not change the temperature of the end of decomposition; (2) Br-ABS also significantly anticipates the beginning of ABS's degradation, without changing the peak nor the end-of-decomposition temperatures; (3) as a consequence, ABS's degradation peak is widened for both samples; (4) as a result, taking into consideration that the areas under the curves remained unchanged, the

peak heat release rates and peak mass loss rates of these samples were significantly reduced further than expected, because the curves were widened and, consequently, "flattened". Other conclusions that that can be made are: (5) TA-FG also exhibited the start-of-curve anticipation, peak widening, and, consequently, PHRR reduction in MCC (likely because of tannic acid's action), but less pronounced than for TA; (6) PA and PA-TA, the next best samples from Phase 1 (behind TA, Br-ABS, and TA-FG), presented the same behavior in a much smaller scale in MCC, and TA-FG and PA-TA presented it in a small scale in TGA as well; (7) PA likely inhibits tannic acid's anticipation of ABS's start of degradation, since the PA-TA curves are all much more similar to PA's curves than to TA's curves, exhibiting only slight peak-start anticipation, peak widening, and PHRR and PMLR reductions.

Taking into consideration that most of the flame-retardation mechanisms seen in cone calorimetry discussed previously (e.g. barrier formation, radical scavenging/flame inhibition, dilution of oxygen concentration) do not occur in MCC, it can be concluded that the flame-retardation mechanism (i.e. the PHRR-reduction mechanism) seen for TA and Br-ABS in MCC is likely due to the additives catalyzing and anticipating the start of the polymer degradation process. (The same can be said for TA-FG, PA, and PA-TA, but in a smaller scale.) This mechanism can also be viewed as a reduction of the activation energy for ABS's degradation. Lyon et al. [115] proposed two methods for calculating a sample's activation energy, E_a, using MCC data for one (eq. (21)) and TGA data for the other (eq. (22)):

$$E_a = \frac{eRT_{p,MCC}{}^2}{\Delta T_{p,MCC}} \tag{21}$$

$$E_a = \frac{RT_{p,TGA}{}^2}{\Delta T_{TGA}} \tag{22}$$

where $T_{p,MCC}$ is the temperature at PHRR from MCC tests, $\Delta T_{p,MCC}$ is the pyrolysis temperature interval as measured by MCC (equal to the half-width of the peak on the temperature axis), $T_{p,TGA}$ is the temperature at peak mass loss rate (T_{dmax}) from TGA tests, ΔT_{TGA} is the characteristic temperature interval for pyrolysis as

measured by TGA, *e* is Euler's number, and *R* is the universal gas constant. $\Delta T_{p,MCC}$ was calculated for each MCC curve as being half of the width between T_1 and T_2, where T_1 is the intersection between the temperature axis and a line tangent to the HRR curve at the inflection point during the curve's rise (before the peak), and T_2 is the analogous point after the peak. ΔT_{TGA} was calculated as the temperature interval between $T_{p,TGA}$ (temperature at PMLR) and the temperature before the peak where the mass loss rate is equal to 69.2% of the PMLR, as described in [115]. These equations assume that the thermal-degradation mechanism does not depend on the heating rate (which is a reasonable assumption) and that the samples undergo a first-order thermal-decomposition reaction; ABS's main degradation peak is actually a combination of 3 overlapping peaks (related to acrylonitrile, butadiene, and styrene) that occur at very similar temperatures, so it must be noted that its consideration as a single first-order-reaction peak is only an approximation.

Table 4.7 presents the calculated activation energies for ABS, Br-ABS, and the bio-based FR composites as calculated by MCC and TGA. The MCC-based values are averages of E_a calculations for 9 specimens for ABS, 4 specimens for PA-TA, and 3 specimens for each of the other compositions; the TGA-based values were obtained from a single run for each sample. There is a good agreement between the values calculated by the two methods for 4 out of the 6 samples (ABS, Br-ABS, PA-TA, and TA); PA and TA-FG, however, displayed much larger values for the TGA-based calculation than for the MCC-based one. The activation energy calculated for ABS is at the high end of the very large range reported in literature: ABS's E_a was calculated to be anywhere between 59.9 and 270.7 kJ/mol but estimated to be, in reality, between 150 and 270 kJ/mol [123]; other researchers reported E_a values of 179 kJ/mol [124], 179.3 kJ/mol [125], 187 kJ/mol [115], 196.6 kJ/mol [126], and 219 kJ/mol [127]. The lowest activation energies were those of Br-ABS and TA, with reductions between 18 and 29% compared to neat ABS. This result corroborates the hypothesis that the additives of these two samples reduce the activation energy for ABS decomposition, bringing the beginning of the polymer's degradation to lower temperatures and, thus, widening the pyrolysis temperature interval and lowering the HRR and MLR (dTG) peaks. TA-FG presented the same E_a as TA when using MCC results, which suggests that the same mechanism occurs for this sample; however, the TGA-based E_a is as high as ABS's value, an unexpected result. PA-TA (MCC and TGA) and PA (only TGA) presented

activation energies higher than those found for Br-ABS, TA, and TA-FG, but still 10–15% lower than that found for ABS; these results were expected, since the decomposition peak is only slightly anticipated for these samples. PA's E_a was found to be higher than ABS's when calculated by TGA, surprisingly. The results correlate well with the relative peak-onset anticipations visually observed for each sample in MCC and TGA; the large differences seen for TA-FG and PA between the two methods (both visually and in terms of E_a) is not yet understood, however. In summary, the data suggests that the large PHRR reductions seen in MCC for the samples that exhibited PHRR values significantly lower than the predicted no-interaction values (and in particular for TA and Br-ABS) were caused by a reduction in ABS's activation energy for decomposition, leading to an earlier onset of degradation and, consequently, to a wider and lower peak.

Table 4.7

Activation energies (E_a) for ABS, commercial brominated ABS, and bio-based FR ABS composites[a]

Sample	E_a from MCC [kJ/mol]	E_a from TGA [kJ/mol]	% Change from ABS (MCC)	% Change from ABS (TGA)
ABS	267 ± 4	265	-	-
Br-ABS	198 ± 5	187	- 26%	- 29%
PA	229 ± 5	281	- 14%	+ 6%
PA-TA	237 ± 9	238	- 11%	- 10%
TA	208 ± 10	218	- 22%	- 18%
TA-FG	212 ± 8	268	- 21%	+ 1%

[a] Gray = controls, Green = bio-based FR composites.

4.4. Pyrolysis-Gas Chromatography-Mass Spectrometry

Pyrolysis-gas chromatography-mass spectrometry (Py-GC-MS) was performed on the six Phase 2 samples as well as on phytic acid sodium salt, tannic acid, and fish gelatin individual powders. Evolved gas analysis (EGA) was performed first in order to visualize each sample's degradation profile. Heart Cut Analysis (HCA) experiments were performed next, using temperature zones that were defined based on the EGA results, for detailed analysis of each sample's decomposition products.

4.4.1.
Degradation Profiles from Evolved Gas Analysis

Figure 4.12 presents the samples' degradation profiles, obtained through EGA experiments. The horizontal axis can represent either the temperature of the pyrolyzer (100–800 °C) or the time elapsed (0–35 min), since the heating rate was constant; both axis labels are shown at the bottom of the figure. Each curve in the figure has been normalized in relation to its peak value; this normalization was necessary because the specimens did not have the same masses. Three curves are shown for ABS, one for Br-ABS, and two for each of the other compounds; curves from the same compound are similar to each other, although some discrepancies can be seen (especially for TA and TA-FG).

Images b–f show that all of the FR ABS samples, except for PA, anticipated the start of ABS's degradation; this is consistent with the TGA results and similar to the MCC results (for which PA also slightly anticipated ABS's degradation). TA and Br-ABS displayed the most pronounced anticipations of the beginning and of the peak of decomposition and widening of the pyrolysis interval, which is in accordance with MCC and TGA results and consistent with the fact that these two compounds have the lowest activation energies out of the materials tested. The other tannic acid-containing composites, TA-FG and PA-TA, also presented some anticipation of the onset of decomposition and widening of the peak, consistent with PA-TA's calculated activation energies and TA-FGs MCC-based E_a. PA, on the other hand, displayed a very similar curve as ABS, with a slight delay of the degradation peak; this was not observed in MCC, but is consistent with the high E_a calculated from TGA. All of the melt-processed samples had peak degradation temperatures in between those found in TGA and in MCC, as shown in Table 4.8; this was expected, since the heating rate used was in between those used in the other two experiments (10, 20, and 60 °C/min for TGA, EGA, and MCC, respectively).

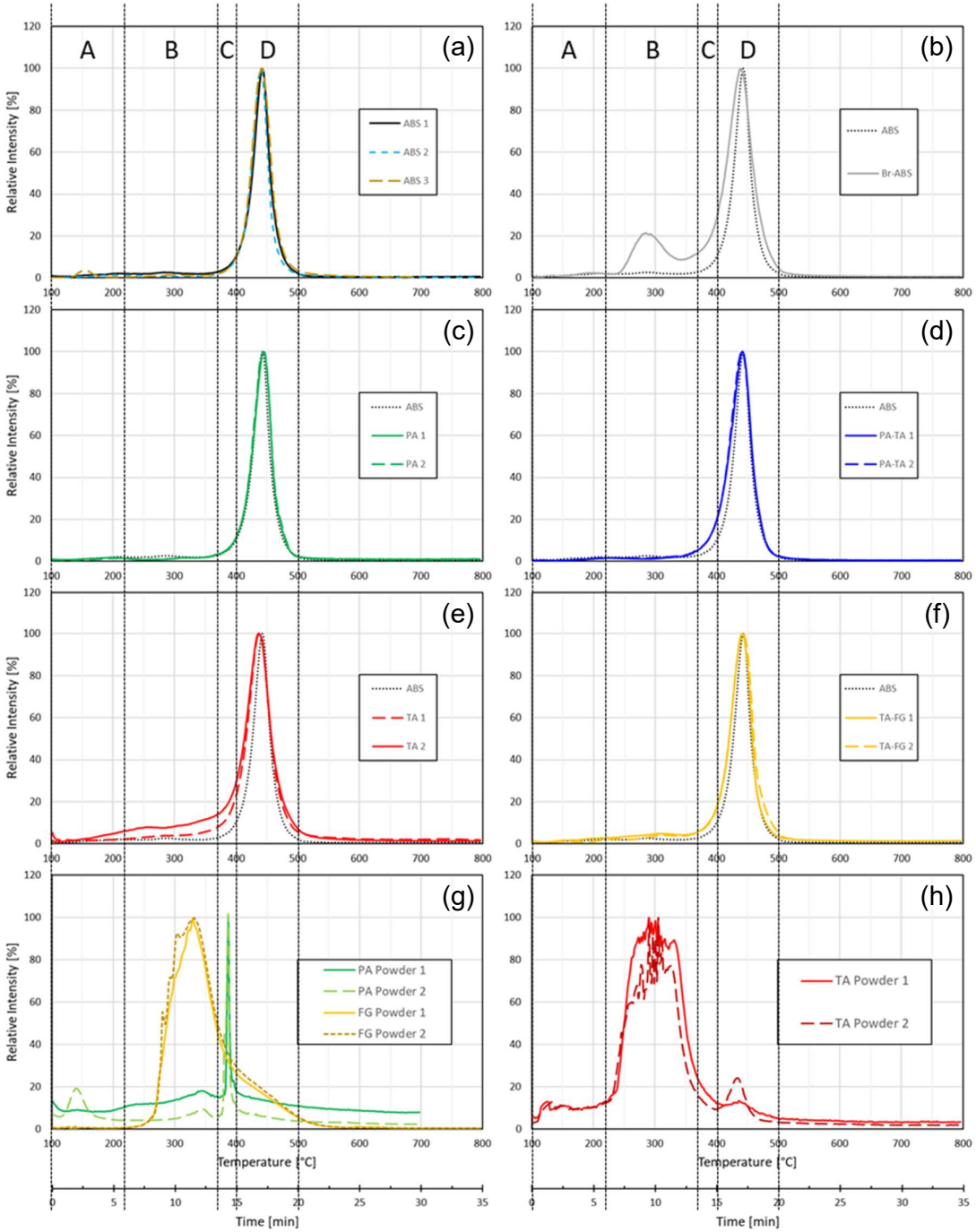

Figure 4.12. EGA curves for (a) ABS, (b) commercial halogenated Br-ABS, (c–f) bio-based FR ABS composites, and (g–h) individual FR powders. The vertical lines delineate the 4 temperature zones (A, B, C, and D) used for HCA experiments.

Table 4.8

Peak degradation temperatures of ABS, commercial brominated ABS, and bio-based FR ABS composites as measured by TGA, EGA, and MCC[a]

Sample	TGA	EGA	MCC[b]
ABS	428	442 ± 1	454 ± 2
Br-ABS	427	438	455 ± 4
PA	428	445 ± 0	455 ± 2
PA-TA	425	440 ± 0	453 ± 3
TA	414	437 ± 2	443 ± 0
TA-FG	424	440 ± 0	444 ± 4

[a] Gray = controls, Green = bio-based FR composites.

[b] For ABS and Br-ABS, the 1st peak was used in MCC; all other samples presented only 1 peak.

TA and TA-FG are the only bio-based FR composites for which it is possible to observe a peak or shoulder referring to the FR additives' degradation (before the main peak). Such a peak is not visible for PA due to the very small amount of volatiles released by phytic acid that are detected by the equipment. A small peak or shoulder was expected to be seen for PA-TA due to the presence of tannic acid, but none can be observed. A clear peak can be seen for Br-ABS's FR additives (~250–350 °C), as expected.

Fish gelatin and tannic acid powders (Figure 4.12g and h) presented similar curves as their respective MCC and TGA data; TA Powder, however, did not display clear distinctions between its peaks as it did in the other tests (likely a side-effect of lower test resolution and other testing conditions) and presented an additional peak at ~440 °C. Phytic acid powder (g) had a strangely large peak at ~390 °C – which was not present in MCC data and appeared only as a small peak in TGA results – and a smaller peak at ~340 °C. It must be taken into account that the amount of gas released by PA powder and captured by the equipment is very small because of the compound's high char yield and because its main degradation product is water, which is too small a molecule to be captured in the tests that were performed; therefore, EGA runs performed on this sample were subject to much noise and imprecision.

For all of the melt-processed samples, a mass-spectrometry (MS) scan of the main degradation peak (i.e. a summation of the mass spectra of the data points along the peak) led to a spectrum that was identified as belonging to ABS according to the EGA library used (as shown in Figure 4.13), as expected. The mass spectrum

of Br-ABS's secondary peak (~250–350 °C) was shown to contain primarily TBBPA according to the compound library used (as shown in Figure 4.14), as expected; the additional peaks near m/z = 449 possibly refer to the presence of other additives in the material. An MS scan of TA powder's EGA peak was shown to contain primarily the compound 1,2,3-benzenetriol, which can be recognized mainly by the m/z = 126 ion, as shown in Figure 4.15; this compound is indeed one of the main thermal-degradation products of tannic acid, being directly derived from tannic acid's outer gallic acid units [71]. The extra peak at m/z = 44 is likely caused by a significant release of CO_2 coming from the ester linkages between the inner and outer gallic acid units [71]. Both the small and the large peaks in PA powder's EGA profile were shown to contain primarily 1,2-benzenediol (catechol) or 1,3-benzenediol (resorcinol), also known collectively as hydroquinone, which can be recognized by the m/z = 110 ion; it is important to consider, once again, that water is the main degradation product of phytic acid, but it was below the detection limit in the experiments. Mass spectra from FG powder's degradation peak were not matched to any specific compound, likely because a large amount of different volatiles were formed without any one compound dominating the spectra. The EGA library was not able to identify tannic acid, phytic acid, and fish gelatin as the generators of the respective EGA profiles; these compounds are likely not included in the library.

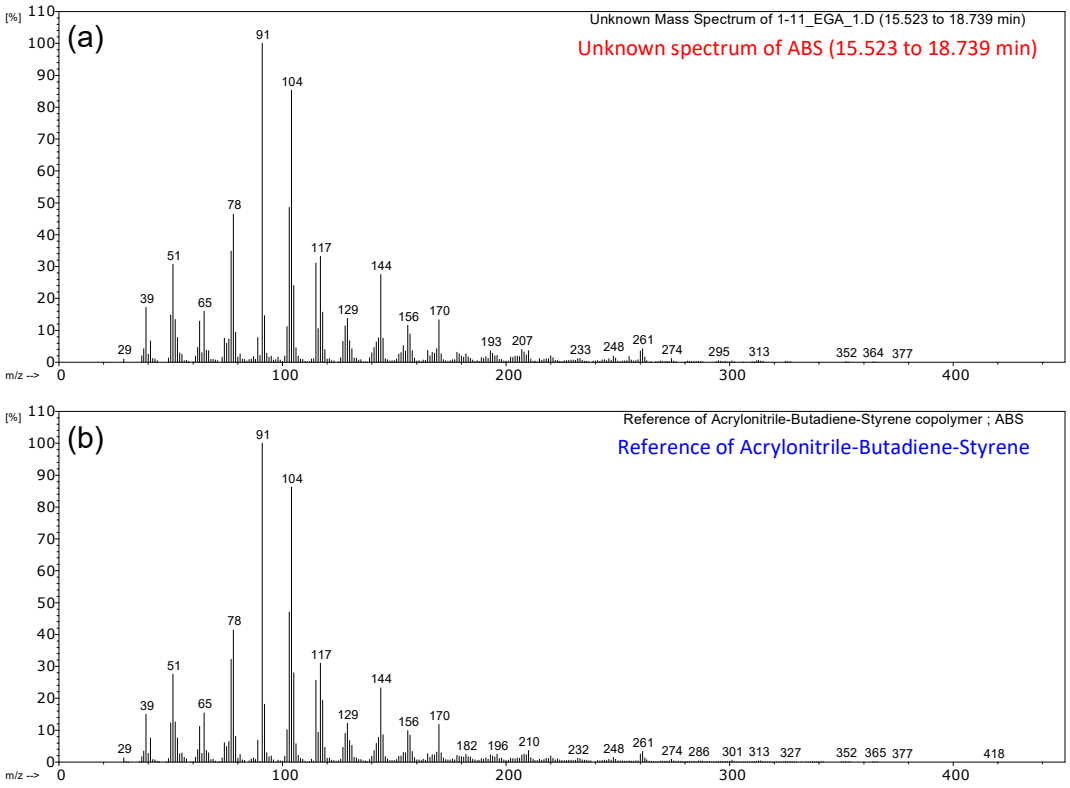

Figure 4.13. (a) Mass-spectrum scan corresponding to the peak in ABS's EGA curve; (b) reference mass spectrum for acrylonitrile-butadiene-styrene.

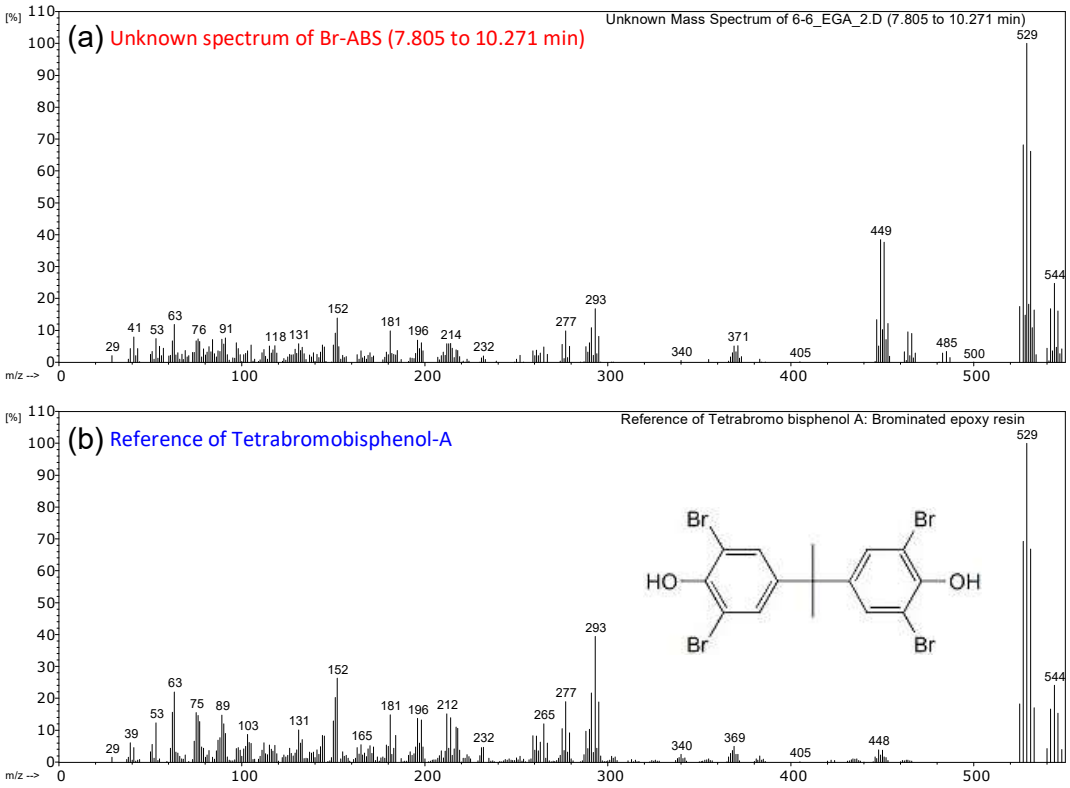

Figure 4.14. (a) Mass-spectrum scan corresponding to the first peak in Br-ABS's EGA curve; (b) reference mass spectrum for tetrabromobisphenol-A (TBBPA).

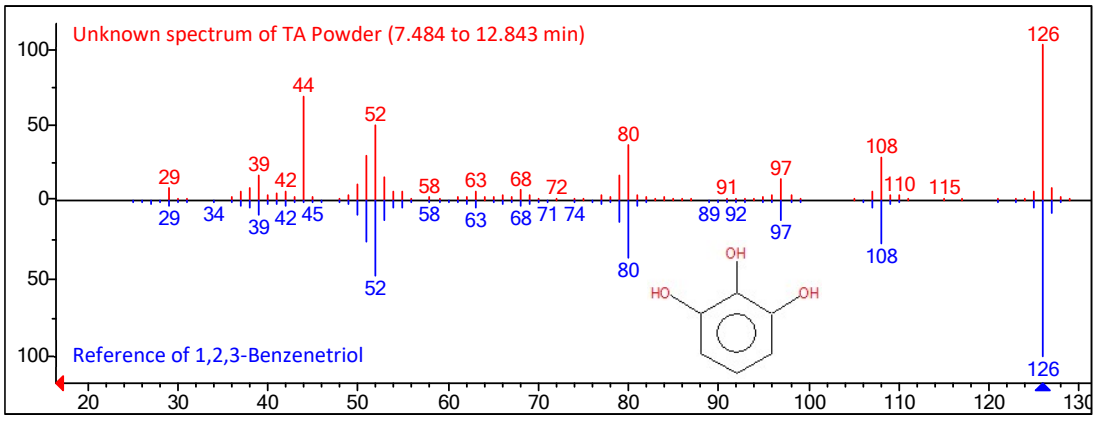

Figure 4.15. Top (red): Mass-spectrum scan corresponding to the main peak in TA Powder's EGA curve; Bottom (blue): reference mass spectrum of 1,2,3-benzenetriol.

The mass spectra related to the initial portion of the bio-based FR ABS composites' EGA profiles (~250–350 °C in Figure 4.12c–f), which refers mainly to the degradation of the FR additives, were not matched to any specific compound in the library, likely because of the relatively low amounts of volatiles from the

additives mixed with some volatiles being released early from ABS. A mass chromatogram of the m/z = 126 ion (Figure 4.16), however, was used to trace 1,2,3-benzenetriol, indicating its presence in TA and, to a lesser extent, in TA-FG and PA-TA, suggesting that this compound continued to be volatilized from tannic acid when it was used as an additive in ABS; the ion was not detected for PA, since this sample does not contain tannic acid. Figure 4.16 shows the presence of the m/z = 126 ion in TA, TA-FG, and PA-TA and its absence in PA. The chromatograms were normalized with relation to the highest intensity of the m/z = 39 ion in each sample (not shown), since this ion is present in many ABS-derived volatile compounds (assumed here to be in approximately equal total amounts in each sample), but in quantities low enough so that the m/z = 126 ion would still visibly appear in the 0–100% scale. The peaks located near the center (~17 min or ~440 °C) of all 4 mass chromatograms (b–e) should be ignored in this analysis, since they correspond to ABS's degradation peak (i.e. ABS-derived volatiles that contain the m/z = 126 ion in low quantities) and not to the additives' degradation peaks, as can be seen by looking at the total ion chromatogram (TIC), or EGA profile, of TA, shown in (a) for reference. A similar tracing of the m/z = 110 ion indicated its presence in very low amounts in TA, TA-FG, and PA-TA's additive-degradation portion (always towards the end of the section), suggesting the release of 1,2-benzenediol in very low quantities from tannic acid's inner gallic acid units in the later stages of tannic acid's degradation; this compound has been reported to be released in considerable amounts when tannic acid is flash-pyrolyzed at a high temperature (750 °C), but in very low amounts when tannic acid is pyrolyzed at a lower temperature (400 °C) or heated gradually, as was the case in the present study [71]. The ion was not observed for PA, since the amount of detectable volatiles generated by phytic acid are insignificant compared to that of ABS's volatiles.

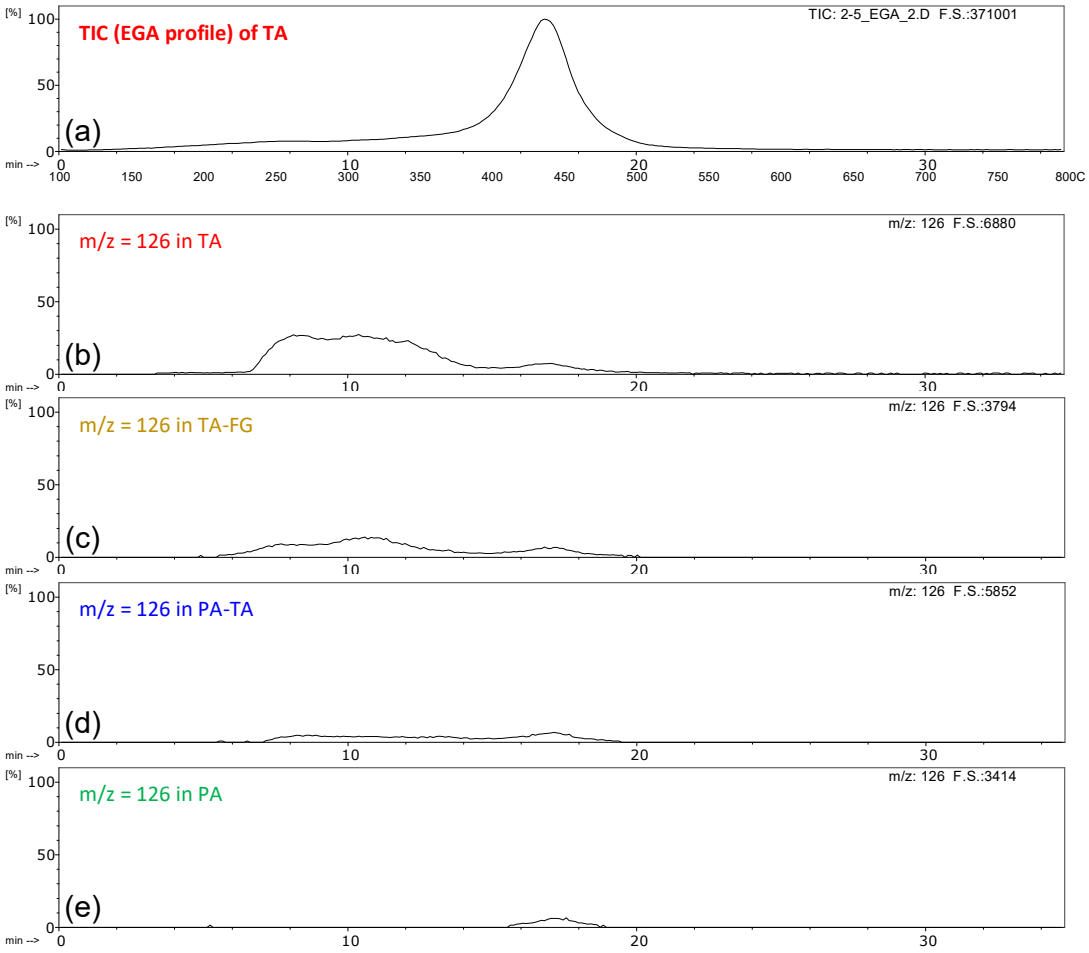

Figure 4.16. (a) Total ion chromatogram (TIC), or EGA curve, of TA; (b–e) mass chromatograms of the m/z = 126 ion in (b) TA, (c) TA-FG, (d) PA-TA, and (e) PA.

In order to perform a detailed analysis of the decomposition products of each sample, it was decided to perform HCA experiments in order to compare the products from the different samples within different temperature zones. The temperature zones were defined, based on the EGA profiles, so that different "events" (i.e. degradation of each of the additives, decomposition of ABS, and mixed zones) could be looked at separately. A premise used was that the temperature ranges would be the same for all of the samples, including the FR powders. The vertical lines in Figure 4.12 depict the temperature zones that were defined:

- Zone A: 100–220 °C (0–6 min);
- Zone B: 220–370 °C (6–13.5 min);
- Zone C: 370–400 °C (13.5–15 min);
- Zone D: 400–500 °C (15–20 min).

Zone A was a "preliminary" region that was expected to contain very few degradation products, since the EGA profiles are almost flat in this zone; some degradation products from tannic acid would possibly be seen for TA and TA Powder. Zone B contains most of tannic acid's degradation, a large part of fish gelatin's decomposition, and a small part of phytic acid's degradation; it would be interesting to see if the products volatilized from the FR powders would be the same as those released by the additives in the composites, and whether or not there would be ABS degradation products in this zone for the composites. Br-ABS's additives also decompose in Zone B. The definition of Zone C had 2 functions: (1) phytic acid decomposes mostly in this zone according to the EGA profile, so the same FR powder vs. composite comparison could possibly be performed; and (2) this zone still contains some TA Powder and FG Powder degradation but also already contains the beginning of ABS's degradation – it would be interesting to see if the fact that TA, TA-FG, PA-TA, and Br-ABS's curves were higher than ABS's curve in this zone was due to late degradation of the additives or indeed to an early degradation of ABS, as proposed earlier. Zone D contains the main portion of ABS's degradation (along with a part of fish gelatin's decomposition and the small final peak for TA Powder). This approach would hopefully enable a decoupling of the different events in order to understand the changes in degradation products released from each component in the samples.

4.4.2. Detailed Analysis of Degradation Products

HCA experiments were conducted on ABS, TA, PA, PA-TA, and individual TA and PA powders in order to try to understand the chemical mechanisms by which TA and PA act to flame retard ABS and by which TA and PA act synergistically with each other, as seen in cone calorimetry. It was decided to focus

on the most promising and scientifically motivating novel formulations (PA, TA, and PA-TA), so fish gelatin, TA-FG, and Br-ABS were not analyzed in this section of the study. The analysis consisted of identifying the degradation products released by each sample in each temperature zone and then comparing the sets of products among the different samples. Questions asked before the analysis and that would seek to be answered included: (1) Were the ABS degradation products generally the same between pure ABS and the bio-based FR composites? (2) If so, was the distribution of ABS products among the 4 temperature zones the same between pure ABS and the composites? (3) Were the tannic acid- and phytic acid-originated products the same between the individual powders and the composites? (4) Was the distribution of products among the 4 temperature zones changed between the pure FR components and the composites? (5) Were the relative proportions between ABS-derived and tannic acid- and/or phytic acid-derived products similar to the expected proportions, in total (both compared to the individual components' Py-GC-MS results and to MCC and TGA results)? (6) What were the relative proportions between ABS-derived and TA- and/or PA-derived products in each temperature zone – were they similar to the expected amounts based on the individual components' tests? (7) Were phosphorus-containing products released during experiments on PA Powder, PA, and PA-TA, indicating a possible gas-phase mechanism? (8) Were there any other notable differences between the individual components' chromatograms and the composites' chromatograms? In general, the objective was to determine whether TA and PA act in the condensed phase or in the gas phase in ABS and to try to elucidate specific chemical mechanisms or interactions occurring between ABS, tannic acid, and/or phytic acid.

4.4.2.1.
Qualitative Analysis

4.4.2.1.1.
ABS

Figure 4.17 presents the total ion chromatograms (TIC) for pure ABS for each temperature zone. The main peaks are labeled in the figure and listed in Table 4.9. Each graph is scaled differently, so that the peaks can be clearly seen. By looking

at the vertical-axis values, it can be seen that Zone D contained the largest amount of degradation products, which is consistent with the location of the main degradation peak in the MCC, TGA, and EGA curves. Zone C has the smallest values on the vertical axis, meaning that less degradation products were evolved in this zone; this is simply a consequence of the short temperature range (and, consequently, short duration) of this zone, spanning only from 370 to 400 °C. The main degradation products in Zone A were CO_2 (1), ethanol, ethylbenzene, styrene (5), and palmitic acid (16); the latter can be either from an impurity or industrial additive in the sample or derived from butadiene (combined with oxygen atoms from an impurity or a leak in the system), given that hydrocarbons with as many as 16 carbon atoms have been detected from the decomposition of 1,4-polybutadiene [128].

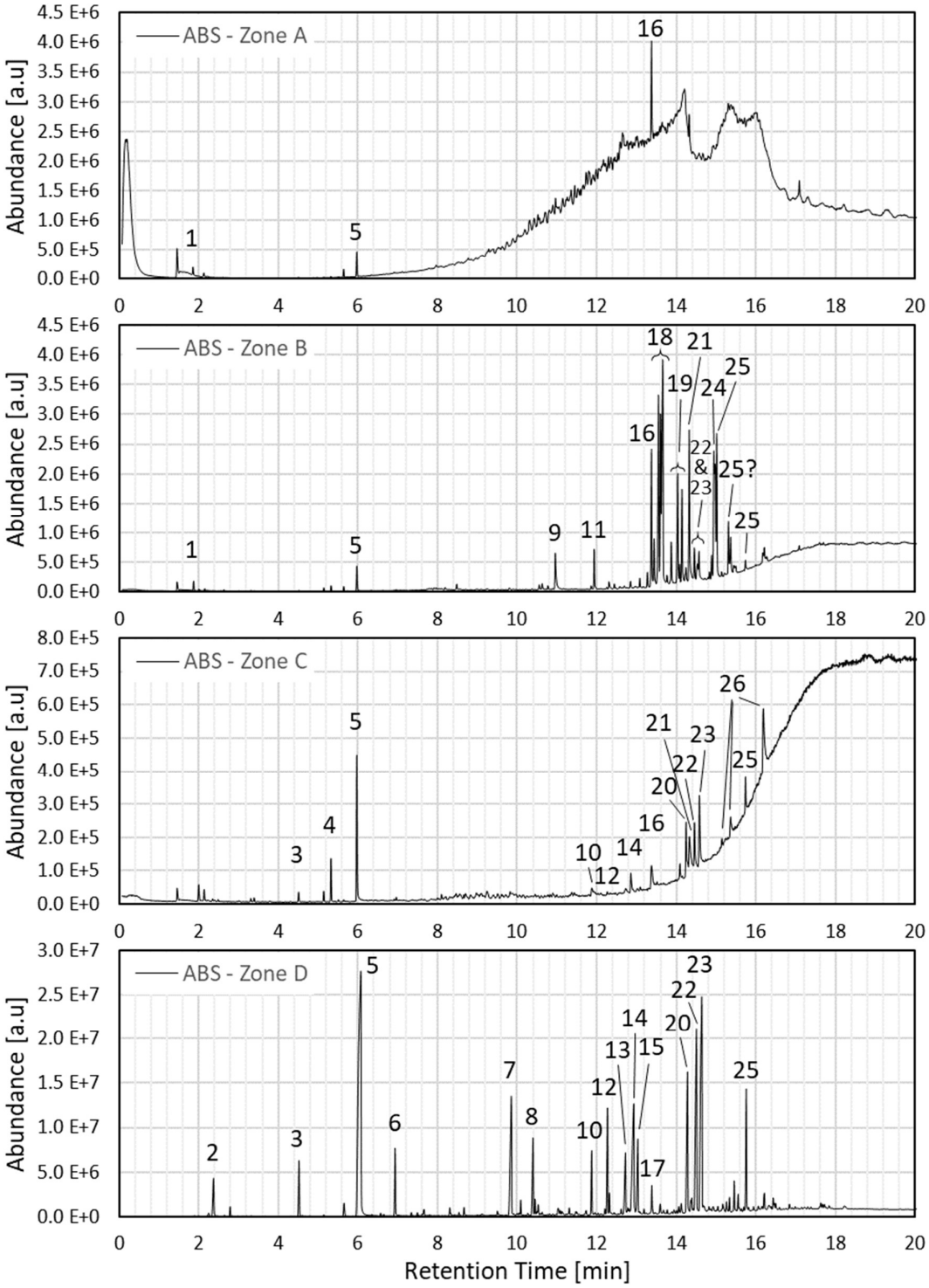

Figure 4.17. Total ion chromatograms for ABS for Zones A, B, C, and D.

Table 4.9

List of main peaks in the total ion chromatograms of ABS, TA, PA, PA-TA, TA Powder, and PA Powder, labeled in Figure 4.17–Figure 4.34 (black = mainly ABS-derived, red = tannic acid-derived compounds)

Peak #	Compound	Structure
1	CO2	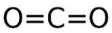
2	Acrylonitrile	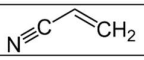
3	Toluene	
4	4-Vinylcyclohexene (Butadiene dimer)	
5	Styrene	
6	α-Methylstyrene	
7	SAN hybrid dimer (AS)	
8	SAN hybrid dimer (SA)	
9	Vinylnaphthalene?	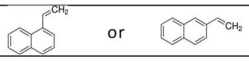
10	1,3-Diphenylpropane	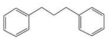
11	Acrylic acid dodecanyl ester??	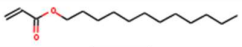
12	Styrene dimer	
13	SAN hybrid trimer (AAS)	
14	SAN hybrid trimer (ASA)	
15	SAN hybrid trimer (SAA)	
16	Palmitic acid	
17	m-Methylstyrene	
18	Isoquinoline or 2-[1-(4-Cyano-1,2,3,4-tetrahydronaphthyl)]propanenitrile	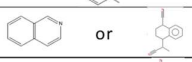
19	Isoquinoline or 3-[1-(4-Cyano-1,2,3,4-tetrahydronaphthyl)]propanenitrile	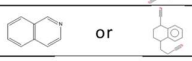
20	SAN hybrid trimer (ASS)	
21	Stearic acid	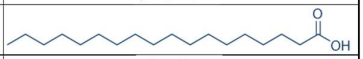
22	SAN hybrid trimer (SSA)	
23	SAN hybrid trimer (SAS)	
24	Propane-1,2-diyldibenzene	
25	Styrene trimer	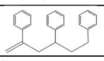
26	Hydroxyethylpalmitamide or 2-Heptadecylimidazole	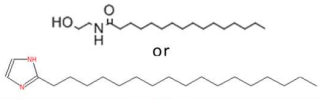
27	1,2,3-Benzenetriol	

Zone B also contained CO_2 (1) and styrene (5), but was dominated by much larger peaks, the three largest corresponding either to isoquinoline or to 2-[1-(4-cyano-1,2,3,4-tetrahydronaphthyl)]propanenitrile (2-CN-Np-PPN; 18); isoquinoline has been previously detected as a degradation product from styrene-acrylonitrile copolymer (SAN) [129], but the latter compound can be derived from a combination of acrylonitrile with either styrene or butadiene. Two more peaks (19) were also identified as either isoquinoline or the slightly different 3-[1-(4-cyano-1,2,3,4-tetrahydronaphthyl)]propanenitrile (3-CN-Np-PPN). Peaks 21, 16, and 11 were identified as stearic acid (octadecanoic acid), palmitic acid (hexadecanoic acid), and acrylic acid dodecanyl ester, respectively; these can be derived either from butadiene groups oxidized by impurities or industrial additives or from impurities or industrial additives themselves. Also present in relatively large amounts were styrene trimers (25) and propane-1,2-diyldibenzene (24), the latter likely derived from head-to-head styrene dimers. Peak 9 was tentatively assigned to vinylnaphthalene. All 6 isomers of SAN hybrid trimers were also observed, but only the SSA (styrene-styrene-acrylonitrile) and SAS (styrene-acrylonitrile-styrene) isomers (22 & 23) appeared in appreciable amounts; it is possible that the compounds with two styrene units and one acrylonitrile unit appeared more than the opposite because ABS typically has a larger styrene than acrylonitrile content [130], making the occurrence of hybrid trimers with more styrene units more probable than the opposite. Very small quantities of 1,3-butadiene, 4-vinylcyclohexene (4VCH; butadiene dimer), acrylonitrile, styrene dimers, and SAN hybrid dimers were observed. Many other compounds, most of them aromatic, were also detected in smaller amounts.

Zone C contained a large amount of styrene monomers (5). The next most abundant compounds were 4-vinylcyclohexene, which is a butadiene dimer (4), and SAN hybrid trimers with two styrene (S) units and one acrylonitrile (A) unit (SAS (23), ASS (20), and SSA (22), in order of abundance). Styrene trimers (25) were once again detected in reasonable amounts, as were stearic acid (21) and palmitic acid (16). Octadecanenitrile (14.1 min) and other long nitrogen-containing groups (26; hydroxyethylpalmitamide (HEP) and 2-heptadecylimidazole (HDI)) were also observed, possibly coming from butadiene chains that reacted with acrylonitrile groups and, for the palmitamide, with oxygen atoms from impurities. SAN hybrid trimers with 2 A units and 1 S unit were also present, with the ASA isomer (14)

appearing more than the others (likely because of the larger presence of styrene than acrylonitrile in ABS, making the probability of having two adjacent A units smaller than having them separated by an S unit). Also visible in the chromatogram are peaks corresponding to 1,3-butadiene (2 min), ethanol (2.15 min), toluene (3), and hexamethylcyclotrisiloxane (5.15 min), the latter probably coming from the GC column and not from the sample. 1,3-diphenylpropane (10; likely derived from head-to-tail styrene dimers) and styrene dimers (12; also head-to-tail) were detected in small amounts. Other compounds detected in small amounts included acrylonitrile, cyclic aliphatic hydrocarbons (likely from butadiene chains), butadiene trimers, and aromatic groups.

Zone D contained the largest amount of volatiles, since the main part of ABS's degradation occurs within this temperature range (400–500 °C). The most abundant compound was, once again, styrene (5). SAN hybrid trimers with 2 S units were the next most abundant (SAS, SSA, and ASS; 23, 22, and 20, respectively), followed by styrene trimers (25), SAN hybrid dimers (AS and SA; 7 and 8, respectively), styrene dimers (12), and SAN hybrid trimers with 2A units (ASA, SAA, and AAS; 14, 15, and 13, respectively). α-methylstyrene (6) was also present in appreciable amounts, as were 1,3-diphenylpropane (10), toluene (3), acrylonitrile (2), and m-methylstyrene (17). Next, in order of abundance, were 1-pentene-2,4-diyldibenzene (similar to a head-to-tail styrene dimer), propane-1,2-diyldibenzene (from head-to-head styrene dimers), ethylbenzene (likely derived from styrene or butadiene), benzylnitrile or tolunitrile, methacrylonitrile, acrylonitrile dimers, isoquinoline, and acetonitrile. Many other compounds were detected in low quantities, such as different varieties of small unsaturated aliphatic compounds (both linear and cyclic; likely derived from butadiene chains) and aromatic groups (such as benzene).

4.4.2.1.2. TA Powder

Figure 4.18 presents the chromatograms for pure tannic acid for each of the temperature zones. It is clear that the main component released during tannic acid's degradation is 1,2,3-benzenetriol (27), while CO_2 (1) is the second most abundant; this is in accordance with results seen from EGA analyses and with the literature

[71]. Most of the degradation occurs in Zone B (220–370 °C), which is consistent with MCC, TGA, and EGA results. The secondary peak in the EGA profile (~400–460 °C), which can also be seen as a very small "hump" in the dTG curves (~400–500 °C) but not in the MCC curves, can be caused by CO_2, which is the only compound abundantly released in Zone D (400–500 °C); CO_2 would not be seen in MCC tests because it does not react with oxygen (i.e. does not undergo combustion). The results are very much in agreement with those obtained by Xia et al. [71] when they studied the thermal degradation of tannic acid: Fourier-transform infrared spectroscopy (FTIR) showed that the main degradation products during the 230–400 °C decomposition step (Zones B and C in the present study) are CO_2 and 1,2,3-benzenetriol, and that there is another decomposition step from 400 to 720 °C during which mainly CO_2 is released. They also performed Py-GC-MS analysis using flash pyrolysis at 400 °C, obtaining a spectrum very similar to Zone B's spectrum in Figure 4.18. The authors explained that cleavage of the ester linkages between the outer and the inner layers of gallic acid units is responsible for the release of the 1,2,3-benzenetriol groups and CO_2.

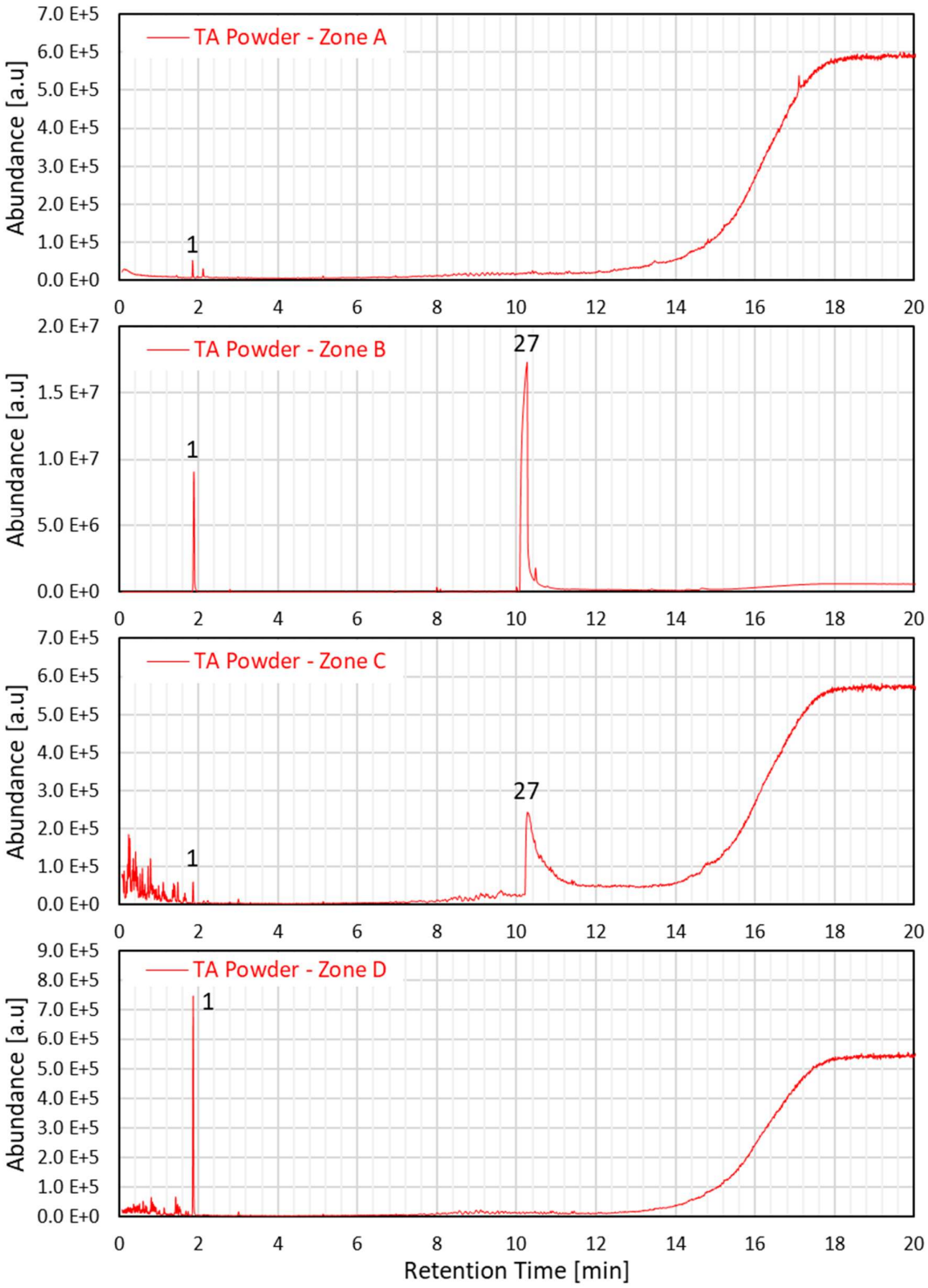

Figure 4.18. Total ion chromatograms for TA Powder for Zones A, B, C, and D.

Zone A presented mainly CO_2, with smaller quantities of ethanol, acetaldehyde, tetrahydrofuran, and toluene being detected as well; the total quantity detected, however, was very small. Xia et al. [71] observed the release of acetic acid and compounds containing C–O groups during this stage; they believed that the former came from the remaining acetate buffer that is used in the preparation of tannic acid. Zone B contained mainly 1,2,3-benzenetriol and CO_2; others compounds detected in this range were 2-methylhydroquinone, phenol, possibly 5-methylfuran-2(3H)-one or levuglucosenone, 2-methylfuran, and 6-methyl-3,4-dihydro-2H-pyran. Even smaller amounts of acetaldehyde, ethanol, acetone, furan, 1,3-cyclopentadiene, pyruvic aldehyde, acetic acid, tetrahydrofuran, benzene, toluene, 5-methyl-2(5H)-furanone, 1,2-benzenediol, and 1,3-benzenediol were identified. The origins of most of these compounds are unclear, especially the furans and pyrans; the benzenediols (hydroquinones) likely come from the inner gallic acid units, which are only released in appreciable amounts when the temperature is higher (e.g. flash pyrolysis at 750 °C) [71]. Xia et al. [71] reported only CO_2, 1,2,3-benzenetriol, groups containing C–O bonds (unspecified), and other aromatic groups (unspecified) in this temperature range. Zone C (370–400 °C) is still the tailing part of tannic acid's main degradation step according to the MCC, TGA, and EGA curves; the main products were therefore the same as before, but in lower amounts: 1,2,3-benzenetriol and CO_2. Very small amounts of ethanol, furan, 2-methylfuran, tetrahydrofuran, benzene, and possibly 1,3-benzenediol and bisphenol-A were also detected. Zone D contained almost only CO_2, with very small amounts of tetrahydrofuran, benzene, and possibly bisphenol-A being detected.

4.4.2.1.3.
TA Composite

Figure 4.19 presents the TICs for TA for each of the 4 temperature zones. In order to discuss TA's results more efficiently, it is desirable to compare them to those of TA's individual components (ABS and tannic acid). TA's chromatograms are therefore compared to those of ABS and TA Powder for each of the temperature zones in Figure 4.20 through Figure 4.23. In these comparison figures, two scaling

procedures were performed in order to enable proper comparisons between the intensities of the different samples' peaks: (1) since different masses were used for each sample and the masses were not recorded, it was necessary to estimate the relative masses between the samples by integrating the chromatograms from all 4 temperature zones for a given sample and dividing by the sample's expected "volatilization yield" (1 minus the expected char yield), providing approximate "relative mass factors" between the samples (this procedure is explained in more detail in the next section, *Semi-Quantitative Analysis*); the chromatograms for each sample were then divided by the sample's "relative mass factor" (considering 1 for ABS) to obtain normalized curves that could theoretically be compared among different samples; (2) ABS's TICs were multiplied by 70%, and TA Powder's were multiplied by 30%, which are the respective mass fractions of each component in the TA composite. The realization of these scaling procedures allows a direct comparison of the curves between the different samples, so that the expected chromatogram for TA is simply the sum of the chromatograms of ABS and TA Powder; in other words, a compound released from ABS and not from TA Powder, for example, "should" have the same intensity in TA as in ABS in the figures below, if no interactions occurred between the components. It should be noted that the procedure for estimating relative mass factors by integrating the chromatograms is only an approximation and is subject to errors; however, most of the analysis described below does not *depend* on this correction, since relative changes are normally referred to (either directly or indirectly) rather than absolute changes. The scaling/mass-correction procedure *does*, though, provide an easy and direct visualization of the arguments presented in the discussion below.

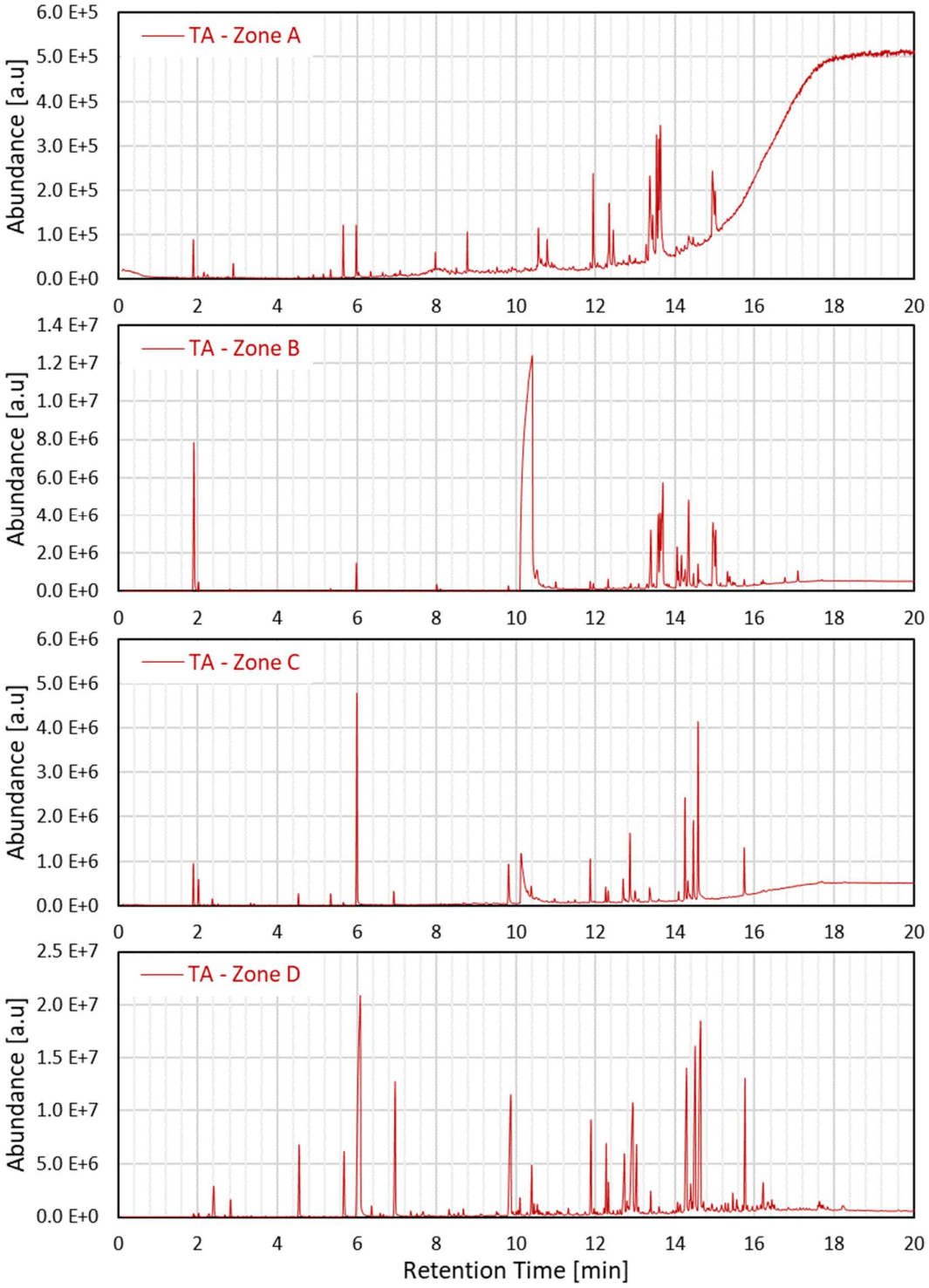

Figure 4.19. Total ion chromatograms for TA for Zones A, B, C, and D.

Figure 4.20 presents the ABS vs. TA Powder vs. TA composite comparison for Zone A. It is immediately clear that TA contains many more degradation products than ABS and TA Powder. A quick look at Figure 4.21a shows that many of these additional products are the same as those that occur for ABS in Zone B. It seems, therefore, that some degradation products from ABS are being anticipated from Zone B (220–370 °C) to Zone A (100–220 °C), which is consistent with the reduction in activation energy from ABS to TA seen in the previous section. Products not seen (or seen in very low amounts) for ABS in Zones A and B are marked in Figure 4.20c: the peaks marked with an "*" correspond to nonanal and dodecanal, which were barely present for ABS in Zone A and are possibly derived from butadiene chains, with the addition of oxygen from impurities; and the peaks marked with a "+" were identified as either 3-cyclohexen-1-ylbenzene or styrene and were present in very low quantities in Zone B for ABS. It should also be noted that the total amount of styrene (peak 5; 6 min) reduced significantly and that the relative quantities between propane-1,2-diyldibenzene (peak 24; 14.9 min) and styrene trimer (peak 25; 15 min) switched from ABS Zone B (styrene trimer was higher) to TA Zone A (propane-1,2-diyldibenzene was higher).

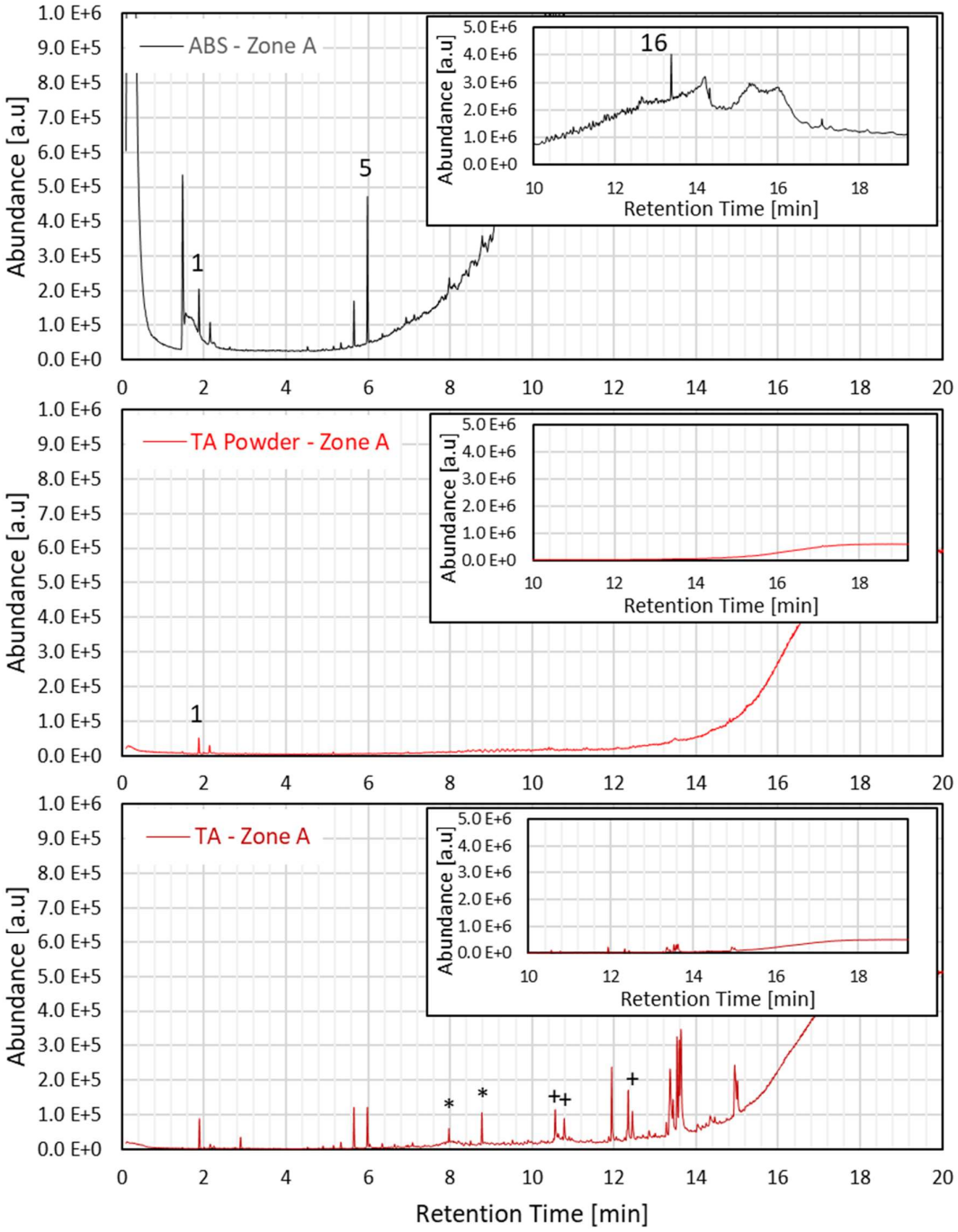

Figure 4.20. Zone A total ion chromatograms for ABS, TA Powder, and TA.

Figure 4.21 shows the comparison for Zone B. TA's behavior in this zone was quite similar to what was expected, since its TIC contains most of ABS and TA Powder's peaks with similar intensities. The most abundant volatiles were 1,2,3-benzenetriol and CO_2, both coming from tannic acid's degradation; these compounds were present in slightly smaller amounts than expected, however. The ABS-derived products are mostly the same as for neat ABS, but the intensities are larger in TA than in the mass-corrected ABS chromatogram; this fact supports the idea, once again, that tannic acid facilitates or anticipates ABS's decomposition, since many of the products are the same in Zones C and D and were anticipated, for TA, to Zone B, increasing the quantities. Some Zone B products that do not appear in Zones C and D, such as the abundant isoquinoline or 2-CN-Np-PPN (18), also appear in larger amounts than expected for TA, suggesting that, besides anticipating ABS's degradation process, tannic acid might be changing the nature and relative proportions of the products. Corroborating this statement is the fact that the relative intensities between the propane-1,2-diyldibenzene (24) and styrene trimer (25) peaks are once again switched, just as seen for TA's Zone A.

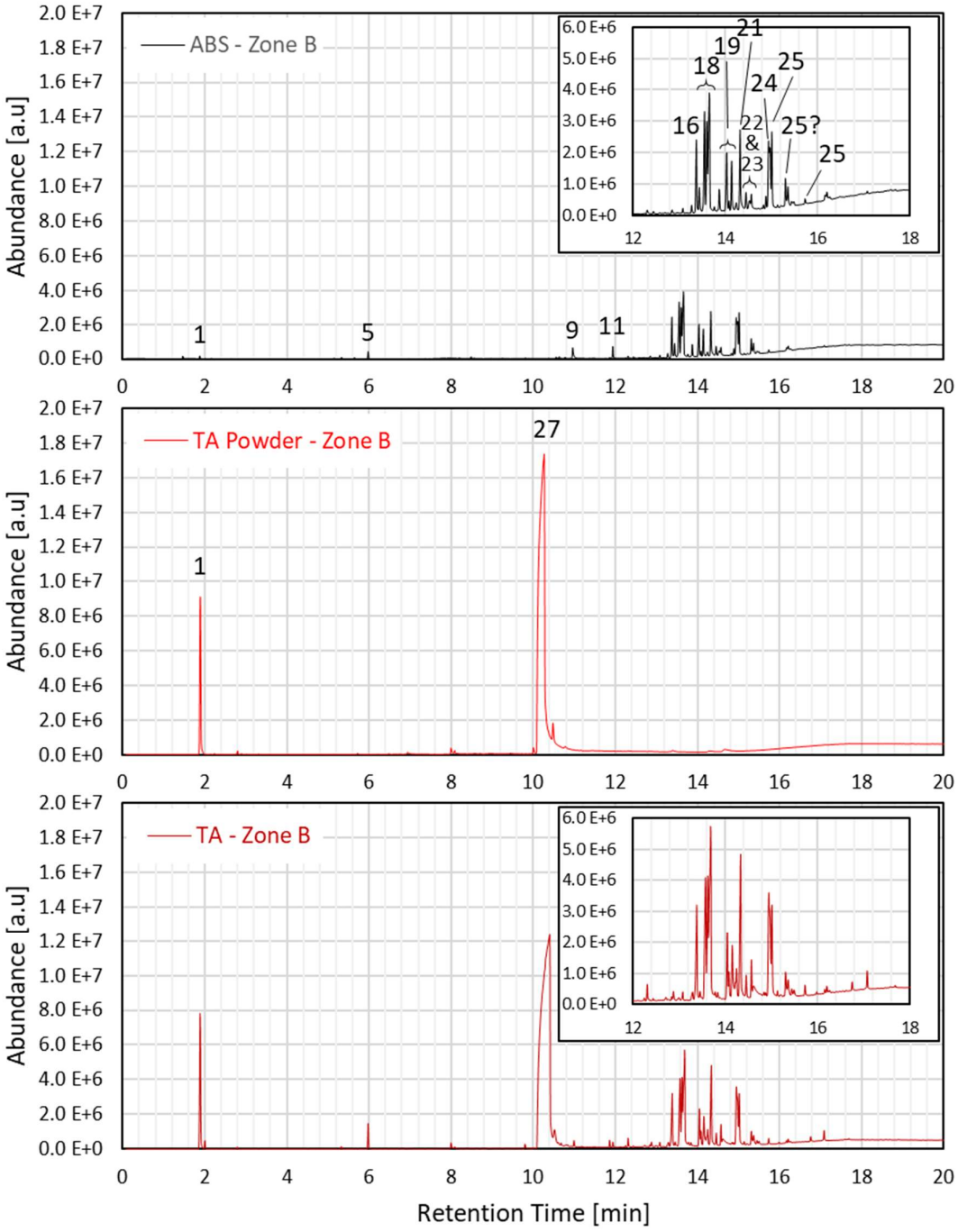

Figure 4.21. Zone B total ion chromatograms for ABS, TA Powder, and TA.

The comparison for Zone C is shown in Figure 4.22. Two facts are clearly visible: (1) the peaks corresponding to tannic acid's degradation products (CO_2 (1) and 1,2,3-benzenetriol (27)) are higher than expected, and (2) the remaining degradation products, derived from ABS, have much higher intensities than expected. CO_2 and 1,2,3-benzenetriol's peaks had been lower than expected for Zone B, so the fact that they are higher than predicted for Zone C suggests that the volatilization of tannic acid degradation products was slightly delayed when the additive was used in ABS; this phenomenon was also observed in the TGA curves. The intensities of the ABS-derived products increased significantly from ABS to TA; almost all of these products also occurred in Zone D for ABS, suggesting that they were anticipated from Zone D into Zone C for TA. The numbered peaks in TA's chromatogram were barely or not-at-all present in Zone C for ABS but were observed in Zone D for ABS (α-methylstyrene (6), SAN hybrid dimers and trimers (7, 8, 13, 14, 15), 1,3-diphenylpropane (10), and styrene dimers (12)), indicating that they were indeed anticipated from Zone D into Zone C. This information is consistent, once again, with the reduced E_a calculated for TA in relation to ABS. The long nitrogen-containing groups HEP and HDI (26) seen for ABS were not observed for TA. An additional peak (*) can be seen for TA, corresponding to either isobutene or 1-butene; the 1,3-butadiene peak, on the other hand, which had been detected in small amounts for ABS, was not identified at all for TA.

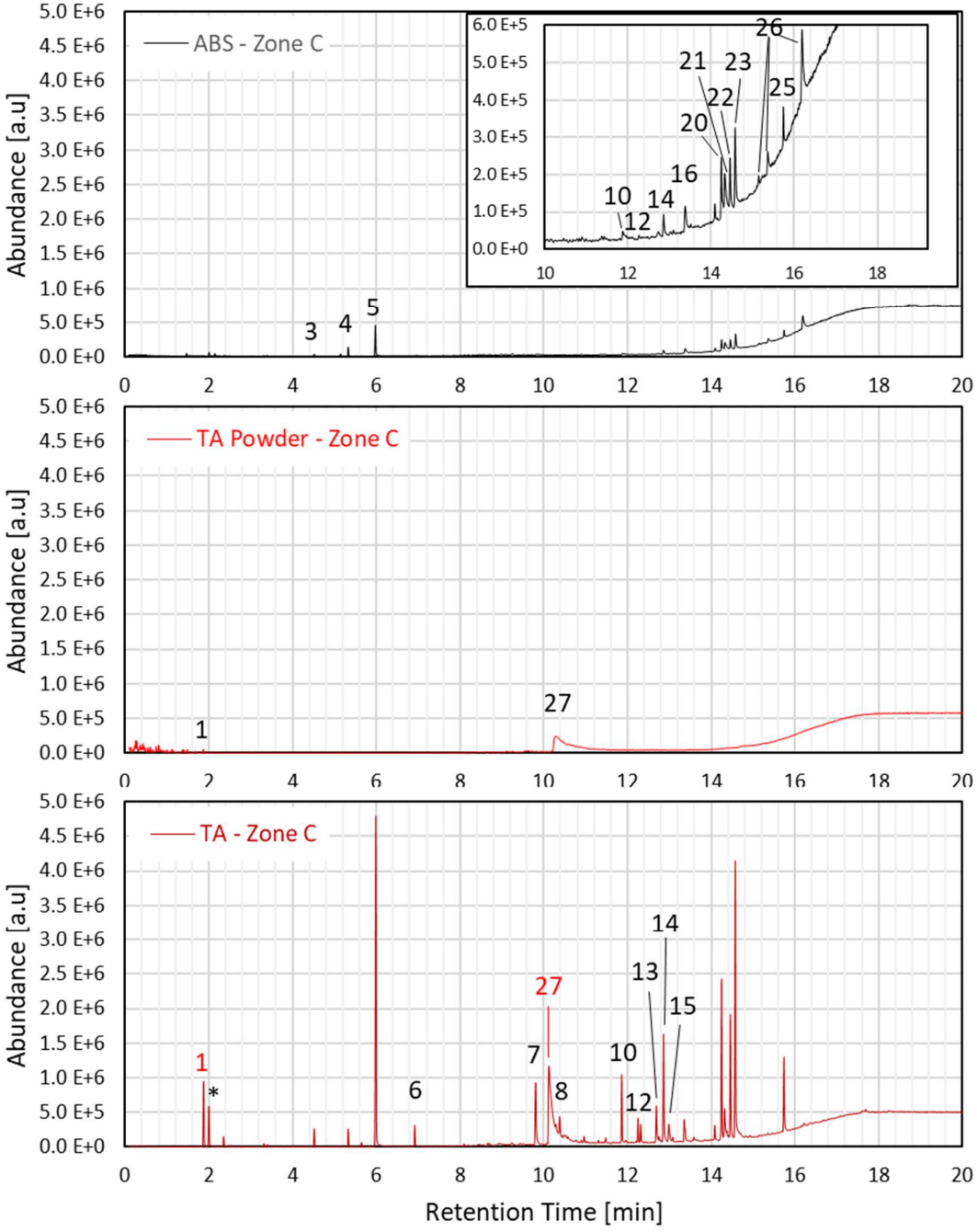

Figure 4.22. Zone C total ion chromatograms for ABS, TA Powder, and TA.

Figure 4.23 contains the TA comparison for Zone D. A quick glance at the chromatograms shows that most of the degradation products are the same between ABS and TA, with lower intensities than expected for TA; this simply reflects the anticipations observed in Zones A through C, leaving less material to be degraded in Zone D. A closer look, however, reveals that a number of peaks (identified by numbers or symbols for TA) maintained or increased their intensities from ABS to TA. Methacrylonitrile (*) increased, while acrylonitrile monomer (2) was reduced; toluene (3), ethylbenzene (+) and α-methylstyrene (6) increased, while styrene monomer (5) was reduced; 1,3-diphenylpropane (10) increased, while styrene dimer (12) was reduced; and SAN hybrid dimers and trimers and styrene trimer were reduced. A pattern can be observed: there was a general reduction in the amounts of monomers, dimers, and trimers of acrylonitrile and styrene (and 1,3-butadiene as well, taking Zone C into consideration), while other products derived from or similar to the monomers, dimers, and trimers became more abundant. This important observation suggests that there might be a change in degradation mechanism caused by the addition of tannic acid into ABS, which can possibly be responsible for the reduced activation energy and, consequently, to the reduced flammability (as measured by PHRR in MCC) of ABS/tannic acid composites.

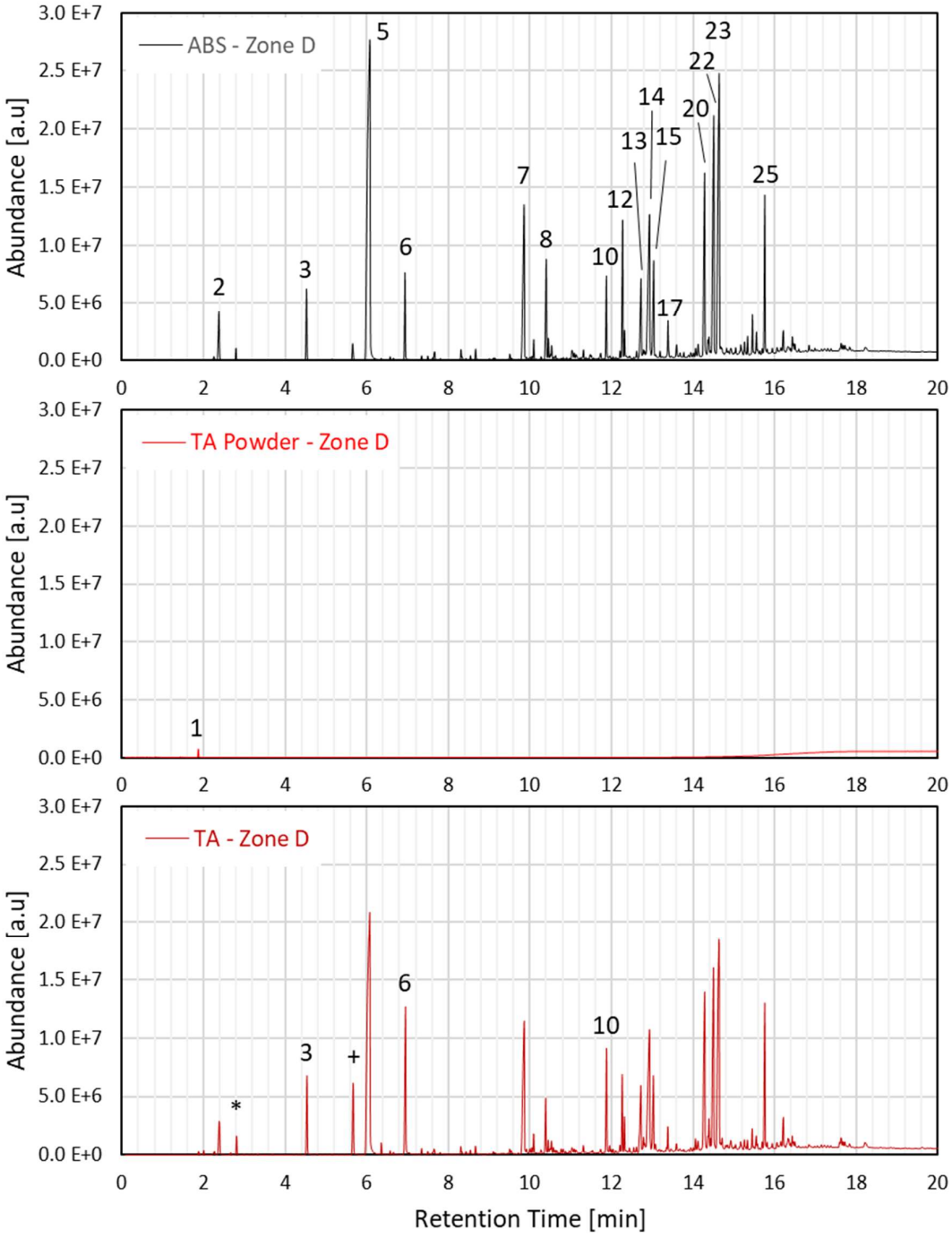

Figure 4.23. Zone D total ion chromatograms for ABS, TA Powder, and TA.

From the analysis of TA's TICs and their comparison to ABS and TA Powder's chromatograms, three main conclusions can be reached: (1) the addition of tannic acid into ABS accelerates the initial degradation of the polymer, causing decomposition products to be released earlier than for the pure polymer – a reduction of the activation energy for ABS's decomposition is suspected to be responsible for this behavior; (2) the degradation of tannic acid seems to be moderately delayed when it is used as an additive in ABS; and (3) the nature and the relative proportions of ABS's decomposition products change when tannic acid is used as an additive, giving preference to the volatilization of products derived from acrylonitrile, butadiene, and styrene monomers, dimers, and trimers rather than to the monomers, dimers, and trimers themselves. It is suspected that the interaction of tannic acid (or of its degradation products) with ABS in the condensed phase partially alters ABS's decomposition mechanism in such a way that initial degradation is facilitated (hence the reduction in activation energy), changing the nature of the evolved fragments in the process. If this proposition is correct, this ABS-tannic acid interaction can be responsible for the reduction in PHRR seen for ABS/TA composites in MCC to values significantly lower than the additively predicted "no-interaction" PHRR.

4.4.2.1.4. PA Powder

Almost no volatiles were detected from the pyrolysis of phytic acid powder, as show in Figure 4.24. This is consistent with the fact that its main volatile degradation product is water, which is too small a molecule to be captured by the equipment in the configurations under which the experiments were performed (i.e. it was below the detection limit). Trace amounts of some compounds were observed: ethanol, acetone, isopropanol, 1,3-cyclohexadiene, and tetrahydrofuran in Zone A; acetaldehyde, ethanol, acrolein, 1,3-cyclohexadiene, tetrahydrofuran, and benzene in Zone B; and tetrahydrofuran and benzene in Zones C and D. Tetradecanoic acid, palmitic acid (16), and squalene (large peak at ~17 min) were also identified in Zone B, but they are likely due to contaminants in the sample or in the system. It is noteworthy that no phosphorus-containing products were detected, indicating that all of the phosphorus remains in the char residue when

phytic acid is degraded. Assuming that the phytic acid sodium salt hydrate product used has a chemical formula of $C_6H_{12}O_{24}P_6.6Na.7H_2O$ (taken from [120], who reportedly used the same product as in the present study; the manufacturer only specifies that the sodium content is ≥ 5 mol/mol and that the compound is a "hydrate"), the mass loss of 19.2% seen in MCC or 18.8% seen in TGA experiments corresponds almost exactly to the loss of 10 H_2O molecules (19.6%) (likely the 7 water-of-crystallization molecules and 3 more water molecules derived from hydroxyl groups), suggesting that all of the phosphorus and sodium atoms and possibly all of the carbon atoms might indeed remain in the char.

Few reports have been published on the thermal degradation of phytic acid, and even less on that of phytic acid sodium salt (or sodium phytate). One study conducted on phytic acid found that, below 500 °C, the product releases almost only water, with a possible small loss of CO_2 at ~360 °C. In their study, a major decomposition step occurred from 600 to 700 °C; this range was not included in the present analysis, but was not seen in MCC, TGA, and EGA experiments. It is possible that phytic acid sodium salt hydrate (or sodium phytate) has a higher thermal stability than unsubstituted phytic acid due to the presence of the sodium ions. The release of almost only water below 500 °C seen by the authors is in agreement with the lack of peaks observed in PA Powder's chromatograms.

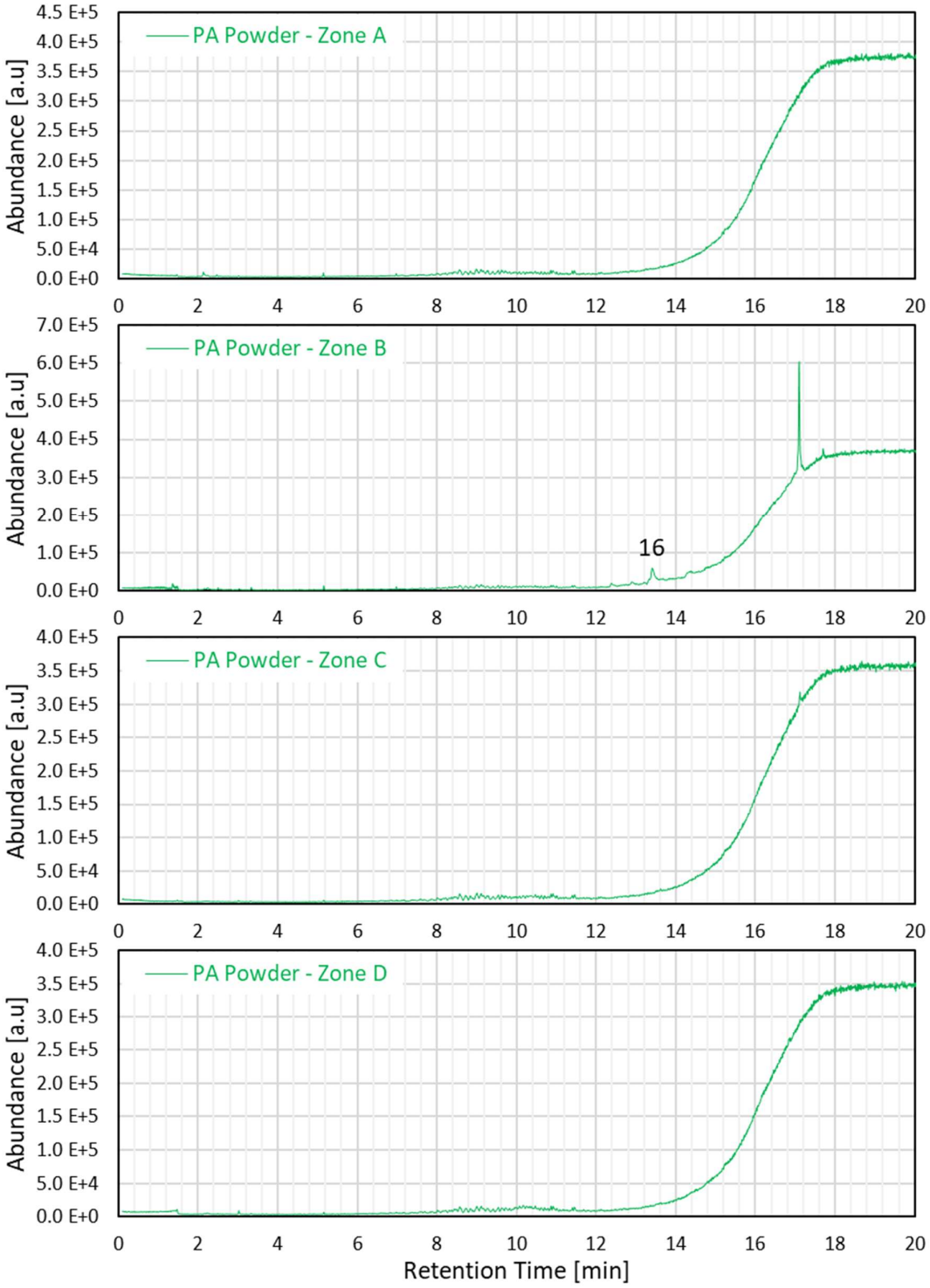

Figure 4.24. Total ion chromatograms for PA Powder for Zones A, B, C, and D.

4.4.2.1.5.
PA Composite

The total ion chromatograms for the ABS/PA composite for each temperature zone are presented in Figure 4.25. As done for TA, the chromatograms will be analyzed in comparison to ABS and PA Powder's results, using Figure 4.26 through Figure 4.29. The same scaling procedure as used for TA was performed.

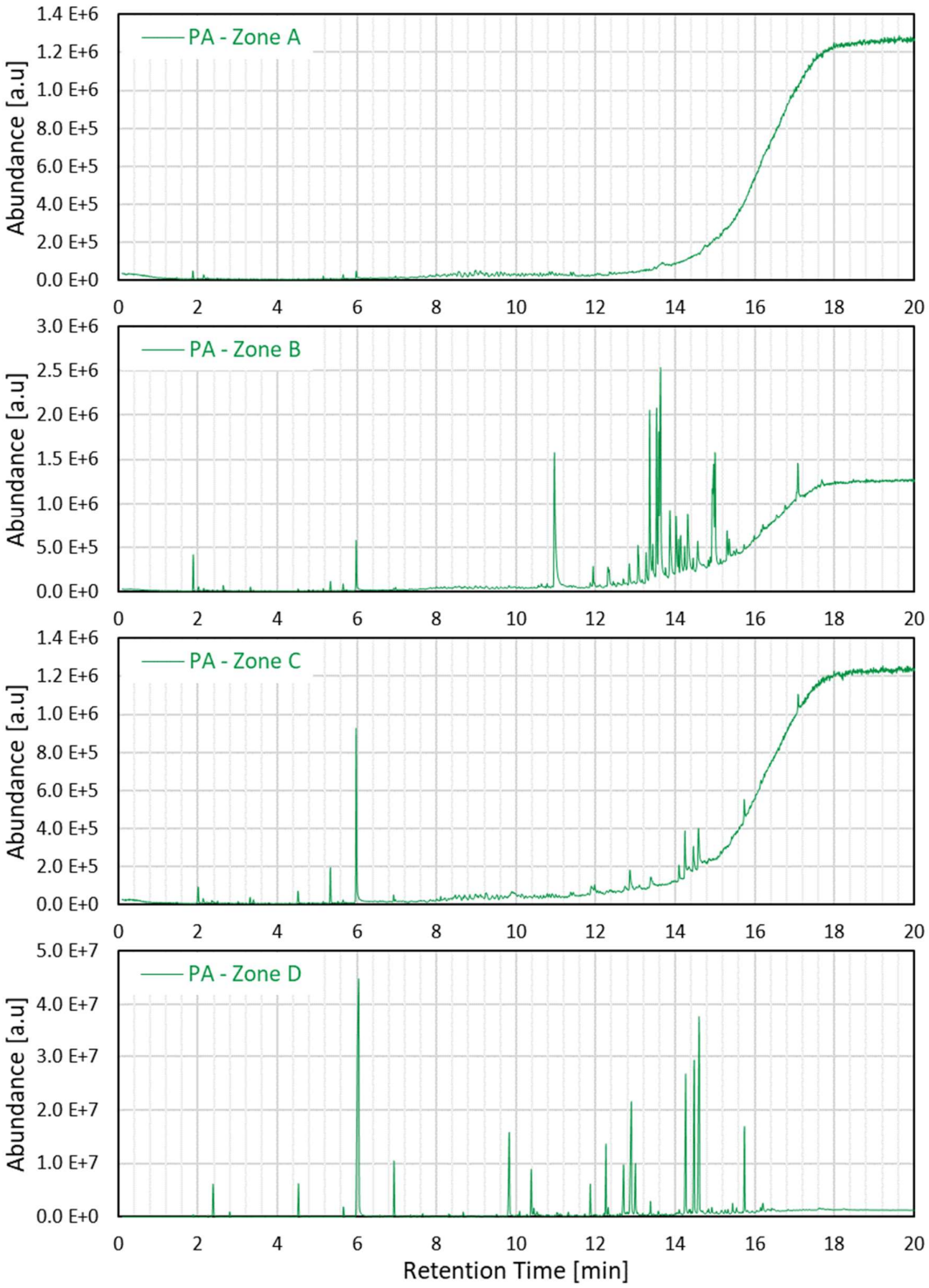

Figure 4.25. Total ion chromatograms for PA for Zones A, B, C, and D.

Figure 4.26 presents the ABS vs. PA Powder vs. PA composite comparison for Zone A. Very little change can be seen, except for a reduction in peak intensities and the suppression of a few small peaks. The addition of a small isoquinoline "peak" (or hump) at 13.6 min can also be seen. Figure 4.27 shows little change in the types of products seen as well; however, there are shifts in some of the relative intensities. Most compounds appeared in lower quantities than expected in PA, most notably the ones labeled in red in Figure 4.27c, including isoquinoline or 2- or 3-CN-Np-PPN (18), propane-1,2-diydibenzene (24), styrene trimer (25), stearic acid (21), and acrylic acid dodecanyl ester (11); vinylnaphthalene or acenaphthalene (9), on the other hand, increased significantly, and CO_2 (1) and styrene (5) increased marginally. In summary, a total reduction in volatile content was seen in both Zone A and Zone B, with vinylnaphthalene or acenaphthalene being the only compound to show a substantial increase in Zone B.

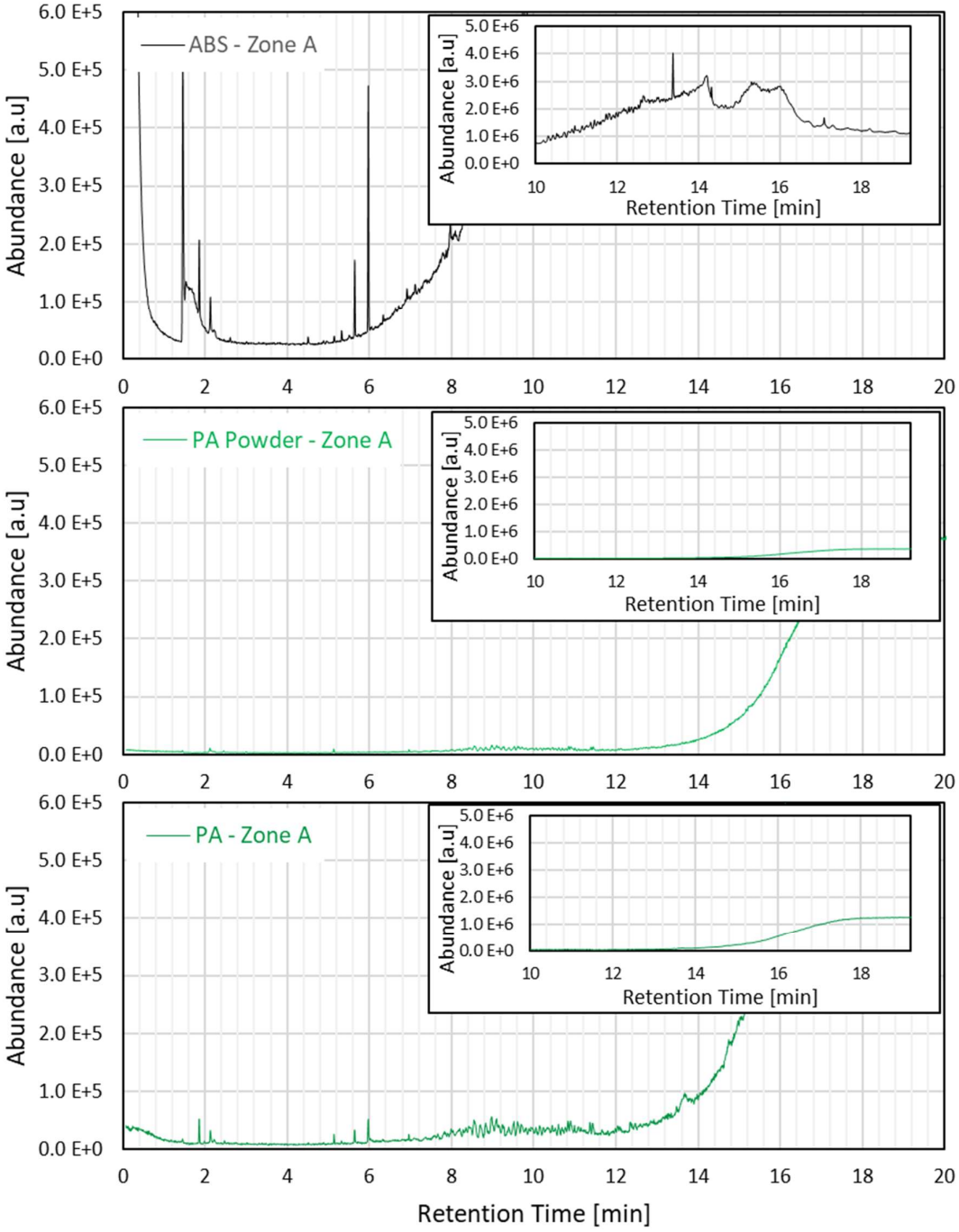

Figure 4.26. Zone A total ion chromatograms for ABS, PA Powder, and PA.

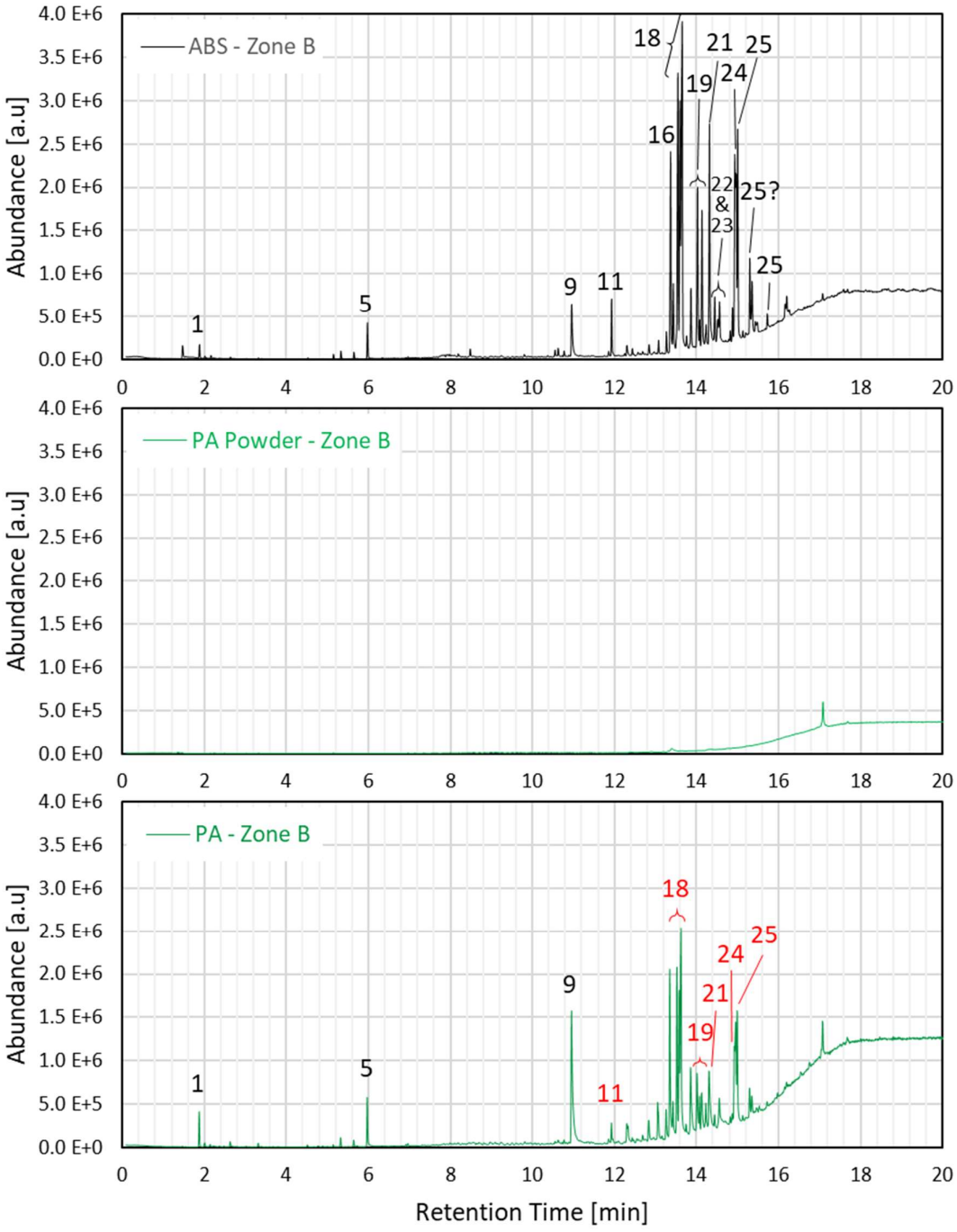

Figure 4.27. Zone B total ion chromatograms for ABS, PA Powder, and PA.

The degradation products for Zone C were almost identical between ABS and PA, with a higher volatile content for the latter (Figure 4.28). Most of the compounds presented higher peak intensities for PA, with the exception of the SAN hybrid trimers with 2 S units and styrene trimer, which remained with approximately the same intensities. The long nitrogen-containing groups HEP and HDI detected for ABS were not seen for PA, as was the case for TA. Figure 4.29 presents almost identical chromatograms between ABS and PA as well, with higher peak intensities for the latter. Especially significant peak growths can be seen for styrene (5), α-methylstyrene (6; less pronounced), SAN hybrid trimer type ASA (14), and all 3 SAN hybrid trimers with 2 S units and 1 A unit (20, 22, and 23); the only observed peak reduction was for 1,3-diphenylpropane (10).

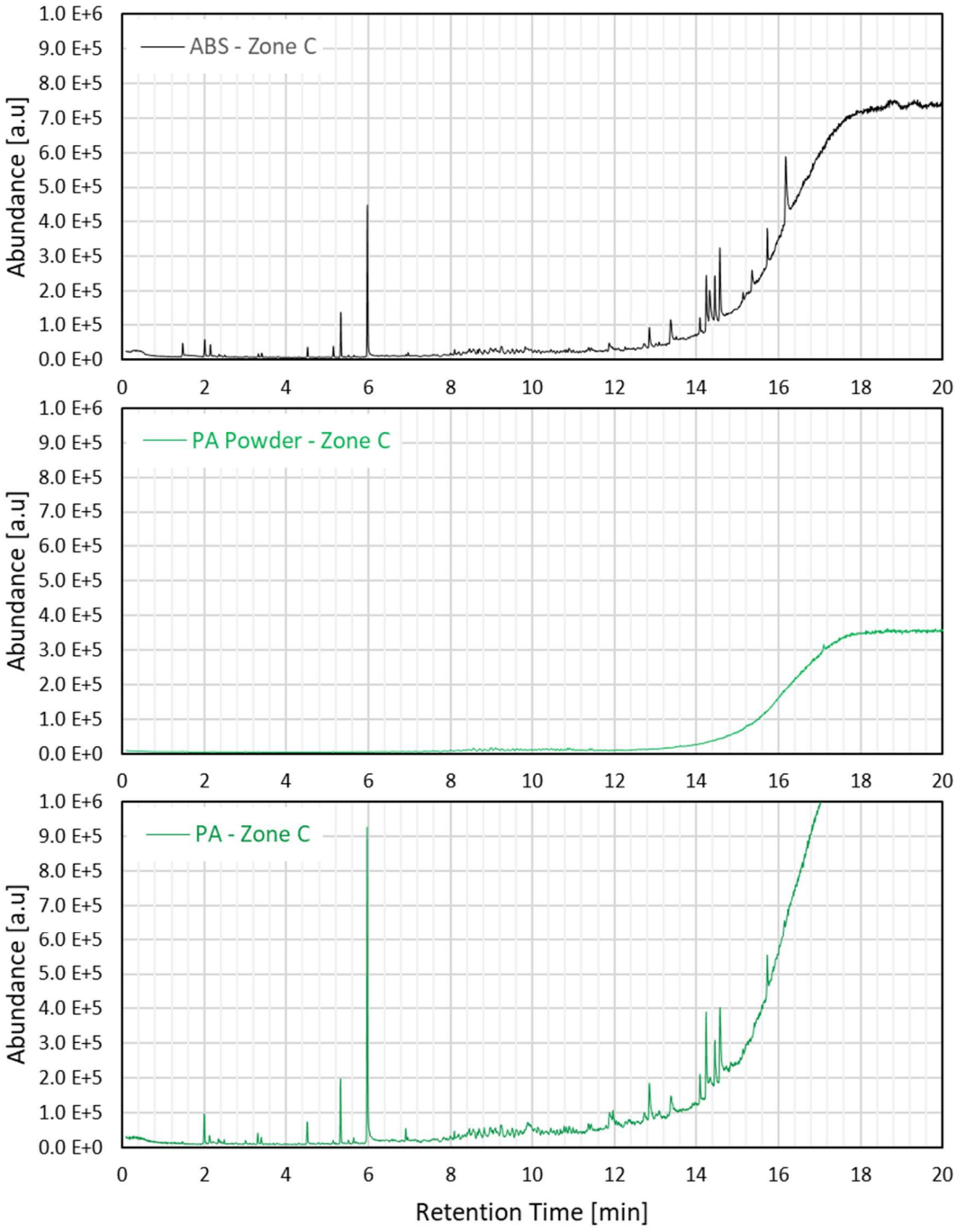

Figure 4.28. Zone C total ion chromatograms for ABS, PA Powder, and PA.

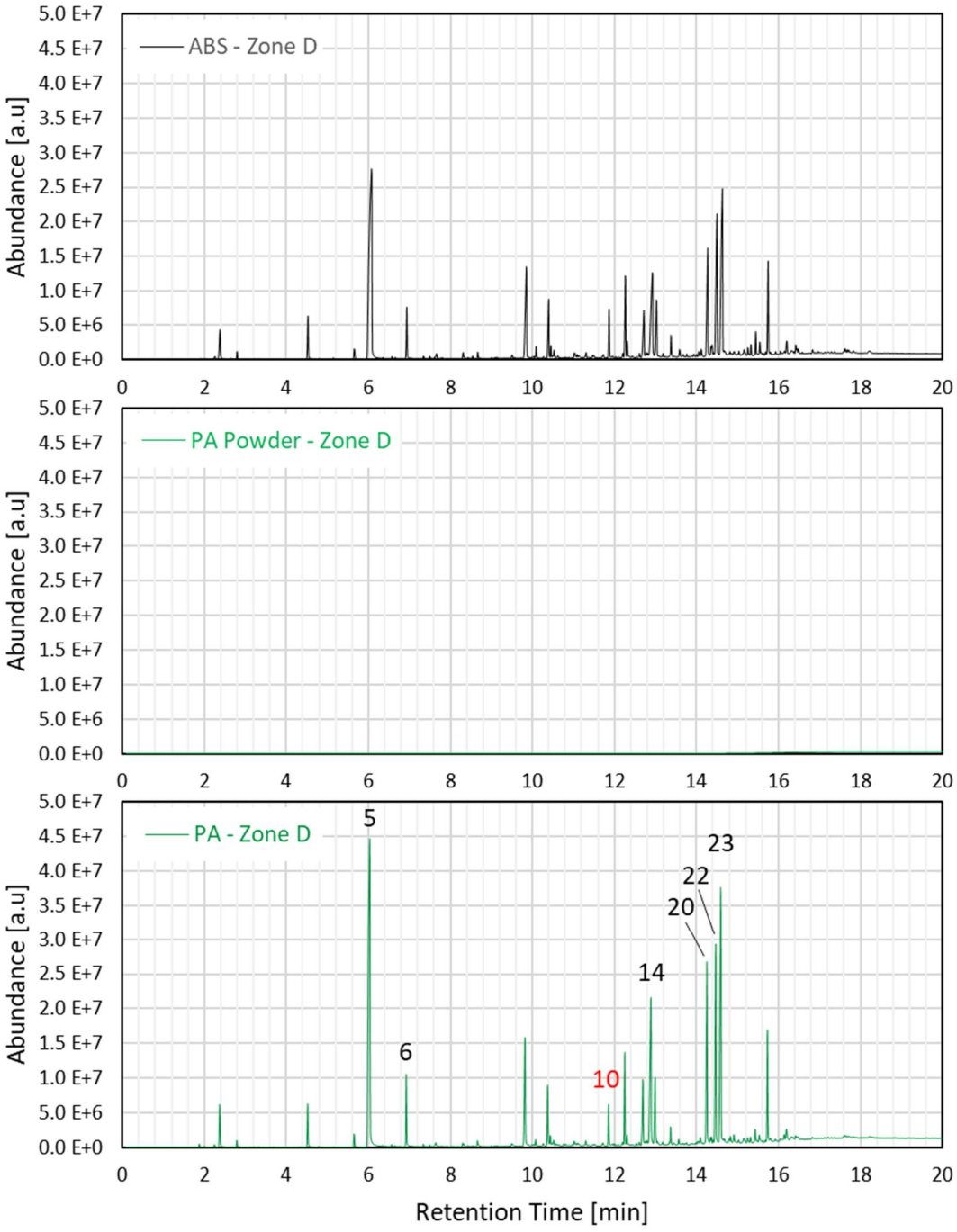

Figure 4.29. Zone D total ion chromatograms for ABS, PA Powder, and PA.

In summary, there is almost no change in the nature and relative proportions of ABS's degradation products between pure ABS and the ABS/PA composite. It appears, however, that there is a slight delay in ABS degradation, since PA has smaller peaks than ABS in Zones A and B but larger peaks in Zones C and D. This delay was not seen in MCC, but it is consistent with the decomposition-peak delay observed in EGA profiles and with the increase in E_a calculated for PA in relation to ABS based on TGA results. It should be noted that no phosphorus-containing products were detected for PA (as was the case for PA Powder), suggesting that gas-phase mechanisms do not play a role in phytic acid's flame-retardation of ABS; this is consistent with the conclusions reached from cone calorimetry data (Table 4.4 and Table 4.5) based on the similar THR Ratios and χ values between ABS and PA (Table 4.3).

4.4.2.1.6.
PA-TA Composite

Figure 4.30 presents the TICs for PA-TA for each of the temperature zones. As was done for the previous samples, PA-TA's chromatograms will be analyzed in the context of comparisons to the other materials tested. Instead of being compared to the individual components (ABS, TA Powder, and PA Powder), however, comparisons between ABS, TA composite, PA composite, and PA-TA composite will be presented and discussed (Figure 4.31–Figure 4.34), enabling the focus to be placed on interactions between tannic acid and phytic acid sodium salt rather than between the additives and ABS (which were already discussed for the other samples). Very few differences had been seen between tannic acid's degradation products in TA Powder and in TA (except for a reduction of the degradation products in Zone B and an increase in Zone C), and no differences had been seen between phytic acid's detected degradation products in PA Powder and in PA (which were practically non-existent), so little visual information will be missed by presenting PA-TA's comparison in relation to TA and PA rather than to TA Powder and PA Powder.

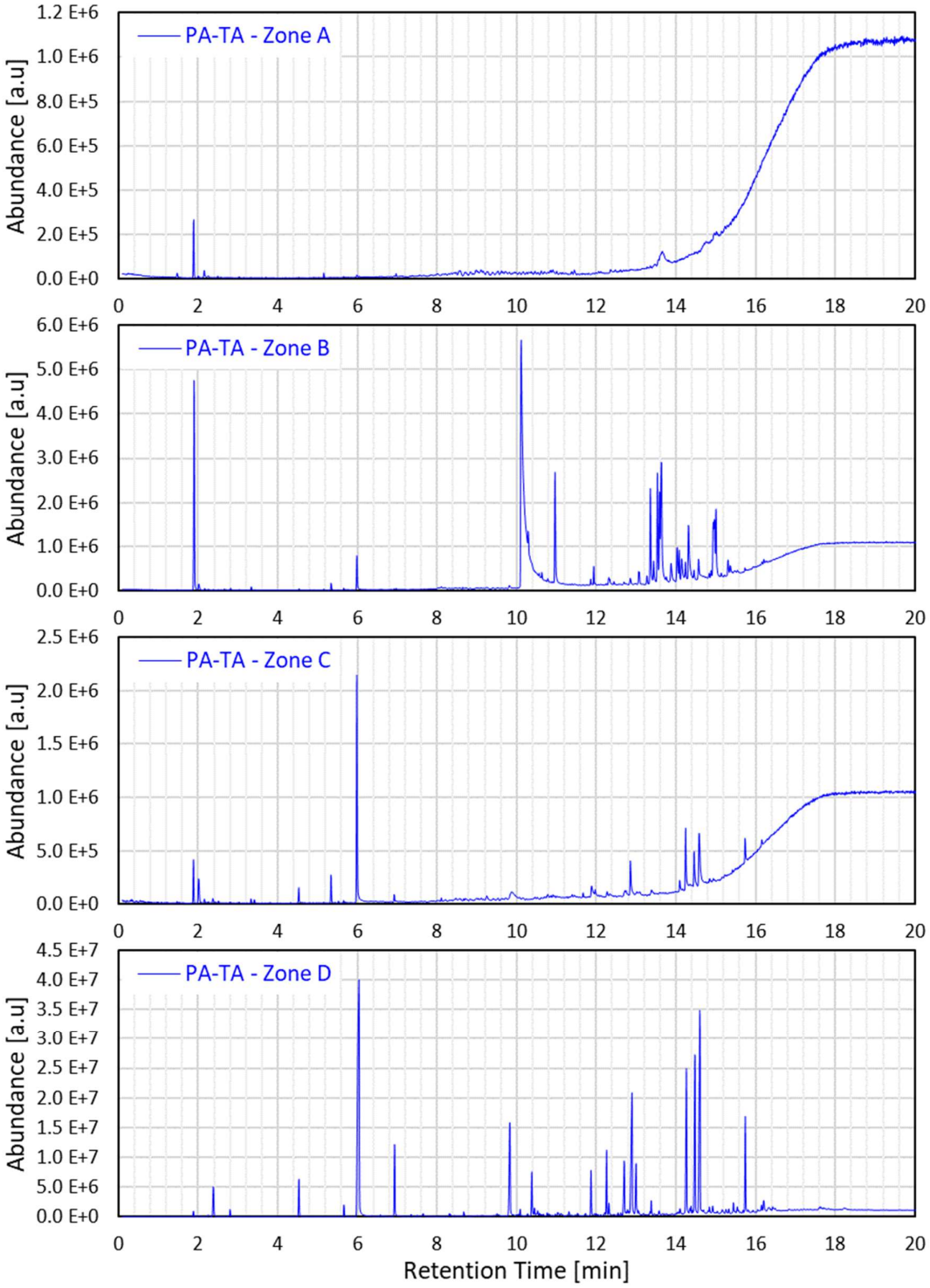

Figure 4.30. Total ion chromatograms for PA-TA for Zones A, B, C, and D.

Zone A chromatograms for ABS, TA, PA, and PA-TA are shown in Figure 4.31. PA-TA's results are much more similar to PA's than to TA's data, having very few peaks and lower peak intensities than those seen for ABS. Judging only from Zone A, it appears that tannic acid's anticipation of ABS's decomposition did not occur for PA-TA, at least not as far as bringing the products' release to below 220 °C. An isoquinoline peak (or hump), which is not present for pure ABS in Zone A, can be seen at 13.6 min; this hump is larger than that present in PA's graph but much smaller than the set of isoquinoline peaks seen at the same retention time for TA, indicating another similarity with PA rather than with TA.

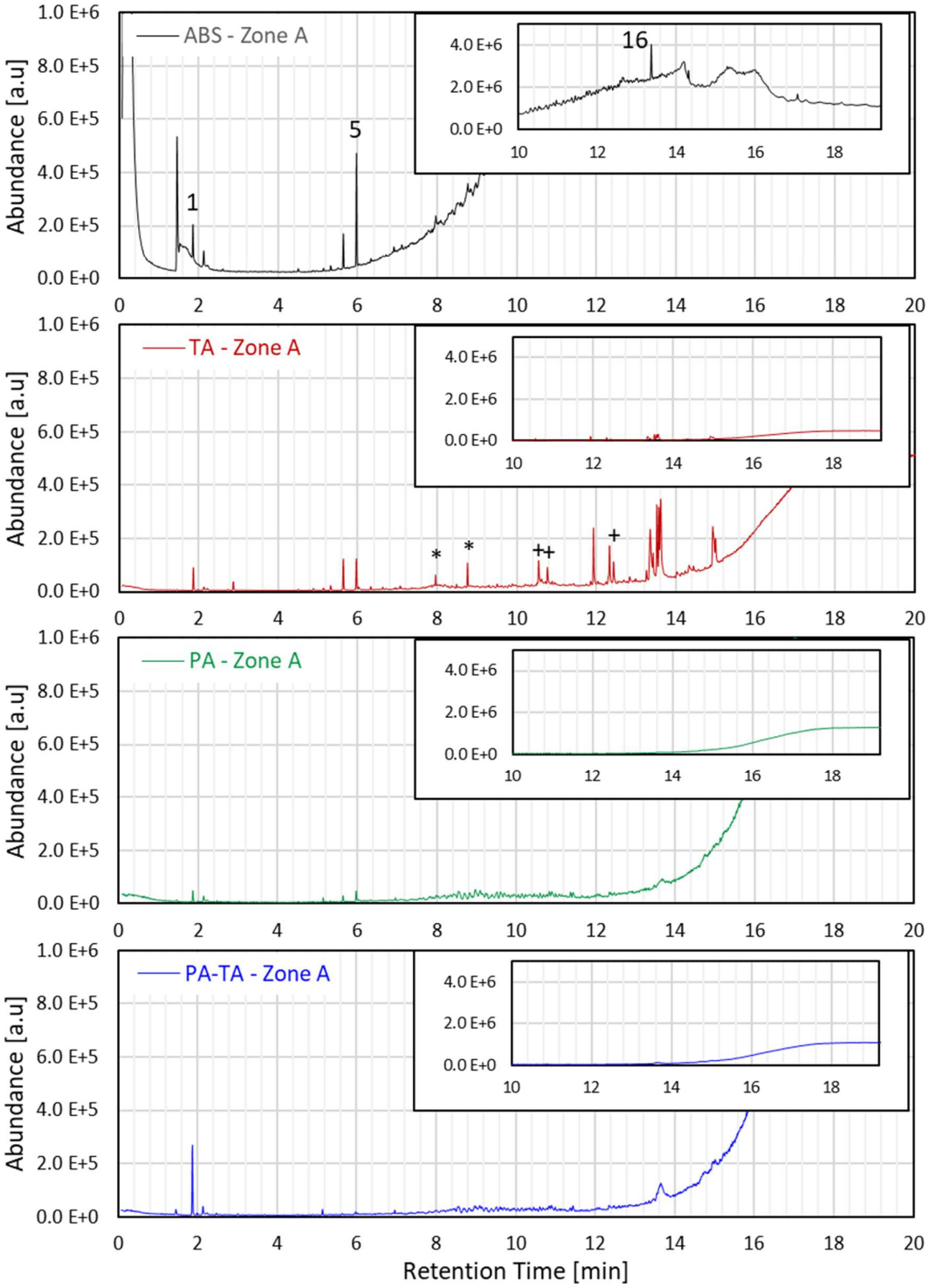

Figure 4.31. Zone A total ion chromatograms for ABS, TA, PA, and PA-TA.

Figure 4.32 presents the chromatograms for the 4 samples for Zone B. The first observation to be made is that the 2 peaks corresponding to tannic acid's degradation (red labels), which are the CO_2 (1) and 1,2,3-benzenetriol (27) peaks, are clearly present for PA-TA. They were expected to be half the size of the respective peaks in TA's chromatogram, since PA-TA contains half the tannic-acid content as TA. CO_2's and 1,2,3-benzenetriol's respective intensities are indeed just over and just under half of TA's values, but it is the peak area (not the peak intensity) that is roughly proportional to a compound's mass when mass detectors are used [131], and it can be seen that 1,2,3-benzenetriol's area for TA is far more than twice its area for PA-TA; therefore, the amount of tannic acid degradation products is lower than expected based on TA. It is important to remember that these peaks were already smaller than expected for TA based on TA Powder's results, so PA-TA's values are considerably smaller than those originally expected based on TA Powder. The remaining peaks, which correspond to the ABS-derived degradation products, are mostly smaller for PA-TA than for ABS, showing a behavior similar to that seen for PA; this fact suggests, once again, that PA-TA does not present an anticipation of ABS's degradation like TA did. The same products as seen for PA presented especially large reductions (indicated in gray for PA). Only 2 compounds visibly were not reduced (the same ones as for PA): styrene (5) and vinylnaphthalene or acenaphthalene (9); in fact, the latter surprisingly increased significantly, more so than for PA. Conclusions from Zone B are: (1) tannic acid degradation products are present in lower quantities than expected; (2) ABS's decomposition is not anticipated into Zone B – on the contrary, less ABS degradation products are present than for ABS, indicating a possible delay; (3) vinylnaphthalene or acenaphthalene is much more abundant than expected; and (4) PA-TA's behavior is, once again, much more similar to PA's than to TA's behavior.

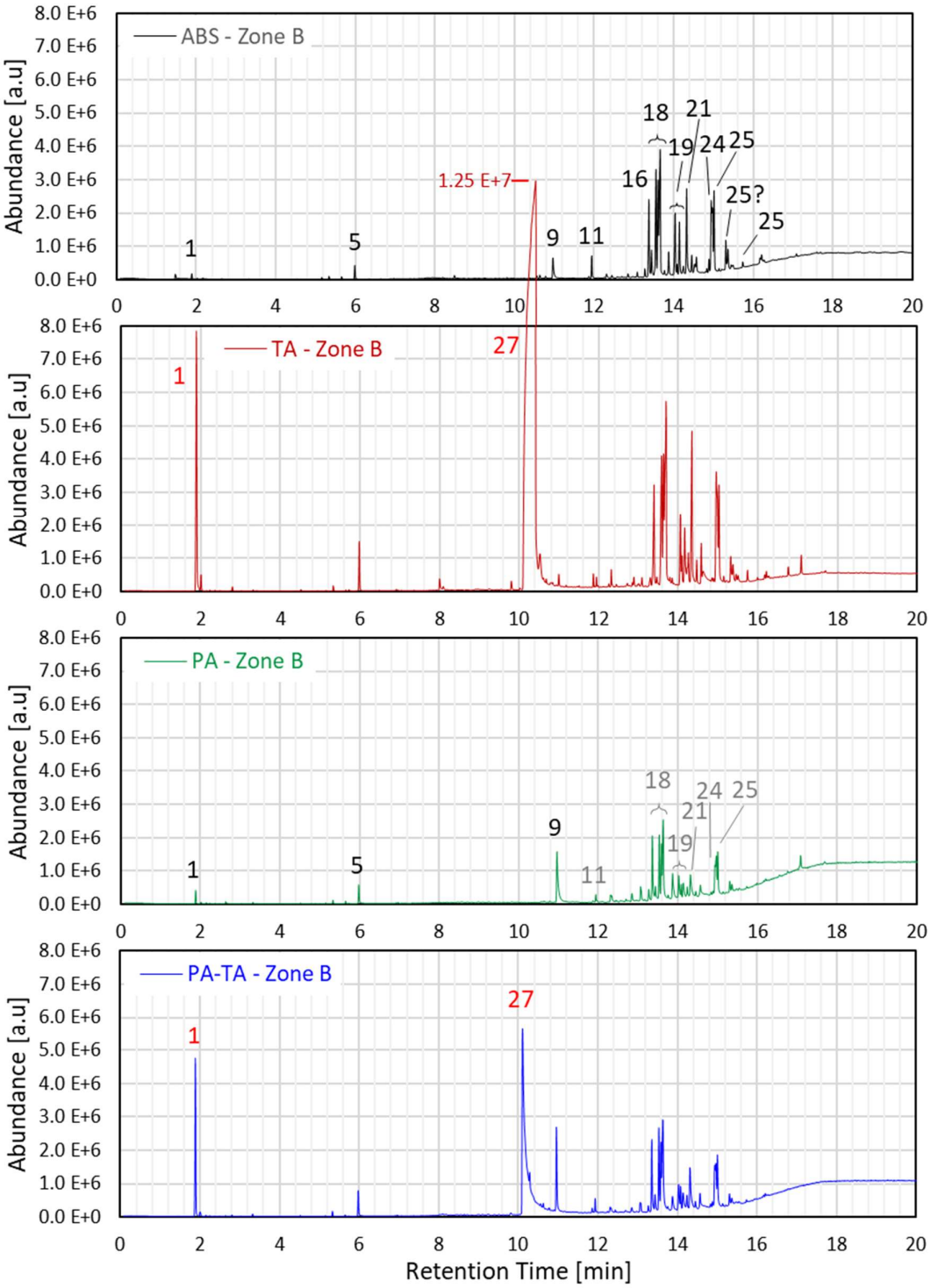

Figure 4.32. Zone B total ion chromatograms for ABS, TA, PA, and PA-TA.

The samples' TICs for Zone C are shown in Figure 4.33. The most notable observation from PA-TA's chromatogram in this zone is the complete absence of the 1,2,3-benzenetriol peak (27)! The CO_2 peak (1) is also smaller than for TA. If these peaks had been larger than expected in Zone B, it could have been said that the degradation of tannic acid was anticipated from Zone C into Zone B; however, the peaks were smaller than expected for Zone B and smaller (for CO_2) or non-existent (for 1,2,3-benzenetriol) for Zone C, indicating that a considerably smaller amount of tannic acid degradation products were released into the gas phase than expected when tannic acid and phytic acid were used together. This finding is consistent with the very low trace for the m/z = 126 ion, which is an indication of the presence of 1,2,3-benzenetriol, observed for PA-TA in comparison to that seen for TA and TA-FG in EGA experiments (Figure 4.16). It can be postulated, therefore, that phytic acid might be helping tannic acid to remain in the condensed phase, possibly by catalyzing crosslinking and char-forming reactions of the latter. This important conclusion will be further discussed in the next section, *Semi-Quantitative Analysis*. Visual analysis of the remaining peaks shows that most of the ABS-derived degradation products were the same as for ABS and PA, but the peak intensities were larger for PA-TA than for the other two.

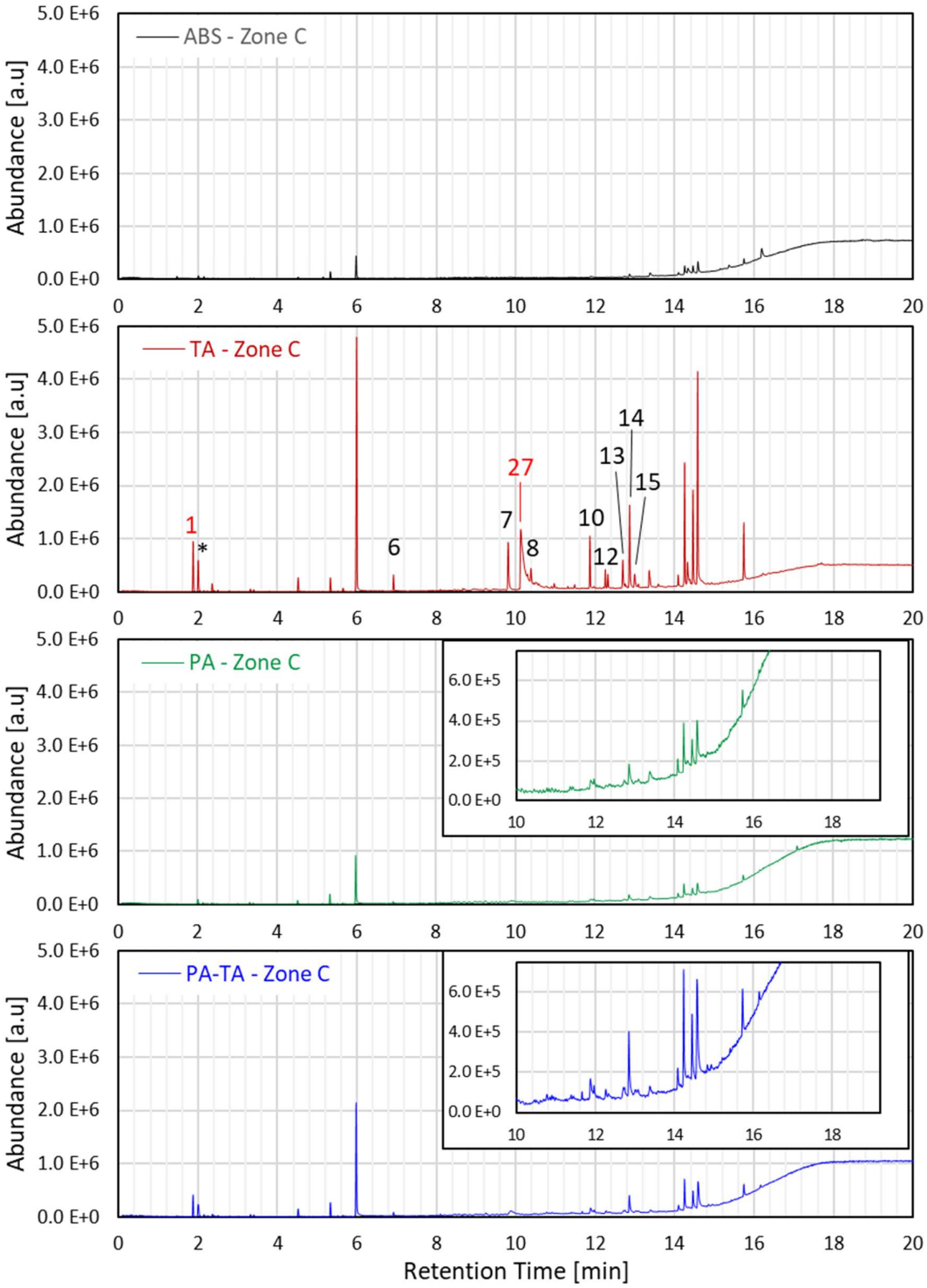

Figure 4.33. Zone C total ion chromatograms for ABS, TA, PA, and PA-TA.

Figure 4.34 presents the chromatograms for Zone D. PA-TA's results are very similar to PA's results, with almost all peak intensities being higher than ABS's peak intensities but slightly lower than PA's. The compounds that presented especially large peak growths were the same as for PA: styrene (5), α-methylstyrene (6; less pronounced), SAN hybrid trimer type ASA (14), and all 3 SAN hybrid trimers with 2 S units and 1 A unit (20, 22, and 23). Importantly, the relative proportions between peaks remained roughly the same between ABS, PA, and PA-TA (except for a larger styrene peak for PA), suggesting that the change in degradation mechanism observed for TA did not occur for PA nor for PA-TA.

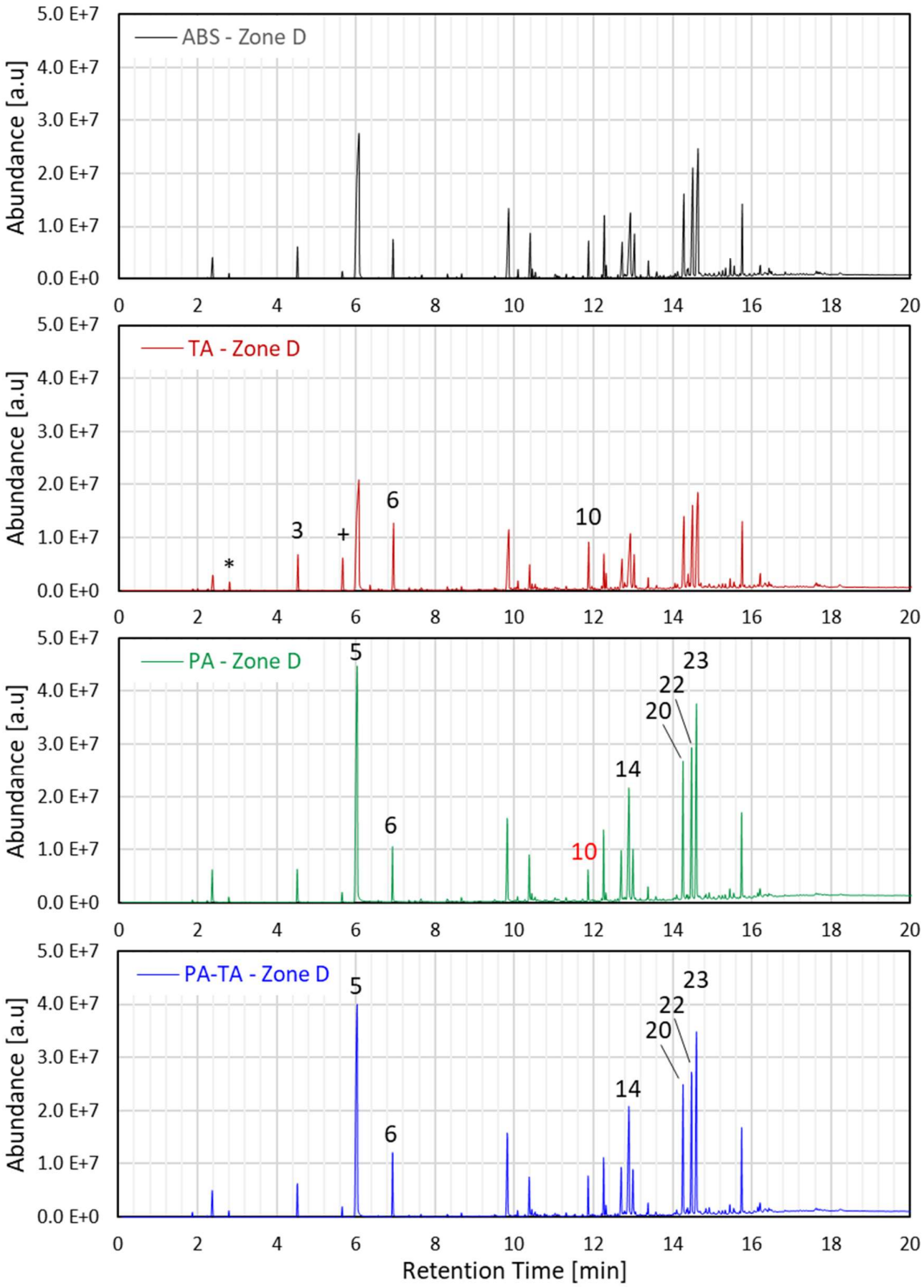

Figure 4.34. Zone D total ion chromatograms for ABS, TA, PA, and PA-TA.

A number of conclusions can be drawn from the analysis of PA-TA's chromatograms and from their comparison to ABS, TA, and PA's results. (1) The changes in ABS's degradation caused by tannic acid's interaction with the polymer, seen for TA (namely, anticipating the decomposition (i.e. reducing the E_a) and changing the nature and relative proportions of the degradation products), were not observed for PA-TA, suggesting that phytic acid inhibited tannic acid's interactions with the polymer. This fact can explain PA-TA's positive Δ_2PHRR value obtained from MCC (i.e. apparent antagonism between phytic acid and tannic acid): it was proposed earlier in this chapter that TA had a largely negative ΔPHRR (large synergistic interaction with ABS) as a consequence of its reduction of the polymer's E_a for decomposition, done by partially changing the degradation pathways; since phytic acid is mostly inhibiting tannic acid's degradation-mechanism-changing action, the large synergy seen between tannic acid and ABS in TA does not occur in PA-TA, so the "antagonism" between phytic acid and tannic acid is simply the former's "cancellation" of the latter's synergy with ABS. (2) PA-TA's behavior (i.e. the nature and amounts of degradation products) is much more similar to PA's than to TA's behavior, which is a reflection of the fact that phytic acid mostly inhibits tannic acid's interaction with ABS, "cancelling" the significant changes seen for TA. (3) PA-TA seems to slightly delay ABS's degradation, since it releases less degradation products than ABS in Zones A and B and more products in Zones C and D; however, the delay is less pronounced than for PA, possibly a simple consequence of having less phytic acid in PA-TA than in PA, assuming that direct or indirect interactions between phytic acid and ABS are responsible for the delay. (4) Tannic acid releases significantly less degradation products for PA-TA than for TA Powder or TA, indicating a larger char formation from tannic acid than expected when in the presence of phytic acid; it is possible that phytic acid catalyzes crosslinking and char-forming reactions of tannic acid (as acid groups are known to do to char formers in intumescent systems, for example), thus making it more difficult and requiring more thermal energy for tannic acid to degrade as much as it normally would. Higher temperatures would likely be needed under the Py-GC-MS conditions in order to fully degrade tannic acid in the PA-TA sample. The reduced degradation of tannic acid in PA-TA observed in the Py-GC-MS experiments supports the hypothesis presented during the discussion on the cone calorimetry results: PA-TA's excellent performance in cone calorimetry, achieving better

results than PA and TA individually, was hypothesized to have been caused by a rapid formation of a strong, cohesive char layer that acts as a thermal and gas barrier, protecting the sample underneath, due to phytic acid's phosphoric acid groups catalyzing tannic acid's crosslinking and char formation; this cohesive and more stable char would consequently require more thermal energy to degrade, being consistent with a lower release of degradation products from tannic acid.

4.4.2.2.
Semi-Quantitative Analysis

Semi-quantitative analyses were performed in order to numerically confirm the observations and conclusions made from the visual observations of the total ion chromatograms. The numerical conclusions, which will be presented in this section, actually assisted in perceiving many of the nuances and observations that were presented above, which were only visually identified after the completion and detailed interpretation of the numerical analysis.

The first premise that was considered was that peak areas, rather than peak intensities, would be used to calculate the quantities of the identified compounds. According to Guiochon and Guillemin [131,132], mass spectrometers are typically equipped with mass flow detectors, whose response signal is proportional to the mass flow rate of the analyte. Assuming that the detector response is linear, the relationship of proportionality between signal and mass flow rate leads to a relationship of proportionality between an analyte's mass and its corresponding signal's peak area. The coefficient of proportionality is unknown in this study, so absolute masses cannot be determined; however, relative masses between components can be estimated or approximated by comparing the peak areas. The peak height is a function of the carrier gas flow rate and of the temperature of the column, parameters that do not or only negligibly affect the peak area, so the extent of errors in quantitative determinations are smaller and the repeatability of results is better when using peak areas than when using peak heights. The second premise that was considered was that the peak area is approximately proportional to a compound's *mass*, as opposed to to its number of moles, volume, or other measurement parameter.

The procedure began with a detailed analysis of each TIC (for each temperature zone for each sample), identifying the grand majority of the peaks using two softwares' compound libraries and calculating their areas (i.e. integrals); the integrals for a given temperature zone for a given sample were calculated semi-automatically (automatic integration followed by manual adjustments) after identification of the peaks of that chromatogram. Over 1200 peaks were analyzed in total. Next, it was attempted to identify the starting material from which each detected compound was derived: acrylonitrile (A), butadiene (B), styrene (S), tannic acid (TA), or phytic acid (PA). The identification of the starting materials was based on literature (sources that present thermal-degradation studies for polyacrylonitrile (PAN), polybutadiene (PB), PS, nitrile-butadiene rubber (NBR), SAN, styrene-butadiene rubber (SBR), ABS, tannic acid, and/or phytic acid or its salts) [71,122,123,128–130,133–142], logical deductions, and, in the case of the composites, knowing for which individual components the compound was detected (ABS, tannic acid powder, and/or phytic acid powder). In many occasions, it was considered that a compound was derived from a combination of starting materials (e.g. SAN hybrid trimers are derived from A and from S combined) or that a compound could be a product of one or another starting material (for which coefficients were defined to consider the probability that the compound was derived from each possible compound). The total area count of compounds derived from each starting material were then calculated for each zone and for each sample; for compounds derived from more than one starting material (e.g. from acrylonitrile and styrene), the mass fraction of the compound "belonging" to each starting unit was estimated, and that compound's area count was divided proportionally between the two or more starting units. These calculations provided the relative amounts of A-, B-, S-, tannic acid-, and phytic acid-derived products being released in each temperature zone for each sample. These relative amounts were then compared to enable conclusions to be drawn. It should be noted that, given the 2 premises described above, the area count can be considered as a mass value with arbitrary units. Care was taken to treat each peak and compound as if it had a significant impact on the final results, even for peaks with very small areas; given the many possible sources of errors and approximations made during this analysis, being as accurate as possible with each component was important to avoid propagations of error that could lead to significant deviations in the final results. A number of

checks were also performed during the analysis, when possible, to ensure that specific proportions between components were consistent with values experimentally measured in other tests and/or with literature.

One additional step was performed in order to facilitate the comparisons between the samples. Since each sample had a different starting mass and the masses were not recorded, area-count values could not be directly compared between different samples; only the relative proportions between compounds and between different temperature zones for the same sample, and the changes in those relative proportions from one sample to another, could be compared. In order to facilitate direct area-count comparisons, the samples' masses were normalized according to a procedure briefly described earlier in this section. Firstly, the integration of all of ABS's peaks, except for those that clearly did not come from the sample (such as hexamethylcyclotrisiloxane and octamethylcyclotetrasiloxane, derived from the dimethylpolysiloxane-based GC column, and squalene), was performed for each temperature zone, obtaining the total area count (or mass, in arbitrary units (a.u.)) of ABS-derived volatile products ($M_{v,ABS}$). Since ABS's experimental char yield for MCC and TGA is close to 0% (i.e. ~100% volatile content (VC)), this value can be considered equal to the ABS sample's starting mass ($M_{ABS} = M_{v,ABS} = Total\ Integral_{ABS}$). The same integrating procedure was performed for tannic acid powder, obtaining the total area count (or mass, in a.u.) of tannic acid-derived volatiles ($M_{v,TAPowder} = Total\ Integral_{TAPowder}$). Considering that TA Powder's experimental char yield in MCC was ~23% ($\mu_{TAPowder} \approx 0.23$), meaning that its volatile content was ~77% ($VC_{TAPowder} = 1 - \mu_{TAPowder} \approx 0.77$), it can be estimated that the starting mass of the TA Powder sample was approximately equal to $M_{TAPowder} = \frac{M_{v,TAPowder}}{VC_{TAPowder}} = \frac{M_{v,TAPowder}}{0.77}$. The mass-correction factor for TA Powder ($f_{TAPowder}$) was then defined so as to normalize the masses based on ABS's sample mass – in other words, to make TA Powder's corrected mass ($M^*_{TAPowder}$) equal to ABS's mass: $M^*_{TAPowder} = f_{TAPowder} * M_{TAPowder} = M_{ABS}$. Therefore, the mass-correction factor was calculated by:

$$f_{TAPowder} = \frac{M_{ABS}}{M_{TAPowder}} = \frac{M_{ABS} * VC_{TAPowder}}{M_{v,TAPowder}} = \frac{M_{ABS} * 0.77}{M_{v,TAPowder}} \quad (23)$$

where M_{ABS} and $M_{v,TAPowder}$ are the total integrals of all of ABS's and TA Powder's TICs, respectively. For TA composite, the same procedure was used, but instead of using TA's experimental char yield (and volatile content) from MCC, TA's predicted no-interaction char yield was used based on ABS and TA Powder's experimental char yield from MCC (i.e. $\mu_{pred,no\_int,TA} = 0.70*\mu_{ABS} + 0.30*\mu_{TAPowder}$ and $VC_{pred,no\_int,TA} = 0.70*VC_{ABS} + 0.30*VC_{TAPowder}$). TA's mass-correction factor was then calculated analogously to eq. (23), by:

$$f_{TA} = \frac{M_{ABS}}{M_{TA}} = \frac{M_{ABS} * VC_{pred,no\_int,TA}}{M_{v,TA}} = \frac{M_{ABS} * (0.7 + 0.3 * 0.77)}{M_{v,TA}} = \frac{M_{ABS} * 0.93}{M_{v,TA}} \quad (24)$$

A similar procedure was used for PA Powder and PA composite; however, the procedure was not as straightforward for these samples, because only an unknown, small fraction of phytic acid's volatile products were detected by the equipment (because its main degradation product is water, which was below the detection limit). To solve this problem, reverse calculations were applied to estimate the proportion of phytic acid volatile content actually detected by the system (d_f, which was expected to be extremely small). PA composite's peak areas were calculated, and the total amounts of ABS-derived and of phytic acid-derived degradation products were estimated by identifying the source of each compound. The total amount of ABS-derived degradation products was then set to be equal to 70% of M_{ABS}, since PA contains 70 wt% of ABS. This equality determined PA's mass-correction factor, f_{PA}. The "detected-volatile-content fraction" was then tweaked in order to make the mass-corrected phytic acid-derived total area count in PA approximately equal to 30% of the mass-corrected phytic acid-derived total area count in PA Powder. The fraction of volatiles that are actually detected by the system from phytic acid's degradation (d_f) was thus estimated to be ~0.75 wt%. Equipped with this value, PA Powder's mass-correction factor was calculated, enabling PA-TA's factor to be calculated in the manner described in eq. (24). The mass-correction factors are listed in Table 4.10. A mass-correction factor of *f* means that ABS's initial mass was approximately *f* times the sample's initial mass ($M_{ABS} \approx f * M_{sample}$). It should be noted that, despite the large efforts made to calculate the

relative mass factors and the errors and approximations related to this procedure, the procedure was not necessary in order to compare the samples and reach conclusions, because most of the observations made directly or indirectly refer to changes, from one sample to another, in the *relative* proportions among compounds and temperature zones *within* a given sample. Normalizing the masses, however, does make it much easier to analyze the numbers and identify trends that would have been more "hidden" without the normalization.

Table 4.10

Reverse-calculated mass-correction factors for the samples in Py-GC-MS experiments

Sample	Mass-correction factor (f_{sample})
ABS	1.00
TA Powder	2.66
TA	0.54
PA Powder	1.91
PA	1.50
PA-TA	1.37

4.4.2.2.1. ABS

Table 4.11 presents the summarized results for pure ABS. The Area Count column provides the total area count (i.e. mass, in a.u.) of all of the volatilized compounds (or parts of compounds, in the case of compounds derived from more than one monomer) that were considered as being derived from each monomer. In other words, it provides the estimated reverse-calculated mass of each monomer in the original polymer (considering 100% ABS degradation). The estimated relative proportions of acrylonitrile, butadiene, and styrene monomers, in wt%, is highlighted in green: 76% styrene, 19% acrylonitrile, and 5% butadiene. The composition of the ABS used was not disclosed by the manufacturer. Literature reports of typical compositions for the terpolymer often do not specify if wt% or mol% values are being referred to, so typical compositions are either 40–60 wt% styrene, 15–35 wt% acrylonitrile, and 5–30 wt% butadiene or 56–75 wt% styrene, 9–25 wt% acrylonitrile, and 3–22 wt% butadiene [130]. The calculated values for acrylonitrile agree with the reported values. The calculated values for styrene are a

little high, but almost within the second range option, and estimated values for butadiene are at the extreme bottom of its reported range. The estimated values might be correct, or it is possible that, for compounds that could come from either butadiene or styrene (e.g. aromatics, which were sometimes split evenly between B and S but sometimes (e.g. α-methylstyrene) considered as coming from S), the portion allocated to styrene was too high. Either way, the values are realistic given the many possible sources of error, suggesting validity of the procedure used.

Table 4.11

Breakdown of ABS degradation products into acrylonitrile-, butadiene-, or styrene-derived for each temperature zone

Zone	Monomer	% of total Zone mass	% of total Monomer mass	Area Count (Mass [a.u.])
Zone A	A	0.0%	0.0%	0
	B	73.6%	7.0%	2,961,166
	S	26.4%	0.2%	1,064,001
	Total	100.0%	0.5%	4,025,167
Zone B	A	18.4%	8.3%	13,000,871
	B	28.6%	47.5%	20,177,809
	S	52.9%	6.0%	37,332,415
	Total	100.0%	8.5%	70,511,095
Zone C	A	14.2%	0.5%	827,147
	B	40.3%	5.5%	2,346,686
	S	45.5%	0.4%	2,645,821
	Total	100.0%	0.7%	5,819,655
Zone D	A	19.3%	91.2%	143,554,316
	B	2.3%	40.0%	17,014,482
	S	78.5%	93.4%	585,001,650
	Total	100.0%	90.3%	745,570,447
Totals	Total A	19.1%	100.0%	157,382,334
	Total B	5.1%	100.0%	42,500,144
	Total S	75.8%	100.0%	626,043,888
	Grand Total	100.0%	100.0%	825,926,365

90% of ABS's degradation was found to occur in Zone D (by weight), 9% in Zone B, 1% in Zone C and ~0% in Zone A. The major part of the decomposition was indeed expected to occur in Zone D; Zone C has such a low value likely because of the very short temperature range of (and, consequently, very short residence time in) this zone. Acrylonitrile's and styrene's degradation breakdowns per zone were similar to the total breakdown per zone. Butadiene presented a different breakdown,

with 48% in Zone B, 40% in Zone D, 6% in Zone C, and 7% in Zone A, suggesting that this monomer degrades earlier than the others. These breakdowns agree with a report on the thermal degradation of ABS [122]. The authors explain that polystyrene degrades between 360 and 450 °C, and that styrene's degradation profile does not change much when it is used in SAN; this range translates to only a small fraction in Zones B and C and the bulk in Zone D. SAN decomposes between 370 and 530 °C (Zones C and D), which means that acrylonitrile-derived products should also appear mainly in Zone D. Polybutadiene, on the other hand, begins degrading at 290 °C and continues to at least 600 °C, so it should, indeed, be spread out from Zone B to Zone D. The authors explain that when SAN is grafted onto PB for the production of ABS, PB's degradation is mostly unchanged (possibly slightly delayed), but PAN begins degrading ~25 °C earlier (at ~335 °C); this would explain acrylonitrile and styrene's products in Zone B being more than just a very small fraction, and actually more than in the short Zone C.

4.4.2.2.2. TA Powder

The main results for TA Powder were the relative amounts of material released in each temperature zone and the breakdown of the different components. 97% of volatile contents were released in Zone B, 2% in Zone C, and < 0.5% in Zones A and D; this breakdown agrees with MCC, TGA, and EGA curves. Zones B and C contained mostly aromatic compounds (91% and 97%, respectively; almost completely 1,2,3-benzentriol), some CO_2 (9% and 2%, respectively), and trace amounts of other components, as expected. Zone D contained 97% CO_2, consistent with the discussion on the EGA curves and with the fact that this zone presented a "hump" in TGA and EGA curves but nothing in MCC curves, since CO_2 does not react with oxygen. The total breakdown was 90 wt% aromatics, 9 wt% CO_2, and 1 wt% other compounds.

4.4.2.2.3.
TA Composite

Table 4.12 summarizes the results from TA and presents comparisons to the "expected" values. The "expected" values consider, for each zone, 70% of ABS's total area count and 30% of TA Powder's total area count (with the mass-correction factors applied) in each zone:

$$M_{ABS\ in\ TA\ sample,\ \ Expected} = \frac{0.70 * f_{ABS} * M_{ABS\ in\ ABS\ sample}}{f_{TA}} \tag{25}$$

$$M_{TA\ in\ TA\ sample,\ \ Expected} = \frac{0.30 * f_{TA\ Powder} * M_{TA\ in\ TA\ Powder}}{f_{TA}} \tag{26}$$

where $M_{ABS\ in\ TA\ sample,\ Expected}$ and $M_{TA\ in\ TA\ sample,\ Expected}$ are the area counts (or masses, in a.u.) listed in the "Expected" column to the right of the "Area Count (Mass [a.u.])" column. The values were used to calculate the other "Expected" columns' values and the "Compared to Expected" values. The same approach was used to calculate the expected amounts of specific components (A, B, and S from ABS and aromatics, CO_2, and others from tannic acid), substituting the "*ABS [or TA] in determined sample*" subscripts by "*[specific component] in determined sample*".

Table 4.12

Breakdown of TA composite's degradation products into ABS- or tannic acid-derived for each temperature zone, and comparison to the expected values[a]

Zone	Component	% of total Zone mass	Expected	% of total Component mass	Expected	Area Count (Mass [a.u.])	Expected	Compared to Expected:	
Zone A	ABS	95%	96%	0.7%	0.5%	7,286,824	5,185,884	+ 2,100,940	+ 41%
	TA	5%	4%	0.1%	0.1%	381,266	224,204	+ 157,062	+ 70%
	Total	100%	100%	0.5%	0.4%	7,668,089	5,410,088	+ 2,258,001	+ 42%
Zone B	ABS	29%	20%	13.6%	8.5%	143,897,548	90,844,025	+ 53,053,523	+ 58%
	TA	71%	80%	94.7%	97.1%	356,560,981	359,577,616	- 3,016,635	- 1%
	Total	100%	100%	35.0%	31.4%	500,458,529	450,421,641	+ 50,036,887	+ 11%
Zone C	ABS	77%	46%	5.5%	0.7%	57,971,588	7,497,840	+ 50,473,748	+ 673%
	TA	23%	54%	4.7%	2.4%	17,664,806	8,736,783	+ 8,928,024	+ 102%
	Total	100%	100%	5.3%	1.1%	75,636,394	16,234,623	+ 59,401,771	+ 366%
Zone D	ABS	100%	100%	80.2%	90.3%	845,367,186	960,566,844	- 115,199,658	- 12%
	TA	0%	0%	0.5%	0.5%	1,760,473	1,705,154	+ 55,319	+ 3%
	Total	100%	100%	59.2%	67.1%	847,127,659	962,271,998	- 115,144,339	- 12%
Totals	Total ABS	74%	74%	100%	100%	1,054,523,145	1,064,094,593	- 9,571,448	- 1%
	Total TA	26%	26%	100%	100%	376,367,526	370,243,757	+ 6,123,769	+ 2%
	Grand Total	100%	100%	100%	100%	1,430,890,671	1,434,338,350	- 3,447,679	- 0%

Predicted Totals	Component	Theoretical 1	Theoretical 2
	Total ABS	75%	77%
	Total TA	25%	23%

[a] Yellow indicates anticipation of ABS's degradation; Orange indicates delay of tannic acid's degradation; Blue indicates overall anticipation of degradation products; Green indicates that the total breakdown agrees with the expected values.

The most important values in the table are highlighted. The yellow highlights show that there was a significant anticipation of ABS's degradation, as was visually observed from the TICs and discussed in the previous *Qualitative Analysis* section. Instead of having 90%, 9%, and 1% of the ABS-derived degradation products released in Zones D, B, and C, respectively, there were 80%, 14%, and 6% in those respective zones. The total mass of ABS products in Zone D decreased 12% (115,000,000 area counts (a.c.); rightmost columns), which is a significant amount considering that this is the main decomposition zone for ABS, containing a very large amount of products; meanwhile, Zone C increased by 673% (50,000,000 a.c.), Zone B increased by 58% (53,000,000 a.c.), and even Zone A increased by 41% (2,000,000 a.c.). This breakdown confirms that the early beginning of the main degradation peak for TA in MCC, TGA, and EGA curves is indeed due to earlier degradation of ABS. Degradation products that would normally be released only above 400 °C (Zone D) were anticipated to as low as the 220–370 °C temperature

range (Zone B), while some products from Zones B and C were anticipated as far as to Zone A.

The orange highlighted values show that tannic acid's decomposition was slightly delayed in TA, as had been discussed previously. Instead of having 97% in Zone B and 2% in Zone C, the breakdown was 95% to 5%. This represented only a 1% decrease for Zone B, but a 100% increase for Zone C (because the expected amount, from tannic acid powder's decomposition, was very small for this zone). It is not clear from the numbers if these changes are within the experimental and procedural errors or if there is indeed a slight delay of tannic acid's decomposition. The fact that small delays were visually observed in the comparisons between the expected and experimental TA curves for MCC and TGA (Section 4.3) and in the TIC visual analyses (previous section) suggests that a delay does indeed occur, even if it is not very pronounced.

The green-highlighted values validate the analysis for TA composite. The relative proportion between ABS- and TA-derived volatiles was 74% to 26%, respectively; this was also the expected proportion based on the numerical Py-GC-MS analysis of pure ABS and TA Powder. The expected results based on char yield from MCC experiments also agreed: considering the observed char yield of each pure component (ABS and tannic acid powder) and their mass fractions in TA (70 wt% and 30 wt%), the calculated weight proportion of released compounds would be 75% to 25% (Theoretical 1), and considering the observed char yield of TA composite in MCC and considering that all of the char yield came from tannic acid (i.e. all of ABS degraded, and the remaining volatile content came from tannic acid), the proportion would be 77% to 23%. There was only a marginal difference in the total area count between TA composite and its expected amount (-0%, -3,000,000 a.c.). This value had been "forced" to be approximately 0 because the mass-correction factors were obtained from the total integrals; the slight difference is due to peaks that were not able to be identified by the libraries (unidentified or unknown), which were counted for the mass-correction-factor determination but not for the current analysis of the breakdown of components and zones. ABS's total amount deviated by only -1% (-9,000,000 a.c.) and tannic acid's by only +2% (+6,000,000 a.c.), which are acceptable deviations considering a grant-total area count of 1.4 billion. In summary, the analysis of TA composite yielded the correct

amount of products derived from ABS and from tannic acid, suggesting that the procedure used is valid.

The blue-highlighted values show the change in total degradation products for each zone, demonstrating increases in Zones A, B, and C and a decrease in Zone D. This is simply a reflection of the anticipation of ABS's degradation products (yellow highlights), slightly attenuated by the small delay of tannic acid-derived products (orange highlights).

Table 4.13 presents the breakdown of A-, B-, and S-derived products. Note that the "ABS Total" lines for each zone, as well as the "ABS Grand Total", are exactly what was presented for ABS in Table 4.12. The green highlights show the reverse-calculated monomeric breakdown of the ABS material used (considering 100% ABS degradation). The values are similar to the ones seen for pure ABS: instead of 76%, 19%, and 5% for S, A, and B, respectively, the values were 74%, 18%, and 8%. These numbers represent a 4% decrease for styrene, 5% decrease for acrylonitrile, and 57% increase for butadiene. These are acceptable errors, given the small total amounts of butadiene found and the already discussed possible inaccuracy in allocating products to styrene or to butadiene. All percentage values given here are in wt%. The changes in the styrene and acrylonitrile breakdowns per zone due to the anticipation of ABS's degradation are similar to the total ABS changes, with 12–15% decreases in Zone D, over 600% increases in Zone C, 50–60% increases in Zone B, and increases in Zone A. Butadiene, on the other hand, presents increases in Zones B, C, and D and a reduction in Zone A; the increases seen are smaller than the total butadiene increase (in area counts), however, so it is unknown whether the increases in the respective zones are real or are just a reflection of the error related to butadiene's identification. It is better, therefore, to look at the difference in breakdown of butadiene products per zone, which did not change much: Zones B and C slightly increased (from 48 and 6% of the total butadiene content to 53 and 7%, respectively) and Zones A and D slightly decreased (from 7 and 40% to 4 and 37%, respectively). These results suggest that the ABS degradation products that were anticipated by tannic acid's action (and that are related to the reduction in activation energy) are mainly acrylonitrile- and styrene-derived products, but not so much butadiene-derived volatiles; this is consistent with the fact that A and S originally degrade later than B, appearing mostly in Zone D while the latter was already split almost evenly between Zones B and D.

Table 4.13

Breakdown of TA composite's ABS-derived degradation products into acrylonitrile-, butadiene-, or styrene-derived for each temperature zone, and comparison to the expected values[a]

Zone	Monomer	% of total Zone mass	Expected	% of total Monomer mass	Expected	Area Count (Mass [a.u.])	Expected	Compared to Expected:	
Zone A	A	8.1%	0.0%	0.3%	0.0%	589,517	0	+ 589,517	+ n/a
	B	46.2%	73.6%	3.9%	7.0%	3,367,899	3,815,062	- 447,164	- 12%
	S	45.7%	26.4%	0.4%	0.2%	3,329,408	1,370,822	+ 1,958,586	+ 143%
	ABS Total	100.0%	100.0%	0.7%	0.5%	7,286,824	5,185,884	+ 2,100,940	+ 41%
Zone B	A	18.4%	18.4%	13.7%	8.3%	26,512,545	16,749,866	+ 9,762,679	+ 58%
	B	31.4%	28.6%	52.6%	47.5%	45,234,123	25,996,383	+ 19,237,741	+ 74%
	S	50.1%	52.9%	9.3%	6.0%	72,150,879	48,097,776	+ 24,053,103	+ 50%
	ABS Total	100.0%	100.0%	13.6%	8.5%	143,897,548	90,844,025	+ 53,053,523	+ 58%
Zone C	A	16.4%	14.2%	4.9%	0.5%	9,503,863	1,065,668	+ 8,438,195	+ 792%
	B	9.8%	40.3%	6.6%	5.5%	5,666,406	3,023,388	+ 2,643,018	+ 87%
	S	73.8%	45.5%	5.5%	0.4%	42,801,319	3,408,784	+ 39,392,535	+ 1156%
	ABS Total	100.0%	100.0%	5.5%	0.7%	57,971,588	7,497,840	+ 50,473,748	+ 673%
Zone D	A	18.5%	19.3%	81.0%	91.2%	156,376,807	184,950,351	- 28,573,544	- 15%
	B	3.8%	2.3%	36.9%	40.0%	31,730,304	21,920,862	+ 9,809,442	+ 45%
	S	77.7%	78.5%	84.7%	93.4%	657,260,075	753,695,631	- 96,435,556	- 13%
	ABS Total	100.0%	100.0%	80.2%	90.3%	845,367,186	960,566,844	- 115,199,658	- 12%
`									
Totals	Total A	18.3%	19.1%	100.0%	100.0%	192,982,732	202,765,885	- 9,783,153	- 5%
	Total B	8.2%	5.1%	100.0%	100.0%	85,998,732	54,755,696	+ 31,243,036	+ 57%
	Total S	73.5%	75.8%	100.0%	100.0%	775,541,681	806,573,013	- 31,031,331	- 4%
	ABS Grand Total	100.0%	100.0%	100.0%	100.0%	1,054,523,145	1,064,094,593	- 9,571,448	- 1%

[a] Yellow indicates anticipation of styrene degradation; Orange indicates anticipation of acrylonitrile degradation; Green indicates that the total breakdown agrees with the expected values, with an increase in total reverse-calculated butadiene content.

Knowing that ABS degradation was anticipated in TA composite, it was important to understand if there was a change in the nature of the degradation products. Were the same products just released earlier? Or, a more likely scenario, was there an alteration in the degradation mechanism caused by tannic acid's interaction, leading to a change in the products being released? Table 4.14 contains the answer to these questions: there is, indeed, a clear change in the types of degradation products being generated. This table presents the difference in area count (i.e. difference in mass, in a.u.) for different groups of compounds between the pure ABS sample and the TA composite (applying the mass-correction factor and multiplying the former by 70% to reflect ABS's weight content in TA) – in other words, the difference between the expected total mass and the actual total mass in TA composite for each compound. Blue values represent increases from ABS to TA, while red values indicate reductions. The compounds are presented in

order of decreasing “Change in Area Count”. The compounds highlighted in gray are the monomers, dimers, and trimers of A, B, and S that were detected (including SAN hybrid dimers and trimers), with trimers in light gray, dimers in a medium shade, and monomers in darker gray. The non-highlighted compound groups are the other detected molecules that are derived from the A, B, and S units: “S-derived compounds” are molecules with one benzene ring (e.g. benzene, toluene, α-methylstyrene, ethylbenzene, allylbenzene); “SS-derived compounds” contain 2 benzene rings (e.g. 1,3-diphenyl propane, 1-butene-1,4-diyldibenzene, 1-pentene-2,4-diyldibenzene, biphenyl); “Long hydrocarbon chains” are saturated long molecules, often oxidized (e.g. tridecanol, dodecanoic acid, palmitic acid, stearic acid, octadecanenitrile), which might be derived from butadiene; “B-derived compounds” are smaller molecules (linear or cyclic, mostly unsaturated) thought to be derived from butadiene – some aromatic groups are also included, multiplied by a pre-determined probability that they “belong” to B and not to S – (e.g. 3-methylcyclopentene, 1-hexene, 1,3-cyclohexadiene, methylhexadiene, benzene, toluene, ethylbenzene, xylene); “1-butene or isobutene” was included separately because, in many samples, it appears when 1,3-butadiene does not, and vice-versa; “A-derived compounds” are nitrogen-containing small molecules thought to be derived only from acrylonitrile (e.g. acetonitrile, methacrylonitrile, pent-2-enenitrile); and “Aromatic nitriles” include benzylnitrile and 2,4-dimethylbenzonitrile.

Table 4.14

Differences in the amounts of certain groups of degradation products between pure ABS and TA composite[a]

Type of Compound	Derived from	Change in Area Count from ABS to TA	% Change
S-derived compounds	S	+ 30,737,972	+ 70%
SS-derived compounds	S	+ 23,484,210	+ 65%
Isoquinoline or CN-Np-PPN	AS or AB	+ 23,262,516	+ 48%
Long hydrocarbon chains	B	+ 11,787,132	+ 55%
B-derived compounds	B	+ 10,430,869	+ 71%
Styrene trimer (SSS)	S	+ 8,454,334	+ 18%
1-butene or isobutene	B	+ 3,966,532	+ N/A
A-derived compounds	A	+ 1,555,497	+ 30%
3-cyclohexen-1-ylbenzene	BS	+ 1,275,489	+ 73%
Butadiene dimer (BB)	B	+ 420,487	+ 70%
Butadiene trimer (BBB)	B	+ 88,887	+ 167%
Butadiene monomer (B)	B	- 247,567	- 100%
Acrylonitrile dimer (AA)	A	- 768,783	- 26%
Aromatic nitriles	AS or AB	- 1,488,486	- 37%
Vinylnaphthalene	BS	- 1,505,658	- 60%
Acryonitrile monomer (A)	A	- 3,566,363	- 24%
SAN hybrid trimers with 2 A units (e.g. ASA)	AS	- 11,566,570	- 9%
SAN hybrid dimers (e.g. AS)	AS	- 12,181,101	- 13%
Styrene dimers (SS)	S	- 18,984,460	- 55%
SAN hybrid trimers with 2 S units (e.g. SAS)	AS	- 26,224,573	- 10%
Styrene monomer (S)	S	- 51,404,871	- 21%

[a] Gray = monomers (dark shade), dimers (medium shade), or trimers (light shade) of acrylonitrile, butadiene, styrene, or SAN.

The results show that almost all of the monomers, dimers, and trimers decreased significantly in amount, while almost all of the other compounds increased significantly! The biggest change was the reduction of styrene monomers and dimers, which were replaced by the S- and SS-derived compounds. SAN hybrid dimers and trimers also suffered a very large reduction. Acrylonitrile monomers and dimers also decreased their amounts, being substituted by the A-derived compounds. Butadiene monomer ceased to be detected, giving way to an increase in 1-butene or isobutene, other B-derived compounds, and the long hydrocarbon chains. Butadiene dimers and trimers almost did not change their amounts; the percent increases are large, but the raw increases are very small. The only true exception to the trend was the increase in the styrene trimer amount. It should be noted that, although the total amounts of the monomers, dimers, and trimers

decreased, the ones that were still released did so earlier than for pure ABS, as shown in Table 4.15: all of these compounds decreased in amount in Zone D, but all of them, with the exception of butadiene monomer, increased in Zones B and C.

Table 4.15

Differences in the amounts of ABS monomers, dimers, and trimers between pure ABS and TA composite for each temperature zone[a]

Compound	Zone A		Zone B		Zone C		Zone D		Total	
	Change in Area Count	% Change	Change in Area Count	% Change	Change in Area Count	% Change	Change in Area Count	% Change	Change in Area Count	% Change
Acryonitrile monomer (A)	0	-	+ 56,138	+ 267%	+ 353,990	+ 1,345%	- 3,976,491	- 26%	**- 3,566,363**	**- 24%**
Butadiene monomer (B)	0	-	- 92,615	- 100%	- 154,952	- 100%	0	-	**- 247,567**	**- 100%**
Styrene monomer (S)	- 618,005	- 67%	+ 2,426,729	+ 233%	+ 11,447,728	+ 1,047%	- 64,661,323	- 27%	**- 51,404,871**	**- 21%**
Acrylonitrile dimer (AA)	0	-	0	-	0	-	- 768,783	- 26%	**- 768,783**	**- 26%**
Butadiene dimer (BB)	- 10,124	- 17%	+ 158,507	+ 73%	+ 272,104	+ 84%	0	-	**+ 420,487**	**+ 70%**
Styrene dimers (SS)	0	-	+ 125,493	+ 178%	+ 665,047	+ 1,723%	- 19,775,001	- 57%	**- 18,984,460**	**- 55%**
SAN hybrid dimers (e.g. AS)	+ 59,923	+ N/A	+ 702,549	+ 334%	+ 3,950,594	+ 7,035%	- 16,894,167	- 18%	**- 12,181,101**	**- 13%**
Butadiene trimer (BBB)	0	-	+ 72,396	-	+ 16,491	+ 31%	0	-	**+ 88,887**	**+ 167%**
Styrene trimer (SSS)	+ 305,599	+ N/A	+ 5,831,728	+ 46%	+ 2,473,264	+ 882%	- 156,256	- 0%	**+ 8,454,334**	**+ 18%**
SAN hybrid trimers with 2 A units (e.g. ASA)	0	-	+ 800,504	+ 128%	+ 6,412,828	+ 1,842%	- 18,779,901	- 15%	**- 11,566,570**	**- 9%**
SAN hybrid trimers with 2 S units (e.g. SAS)	0	-	+ 4,446,599	+ 119%	+ 18,888,566	+ 954%	- 49,559,738	- 19%	**- 26,224,573**	**- 10%**

[a] Positive (blue) values indicate a larger presence in TA than in ABS; negative (red) values indicate a smaller presence in TA than in ABS.

It is hypothesized that the presence of tannic acid leads to acid catalysis of ABS, causing an earlier and less "orderly" decomposition process, thus yielding less "ordered" structures. PS's decomposition normally contains a considerable amount of unzipping, yielding a considerable monomer content, with some intramolecular transfer, yielding dimers and trimers [139,143]; SAN has basically the same degradation mechanism as PS, with the acrylonitrile units not interfering much in the unzipping process (although a slightly higher dimer and trimer content, relative to the monomer content, is observed compared to PS) [143]. Perhaps tannic acid-derived radicals attack random points in the SAN chains before the unzipping reactions begin, leading to more random chain scissions and, possibly, the release of side groups rather than predominant unzipping. This phenomenon would lead to an earlier degradation process that would yield a much lower monomer content, and also a lower amount of acrylonitrile, styrene, and hybrid dimers and trimers, which is what was observed. The increase in styrene trimers in relation to dimers and monomers is also consistent with this explanation, but not the total increase in styrene trimers. A partial explanation could be that styrene trimers were already released in very large amounts in Zone B for ABS (proportionally decreasing for the higher zones while the dimer and monomer amounts increased), so they were

less influenced by the anticipated degradation because they were already released early.

4.4.2.2.4.
PA Powder

There is not much to be learned from the analysis of PA Powder, because its main degradation product, water, was below the detection limit. As mentioned earlier, it was estimated that the detected products account for less than 1% (by weight) of the total amount of volatiles. Of the products that were detected, ~80% was released in Zone B, ~10% in Zone A, and ~5% in each of Zones C and D. The fact that the majority of non-water products were released in Zone B is in agreement with the MCC curves, which also don't reflect the release of water, since MCC curves show phytic acid's degradation peak to occur mainly in Zone B, with a tail going into Zones C and D.

4.4.2.2.5.
PA Composite

Table 4.16 presents the breakdown of PA's decomposition products into ABS-derived and phytic acid-derived products in each temperature zone. The main information to be learned from the table is that there was a slight delay in ABS's degradation (yellow highlights), as was discussed earlier. Zones A and B decreased from containing 0.5% and 9% of total ABS-derived products to containing 0.1% and 6%, respectively, while Zone D increased from 90% to 93%. Zones A and B presented 89% (2,000,000 a.c.) and 32% (11,000,000, a.c.) reductions, respectively, in the total area count (i.e. mass), while Zones C and D presented 13% (300,000 a.c.) and 4% (13,000,000 a.c.) increases, respectively. The changes are relatively small, but they agree with the visual observations of the TICs, with the EGA curves, and with the TGA-calculated E_a, which was larger than ABS's. It is possible that the large release of water acts as a heat sink, absorbing much thermal energy for the heating and vaporization of the water molecules; this would mean that the actual sample temperature in Py-GC-MS experiments was actually slightly lower than the nominal temperature, explaining the release of products at apparently higher

temperatures. The position of TGA curves would not be influenced, since the horizontal axis in TGA curves reflects the actual sample temperature measured by a thermopar, and not the nominal temperature; however, the considerable absorption of thermal energy by the water molecules would cause an apparent increase in activation energy, since more total energy would be required to degrade ABS because a portion of the energy would be "lost" in the heat sink. The MCC curves would also not have their position changed, as was the case, for the same reason as the TGA curves; what would remain unexplained, however, is the slightly earlier beginning of the main degradation peak in MCC curves and the lower MCC-calculated E_a for PA than for ABS. The delayed time to ignition (TTI) in cone calorimetry experiments is also consistent with this hypothesis.

Table 4.16

Breakdown of PA composite's degradation products into ABS- or phytic acid-derived for each temperature zone, and comparison to the expected values

Zone	Component	% of total Zone mass	Expected	% of total Component mass	Expected	Area Count (Mass [a.u.])	Expected	Compared to Expected:	
Zone A	ABS	82%	98%	0.1%	0.5%	198,967	1,877,311	- 1,678,345	- 89%
	PA	18%	2%	18.3%	11.8%	43,576	29,429	+ 14,146	+ 48%
	Total	100%	100%	0.1%	0.5%	242,542	1,906,741	- 1,664,199	- 87%
Zone B	ABS	100%	99%	5.8%	8.5%	22,355,246	32,885,909	- 10,530,663	- 32%
	PA	0%	1%	38.2%	81.6%	91,068	203,749	- 112,681	- 55%
	Total	100%	100%	5.8%	8.6%	22,446,314	33,089,658	- 10,643,344	- 32%
Zone C	ABS	98%	100%	0.8%	0.7%	3,066,263	2,714,249	+ 352,014	+ 13%
	PA	2%	0%	21.3%	2.9%	50,823	7,310	+ 43,512	+ 595%
	Total	100%	100%	0.8%	0.7%	3,117,086	2,721,559	+ 395,527	+ 15%
Zone D	ABS	100%	100%	93.4%	90.3%	360,528,471	347,729,130	+ 12,799,341	+ 4%
	PA	0%	0%	22.1%	3.7%	52,642	9,315	+ 43,327	+ 465%
	Total	100%	100%	93.3%	90.2%	360,581,113	347,738,445	+ 12,842,668	+ 4%
Totals	Total ABS	99.9%	99.9%	100%	100%	386,148,946	385,206,599	+ 942,347	+ 0%
	Total PA	0.1%	0.1%	100%	100%	238,108	249,803	- 11,695	- 5%
	Grand Total	100%	100%	100%	100%	386,387,054	385,456,402	+ 930,652	+ 0%

Estimated totals including volatilized water	Component	Actual	Theoretical 1	Theoretical 2
	Total ABS	92.4%	92.4%	89.6%
	Total PA	7.6%	7.6%	10.4%

[a] Yellow indicates delay of ABS's degradation; Green indicates that the total breakdown agrees with the expected values.

The green highlights show that the total amount of ABS (+0%, +900,000 a.c.) and total amount of detected PA (-5%, -10,000 a.c.) were close to the expected values. Using the estimated "detected volatile content" value of 0.75% by weight,

the reverse-calculated proportion between ABS- and phytic acid-derived products was 92.4% to 7.6%, which agrees perfectly with the Theoretical 1 value (based on MCC char yields for pure ABS and pure PA Powder) and is sufficiently close to the Theoretical 2 value (which considers PA composite's char yield in MCC), suggesting validity of the analysis. It is true that the mass-correction factors for PA Powder and for PA, as well as the "detected volatile content", were determined in such a way that would force these approximate equalities.

The reverse-calculated monomeric breakdown for ABS in PA composite was 77%, 19%, and 4% for S, A, and B, respectively, as shown in Table 4.17. These values are very similar to those calculated for pure ABS. Styrene presented a reduction in Zone B and increases in Zones C and D, and acrylonitrile presented a decrease in Zone B, no change (-20,000 a.c. can be considered insignificant) in Zone C, and an increase in Zone D; these results agree with the total ABS changes. B presented reductions in all zones, but these reductions were smaller than the total B reduction, so they are not necessarily real; looking at the "% of total Monomer mass" and corresponding "Expected" columns, it can be seen that, proportionally to each other, there were small reductions in Zones B and C and an increase in Zone D for butadiene, also agreeing with a small delay in ABS degradation.

Table 4.17

Breakdown of PA composite's ABS-derived degradation products into acrylonitrile-, butadiene-, or styrene-derived for each temperature zone, and comparison to the expected values[a]

Zone	Monomer	% of total Zone mass	Expected	% of total Monomer mass	Expected	Area Count (Mass [a.u.])	Expected	Compared to Expected:	
Zone A	A	10.7%	0.0%	0.0%	0.0%	21,338	0	+ 21,338	+ n/a
	B	31.3%	73.6%	0.4%	7.0%	62,299	1,381,068	- 1,318,770	- 95%
	S	58.0%	26.4%	0.0%	0.2%	115,330	496,243	- 380,913	- 77%
	ABS Total	100.0%	100.0%	0.1%	0.5%	198,967	1,877,311	- 1,678,345	- 89%
Zone B	A	15.4%	18.4%	4.6%	8.3%	3,433,012	6,063,520	- 2,630,508	- 43%
	B	31.1%	28.6%	44.9%	47.5%	6,962,527	9,410,797	- 2,448,270	- 26%
	S	53.5%	52.9%	4.0%	6.0%	11,959,707	17,411,592	- 5,451,885	- 31%
	ABS Total	100.0%	100.0%	5.8%	8.5%	22,355,246	32,885,909	- 10,530,663	- 32%
Zone C	A	11.8%	14.2%	0.5%	0.5%	362,427	385,776	- 23,349	- 6%
	B	23.3%	40.3%	4.6%	5.5%	712,987	1,094,479	- 381,492	- 35%
	S	64.9%	45.5%	0.7%	0.4%	1,990,848	1,233,994	+ 756,854	+ 61%
	ABS Total	100.0%	100.0%	0.8%	0.7%	3,066,263	2,714,249	+ 352,014	+ 13%
Zone D	A	19.7%	19.3%	94.9%	91.2%	71,173,748	66,952,784	+ 4,220,964	+ 6%
	B	2.2%	2.3%	50.1%	40.0%	7,778,922	7,935,442	- 156,520	- 2%
	S	78.1%	78.5%	95.2%	93.4%	281,575,801	272,840,904	+ 8,734,897	+ 3%
	ABS Total	100.0%	100.0%	93.4%	90.3%	360,528,471	347,729,130	+ 12,799,341	+ 4%
Totals	Total A	19.4%	19.1%	100.0%	100.0%	74,990,526	73,402,080	+ 1,588,445	+ 2%
	Total B	4.0%	5.1%	100.0%	100.0%	15,516,735	19,821,786	- 4,305,051	- 22%
	Total S	76.6%	75.8%	100.0%	100.0%	295,641,686	291,982,732	+ 3,658,953	+ 1%
	ABS Grand Total	100.0%	100.0%	100.0%	100.0%	386,148,946	385,206,599	+ 942,347	+ 0%

[a] Green indicates that the total breakdown agrees with the expected values.

4.4.2.2.6. PA-TA Composite

Table 4.18 presents the breakdown between ABS-, tannic acid-, and detectable phytic acid-derived degradation products for each temperature zone. The "Area Count (Mass [a.u.])" column has been suppressed for the sake of reducing the table size because of the additional "Expected 2" columns. The "Expected 1" columns are the predicted values considering the pure individual components (*Expected 1 = 0.70*ABS + 0.15*TA Powder + 0.15*PA Powder*), considering the mass-correction factors; the "Expected 2" columns are based on the TA and PA composites (*Expected 2 = 0.5*TA + 0.5*PA*), also considering the mass-correction factors.

Table 4.18

Breakdown of PA-TA's degradation products into ABS-, tannic acid-, or phytic acid-derived for each temperature zone, and comparison to the expected values

Zone	Component	% of total Zone mass	Expected 1[a]	Expected 2[b]	% of total Component mass	Expected 1[a]	Expected 2[b]	Compared to Expected 1[a]:		Compared to Expected 2[b]:	
Zone A	ABS	50%	97%	94%	0%	0%	0%	- 1,753,210	**- 85%**	- 1,248,796	**- 80%**
	TA	44%	2%	5%	1%	0%	0%	+ 228,376	**+ 512%**	+ 197,128	**+ 260%**
	PA	5%	1%	1%	32%	12%	18%	+ 17,407	**+ 108%**	+ 9,632	**+ 40%**
	Total	100%	100%	100%	0%	0%	0%	- 1,507,427	**- 71%**	- 1,042,036	**- 63%**
Zone B	ABS	48%	34%	37%	7%	9%	10%	- 5,002,377	**- 14%**	- 9,770,058	**- 24%**
	TA	52%	66%	63%	94%	97%	95%	- 38,305,528	**- 54%**	- 37,705,354	**- 53%**
	PA	0%	0%	0%	39%	82%	38%	- 70,858	**- 63%**	- 8,929	**- 18%**
	Total	100%	100%	100%	14%	22%	23%	- 43,378,763	**- 40%**	- 47,484,341	**- 42%**
Zone C	ABS	95%	63%	79%	2%	1%	3%	+ 5,033,510	**+ 169%**	- 5,201,956	**- 39%**
	TA	5%	37%	21%	1%	2%	5%	- 1,302,619	**- 75%**	- 3,078,893	**- 88%**
	PA	0%	0%	0%	12%	3%	21%	+ 8,743	**+ 218%**	- 15,171	**- 54%**
	Total	100%	100%	100%	2%	1%	3%	+ 3,739,635	**+ 79%**	- 8,296,021	**- 49%**
Zone D	ABS	100%	100%	100%	91%	90%	87%	- 1,139,425	**- 0%**	+ 14,745,688	**+ 4%**
	TA	0%	0%	0%	4%	0%	0%	+ 1,069,490	**+ 315%**	+ 1,058,483	**+ 302%**
	PA	0%	0%	0%	16%	4%	22%	+ 12,065	**+ 236%**	- 11,748	**- 41%**
	Total	100%	100%	100%	84%	77%	74%	- 57,871	**- 0%**	+ 15,792,424	**+ 4%**
Totals	Total ABS	92.2%	85.2%	84.9%	100%	100%	100%	- 2,861,502	**- 1%**	- 1,475,123	**- 0%**
	Total TA	7.8%	14.8%	15.1%	100%	100%	100%	- 38,310,282	**- 52%**	- 39,528,636	**- 53%**
	Total PA	0.0%	0.0%	0.0%	100%	100%	100%	- 32,643	**- 24%**	- 26,215	**- 20%**
	Grand Total	100%	100%	100%	100%	100%	100%	- 41,204,426	**- 8%**	- 41,029,974	**- 8%**

Estimated totals including volatilized water	Component	Actual	Theoretical 1	Theoretical 2
	Total ABS	89.5%	82.9%	81.3%
	Total TA	7.5%	13.7%	15.0%
	Total PA	3.0%	3.4%	3.7%

[a] Based on individual components' results (0.70*ABS + 0.15*TA Powder + 0.15*PA Powder).

[b] Based on TA and PA composites' results (0.5*TA + 0.5*PA).

[c] Yellow indicates slight delay of ABS's degradation compared to Expected 1; Orange indicates inhibition or attenuation of tannic acid's catalysis of ABS's degradation; Red indicates reduction in total amount of tannic acid-derived volatiles; Green indicates expected values.

Analyzing ABS's per-zone breakdown in relation to Expected 1 (yellow highlights), it can be seen that there was a very slight delay of ABS's degradation from Zone B to Zone C, since Zone B decreased from 9% to 7% of total ABS degradation products while Zone C increased from 1% to 2%; Zone D barely changed (90% to 91%). In terms of area counts (i.e. total mass), Zone B decreased by 14% (-5,000,000 a.c.), Zone B increased by 170% (+5,000,000 a.c.), while Zone D barely changed (-0%, -1,000,000 a.c.). These changes were less attenuated than those seen for PA: the total reduction of Zones A and B combined was of 35% for PA but only 17% for PA-TA, and the total increase of Zones C and D combined was of 4% for PA but only 1% for PA-TA. This attenuation of the decomposition

delay makes sense, because PA-TA contains half the amount of phytic acid as PA; if the heat sink created by the large amount of water generation is indeed responsible for the apparent delay in ABS's decomposition, less phytic acid means less water and, consequently, a lower heat-sink effect and less apparent delay. (Even if the heat-sink hypothesis is incorrect, the mechanism used by phytic acid to delay ABS degradation has a less significant effect if there is less phytic acid present.) It is worth mentioning that, in terms of individual monomers, all 3 decreased in Zone B and increased in Zone C; butadiene also increased in Zone D, while acrylonitrile and styrene barely changed. The total monomeric breakdown was 76, 19, and 5% for S, A, and B, exactly the same as those seen for pure ABS.

The orange-highlighted values focus on the comparison of ABS's per-zone breakdown in comparison to Expected 2. Expected 2 considers the average of TA and PA composites; since TA experienced a *very pronounced* anticipation of ABS degradation from Zone D to Zones C, B, and even A, while PA underwent *only a slight* delay from Zones A and B to Zones C and D, Expected 2 is dominated by TA's changes (which is why it shows a smaller Zone D value and higher Zones B and C values in the "% of total Component mass"-related columns than Expected 1). The per-zone breakdown showed a decrease in Zone B compared to Expected 2 (10% to 7%; -24%, -10,000,000 a.c.), showing that tannic acid's anticipation, or catalysis, of ABS's decomposition was cancelled or much attenuated because of the presence of phytic acid. Likewise, Zone C decreased from 3% to 2% (-39%, -5,000,000 a.c.) and Zone D increased from 87% to 91% (+4%, +15,000,000 a.c.), showing that tannic acid's catalysis of ABS's decomposition was indeed much lessened or cancelled.

Perhaps the most noticeable trait that can be seen in Table 4.18 is the reduction in the total amount of tannic-acid derived degradation products (highlighted in red). The per-zone breakdown did not change much, showing a decrease in Zone B from 97 or 95% to 94% of total TA-degradation products and in Zone C from 2 or 5% to 1%; the remaining portion of the products migrated to Zone D (0% to 4%). The total area count (i.e. mass) of degradation products, however, decreased by ~54% (38,000,000 a.c.) in Zone B and by 75% (1,300,000 a.c.) or 88% (3,000,000 a.c.) in Zone C. Most importantly, the total amount of tannic-acid derived degradation products decreased by ~53% (~39,000,000 a.c.)! It is important to note that this drastic reduction is not just an error created by

potentially wrong mass-correction factors, because the total amount of ABS degradation products was almost exactly as expected (-1%, -2,900,000 a.c.). If the mass-correction factor was tweaked to bring tannic acid's total area-count change to approximately zero, the total amount of ABS degradation products would be increased by +110% compared to the expected, which is impossible because pure ABS already had almost all of its mass degraded into volatiles (~100% volatile content). The huge reduction in tannic acid-derived degradation products is therefore real. The main component group responsible for this reduction was, as expected, the aromatics – especially 1,2,3-benzenetriol, which was the main degradation product and showed clear decreases upon visual observations of the TICs. The release of aromatics showed a total decrease of 56% by weight, with a 56% reduction in Zone B and a 99% reduction in Zone C. CO_2 decreased by only 7%, and other compounds decreased by 61% (but the latter group comprises a negligible amount of tannic acid's degradation products). The volatilized aromatics:CO_2 ratio changed from 90:9 (w/w) to 82:17 (w/w).

The total reduction in all degradation products was -8% (-41,000,000 a.c.), due to the large decrease in tannic acid products. The breakdown between ABS and tannic acid detected degradation products was 92 to 8% instead of the predicted 85 to 15%. Considering phytic acid's "detected volatile content" of 0.75%, the reverse-calculated total proportion of decomposition products, shown in the bottom 3 rows in red, was 90%, 8%, and 3% for ABS-, tannic acid-, and phytic acid-derived products, respectively; the theoretical amounts based on the experimental MCC-obtained char yields of the individual components (Theoretical 1) were 83%, 14%, and 3%, and the theoretical proportion based on PA-TA's MCC-obtained char yield was 81%, 15%, and 4%, respectively. There was clearly a larger proportion of ABS compounds and a lower fraction of tannic acid compounds than expected. This reduction in tannic acid's volatilization corresponds to a decrease of ~50% in tannic acid's volatile content, or an increase in tannic acid's char yield from 23% to ~62% (2.7 times the original value)! Considering this corrected char yield for tannic acid, the reverse-calculated theoretical proportions would be 89%, 7%, and 4% for ABS, TA, and PA, very close to the observed values. It is worth noting that phytic acid's estimated "detected volatile content" of 0.75% led to an almost exactly correct total amount of phytic acid degradation products, showing that this estimate, as well as the mass-correction factors of the other samples, are realistic.

From the analysis of PA-TA, is possible to conclude that (1) there is a very large increase in tannic acid's char yield (i.e. much lower volatilization of tannic acid), (2) tannic acid's effect of anticipating ABS's degradation is much attenuated or possibly completely cancelled, and (3) phytic acid causes a small delay in ABS's decomposition, but less so than for PA. It is hypothesized that phosphoric acid groups from phytic acid catalyze crosslinking and char-forming reactions in tannic acid, which is commonly seen in intumescent systems. Consequently, much more energy is needed to release tannic acid fragments, leading to a lower volatile content and a higher char yield for this additive; temperatures greater than 500 °C (the maximum temperature of Zone D) would be needed to considerably degrade tannic acid. This hypothesis would naturally lead to conclusion 2 above: much less tannic acid radical fragments would be released, so less radicals would be available to attack the SAN chains and cause an anticipation of ABS's degradation; therefore, tannic acid's interactions with ABS observed in TA would be attenuated or even inhibited in PA-TA. The hypothesis that phytic acid catalyzes crosslinking and char-forming reactions in tannic acid could explain PA-TA's promising performance in cone calorimetry experiments: with phytic acid catalyzing tannic acid's crosslinking and char formation, a protective char layer is formed faster than for the other samples, leading to an earlier break of the HRR increase since the sample is quickly protected by an effective thermal and gas barrier; therefore, PA-TA's PHRR is lower that TA's and PA's PHRRs. Conclusion 3 can possibly be explained by the release of a large amount of water molecules by phytic acid, which act as heat sinks, reducing the actual sample temperature and causing the degradation products to be released at an apparently higher temperature (as explained for PA composite). The fact that there is only half the amount of phytic acid in PA-TA than in PA would naturally lead to a lower apparent-delay effect, as is seen.

There is one more question to be answered about PA-TA, based on the hypotheses related to conclusions 1 and 2 above: why are the char yields in MCC and TGA not higher than the no-interaction predicted char yields if phytic acid is causing a much higher tannic acid residue? Based on the 62% (instead of 23%) char yield for tannic acid estimated above, the total PA-TA char yield observed should have been 22% for MCC and 23% for TGA instead of the experimentally obtained 14% for MCC and 17% for TGA. The fact that Py-GC-MS experiments only went

until 500 °C is not a complete answer, because TGA, MCC, and EGA curves show that PA-TA degradation is totally or almost complete by this temperature. The hypothesis to answer this question and connect PA-TA's mechanisms throughout all of the experiments is the following: phytic acid is indeed catalyzing tannic acid's char formation, leading to a quicker formation of char in all of the tests (cone calorimetry, MCC, TGA, EGA, and Py-GC-MS). The effect of this early char formation is only observable in cone calorimetry, however, because the relatively large sample mass allows for the increased amount of char to quickly form a protective barrier, shielding the sample underneath; in all of the other tests, the sample size is so small that a protective barrier cannot be formed (it has been repeated throughout this study that barrier effects are not observed in MCC because of the small sample size – the same is naturally true for TGA, EGA, and Py-GC-MS). The quickly formed char is not necessarily stable, however; the material needs time to form a sufficiently crosslinked network that makes it thermally stable enough to "survive" beyond 500 °C. For this reason, the char is completely burned in cone calorimetry (oxidation also plays a part in this case), and the "additional" char also does not survive in MCC, EGA, and TGA, which have heating rates of 60, 20, and 10 °C/min. Py-GC-MS experiments had a heating rate of 40 °C/min, BUT the time taken between temperature zones caused the sample to remain at a much longer time at low temperatures than for the other tests! As explained in the Experimental section (Chapter 2), the sample was cooled down to 100 °C between Zones A and B and between Zones B and C, where it remained for ~26 min each time to allow for processing of the released volatiles by the GC-MS; between Zone C and D, the sample was cooled to 220 °C for ~26 min. Additionally, there was an ~2-min wait at the initial temperature of Zones B, C, and D before the zones actually began. Consequently, the time spent at or above 100 °C before the sample surpassed 220 °C (the approximate initial temperature of tannic acid's degradation) was 2, 6, and 12 min for MCC, EGA, and TGA, respectively, but was 31 min for Py-GC-MS! Crosslinking could be occurring at these temperatures, preparing the formation of a more thermally stable char. Times spent below or at 500 °C were 6.7, 20, 40, and 94 min for MCC, EGA, TGA, and Py-GC-MS, respectively; for the latter, 83 out of the 94 min were spent below or at 220 °C. Additionally, PA-TA's char yield in TGA was higher than in MCC, supporting this hypothesis. It is possible, therefore, that the additional time spent at low temperatures by the PA-TA sample

in Py-GC-MS experiments allowed sufficient tannic acid crosslinking to take place, catalyzed by the presence of phytic acid, before considerable tannic acid decomposition temperatures were reached, creating a crosslinked network that was thermally stable enough to withstand temperatures greater than 500 °C. The final conclusion from these analyses is that phytic acid does seem to catalyze tannic acid's crosslinking and char formation early on, quickly creating a protective barrier that shields the sample in cone calorimetry-mass-scaled tests; however, in order for the char to be thermally stable and withstand higher temperatures without degrading, the sample needs to remain at relatively low temperatures (but high enough for crosslinking reactions to take place) for a considerable amount of time, which occurred in Py-GC-MS tests but not in MCC and TGA experiments.

4.5. Mechanical Properties

The six compositions that were chosen to be scaled up and further analyzed in Phase 2 (listed in Table 4.1) were also mechanically tested. Specimens were prepared through extrusion followed by injection molding and were then submitted to tensile testing and notched Izod impact testing.

4.5.1. Tensile Testing

Representative tensile stress-strain curves for the six samples are shown in Figure 4.35. A quick look at the curves reveals that pristine ABS and the commercial brominated Br-ABS are more ductile than the bio-based flame-retarded samples, which was expected due to the high filler content of the particle-filled composites. The tensile strengths of the composites are similar to those of ABS and Br-ABS, which is interesting since the addition of a high content of filler particles often leads to a decrease in tensile strength, suggesting that that there is interfacial adhesion between the FRs and the matrix [144]. It can also be seen that the composites have a higher elastic modulus (represented by the initial slopes of the curves) than the controls.

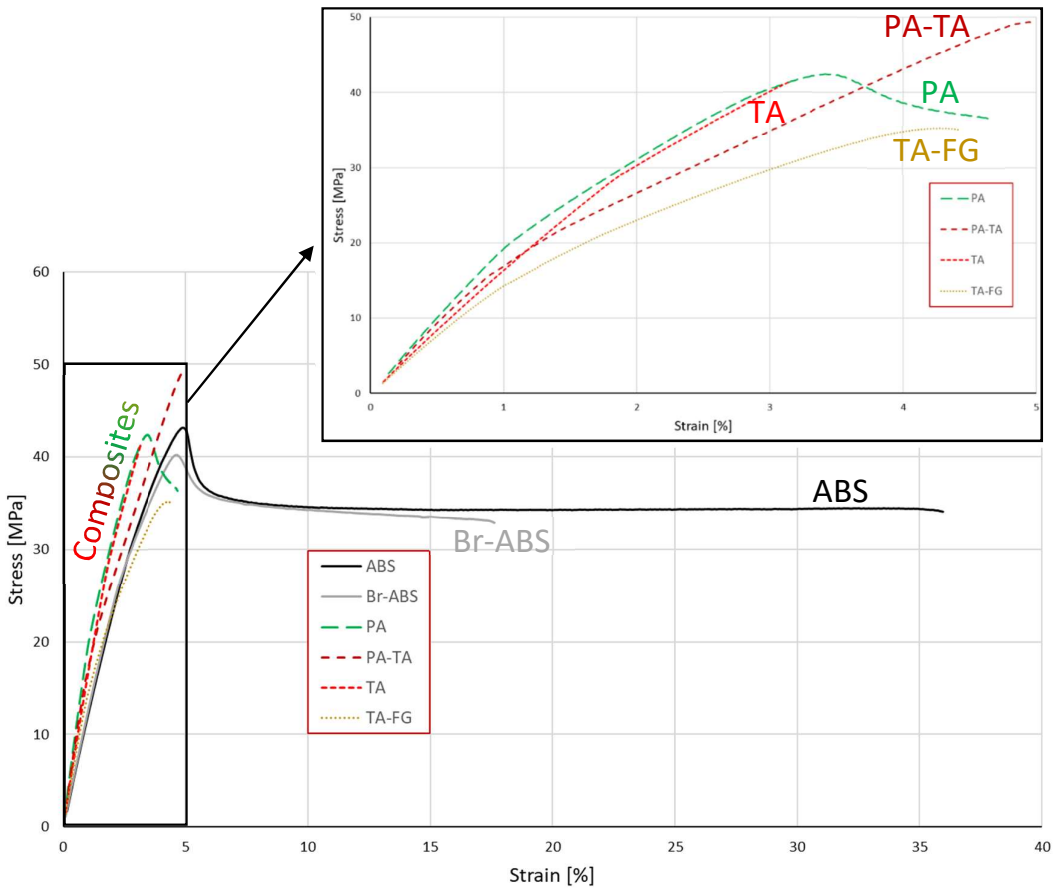

Figure 4.35. Representative tensile stress-strain curves for neat ABS (black), commercial halogenated Br-ABS (gray), and bio-based FR ABS composites (colored). Inset: Enlargement of the bio-based FR ABS composites' tensile stress-strain curves.

Average tensile properties (elastic modulus, tensile strength, strain at break, and toughness) and their standard deviations are shown in Figure 4.36. Five specimens were tested for each composition. As can be seen in Figure 4.36a, all of the composites have a considerably higher elastic modulus than ABS and Br-ABS. The sample containing 30 wt% phytic acid sodium salt (PA) exhibited the highest modulus (1.96 ± 0.10 GPa), with an increase of 70% compared to pristine ABS. The sample with 30 wt% tannic acid (TA) presented an increase of 45% relative to pure ABS (1.67 ± 0.05 GPa). As expected, the elastic modulus of PA-TA, which contains 15 wt% of each filler, is about halfway between those of PA and TA, at 62% higher than the control (1.86 ± 0.01 GPa). Fish gelatin used together with tannic acid (TA-FG) presented the lowest modulus out of the composites (1.50 ± 0.06 GPa), but it is still 30% more rigid than the pure polymer. It is reasonable to

hypothesize that the increases in elastic modulus are due to the addition of a high content of rigid particles, which act as reinforcement, into the polymeric matrix [26]. The elastic modulus of Br-ABS (1.17 ± 0.06 GPa) is statistically the same as that of pure ABS (1.15 ± 0.07 GPa).

Figure 4.36b shows the average tensile strength for each sample, which corresponds to the point of highest stress in the stress-strain curve. (For ABS, Br-ABS, and PA, this is the "yield strength"; for the other composites, which break before yielding, this is the "tensile strength at break".) All of the samples exhibited values similar to that of pristine ABS (within ± 20%), suggesting that there is significant interfacial adhesion between the matrix and the additives, since, according to a model proposed by Nicolais & Narkis [144], a composite with spherical filler particles that experience no interfacial adhesion with the matrix at a volumetric loading level between 15 and 25 vol% (which is the estimated volumetric content for the composites in this study) would show a reduction of about 35 to 50% in tensile strength compared to the pure polymer. The commercial Br-ABS (39.8 ± 0.3 MPa) is almost as strong as pristine ABS (42.8 ± 0.3 MPa), showing a decrease of only 7%. TA-FG presented the lowest tensile strength (34.6 ± 0.5 MPa), 19% lower than pure ABS. Tannic acid caused a minor reduction, of only 5% (40.8 ± 0.8 MPa), and phytic acid sodium salt did not induce any change in the polymer's strength (42.2 ± 0.4 MPa). Surprisingly, when phytic acid and tannic acid were used together, there was a sharp increase in tensile strength (48.1 ± 1.0 MPa for PA-TA), which is higher than when each component was used individually and 12% higher than pure ABS. It is interesting to see that PA and TA act synergistically with each other in terms of both flammability (when tested through cone calorimetry) and mechanical properties. It is possible that crosslinking reactions in tannic acid catalyzed by the presence of phytic acid, discussed previously in this chapter in the context of pyrolysis and combustion experiments, began to occur in the sample during melt processing, since nominal temperatures of up to 220 °C, which are higher than the initial degradation temperatures of both phytic acid and tannic acid, were seen during extrusion. A crosslinked network of tannic acid could lead to a superior performance in tensile strength. It is also possible that tannic acid's crosslinking was extended to involve ABS chains, building bridges between them and forming an extensive network, which would surely cause a significant increase in tensile strength due to the increased interfacial

adhesion and the crosslinked polymeric network. It has been reported that crosslinked composites of LDPE with organic (beech wood) fillers have a higher tensile strength than uncrosslinked LDPE/organic filler composites, caused by the formation of direct covalent bonds between the matrix and the fillers, which results in improved interfacial adhesion [145].

Similar synergy in mechanical performance was observed by Costes et al. [72] when phytic acid and lignin were used together in PLA, keeping in mind that lignin and tannic acid have similar structures: the tensile strengths of the PLA/lignin/phytic acid composites were significantly higher than those of the PLA/lignin and PLA/phytic acid composites. It is important to note that the total filler content was maintained constant both in their work (20 wt%) and in the present work (30 wt%) for all compositions. The previous workers attributed the synergistic effect to the fact that phytic acid was preventing lignin from accelerating the degradation of PLA during processing, since lignin's reactive end groups were preferentially reacting with phytic acid as opposed to inducing chain scissions in the polymer. The PA-TA mechanical synergy seen in the present work, however, is not based on the same mechanism, since the ABS/TA and ABS/PA composites have tensile strengths equivalent to that of pure ABS, while PLA/lignin and PLA/phytic acid had much lower tensile strengths than pure PLA due to the accelerated degradation during processing.

The strain at break (i.e. ductility) of each sample is shown in Figure 4.36c. Pristine ABS and the commercial brominated Br-ABS have a higher ductility than the composites, which was expected due to the high filler content (30 wt%) of the particle-filled composites. ABS's average strain at break (26%) is much higher than that of Br-ABS (17%), but the values are not statistically different because of the large standard deviation associated to ABS (± 11%). It is hypothesized that ABS's ductility is indeed higher than Br-ABS's (despite the large error bar), but localized imperfections (such as surface defects, voids, and impurities), which were likely created during the injection-molding process and can act as sources for crack initiation and propagation, caused an early fracture in some of the ABS specimens, leading to failure before the actual intrinsic limit of the material was reached. The four composite samples have very similar strain at break values amongst themselves, with tannic acid being slightly more brittle than the other three. It is interesting to note that the PA sample is the only composite that shows a true yield

point and presents some plastic strain before fracturing, as can be seen in Figure 4.35. The TA-FG specimens reach a yield point and then immediately break, while the TA and the PA-TA specimens present brittle fractures, failing while still in the elastic domain. This result suggests that phytic acid sodium salt and fish gelatin are not as harmful to the ductility as tannic acid.

The toughness, which is the amount of energy absorbed by the sample before fracturing (i.e. the area under the tensile stress-strain curve), follows the same trend as the strain at break, as can be seen in Figure 4.36d; this was expected, because the differences in ductility among the samples are much larger than the differences in tensile strength. ABS and Br-ABS have a significantly higher toughness than the particle-filled composites, a reflection of their higher ductility. ABS's average toughness is the highest, but the two error bars overlap due to the large standard deviation associated to the ABS specimens, as discussed above. PA and PA-TA present a slightly higher toughness than TA and TA-FG, once again indicating a slight superiority of PA in relation to TA in terms of mechanical properties.

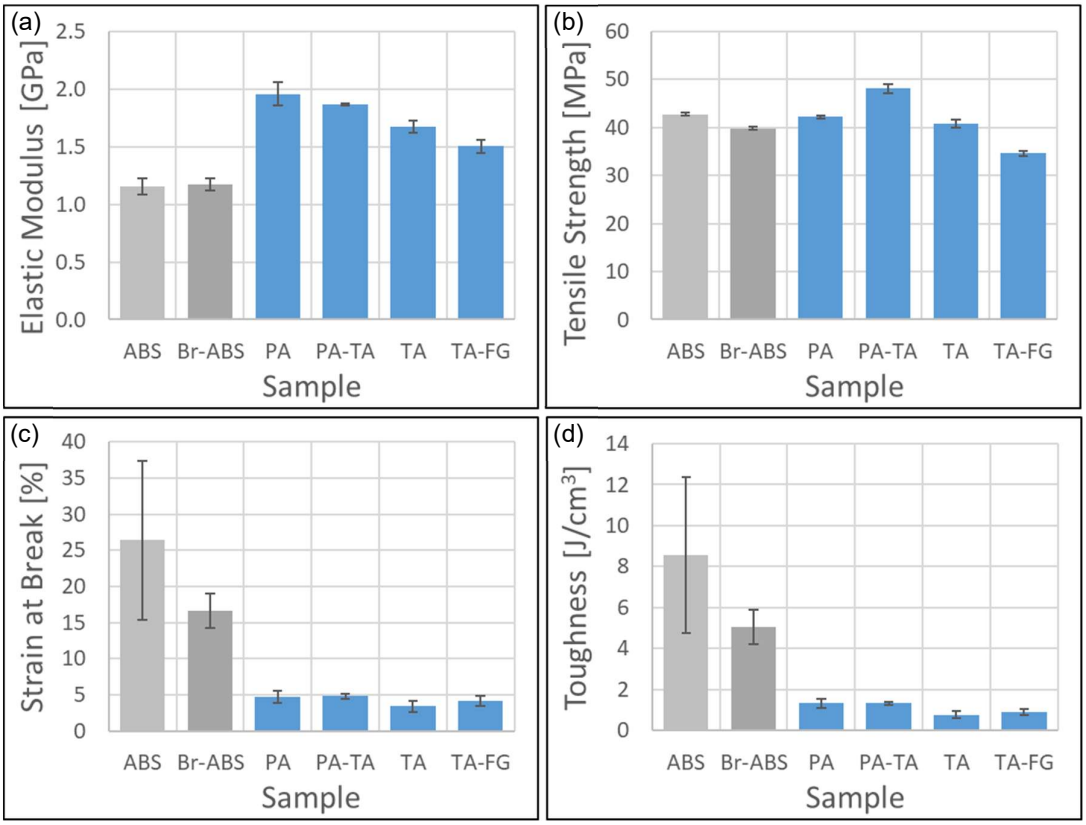

Figure 4.36. Average tensile properties for neat ABS (light gray), commercial halogenated Br-ABS (dark gray), and bio-based FR ABS composites (blue), with standard deviations: (a) elastic modulus, (b) tensile strength, (c) strain at break, and (d) toughness.

The location of the rupture on each specimen (top, middle, or bottom) was also recorded in order to determine if the samples were stronger on one end than on the other and/or if the testing process was preferentially causing fracture on one specific end of the equipment. In order to separate the two effects, the specimens were tested in different orientations relative to the direction of melt flow during injection molding: 3 specimens of each composition were placed with the flow direction facing downwards, and the other 2 were placed with the flow direction facing upwards.

Out of the 30 specimens that were tested, 26 of them (87%) fractured closer to the end of the melt flow (including all 5 of the ABS, Br-ABS, PA, and TA-FG specimens), only 2 fractured closer to the start of the melt flow (both TA), and 2 fractured near the middle of the bar (1 PA-TA and 1 TA). This pattern indicates that the half of the dog-bone specimens that corresponds to the end of the injection-molding melt flow is weaker than the half where the melt flow began, suggesting

either a lack of homogeneity or an uneven distribution of residual stress in the samples caused by the injection-molding process itself. In relation to the tensile-testing process, no abnormality was found, since 15 samples broke at the top end of the testing apparatus, 13 broke at the bottom end, and 2 broke in the middle.

In summary, tensile-test results mostly showed typical behaviors for particle-filled composites: elastic moduli were higher while ductility and toughness were lower for the composites than for the pure polymer. Phytic acid caused the highest increase in modulus, with tannic acid and fish gelatin causing progressively lower increases. Tensile strengths were all within ± 20% of ABS, suggesting significant interfacial adhesion between the matrix and the additives. Clear synergy was observed between tannic acid and phytic acid in terms of tensile strength, as PA-TA's performance was significantly better than both TA's (+18%) and PA's (+14%) performances and 12% better than ABS's results. It is hypothesized that crosslinking reactions in tannic acid were catalyzed by the presence of phytic acid during melt processing, leading to a crosslinked tannic acid network that was responsible for the synergy; it is possible that the crosslinking reactions were extended to involve ABS chains as well, creating an extensive ABS-tannic acid network with improved interfacial adhesion that significantly improved the tensile strength.

4.5.2. Impact Testing

The notched Izod impact resistance was also determined for the 6 samples listed in Table 4.1 as part of the Detailed Analysis and Mechanistic Study Phase. The specimens were clamped in the equipment's vise, and the Izod pendulum was released in order to impact and break the specimens. The amount of energy lost by the pendulum per unit width of each specimen was recorded as the "original Izod impact resistance". According to ASTM D256, for samples with a small impact resistance (less than 27 J/m), the energy required to toss the broken part of the specimen makes up a significant part of the original energy reading, so the toss energy should be estimated separately and subtracted in order to calculate the amount of energy required to actually break the sample (i.e. the "net Izod impact resistance"). Since the composite samples presented an original Izod impact

resistance close to 27 J/m, the toss energy correction procedure was performed on all of the specimens that presented a complete break (i.e. all of the composite specimens): the tossed part was re-placed on top of the clamped part and the pendulum was once again released. The amount of energy lost by the pendulum during its second swing per unit width was recorded as the "estimated toss energy". The estimated toss energy per unit width was then subtracted from the original Izod impact resistance to obtain the net Izod impact resistance of each specimen.

Figure 4.37 presents the original (a) and the net (b) Izod impact resistances of each sample, taken as the average of 10 test specimens, along with the standard deviations. The control samples (ABS and Br-ABS) have a higher impact resistance than the composites, which was expected due to the high filler content of the particle-filled composites; impact strength generally tracks with mechanical toughness. It should be noted that all of the composite specimens presented a Complete Break (failure type C) when tested, meaning that they actually broke into two separate parts, while all of the ABS and Br-ABS specimens presented only a Partial Break (failure type P), which means that they were bent but not broken into two separate pieces. This fact suggests that the difference in impact strength between the controls and the composites is even larger than that presented in the graph, since more energy would be required in order to fully break the controls. There is not much change between the trends of the original and the net impact strengths, because the average toss energies of the composite samples were all very similar (between 17 and 19 J/m) and the toss-energy-correction procedure was not applied to the control samples because they did not fully break, so there was no toss involved. There is no significant difference between the impact resistance of pristine ABS and that of the brominated Br-ABS. The impact strengths of the four composite samples are also similar amongst themselves. It is interesting to point out, however, that the PA sample showed a slightly higher average net Izod impact resistance than the other composites, which is in agreement with the fact that it was the only composite sample that presented a true yield point and showed some plastic strain during the tensile tests (see Figure 4.35). The overall impact-testing results are consistent with the ductility and toughness results obtained from tensile testing, which was expected since both the impact resistance and the toughness calculated from the stress-strain curves are a measure of the amount of energy absorbed by the sample before fracturing.

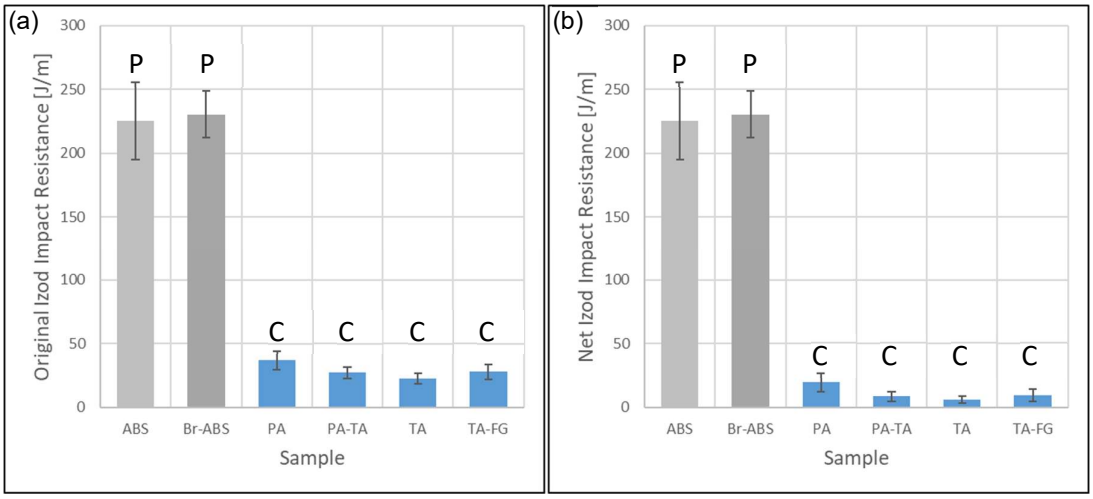

Figure 4.37. (a) Original Izod impact resistances and (b) net Izod impact resistances for neat ABS (light gray), commercial halogenated Br-ABS (dark gray), and bio-based FR ABS composites (blue). Error bars indicate standard deviations. C = Complete break, P = Partial break.

In order to investigate whether the difference in mechanical performance between the two ends of the injection-molded bars seen in the tensile tests would be confirmed by the impact tests, the results from the specimens that were the "top halves" of the molded flexural bars (where the melt flow began) were compared to those from the specimens that were the "bottom halves" (where the melt flow ended). ABS and Br-ABS did present a significant difference between the performances of the two halves, as can be seen in Figure 4.38, and the trend was the same as before: the half of the flexural bars that corresponds to the beginning of the injection-molding melt flow ("top") is stronger than the half where the melt flow ended ("bottom"). For ABS, the "top halves" were on average 23% stronger than the "bottom halves"; for Br-ABS, they were 15% stronger. For each of the composite samples, the "top halves" also had a better average impact strength than the "bottom halves", being 25 to 41% stronger; however, due to the composites' low impact strengths, the differences are not significant when the error bars are taken into consideration.

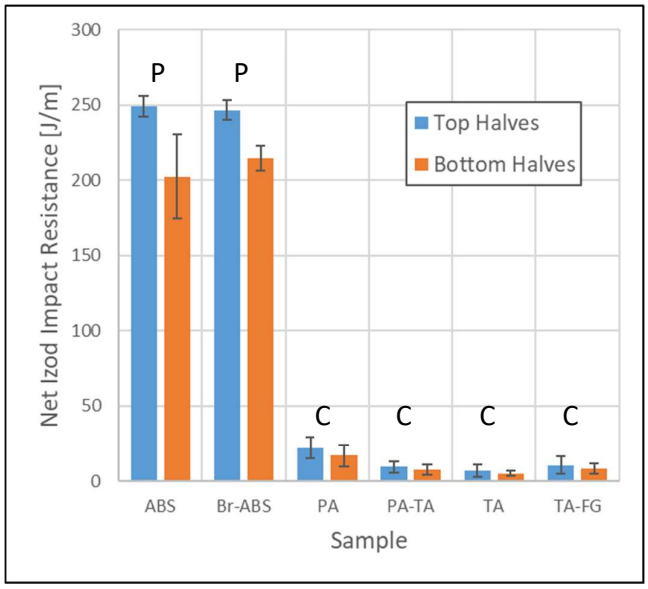

Figure 4.38. Comparison between specimens that were the "top halves" of the injection-molded bars (i.e. where the injection melt-flow began) and those that were the "bottom halves" of the bars (i.e. where the injection melt-flow ended), in terms of net Izod impact resistance, for neat ABS, commercial halogenated Br-ABS, and bio-based FR ABS composites. Error bars indicate standard deviations. C = Complete break, P = Partial break.

4.6. Conclusions

In the present chapter, it was shown that bio-based flame retardants can be used to significantly reduce ABS's flammability while acceptable mechanical properties are maintained. A combination of tannic acid with phytic acid sodium salt (PA-TA) presented the best results; the pair showed clear synergy in terms of both flammability and mechanical performance, achieving better results than when each additive was used individually and obtaining flammability results equivalent to commercial halogenated ABS (Br-ABS). The mechanisms of flame retardation of the bio-based FR composites were studied in detail by combining data from cone calorimetry, MCC, TGA, EGA-MS, and Py-GC-MS experiments, and appear to differ significantly between MCC and cone calorimetry tests; hypotheses for the additives' modes-of-action, as well as to explain the interactions between the different components, were formulated.

TA presented PHRRs significantly below the predicted values in both MCC and cone calorimetry experiments (43% and 53% reductions, respectively,

compared to ABS), but the performances were based on completely different mechanisms. When milligram-scale sample masses are used (as in MCC), it is hypothesized that tannic acid lowers ABS's activation energy for degradation by catalyzing its decomposition through acid catalysis; the polymer's degradation pathway and the nature of the released volatile products are partially changed as the additive is suspected to electrophilically attack the polymer chains, promoting random chain scissions and the loss of side groups rather than the normally predominant unzipping reactions. The onset of ABS's decomposition peak is anticipated due to the lower activation energy, but the end of the polymer's degradation and the THR remain the same; as a result, the HRR curve is widened and, consequently, "flattened", causing a reduction in the PHRR. In cone calorimetry tests, the sample size is sufficiently large so that barrier effects can play a role: tannic acid forms a protective char layer that quickly limits the HRR growth by acting as a thermal and gas barrier, shielding the material underneath. The PHRR is greatly reduced as a result. The char layer is eventually cracked, leading to a second peak just as high as the first. At the very end of the test, the remaining char suffers thermo-oxidative degradation, volatilizing completely. In terms of mechanical properties, typical particle-filled-composite behavior was observed: elastic modulus increased, while ductility and toughness decreased; tensile strength remained the same, suggesting that there is significant interfacial adhesion between the matrix and the filler.

PA showed a small anticipation of ABS's decomposition peak and a reduction in activation energy in MCC tests, but much less pronounced than for TA; as a result, the PHRR reduction was not as high as for TA (38% reduction compared to ABS). In TGA, on the other hand, no anticipation was observed and the activation energy was higher than for pure ABS. EGA and Py-GC-MS results agreed with TGA data, indicating a small delay in ABS's degradation without changing the nature of the products evolved. It is suspected that the large content of water released from phytic acid sodium salt hydrate acts as a heat sink, lowering the material's temperature and, consequently, increasing the apparent decomposition temperatures; the apparent activation energy is also higher, since a significant portion of the thermal energy is absorbed by the water molecules. The difference in the MCC behavior remains unexplained. PA's positive performance in cone calorimetry (56% reduction in PHRR compared to ABS) is suspected to be caused

solely by condensed-phase mechanisms, specifically the formation of a cohesive char layer that acts as a protective thermal and gas barrier; gas-phase mechanisms are not involved, since phosphorus remains in the residue. Ignition was delayed compared to ABS, which is consistent with the heat-sink effect caused by the large amount of water released, as stated above. The char began to form faster than for TA (slowing down the increase in HRR), but it was initially not as effective (taking longer to reach a peak). The char formed, however, was more thermally stable than for the other samples, since it did not crack after a peak was reached and did not undergo thermo-oxidative degradation at the end of the test as occurred for all other materials; PA was therefore the only sample to display a significant char yield at the end of the test (~20%). It is suspected that the delayed ignition gave the material time to form a more thermally stable char due to increased crosslinking before degradation began, allowing the residue to stay intact for the entire duration of the experiment. Mechanical properties were typical for particle-filled composites with significant interfacial adhesion: elastic modulus increased, ductility and toughness decreased, and tensile strength was maintained.

PA-TA presented the best cone calorimetry performance, improving upon PA's, TA's, and ABS's PHRRs by 20%, 25%, and 65%, respectively. Condensed-phase mechanisms are hypothesized to be responsible for the enhanced flame retardation and for the synergy between the two additives: phosphoric acid groups from phytic acid catalyze crosslinking and char-forming reactions in tannic acid, allowing for the rapid formation of a cohesive char layer that acts as a thermal and gas barrier, leading to the quick attainment of a peak in the HRR curve. Char-forming reactions continue throughout the test, as the char cracks but is immediately restored, forming a second peak. At the end of the experiment, the char undergoes thermo-oxidative degradation, volatilizing almost completely. Gas-phase FR mechanisms (flame inhibition) are suspected to occur only during volatilization of the char as phosphorus is released from the degrading residue, decreasing the combustion efficiency and effective heat of combustion of the remaining char; although scientifically interesting, the occurrence of this mechanism after the sample has burned has little practical significance. MCC, TGA, EGA, and Py-GC-MS results suggest that phytic acid partially inhibits tannic acid's catalysis of ABS's degradation in milligram-scale tests, leading to a less pronounced PHRR reduction in MCC (36% reduction from ABS) than was achieved by TA; PA-TA's

behavior is much more similar to PA's than to TA's behavior in all milligram-scale tests as a result. Py-GC-MS indicates a 50% reduction in the release of 1,2,3-benzenetriol and CO_2, tannic acid's main degradation products, compared to the predicted amount, suggesting a significant reduction in the compound's volatilization. Elastic modulus increased, while ductility and toughness decreased, typical results for particle-filled composites. Surprisingly, tensile strength was higher than for both TA and PA, showing clear synergy between the additives. A hypothesis has been formulated to explain PA-TA's behaviors in all of the experiments. It is proposed that phytic acid catalyzes crosslinking and char-forming reactions in tannic acid during melt processing, leading to a crosslinked network of tannic acid (and possibly ABS chains) that increases the material's tensile strength. During heating or combustion experiments, phytic acid-catalyzed crosslinking and char formation are intensified, leading to the rapid formation of a cohesive char layer. The effects of the char layer can only be observed in cone calorimetry tests (reflected in the low PHRR), since the sample size is too small in the other experiments to account for barrier effects. In Py-GC-MS, the sample's long residence time at temperatures between 100 and 220 °C gives time for the creation of an extensive crosslinked tannic acid network; tannic acid consequently takes longer to degrade, so TA-derived radical fragments are not available in significant amounts to attack ABS chains; acid catalysis of ABS is therefore mostly inhibited in Py-GC-MS, canceling TA's anticipation of ABS's degradation and leading to a slight overall delay in ABS decomposition. The same idea occurs in TGA, EGA, and MCC experiments, but to a lesser extent because of their faster heating rates compared to Py-GC-MS's: the availability of TA-derived radical fragments to attack ABS chains is reduced, but not as much as for Py-GC-MS; consequently, acid catalysis of ABS is attenuated, reducing TA's synergistic interaction with ABS but still allowing for a reduction in activation energy and a slight overall anticipation of ABS's degradation in those tests. In TGA, EGA, MCC, and cone calorimetry experiments, the additional PA-catalyzed char eventually degrades with increasing temperature. In Py-GC-MS, however, the sample's long residence time at temperatures between 100 and 220 °C gives time for sufficient crosslinking to take place, making the additional char stable until higher temperatures. It can be said, therefore, that PA-TA presents modest results in milligram-scale tests because TA's synergistic interaction with ABS is attenuated or inhibited, but it displays an

excellent performance in larger-scale experiments because of the synergy between tannic acid and phytic acid.

Despite TA-FG's promising performance in MCC (39% PHRR reduction compared to ABS), second only to TA, it did not exhibit significant flame retardance in cone calorimetry compared to the other bio-based FR composites (38% PHRR reduction compared to ABS). The MCC results were likely caused by the same mechanisms as for TA, with tannic acid catalyzing ABS decomposition, leading to a wider curve and, consequently, a lower peak. In cone calorimetry, char formation did not appear to be significant, as a protective barrier was not formed; the PHRR reduction was mostly due to dilution of the fuel content. Mechanical results were also typical of particle-filled composites with significant interfacial adhesion, although the tensile strength was lower than those of the other composites.

Br-ABS, the commercial brominated control, had equivalent performances to TA in MCC and to PA-TA in cone calorimetry. In MCC, where flame inhibition effects do not occur, the sample's PHRR reduction was attributed to a reduction in ABS's measured activation energy for decomposition, which led to an earlier onset temperature, a wider peak, and, consequently, a lower PHRR. The sample's performance in cone calorimetry was attributed to gas-phase mechanisms, specifically radical scavenging (flame inhibition) by bromine atoms, thus greatly reducing the combustion efficiency.

The present chapter has attempted to elucidate some of the complex mechanisms involved in the thermal degradation and flame retardation of ABS containing bio-based additives, especially tannic acid and phytic acid sodium salt. The mechanisms strongly depend on testing conditions, such as sample size and heating rate. The combination of data from multiple experiments was used to generate hypotheses for the modes-of-action of the bio-based FRs. The results have also demonstrated that it is possible to achieve results comparable to those produced by halogenated FRs using low-toxicity, bio-based FRs in ABS.

5
Conclusions and Recommendations for Future Work

5.1.
Conclusions

In the present work, a systematic screening experiment was performed to evaluate the flammability of ABS composites containing 8 different bio-based or low-toxicity flame retardants, and detailed analyses were conducted on the most promising samples in order to further evaluate their flammability and mechanical properties and to comprehend their mechanisms of flame retardation. The initial objectives of the study were accomplished: (1) ABS's flammability was significantly reduced using bio-based FRs while acceptable mechanical properties were maintained, and (2) the probable flame-retardation mechanisms of ABS composites containing tannic acid, phytic acid sodium salt, or both were elucidated.

Two main conclusions – one performance-based and one science-related/mechanistic – can be drawn from the present research:

(1) **Performance-based conclusion**: It is possible to significantly reduce ABS's flammability using bio-based and low-toxicity flame retardants – especially tannic acid (TA), phytic acid sodium salt (PA), a tannic acid-phytic acid mixture (PA-TA), and a tannic acid-fish gelatin mixture (TA-FG) –, reaching PHRR results equivalent to a commercial halogenated grade of ABS (Br-ABS), while maintaining acceptable mechanical properties;

(2) **Science-related/mechanistic conclusion:** The 4 flame-retarded ABS composites mentioned above most likely act through condensed-phase mechanisms, and notable synergy occurs between tannic acid and phytic acid in terms of both flammability and mechanical performance.

The main conclusions can be broken down into more specific findings, listed below.

5.1.1.
Performance-Based Conclusions

MCC

(A) When tested by MCC, **all 30 ABS composites containing the screened bio-based and/or low-toxicity FRs** – tannic acid, phytic acid sodium salt, fish gelatin, DNA, magnesium hydroxide, alumina trihydrate, melamine poly(magnesium phosphate) (Safire™ 600), and melamine – **perform significantly better than ABS** in terms of PHRR, THR, and, in all cases but one, char yield;

(B) **The bio-based FRs perform better than the commercial additives** in MCC, since the best 4 compositions, and 5 out of the 7 best, contain fully nature-derived FRs systems;

(C) **The best performing composite in MCC is TA, which has a performance equivalent to a commercial halogenated grade of ABS (Br-ABS)**, achieving a 43% PHRR reduction in relation to pure ABS – the next most effective compositions are TA-FG, PA, and PA-TA;

(D) The 4 above-mentioned samples, along with TA-D, PA-ME, and PA-TA-ME, present PHRRs below the predicted no-interaction values, indicating that **synergies occur between the FRs and ABS and/or among the different FRs**.

Cone Calorimetry

(E) When tested by cone calorimetry, **PA-TA, PA, TA, and TA-FG** (in order of performance) **perform significantly better than ABS** in terms of both PHRR and THR;

(F) **The best performing sample in cone calorimetry is PA-TA**, which has a better performance than both PA and TA (**indicating clear synergy between the 2 FRs**), presents a 65% PHRR reduction compared to neat ABS, and **achieves a PHRR performance equivalent to Br-ABS**;

Mechanical Properties

(G) All 4 samples present higher elastic modulus, lower ductility and toughness, and tensile strength similar to those of ABS and Br-ABS – these **mechanical**

results are typical for particle-filled composites with significant matrix-filler interfacial adhesion and suggest that the samples have **acceptable mechanical properties** which, in the case of ductility and toughness, can likely be improved with the addition of plasticizers if properly investigated;

(H) PA-TA presents a higher tensile strength than both PA and TA, indicating **clear synergy between phytic acid sodium salt and tannic acid in terms of mechanical performance**.

5.1.2. Science-Related/Mechanistic Conclusions

(A) PA, TA, PA-TA, and TA-FG likely act through condensed-phase mechanisms to reduce ABS's flammability in both milligram-scale (e.g. MCC) and medium-scale (e.g. cone calorimetry) tests, while Br-ABS acts through condensed-phase mechanisms in the former and gas-phase mechanisms in the latter;

(B) In MCC, TA reduces ABS's flammability by decreasing the polymer's activation energy for decomposition, making the degradation peak begin earlier and, consequently, widening and lowering the height of the degradation peak – tannic acid is hypothesized to catalyze ABS's decomposition by attacking the polymer chains early and reducing the extent of unzipping reactions, thus anticipating the beginning of decomposition, altering the degradation mechanism, and changing the nature of the products of degradation (decreasing the amounts of acrylonitrile, butadiene, styrene, and hybrid SAN monomers, dimers, and trimers (with the exception of styrene trimers) and increasing the amounts of products derived from them);

(C) In cone calorimetry, TA acts through the formation of a protective char layer, shielding the material underneath and reducing the PHRR – the char, however, eventually cracks, and it suffers thermo-oxidative degradation at the end of the test;

(D) TA-FG is suspected to act through the same mechanism as TA in MCC tests, though to a lesser extent because of the lower quantity of tannic acid – fish gelatin presents synergy with tannic acid in these tests through an unknown mechanism;

(E) TA-FG does not present a significantly protective char layer in cone calorimetry tests, reducing ABS's flammability mainly by diluting the fuel content;

(F) PA's mechanism in milligram-scale tests in difficult to define, since phytic acid seems to decrease ABS's activation energy for decomposition in MCC (slightly anticipating the start of the peak, thus decreasing its height) but increases it in TGA tests and causes a small delay in degradation in EGA and Py-GC-MS tests – the delay and E_a increase seen in the latter tests is possibly due to the release of a large amount of water, which acts as a heat sink, lowering the sample's actual temperature and, consequently, raising the apparent degradation temperature and activation energy;

(G) In cone calorimetry, PA appears to act only through condensed-phase mechanisms (flame inhibition is suspected not to play a role): ignition is delayed (possibly due to the water heat-sink effect), allowing for the formation of a cohesive and thermally stable char layer that acts as a protective thermal and gas barrier – limiting the PHRR slightly more effectively than TA – and remains intact for the entire duration of the test;

(H) PA-TA's main flame-retardation mechanism is suspected to be based upon synergy between phytic acid sodium salt and tannic acid, through which the former catalyzes crosslinking and char-forming reactions in the latter – it is hypothesized that the PA-catalyzed crosslinking of TA: (1) occurs first during melt processing, leading to an increase in tensile strength due to the crosslinked TA network and, if ABS chains are involved in the crosslinking reactions, possibly due to the improved interface between TA and ABS; (2) leads to the rapid formation of a strong and cohesive char layer that acts as a protective thermal and gas barrier, which quickly limits the HRR growth (leading to a low PHRR) and, after cracking, quickly restores itself (leading to a 2nd intermediary PHRR), even though it eventually cracks again and undergoes thermo-oxidative degradation towards the end of the test; (3) leads to a more difficult volatilization of TA-derived radical fragments, which, if given enough time at low temperatures, can significantly increase tannic acid's char yield by reducing (or significantly delaying) the volatilization of tannic acid's main degradation products; (4) if given enough time, inhibits tannic acid's aforementioned catalysis of ABS's decomposition due to the reduction or delay

of tannic acid's degradation, thus causing a reduction in the amount of TA-derived radicals available to attack the ABS chains;

(I) If PA-TA is not given enough time at low temperatures, tannic acid's action is not completely inhibited (likely because the extent of TA crosslinking is not sufficient), leading to a moderate reduction of ABS's activation energy for decomposition and, consequently, a slight anticipation and lowering of ABS's degradation peak in MCC, TGA, and EGA experiments and to an earlier ignition in cone calorimetry tests;

(J) Br-ABS seems to reduce ABS's activation energy for decomposition in milligram-scale tests as much as TA, leading to an equivalent PHRR reduction;

(K) In cone calorimetry, Br-ABS reduces ABS's flammability through gas-phase mechanisms, by which bromine and antimony-containing radicals act through radical scavenging (i.e. flame inhibition), a mechanism that is well established in literature for these kinds of FRs.

5.1.3. Other General Conclusions

(A) MCC, though a valid and useful instrument for a variety of reasons, is not an excellent screening tool of FR additives for larger-scale fire experiments such as cone calorimetry, because the mechanisms of flammability reduction in MCC are very different than those which occur in cone calorimetry – cone calorimetry often relies on thermal- and gas-barrier effects and on flame inhibition (radical scavenging), which are not present in MCC; MCC, on the other hand, has a limited amount of mechanisms at its disposal. In the experiments conducted, the composite samples that ranked 1, 2, 3, and 4 in MCC tests ranked 3, 4, 2, and 1 in cone calorimetry (in terms of PHRR), because the mechanisms that were dominant in each test were completely different. MCC is a very important tool that can yield useful material properties and valuable mechanistic information both when its data is analyzed independently and when it is combined with data from other analysis techniques, such as cone calorimetry and TGA; valuable information was certainly obtained from having performed MCC on the Phase 2 samples. It is not clear, however, how much was gained from performing MCC on the other

26 Phase 1 composite samples, since there is no indication that other samples, which did not perform as well as the first 4 in MCC, wouldn't have performed better than them in cone calorimetry experiments because of strong synergistic mechanisms that are not captured in MCC. It is possible that selecting flame retardants and samples to be analyzed in detail based on theory and on their expected FR mechanisms in larger scale tests would have had as likely a probability of choosing the best compositions as selecting them based on MCC results. The decision of using MCC as a screening tool was not incorrect, as there is currently no other small-scale test that can serve as an accurate screening tool for larger-scale combustion tests, and MCC is possibly the one that comes closest. MCC, however, has significant limitations as a screening tool of FRs for larger-scale fire tests, since it does not necessarily lead to the best choice of the most promising flame retardants, and it is not clear that using MCC results can lead to a more accurate selection than using the available scientific, theoretical, and experimental knowledge on each flame retardant's performance and mechanisms in larger-scale flaming tests.

(B) It is believed that the findings of the present research can contribute to the field of bio-based flame retardation of polymers in a general sense and, more specifically, to the search of a bio-based and/or low-toxicity flame-retardant system for ABS. The results have shown that it is possible to achieve flammability results comparable to those produced by halogenated additives using low-toxicity, bio-based FRs, and probable flame-retardation mechanisms of promising bio-based additives in ABS were explained. Building upon the findings of the current study and using the performance and mechanistic information shared by the present research can be a promising path towards developing commercially viable, environmentally friendly, bio-based FR systems for ABS and towards substituting halogenated FRs with bio-based ones for commercial use in ABS in the near future.

5.2.
Recommendations for Future Work

Further research needs to be done in order to transfer the promising flame-retardation results seen in MCC and cone calorimetry to real-world fire scenarios and to obtain FR ABS products that are ready to be commercialized. Although ABS's flammability was significantly decreased, the flammability of the samples still requires further reduction in order to achieve the efficiency of halogenated FRs. Mechanical properties need to be worked on as well, specifically in the sense of increasing the ductility and toughness of the FR ABS composites, before the products are ready to be commercialized. The cost of the bio-based FR additives should also be taken into consideration: tannic acid and fish gelatin are relatively low-cost materials, but phytic acid is relatively expensive. It is possible that the successful development of a phytic acid-based FR system for ABS that can effectively substitute halogenated systems in terms of performance can create a large market demand for phytic acid that will lead to a drastic reduction in its cost, making it a viable raw material for use in commercial applications; current material costs, however, favor the use of tannic acid over phytic acid. Provided below are recommendations for further research that can lead to the achievement of bio-based or low-toxicity FR ABS materials that can be successfully commercialized and to the increase in the scientific knowledge regarding the flame-retardation mechanisms of the bio-based additives in ABS.

(1) Improving the compatibility between ABS and the additives by experimenting with the content of compatibilizer in the samples and by trying different compatibilizers is suggested – it was discovered towards the end of the project that there are a variety of commercially available styrene-maleic anhydride copolymers that can be used as compatibilizers for organic additive-filled ABS systems, the most appropriate of which can possibly be determined by seeking recommendations from companies that specialize in these copolymers (such as Polyscope Polymers, for example) and performing related experiments;

(2) Optimizing the melt-processing parameters for ABS composites is suggested in order to improve the distribution and dispersion of the fillers and reduce material degradation during processing;

(3) The measurement of ABS's activation energy for degradation (for neat ABS and ABS composites) through the traditional method of performing experiments using different heating rates is recommended, as it can provide more accurate measurements than the method used in this study, which was based on a single heating rate – it is recommended to perform this type of calculation (based on many heating rates) using both MCC [107] and TGA, since some samples presented very different E_a results when tested through each instrument in the present work;

(4) Analyzing the samples' char residues from complete and partial cone calorimetry, vertical burning, MCC, and/or TGA experiments through techniques such as Raman spectroscopy, Fourier-transform infrared spectroscopy (FTIR), x-ray photoelectron spectroscopy (XPS), energy-dispersive x-ray spectroscopy (EDX), and/or scanning electron microscopy (SEM) – most importantly the first three techniques – is recommended to enable a better understanding of the condensed phase and of the char-forming mechanisms;

(5) It would be useful to better understand the mechanical behavior of the bio-based ABS composites in mechanistic terms, especially with the intent of confirming the hypothesis given in the present work for the clear synergy observed in PA-TA in terms of tensile strength;

(6) Improving the ductility and toughness of the bio-based ABS composites, through experimenting the use of plasticizers in the samples or through other techniques, is recommended;

(7) The relative contents of the bio-based FRs (TA, PA, and FG) should be changed in a systematic experiment in order to find optimal loadings for the best possible flame retardance – this is particularly important for PA-TA

composites, for which the synergistic behavior can be better understood and significant increases in synergy can possibly be obtained by changing the relative proportions of the additives;

(8) It would also be useful to experiment with different total filler contents in the bio-based ABS composites;

(9) It is recommended to experiment with different FRs and FR combinations not evaluated in the present study – both in combination with PA, TA, and FG and in completely new compositions – to attempt to achieve even better results than those achieved in this work, particularly to achieve a V-0 classification in vertical burn tests and lower PHRR and THR values in cone calorimetry – preliminary tests with ammonium polyphosphate (APP) in combination with PA and TA have shown indications of promising results;

(10) It is particularly recommended to test the use of phosphorus-based flame retardants that are known to act in the gas phase, since the most successful FRs for ABS to date, halogenated additives, act through gas-phase mechanisms;

(11) It was observed during the present research that phytic acid undergoes considerable degradation even at ambient temperatures, leading to changes in the phytic acid-containing ABS composites over time – the aging effect of phytic acid is recommended to be studied systematically and in more detail (a useful report [120] on the subject is available in literature) since this factor can be a determinant of whether this additive can be viably used as an FR in commercial uses.

6
References

[1] O. Segev, A. Kushmaro, A. Brenner, Environmental Impact of Flame Retardants (Persistence and Biodegradability), Int. J. Environ. Res. Public Health. 6 (2009) 478–491. https://doi.org/10.3390/ijerph6020478.

[2] Environmental Health Criteria 192. Flame Retardants: A General Introduction, World Health Organization, Geneva, Switzerland, 1997.

[3] U. Sellström, Determination of some polybrominated flame retardants in biota, sediment and sewage sludge, Stockholm University, 1999.

[4] A. Sjödin, L. Hagmar, E. Klasson-Wehler, K. Kronholm-Dlab, E. Jakobsson, Å. Bergman, Flame retardant exposure: Polybrominated diphenyl ethers in blood from Swedish workers, Environ. Health Perspect. 107 (1999) 643–648. https://doi.org/10.1289/ehp.99107643.

[5] U. Sellström, P. Lindberg, L. Häggberg, C. de Wit, Higher brominated PBDEs found in eggs of peregrine falcons (Falco peregrinus) breeding in Sweden, in: 2nd Int. Work. Brominated Flame Retard., AB Firmatryck, Stockholm, 2001: pp. 159–162.

[6] A. Sjödin, D.G. Patterson, A. Bergman, Brominated flame retardants in serum from US blood donors, Environ. Sci. Technol. 35 (2001) 3830–3833. https://doi.org/10.1021/es010815n.

[7] D. Herzke, R. Kallenborn, T. Nygard, T. Sandanger, Species dependent distribution of polybrominated biphenyls and diphenyl ethers in eggs of Norwegian bird of prey, in: 2nd Int. Work. Brominated Flame Retard., AB Firmatryck, Stockholm, 2001: pp. 321–324.

[8] H.-B. Lee, T.E. Peart, Organic Contaminants in Canadian Municipal Sewage Sludge. Part I. Toxic or Endocrine-Disrupting Phenolic Compounds, Water Qual. Res. J. 37 (2002) 681–696. https://doi.org/10.2166/wqrj.2002.046.

[9] C.A. de Wit, An overview of brominated flame retardants in the

environment, Chemosphere. 46 (2002) 583–624. https://doi.org/10.1016/S0045-6535(01)00225-9.

[10] M. Alaee, P. Arias, A. Sjödin, Å. Bergman, An overview of commercially used brominated flame retardants, their applications, their use patterns in different countries/regions and possible modes of release, Environ. Int. 29 (2003) 683–689. https://doi.org/10.1016/S0160-4120(03)00121-1.

[11] R.J. Law, C.R. Allchin, J. de Boer, A. Covaci, D. Herzke, P. Lepom, S. Morris, J. Tronczynski, C.A. de Wit, Levels and trends of brominated flame retardants in the European environment, 64 (2006) 187–208. https://doi.org/10.1016/j.chemosphere.2005.12.007.

[12] N. Kajiwara, S. Kamikawa, K. Ramu, D. Ueno, T.K. Yamada, A. Subramanian, P.K.S. Lam, T.A. Jefferson, M. Prudente, K.-H. Chung, S. Tanabe, Geographical distribution of polybrominated diphenyl ethers (PBDEs) and organochlorines in small cetaceans from Asian waters, Chemosphere. 64 (2006) 287–295. https://doi.org/10.1016/j.chemosphere.2005.12.013.

[13] Environmental Health Criteria 152. Polybrominated biphenyls, World Health Organization, Geneva, Switzerland, 1994.

[14] L. Costes, F. Laoutid, S. Brohez, P. Dubois, Bio-based flame retardants: When nature meets fire protection, Mater. Sci. Eng. R. 117 (2017) 1–25. https://doi.org/10.1016/j.mser.2017.04.001.

[15] R. Sonnier, A. Taguet, L. Ferry, J.-M. Lopez-Cuesta, Towards Bio-based Flame Retardant Polymers, Springer International Publishing, Cham, 2018. https://doi.org/10.1007/978-3-319-67083-6.

[16] C. Hobbs, Recent Advances in Bio-Based Flame Retardant Additives for Synthetic Polymeric Materials, Polymers (Basel). 11 (2019) 224–254. https://doi.org/10.3390/polym11020224.

[17] D.A.V. Watson, D.A. Schiraldi, Biomolecules as Flame Retardant Additives for Polymers: A Review, Polymers (Basel). 12 (2020) 849–879. https://doi.org/10.3390/polym12040849.

[18] T. Deans, Using Nature As a Way To Flame Retard Synthetic Materials, Case Western Reserve University, 2017.

[19] H. Wang, X. Zhou, M. Abro, M. Gao, M. Deng, Z. Qin, Y. Sun, L. Yue,

X. Zhang, Mussel-Inspired General Interface Modification Method and Its Application in Polymer Reinforcement and as a Flame Retardant, ACS Omega. 3 (2018) 4891–4898. https://doi.org/10.1021/acsomega.8b00182.

[20] L.-L. Ge, H.-J. Duan, X.-G. Zhang, C. Chen, J.-H. Tang, Z.-M. Li, Synergistic effect of ammonium polyphosphate and expandable graphite on flame-retardant properties of acrylonitrile-butadiene-styrene, J. Appl. Polym. Sci. 126 (2012) 1337–1343. https://doi.org/10.1002/app.36997.

[21] E.J. Price, J. Covello, A. Tuchler, G.E. Wnek, Intumescent, Epoxy-Based Flame-Retardant Coatings Based on Poly(acrylic acid) Compositions, ACS Appl. Mater. Interfaces. 12 (2020) 18997–19005. https://doi.org/10.1021/acsami.0c00567.

[22] K.S. Lim, S.T. Bee, L.T. Sin, T.T. Tee, C.T. Ratnam, D. Hui, A.R. Rahmat, A review of application of ammonium polyphosphate as intumescent flame retardant in thermoplastic composites, Compos. Part B Eng. 84 (2016). https://doi.org/10.1016/j.compositesb.2015.08.066.

[23] J. Alongi, Z. Han, S. Bourbigot, Intumescence: Tradition versus novelty. A comprehensive review, Prog. Polym. Sci. 51 (2015) 28–73. https://doi.org/10.1016/j.progpolymsci.2015.04.010.

[24] J.H. Song, Typical flame retardant/additive chemicals for commercial FR-HIPS and FR-ABS resins, J. Vinyl Addit. Technol. 1 (1995) 46–50. https://doi.org/10.1002/vnl.730010112.n.

[25] E.D. Weil, S. V. Levchik, Flame Retardants for Plastics and Textiles, Carl Hanser Verlag GmbH & Co. KG, München, 2009. https://doi.org/10.3139/9783446430655.

[26] P. Song, Z. Cao, Q. Meng, S. Fu, Z. Fang, Q. Wu, J. Ye, Effect of lignin incorporation and reactive compatibilization on the morphological, rheological, and mechanical properties of ABS resin, J. Macromol. Sci. Part B Phys. 51 (2012) 720–735. https://doi.org/10.1080/00222348.2011.609794.

[27] B. Prieur, M. Meub, M. Wittemann, R. Klein, S. Bellayer, G. Fontaine, S. Bourbigot, Phosphorylation of lignin to flame retard acrylonitrile

butadiene styrene (ABS), Polym. Degrad. Stab. 127 (2015) 32–43. https://doi.org/10.1016/j.polymdegradstab.2016.01.015.

[28] S. V. Levchik, E.D. Weil, New developments in flame retardancy of styrene thermoplastics and foams, Polym. Int. 57 (2008) 431–448. https://doi.org/10.1002/pi.2282.

[29] H. Ma, L. Tong, Z. Xu, Z. Fang, Y. Jin, F. Lu, A novel intumescent flame retardant: Synthesis and application in ABS copolymer, Polym. Degrad. Stab. 92 (2007) 720–726. https://doi.org/10.1016/j.polymdegradstab.2006.12.009.

[30] H.-Y. Ma, L.-F. Tong, Z.-B. Xu, Z.-P. Fang, Functionalizing Carbon Nanotubes by Grafting on Intumescent Flame Retardant: Nanocomposite Synthesis, Morphology, Rheology, and Flammability, Adv. Funct. Mater. 18 (2008) 414–421. https://doi.org/10.1002/adfm.200700677.

[31] J. Alongi, F. Cuttica, F. Carosio, DNA Coatings from Byproducts: A Panacea for the Flame Retardancy of EVA, PP, ABS, PET, and PA6?, ACS Sustain. Chem. Eng. 4 (2016) 3544–3551. https://doi.org/10.1021/acssuschemeng.6b00625.

[32] H. Tributsch, S. Fiechter, The material strategy of fire-resistant tree barks, in: High Perform. Struct. Mater. IV, WIT Press, Southampton, UK, 2008: pp. 43–52. https://doi.org/10.2495/HPSM080051.

[33] P. Song, Z. Cao, S. Fu, Z. Fang, Q. Wu, J. Ye, Thermal degradation and flame retardancy properties of ABS/lignin: Effects of lignin content and reactive compatibilization, Thermochim. Acta. 518 (2011) 59–65. https://doi.org/10.1016/j.tca.2011.02.007.

[34] H. Moustafa, A.M. Youssef, S. Duquesne, N.A. Darwish, Characterization of bio-filler derived from seashell wastes and its effect on the mechanical, thermal, and flame retardant properties of ABS composites, Polym. Compos. 38 (2017) 2788–2797. https://doi.org/10.1002/pc.23878.

[35] W.E. Clark, Firefighting Principles and Practices: 2nd Edition, illust., PennWell Books, New Jersey, 1991.

[36] A.M. Hasofer, V.R. Beck, I.D. Bennetts, Risk Analysis in Building Fire Safety Engineering, 1st ed., Elsevier Ltd, Oxford, 2006.

[37] W.M. Haessler, The extinguishment of fire, Rev. ed., National Fire Protection Association, Boston, 1974.

[38] J.H. Troitzsch, International plastics flammability handbook: principles, regulations, testing and approval, 2nd ed., Hanser Publishers, Munich, 1990.

[39] C.F. Cullis, Bromine Compounds as Flame Retardants, in: Proc. Int. Conf. Fire Safety, Vol. 12, Product Safety Corporation, Milbrae, California, 1987: pp. 307–323.

[40] R.R. Hindersinn, Historical Aspects of Polymer Fire Retardance, in: G.L. Nelson (Ed.), Fire Polym., American Chemical Society, Washington, D.C., 1990: pp. 87–96. https://doi.org/10.1021/bk-1990-0425.ch007.

[41] A.U.R. Shah, M.N. Prabhakar, J.-I. Song, Current advances in the fire retardancy of natural fiber and bio-based composites – A review, Int. J. Precis. Eng. Manuf. - Green Technol. 4 (2017) 247–262. https://doi.org/10.1007/s40684-017-0030-1.

[42] Environmental health criteria 110. Tricresyl phosphate, World Health Organization, Geneva, Switzerland, 1990.

[43] Environmental health criteria 111. Triphenyl phosphate, World Health Organization, Geneva, Switzerland, 1991.

[44] Environmental health criteria 173. Tris(2,3-dibromopropyl) phosphate and bis(2,3-dibromopropyl) phosphate, World Health Organization, Geneva, Switzerland, 1995.

[45] S. Nikkeshi, Agent for imparting flame retardancy to thermoplastic resin, US 6624258 B1, 2003.

[46] A. Gani, I. Naruse, Effect of cellulose and lignin content on pyrolysis and combustion characteristics for several types of biomass, Renew. Energy. 32 (2007) 649–661. https://doi.org/10.1016/j.renene.2006.02.017.

[47] G. Tondi, A. Pizzi, Tannin-based rigid foams: Characterization and modification, Ind. Crops Prod. 29 (2009) 356–363. https://doi.org/10.1016/j.indcrop.2008.07.003.

[48] G. Tondi, W. Zhao, A. Pizzi, G. Du, V. Fierro, A. Celzard, Tannin-based rigid foams: A survey of chemical and physical properties,

Bioresour. Technol. 100 (2009) 5162–5169. https://doi.org/10.1016/j.biortech.2009.05.055.

[49] S. Ravichandran, R.M. Bouldin, J. Kumar, R. Nagarajan, A renewable waste material for the synthesis of a novel non-halogenated flame retardant polymer, J. Clean. Prod. 19 (2011) 454–458. https://doi.org/10.1016/j.jclepro.2010.09.010.

[50] R.N. Walters, R.E. Lyon, Molar group contributions to polymer flammability, J. Appl. Polym. Sci. 87 (2003) 548–563. https://doi.org/10.1002/app.11466.

[51] J. Zhang, Q. Ji, X. Shen, Y. Xia, L. Tan, Q. Kong, Pyrolysis products and thermal degradation mechanism of intrinsically flame-retardant calcium alginate fibre, Polym. Degrad. Stab. 96 (2011) 936–942. https://doi.org/10.1016/J.POLYMDEGRADSTAB.2011.01.029.

[52] G. Laufer, C. Kirkland, A.A. Cain, J.C. Grunlan, Clay-chitosan nanobrick walls: Completely renewable gas barrier and flame-retardant nanocoatings, ACS Appl. Mater. Interfaces. 4 (2012) 1643–1649. https://doi.org/10.1021/am2017915.

[53] G. Laufer, C. Kirkland, A.B. Morgan, J.C. Grunlan, Intumescent multilayer nanocoating, made with renewable polyelectrolytes, for flame-retardant cotton, Biomacromolecules. 13 (2012) 2843–2848. https://doi.org/10.1021/bm300873b.

[54] F. Carosio, J. Alongi, G. Malucelli, Layer by Layer ammonium polyphosphate-based coatings for flame retardancy of polyester-cotton blends, Carbohydr. Polym. 88 (2012) 1460–1469. https://doi.org/10.1016/j.carbpol.2012.02.049.

[55] J. Alongi, F. Carosio, G. Malucelli, Layer by layer complex architectures based on ammonium polyphosphate, chitosan and silica on polyester-cotton blends: Flammability and combustion behaviour, Cellulose. 19 (2012) 1041–1050. https://doi.org/10.1007/s10570-012-9682-8.

[56] A. Pawlak, M. Mucha, Thermogravimetric and FTIR studies of chitosan blends, Thermochim. Acta. 396 (2003) 153–166. https://doi.org/10.1016/S0040-6031(02)00523-3.

[57] L. Zeng, C. Qin, L. Wang, W. Li, Volatile compounds formed from the

pyrolysis of chitosan, Carbohydr. Polym. 83 (2011) 1553–1557. https://doi.org/10.1016/j.carbpol.2010.10.007.

[58] G. Tondi, S. Wieland, T. Wimmer, M.F. Thevenon, A. Pizzi, A. Petutschnigg, Tannin-boron preservatives for wood buildings: Mechanical and fire properties, Eur. J. Wood Wood Prod. 70 (2012) 689–696. https://doi.org/10.1007/s00107-012-0603-1.

[59] J. Alongi, R.A. Carletto, A. Di Blasio, F. Cuttica, F. Carosio, F. Bosco, G. Malucelli, Intrinsic intumescent-like flame retardant properties of DNA-treated cotton fabrics, Carbohydr. Polym. 96 (2013) 296–304. https://doi.org/10.1016/j.carbpol.2013.03.066.

[60] F. Carosio, A. Di Blasio, J. Alongi, G. Malucelli, Green DNA-based flame retardant coatings assembled through Layer by Layer, Polymer (Guildf). 54 (2013) 5148–5153. https://doi.org/10.1016/j.polymer.2013.07.029.

[61] G. Malucelli, F. Bosco, J. Alongi, F. Carosio, A. Di Blasio, C. Mollea, F. Cuttica, A. Casale, Biomacromolecules as novel green flame retardant systems for textiles: An overview, RSC Adv. 4 (2014) 46024–46039. https://doi.org/10.1039/c4ra06771a.

[62] X. Lang, Low Flammability Foam-Like Materials Based on Epoxy, Tannic Acid, Sodium Montmorillonite Clay, Case Western Reserve University, 2014.

[63] J. Wang, Q. Ren, W. Zheng, W. Zhai, Improved Flame-Retardant Properties of Poly(lactic acid) Foams Using Starch as a Natural Charring Agent, Ind. Eng. Chem. Res. 53 (2014) 1422–1430. https://doi.org/10.1021/ie403041h.

[64] B.A. Howell, Y.G. Daniel, Thermal degradation of phosphorus esters derived from isosorbide and 10-undecenoic acid, J. Therm. Anal. Calorim. 121 (2015) 411–419. https://doi.org/10.1007/s10973-015-4487-2.

[65] L. Costes, F. Laoutid, L. Dumazert, J.M. Lopez-Cuesta, S. Brohez, C. Delvosalle, P. Dubois, Metallic phytates as efficient bio-based phosphorous flame retardant additives for poly(lactic acid), Polym. Degrad. Stab. 119 (2015) 217–227. https://doi.org/10.1016/j.polymdegradstab.2015.05.014.

[66] P. Wang, F. Yang, Z. Cai, Synergistic effect of organo-montmorillonite and DOPO-based oligomer on improving the flame retardancy of epoxy thermoset, J. Therm. Anal. Calorim. 128 (2017) 1429–1441. https://doi.org/10.1007/s10973-016-6051-0.

[67] K. Shang, W. Liao, J. Wang, Y.T. Wang, Y.Z. Wang, D.A. Schiraldi, Nonflammable Alginate Nanocomposite Aerogels Prepared by a Simple Freeze-Drying and Post-Cross-Linking Method, ACS Appl. Mater. Interfaces. 8 (2016) 643–650. https://doi.org/10.1021/acsami.5b09768.

[68] H.B. Chen, P. Shen, M.J. Chen, H.B. Zhao, D.A. Schiraldi, Highly Efficient Flame Retardant Polyurethane Foam with Alginate/Clay Aerogel Coating, ACS Appl. Mater. Interfaces. 8 (2016) 32557–32564. https://doi.org/10.1021/acsami.6b11659.

[69] S.A. Isarov, P.W. Lee, J.H. Towslee, K.M. Hoffman, R.D. Davis, J.M. Maia, J.K. Pokorski, DNA as a flame retardant additive for low-density polyethylene, Polymer (Guildf). 97 (2016) 504–514. https://doi.org/10.1016/j.polymer.2016.05.060.

[70] L. Liu, M. Qian, P. Song, G. Huang, Y. Yu, S. Fu, Fabrication of Green Lignin-based Flame Retardants for Enhancing the Thermal and Fire Retardancy Properties of Polypropylene/Wood Composites, ACS Sustain. Chem. Eng. 4 (2016) 2422–2431. https://doi.org/10.1021/acssuschemeng.6b00112.

[71] Z. Xia, A. Singh, W. Kiratitanavit, R. Mosurkal, J. Kumar, R. Nagarajan, Unraveling the mechanism of thermal and thermo-oxidative degradation of tannic acid, Thermochim. Acta. 605 (2015) 77–85. https://doi.org/10.1016/j.tca.2015.02.016.

[72] L. Costes, F. Laoutid, S. Brohez, C. Delvosalle, P. Dubois, Phytic acid–lignin combination: A simple and efficient route for enhancing thermal and flame retardant properties of polylactide, Eur. Polym. J. 94 (2017) 270–285. https://doi.org/10.1016/j.eurpolymj.2017.07.018.

[73] Y.T. Wang, H.B. Zhao, K. DeGracia, L.X. Han, H. Sun, M. Sun, Y.Z. Wang, D.A. Schiraldi, Green Approach to Improving the Strength and Flame Retardancy of Poly(vinyl alcohol)/Clay Aerogels: Incorporating Biobased Gelatin, ACS Appl. Mater. Interfaces. 9 (2017) 42258–

42265. https://doi.org/10.1021/acsami.7b14958.

[74] Z. Xia, W. Kiratitanavit, P. Facendola, S. Thota, S. Yu, J. Kumar, R. Mosurkal, R. Nagarajan, Fire resistant polyphenols based on chemical modification of bio-derived tannic acid, Polym. Degrad. Stab. 153 (2018) 227–243. https://doi.org/10.1016/j.polymdegradstab.2018.04.020.

[75] D.F. Li, X. Zhao, Y.W. Jia, X.L. Wang, Y.Z. Wang, Tough and flame-retardant poly(lactic acid) composites prepared via reactive blending with biobased ammonium phytate and in situ formed crosslinked polyurethane, Compos. Commun. 8 (2018) 52–57. https://doi.org/10.1016/j.coco.2018.04.001.

[76] F. Laoutid, H. Vahabi, M. Shabanian, F. Aryanasab, P. Zarrintaj, M.R. Saeb, A new direction in design of bio-based flame retardants for poly(lactic acid), Fire Mater. 42 (2018) 914–924. https://doi.org/10.1002/fam.2646.

[77] Z. Cheng, K. DeGracia, D. Schiraldi, Sustainable, Low Flammability, Mechanically-Strong Poly(vinyl alcohol) Aerogels, Polymers (Basel). 10 (2018) 1102–1111. https://doi.org/10.3390/polym10101102.

[78] Z. Cheng, Mechanically Strong/Low Flammability Poly(vinyl alchohol) Aerogels, Case Western Reserve University, 2019.

[79] Y.X. Yang, L. Haurie, J. Zhang, X.-Q. Zhang, R. Wang, D.-Y. Wang, Effect of bio-based phytate (PA-THAM) on the flame retardant and mechanical properties of polylactide (PLA), EXPRESS Polym. Lett. 14 (2020) 705–716.

[80] A. Cayla, F. Rault, S. Giraud, F. Salaün, R. Sonnier, L. Dumazert, Influence of ammonium polyphosphate/lignin ratio on thermal and fire behavior of biobased thermoplastic: The case of Polyamide 11, Materials (Basel). 12 (2019). https://doi.org/10.3390/ma12071146.

[81] K. DeGracia, Sustainable, Flame-Retarded Poly(butylene terephthalate), Case Western Reserve University, 2019.

[82] Y.-Y. Gao, C. Deng, Y.-Y. Du, S.-C. Huang, Y.-Z. Wang, A novel bio-based flame retardant for polypropylene from phytic acid, Polym. Degrad. Stab. 161 (2019) 298–308. https://doi.org/10.1016/J.POLYMDEGRADSTAB.2019.02.005.

[83] H. Yang, B. Yu, X. Xu, S. Bourbigot, H. Wang, P. Song, Lignin-derived bio-based flame retardants toward high-performance sustainable polymeric materials, Green Chem. 22 (2020) 2129–2161. https://doi.org/10.1039/d0gc00449a.

[84] W.J. Work, K. Horie, M. Hess, R.F.T. Stepto, Definition of terms related to polymer blends, composites, and multiphase polymeric materials (IUPAC Recommendations 2004), Pure Appl. Chem. 76 (2004) 1985–2007. https://doi.org/10.1351/pac200476111985.

[85] X. Lang, K. Shang, Y.-Z. Wang, D.A. Schiraldi, Low flammability foam-like materials based on epoxy, tannic acid, and sodium montmorillonite clay, Green Mater. 3 (2015) 43–51. https://doi.org/10.1680/gmat.14.00019.

[86] W. Kiratitanavit, Z. Xia, A. Singh, R. Mosurkal, R. Nagarajan, Tannic Acid: A Bio-based Intumescent Char-forming Additive for Nylon 6, in: SPE ANTEC, Indianapolis, 2016: pp. 1411–1415.

[87] Y. Feng, Y. Zhou, D. Li, S. He, F. Zhang, G. Zhang, A plant-based reactive ammonium phytate for use as a flame-retardant for cotton fabric, Carbohydr. Polym. 175 (2017) 636–644. https://doi.org/10.1016/j.carbpol.2017.06.129.

[88] X.-W. Cheng, J.-P. Guan, R.-C. Tang, K.-Q. Liu, Phytic acid as a bio-based phosphorus flame retardant for poly(lactic acid) nonwoven fabric, J. Clean. Prod. 124 (2016) 114–119. https://doi.org/10.1016/J.JCLEPRO.2016.02.113.

[89] J. Alongi, R.A. Carletto, A. Di Blasio, F. Carosio, F. Bosco, G. Malucelli, DNA: A novel, green, natural flame retardant and suppressant for cotton, J. Mater. Chem. A. 1 (2013) 4779–4785. https://doi.org/10.1039/c3ta00107e.

[90] J. Alongi, A. Di Blasio, F. Cuttica, F. Carosio, G. Malucelli, Bulk or surface treatments of ethylene vinyl acetate copolymers with DNA: Investigation on the flame retardant properties, Eur. Polym. J. 51 (2014) 112–119. https://doi.org/10.1016/j.eurpolymj.2013.12.009.

[91] F. Carosio, F. Cuttica, A. Di Blasio, J. Alongi, G. Malucelli, Layer by layer assembly of flame retardant thin films on closed cell PET foams: Efficiency of ammonium polyphosphate versus DNA, Polym. Degrad.

Stab. 113 (2015) 189–196. https://doi.org/10.1016/j.polymdegradstab.2014.09.018.

[92] J. Alongi, A. Di Blasio, F. Cuttica, F. Carosio, G. Malucelli, Flame Retardant Properties of Ethylene Vinyl Acetate Copolymers Melt-Compounded with Deoxyribonucleic Acid in the Presence of α-cellulose or β-cyclodextrins, Curr. Org. Chem. 18 (2014) 1651–1660. https://doi.org/10.2174/1385272819666140616181108.

[93] L. Ferry, G. Dorez, A. Taguet, B. Otazaghine, J.M. Lopez-Cuesta, Chemical modification of lignin by phosphorus molecules to improve the fire behavior of polybutylene succinate, Polym. Degrad. Stab. 113 (2015) 135–143. https://doi.org/10.1016/j.polymdegradstab.2014.12.015.

[94] L. Costes, F. Laoutid, M. Aguedo, A. Richel, S. Brohez, C. Delvosalle, P. Dubois, Phosphorus and nitrogen derivatization as efficient route for improvement of lignin flame retardant action in PLA, Eur. Polym. J. 84 (2016) 652–667. https://doi.org/10.1016/j.eurpolymj.2016.10.003.

[95] P.L.M. Barreto, A.T.N. Pires, V. Soldi, Thermal degradation of edible films based on milk proteins and gelatin in inert atmosphere, Polym. Degrad. Stab. 79 (2003) 147–152. https://doi.org/10.1016/S0141-3910(02)00267-7.

[96] W.M. Ames, Heat degradation of gelatin, J. Soc. Chem. Ind. 66 (1947) 279–284. https://doi.org/10.1002/jctb.5000660808.

[97] J. Alongi, A. Di Blasio, J. Milnes, G. Malucelli, S. Bourbigot, B. Kandola, G. Camino, Thermal degradation of DNA, an all-in-one natural intumescent flame retardant, Polym. Degrad. Stab. 113 (2015) 110–118. https://doi.org/10.1016/j.polymdegradstab.2014.11.001.

[98] L. Costa, G. Camino, Thermal behaviour of melamine, J. Therm. Anal. 34 (1988) 423–429. https://doi.org/10.1007/BF01913181.

[99] L. Costa, G. Camino, M.P. Luda di Cortemiglia, Mechanism of Thermal Degradation of Fire-Retardant Melamine Salts, in: G.L. Nelson (Ed.), Fire Polym. Hazards Identif. Prev., American Chemical Society, Washington, DC, 1990: pp. 211–238. https://doi.org/10.1021/bk-1990-0425.ch015.

[100] R.G. Puri, A.S. Khanna, Intumescent coatings: A review on recent progress, J. Coatings Technol. Res. 14 (2017) 1–20. https://doi.org/10.1007/s11998-016-9815-3.

[101] J.P. Siregar, S.M. Sapuan, M.Z.A. Rahman, H.M.D.K. Zaman, The Effect of Compatibilising Agent and Surface Modification on the Physical Properties of Short Pineapple Leaf Fibre (PALF) Reinforced High Impact Polystyrene (HIPS) Composites, Polym. Polym. Compos. 17 (2009) 379–384. https://doi.org/10.1177/096739110901700606.

[102] S. Wacharawichanant, L. Noichin, S. Bannarak, S. Thongyai, Morphology and Properties of Acrylonitrile-Butadiene-Styrene/ZnO Nanocomposites with Compatibilizer, Macromol. Symp. 354 (2015) 163–169. https://doi.org/10.1002/masy.201400111.

[103] T.S. Lin, J.M. Cogen, R.E. Lyon, Correlations between Microscale Combustion Calorimetry and Conventional Flammability Tests for Flame Retardant Wire and Cable Compounds, in: Proc. 56th Int. Wire Cable Symp., 2007: pp. 176–185.

[104] B. Schartel, K.H. Pawlowski, R.E. Lyon, Pyrolysis combustion flow calorimeter: A tool to assess flame retarded PC/ABS materials?, Thermochim. Acta. 462 (2007) 1–14. https://doi.org/10.1016/J.TCA.2007.05.021.

[105] H. Lu, C.A. Wilkie, Synergistic effect of carbon nanotubes and decabromodiphenyl oxide/Sb2O3 in improving the flame retardancy of polystyrene, Polym. Degrad. Stab. 95 (2010) 564–571. https://doi.org/10.1016/j.polymdegradstab.2009.12.011.

[106] J.M. Cogen, T.S. Lin, R.E. Lyon, Correlations between pyrolysis combustion flow calorimetry and conventional flammability tests with halogen-free flame retardant polyolefin compounds, Fire Mater. 33 (2009) 33–50. https://doi.org/10.1002/fam.980.

[107] R. Sonnier, H. Vahabi, L. Ferry, J.M. Lopez-Cuesta, Pyrolysis-combustion flow calorimetry: A powerful tool to evaluate the flame retardancy of polymers, ACS Symp. Ser. 1118 (2012) 361–390. https://doi.org/10.1021/bk-2012-1118.ch024.

[108] R.E. Lyon, R.N. Walters, S.I. Stoliarov, Screening flame retardants for

plastics using microscale combustion calorimetry, Polym. Eng. Sci. 47 (2007) 1501–1510. https://doi.org/10.1002/pen.20871.

[109] G. Ozkoc, G. Bayram, E. Bayramli, Short glass fiber reinforced ABS and ABS/PA6 composites: Processing and characterization, Polym. Compos. 26 (2005) 745–755. https://doi.org/10.1002/pc.20144.

[110] S.-Y. Fu, B. Lauke, Fracture resistance of unfilled and calcite-particle-filled ABS composites reinforced by short glass fibers (SGF) under impact load, Compos. Part A Appl. Sci. Manuf. 29 (1998) 631–641. https://doi.org/10.1016/S1359-835X(97)00111-5.

[111] J. Sudeepan, K. Kumar, T.K. Barman, P. Sahoo, Study of Friction and Wear of ABS/ZnO Polymer Composite Using Taguchi Technique, Procedia Mater. Sci. 6 (2014) 391–400. https://doi.org/10.1016/j.mspro.2014.07.050.

[112] M.L. Shofner, F.J. Rodríguez-Macías, R. Vaidyanathan, E. V. Barrera, Single wall nanotube and vapor grown carbon fiber reinforced polymers processed by extrusion freeform fabrication, Compos. Part A Appl. Sci. Manuf. 34 (2003) 1207–1217. https://doi.org/10.1016/j.compositesa.2003.07.002.

[113] R.E. Lyon, R.N. Walters, Microscale Combustion Calorimeter, US 5981290 A, 1999.

[114] B. Schartel, T.R. Hull, Development of fire-retarded materials—Interpretation of cone calorimeter data, Fire Mater. 31 (2007) 327–354. https://doi.org/10.1002/fam.949.

[115] R.E. Lyon, R.N. Walters, S.I. Stoliarov, N. Safronava, Principles and Practice of Microscale Combustion Calorimetry, Renton, WA, 2014.

[116] R.E. Lyon, M.L. Janssens, Polymer Flammability, Washington, DC, 2005.

[117] P.M. Hergenrother, C.M. Thompson, J.G. Smith, J.W. Connell, J.A. Hinkley, R.E. Lyon, R. Moulton, Flame retardant aircraft epoxy resins containing phosphorus, Polymer (Guildf). 46 (2005) 5012–5024. https://doi.org/10.1016/j.polymer.2005.04.025.

[118] R. Sonnier, B. Otazaghine, L. Ferry, J.M. Lopez-Cuesta, Monitoring the combustion efficiency in Pyrolysis Combustion Flow Calorimeter (PCFC) – Correlation with Cone Calorimeter, in: 23rd Annu. Conf.

Recent Adv. Flame Retard. Polym. Mater., BCC Research, Stamford, 2012: pp. 16–17.

[119] R.N. Walters, Molar group contributions to the heat of combustion, Fire Mater. 26 (2002) 131–145. https://doi.org/10.1002/fam.802.

[120] A.L. Doolette, R.J. Smernik, Facile decomposition of phytate in the solid-state: Kinetics and decomposition pathways, Phosphorus. Sulfur. Silicon Relat. Elem. 193 (2018) 192–199. https://doi.org/10.1080/10426507.2017.1416614.

[121] R. Sonnier, L. Ferry, C. Longuet, F. Laoutid, B. Friederich, A. Laachachi, J.M. Lopez-Cuesta, Combining cone calorimeter and PCFC to determine the mode of action of flame-retardant additives, Polym. Adv. Technol. 22 (2011) 1091–1099. https://doi.org/10.1002/pat.1989.

[122] M. Suzuki, C.A. Wilkie, The thermal degradation of acrylonitrile-butadiene-styrene terpolymer as studied by TGA/FTIR, Polym. Degrad. Stab. 47 (1995) 217–221. https://doi.org/10.1016/0141-3910(94)00122-O.

[123] H.C. Jun, S.C. Oh, H.P. Lee, H.T. Kim, K.O. Yoo, Pyrolysis Characteristics of Acrylonitrile-Butadiene-Styrene Resin, J. Ind. Eng. Chem. 5 (1999) 143–149.

[124] M.H. Yang, Thermal degradation of acrylonitrile-butadiene-styrene terpolymer under various gas conditions, Polym. Test. 19 (2000) 105–110. https://doi.org/10.1016/S0142-9418(98)00067-1.

[125] H.Y. Yen, F.S. Lee, M.H. Yang, Thermal degradation of polysulfones. VI: Evaluation of thermal pyrolysis of acrylonitrile-butadiene-styrene terpolymer, Polym. Test. 22 (2003) 31–36. https://doi.org/10.1016/S0142-9418(02)00045-4.

[126] Y. Wang, J. Zhang, Thermal stabilities of drops of burning thermoplastics under the UL 94 vertical test conditions, J. Hazard. Mater. 246–247 (2013) 103–109. https://doi.org/10.1016/j.jhazmat.2012.12.020.

[127] J. Li, S.I. Stoliarov, Measurement of kinetics and thermodynamics of the thermal degradation for non-charring polymers, Combust. Flame. 160 (2013) 1287–1297.

https://doi.org/10.1016/j.combustflame.2013.02.012.

[128] T.S. Radhakrishnan, M.R. Rao, Thermal decomposition of polybutadienes by pyrolysis gas chromatography, J. Polym. Sci. Polym. Chem. Ed. 19 (1981) 3197–3208. https://doi.org/10.1002/pol.1981.170191214.

[129] A. Alajbeg, P. Arpino, Đ. Deur-Šiftar, G. Guiochon, Investigation of some vinyl polymers by pyrolysis—gas chromatography—mass spectrometry, J. Anal. Appl. Pyrolysis. 1 (1980) 203–212. https://doi.org/10.1016/0165-2370(80)80003-9.

[130] L.W. McKeen, Styrenic Plastics, in: Eff. Temp. Other Factors Plast. Elastomers, Second Ed., William Andrew Inc., Norwich, 2008: pp. 41–95. https://doi.org/10.1016/B978-081551568-5.50004-9.

[131] G. Guiochon, C.L. Guillemin, eds., Quantitative Analysis By Gas Chromatography: Basic Problems, Fundamental Relationships, Measurement of the Sample Size, in: Quant. Gas Chromatogr. Lab. Anal. On-Line Process Control, Elsevier, 1988: pp. 563–586. https://doi.org/10.1016/S0301-4770(08)70085-X.

[132] G. Guiochon, C.L. Guillemin, eds., Quantitative Analysis By Gas Chromatography: Measurement of Peak Area and Derivation of Sample Composition, in: Quant. Gas Chromatogr. Lab. Anal. On-Line Process Control, Elsevier, 1988: pp. 629–659. https://doi.org/10.1016/S0301-4770(08)70087-3.

[133] I.C. McNeill, W.T.K. Stevenson, Thermal degradation of styrene-butadiene diblock copolymer: Part 1-Characteristics of polystyrene and polybutadiene degradation, Polym. Degrad. Stab. 10 (1985) 247–265. https://doi.org/10.1016/0141-3910(85)90006-0.

[134] M.A. Golub, M. Sung, Thermal Cyclization of 1,2-Polybutadiene and 3,4-Polyisoprene, Polym. Lett. Ed. 11 (1973) 129–138.

[135] P. Kusch, G. Knupp, A. Morrisson, Analysis of Synthetic Polymers and Copolymers by Pyrolysis-Gas Chromatography/Mass Spectrometry, in: Robert K. Bregg (Ed.), Horizons Polym. Res., Nova Science Publishers, Inc., New York, 2005: pp. 141–191.

[136] S.S. Choi, Characteristics of the pyrolysis patterns of styrene-butadiene rubbers with differing microstructures, J. Anal. Appl.

Pyrolysis. 62 (2002) 319–330. https://doi.org/10.1016/S0165-2370(01)00128-0.

[137] P. Kusch, Pyrolysis-Gas Chromatography/Mass Spectrometry of Polymeric Materials, in: M.A. Mohd (Ed.), Adv. Gas Chromatogr. - Prog. Agric. Biomed. Ind. Appl., InTech, Rijeka, 2012: pp. 343–362. https://doi.org/10.5772/32323.

[138] M. Surianarayanan, R. Vijayaraghavan, K. V. Raghavan, Spectroscopic investigations of polyacrylonitrile thermal degradation, J. Polym. Sci. Part A Polym. Chem. 36 (1998) 2503–2512. https://doi.org/10.1002/(SICI)1099-0518(199810)36:14<2503::AID-POLA9>3.0.CO;2-T.

[139] C.L. Beyler, M.M. Hirschler, Thermal Decomposition of Polymers, in: SFPE Handb. Fire Prot. Eng. 3rd Ed., 2005: pp. 110–131. https://doi.org/10.1021/cm200949v.

[140] J. V. Rutkowski, B.C. Levin, Acrylonitrile-Butadiene-Styrene Copolymers (ABS): Pyrolysis and Combustion Products and their Toxicity - A Review of the Literature, Fire Mater. 10 (1986) 93–105. https://doi.org/10.1002/fam.810100303.

[141] I.C. Mcneill, L. Ackerman, S.N. Gupta, Degradation of Polymer Mixtures. IX. Blends of Polystyrene with Polybutadiene, J. Polym. Sci. Polym. Chem. Ed. 16 (1978) 2169–2181.

[142] B. Schneider, D. Doskočilová, J. Štokr, M. Svoboda, Study of thermal degradation of polybutadiene in inert atmosphere: 1. Evidence of temperature and time of heating in i.r. and n.m.r. spectra, Polymer (Guildf). 34 (1993) 432–436. https://doi.org/10.1016/0032-3861(93)90103-H.

[143] N. Grassie, D.R. Bain, Thermal degradation of copolymers of styrene and acrylonitrile. I. Preliminary investigation of changes in molecular weight and the formation of volatile products, J. Polym. Sci. Part A-1 Polym. Chem. 8 (1970) 2653–2664. https://doi.org/10.1002/pol.1970.150080930.

[144] L. Nicolais, M. Narkis, Stress-strain behavior of styrene-acrylonitrile/glass bead composites in the glassy region, Polym. Eng. Sci. 11 (1971) 194–199. https://doi.org/10.1002/pen.760110305.

[145] I. Chodák, Z. Nógellová, B. V. Kokta, Mechanical properties of crosslinked polyolefin-based materials, Macromol. Symp. 147 (1999) 83–90. https://doi.org/10.1002/masy.19991470109.